MECHANOCHEMICAL SYNTHESIS AND COMPUTATIONAL INVESTIGATION OF ORGANO-MAIN GROUP SPECIES WITH DELOCALIZED LIGANDS

By

Ross Forrest Koby

Dissertation
Submitted to the Faculty of the
Graduate School of Vanderbilt University
in partial fulfillment of the requirements
for the degree of

DOCTOR OF PHILOSOPHY
in
Chemistry

June 30th, 2021

Nashville, Tennessee

Approved
Timothy P. Hanusa, Ph.D.
Nathan D. Schley, Ph.D.
Janet E. Macdonald, Ph.D.
Brian K. Long, Ph.D.

Acknowledgements

Since this would not be possible otherwise, I must start by thanking all my research supervisors and teachers who always believed in my potential. I am especially grateful that I had the opportunity to work under Tomislav Friščić and José Gregorio Hernández, who got me hooked on mechanochemistry and organometallic chemistry and really took a chance on me. I would like to also thank Alan Remaley and the rest of the Remaley lab for providing many enriching opportunities during my time at the NIH. I must also thank Jean-Louis Do, the rest of the Friščić lab, and everyone we shared lab and office space with for being patient and supportive of me as an undergraduate researcher. With Igor, Patrick, Davin, Kruno, Vjeko, and many more serving as role models, providing mentoring, and continuing to be supportive of my career, it has felt like I had a whole team behind me during my PhD.

However, the biggest thanks must go to my doctoral supervisor, Dr. Timothy Hanusa. He modeled the pure enthusiasm and joy of being a chemist, teacher, and supervisor that I hope to hold onto for my whole life. As my friends all know, every day is a great day for chemistry. Dr. Hanusa's unwavering support of me and my coworkers demonstrated that the most important part of being a supervisor is not simply transferring chemistry knowledge, but unconditionally supporting students. His door has always been open for discussions and updates, chemistry-related or not. I will always look back fondly on the evening discussions on myriad topics, or being pulled into his office to see a new handout he has developed or gizmo he has acquired. He has provided the framework for me to develop into a more independent scientist, while still remaining involved and supportive, and for that I will always be appreciative.

I am especially appreciative of my family, notably my parents Betty and Myles and my siblings Jay, Daniel, and Sara. The older I get, the more I realize the untold sacrifices they have made so I could pursue my dream to study and do chemistry. I must also thank all the attentive doctors, nurses, and other medical staff who have helped me be healthy enough to be successful in my PhD, especially Dr. Michael Morris.

My coworkers in the Hanusa group have also been an integral part of my success, and have helped me grow every day as a person and a scientist, especially my cohort-mate, Isaiah Speight. I feel very fortunate to have had the opportunity to work with all my lab mates and watch them put their own spin on mechanochemistry and develop their interests in the lab, especially Henry DeGroot and Lauren Wenger. It has also been very rewarding to work with some talented and motivated undergraduates, including Hogan Sherrow, Grant Steelman, and Kev Jung.

I must also thank the Nicks (Boyde and Rightmire). Nick Boyde showed Isaiah and me the ropes while finishing his PhD, and has continued to be a friend and helpful resource. Nick Rightmire started the mechanochemical research in the Hanusa lab and his hard work and ambitious exploration laid the foundation for much of my work.

The students in the department who I owe thanks extend beyond my group, including all of the students on the 8th floor, especially Jamin Keith and the rest of my neighbors in the Townsend group, Kelly Richardson across the hall, and my DFT buddy Andrew Puente. I also cannot overstate the impact of the Schley group on my graduate

career, having gone above and beyond as friends and colleagues, including Caleb Fast, Scott Chapp, Ben Mueller, and especially Caleb Jones, who was always ready for a beer and chat at Kaybob's.

To the other members of my committee, Profs. Janet Macdonald, Nathan Schley, and Brian Long, thank you for being very engaged and investing time and effort into my education. Dr. Schley in particular has been very supportive, lending his expertise and time as crystallographer on countless occasions. Without him, many of my projects would be unpublishable and unfinished. In addition, he took time to share his expertise in a variety of subjects, including pump maintenance, setting up a lab, crystallography, and of course organometallic chemistry. His encouragement to never settle or give up on a promising result helped me grow as a chemist and push through challenging projects.

Former Hanusa group members Dr. Keith Quisenberry, Dr. Steve Chmely, and Dr. Nick Rightmire have been supportive and encouraging, especially during my search for postdoctoral positions and the writing of my thesis.

My PhD has challenged me in many ways, especially the last year, but this has only made me more appreciative of the friends I have made, whether they be from Maryland, Montreal, Nashville, or on Twitter and elsewhere. Every friend who has checked in on me, enjoyed a beer, proof-read a paper or application, or simply sent a good meme has helped me get one step closer towards finishing. A few friends have been particularly important to me during my PhD. Jesse and Sheena have inspired me to be a better scientist and student, but more importantly to be kind. My squad of friends from Maryland; Austin, Conor, Greg, and Andrew have kept me grounded and reminded me to hold on to the joy of music. In particular, ever since I convinced him to move to Nashville, Conor has made every day in town a blast and for that I am grateful.

I would be remiss to leave out the people behind the scenes who work hard to keep everything working in the department, especially those in maintenance, facilities, VEH&S, the office staff, and Don Stec and Markus Voehler who have facilitated a huge variety of heteronuclear experiments and last-minute low temperature experiments with gusto.

This would not have been possible without financial support by the National Science Foundation (CHE-1112181), ACS PRF (56027-ND3), and a Charles M. Lukehart Fellowship.

Preface

Like the Roman god Janus, scientists look both ahead and behind, caught between the pull of progress and glory-anchored history. Over the course of my doctoral work, I have felt the pull from both sides. Moreso than many students in the department, much of my work is classical or old-school in both scope and mentality. The work I have found stimulating, and that follows in this thesis, is heavily influenced by the intrepid and curious chemists of yesteryear, who toiled ceaselessly to unlock the secrets of the metal-carbon bond. It has been immensely rewarding to contribute to some of these remaining challenges discussed herein, bring them into the 21st century, and push them even an inch further towards understanding. Digging through the literature has allowed me to travel back in time and feel like I am standing next to these researchers, discovering diethylzinc (identified by both the green-blue flame and resulting zinc poisoning, I am quite happy to miss out on that!) or ferrocene for the first time. Delving into very fundamental questions (why are group 2 compounds bent? Why are there only η^1-coordinated allyls on magnesium? What is the structure of beryllocene?) has made me feel truly connected to the birth of modern inorganic and organometallic chemistry and it is an honor and privilege to align myself with this truly amazing field. As a musician and a chemist, the scientific literature is the longest song I know, and whatever happens next, I hope I have added a few good words.

Table of Contents

List of Tables

List of Figures

Chapter 1:

Introduction

1.1 Introduction to mechanochemistry

Mechanochemistry has seen an explosion in interest in the last decade alone, going from a tool for co-crystal formation to an all-purpose synthetic technique. Recently, many reviews and books have been published on its use in different subfields, on specific mechanochemical techniques[1,2], and on our fundamental understanding of it.[3]

Mechanochemistry in the broadest sense can be described as chemical transformations that are initiated or driven by mechanical force.[4] Since the term was coined by Wilhelm Ostwald,[5] this expansive technique has united mechanochemists across a broad range of subdisciplines. Researchers are applying mechanochemical techniques to a variety of synthetic challenges, including functional materials[6] and co-crystals,[7–10] inorganic and organometallic chemistry,[11–17] biomolecules and other organic compounds,[1,18–24] catalysis,[25–29] polymer synthesis,[30,31] and more. This results in a broad range of methods. In terms of scale, mechanochemistry ranges from very small (bending individual crystals[32] or breaking bonds in a single molecule with an atomic force microscope (AFM)[33]) to very large (using industrial tumblers or twin-screw extruders for kilogram-scale synthesis).[34]

Thorough investigation by Prof. Takacs chronicles the history of mechanochemistry starting from antiquity.[35–38] The development of mechanochemistry is often attributed to Theophrastus of Eresos, Michael Faraday, M. Carey Lea, and Wilhelm Ostwald. Theophrastus of Eresos, a 4th century BCE student of Aristotle, equally renowned for his works both dramatic and on natural philosophy, ground cinnabar (HgS) with vinegar in a copper vessel. This resulted in the displacement reaction producing mercury metal and copper sulfide, the first reported example of mechanochemistry, though of course it was not referred to as such.[39] After a ~2000 year gap, the next reported example was in 1820, when Faraday investigated the reduction of AgCl with other metals done "in the dry way". The way this paper was written implies that knowledge of mechanochemical reactivity was relatively common, though poorly documented.[35,40] Unfortunately, since the reactions attempted in this work can also be completed thermally, they do not serve to differentiate mechanochemistry from thermochemistry. In the 1880's, Walthère Spring, a Belgian professor, developed an apparatus to place samples under very high pressure (~6000 atm). Being a professor of chemistry and mineralogy, he used this to study the effects of pressure on materials and imitate the immense pressure of geologic conditions. Though he demonstrated mechanochemical reactivity, the reaction conditions were complicated, consisting of repeated crushing and pelleting of samples until reaction completion. Given

the ill-defined conditions, even contemporary scientists speculated as to the role of moisture and what part of the pressure or grinding was responsible for reactivity.[41] It was not until 1893 that M. Carey Lea definitively demonstrated divergent reactivity from grinding versus heating.[42] In this work, Lea reported the decomposition of mercuric and silver chlorides upon grinding, while heating caused sublimation or melting. In another work, he demonstrated that the grinding action significantly increased the rate of reactivity compared to simply applying pressure. Compared to the static pressure of 6900 atm, lightly grinding silver halides in a mortar and pestle caused rapid decomposition.[43] Lea's work is still frequently cited, and shows that the unique properties of mechanochemistry are not simply related to applying pressure to reagents, or aiding mixing.

The vast majority of synthetic work covered in this thesis has been done mechanochemically, which has been the basis for much of the success and discovery discussed herein. While many synthetic chemists worry about choosing the proper solvent for a reaction, it is important to remember that not choosing is also always a choice. By choosing to not use a solvent, and instead grind reagents together, the Hanusa group has succeeded in isolating and characterizing a variety of astounding compounds that challenge the way chemists think about synthesis and main-group chemistry. It is our hope that our work will contribute to mechanochemistry becoming a technique that has similar popularity and is held in similar esteem to electrochemistry, photochemistry, microwave-assisted chemistry, and other alternative techniques.

In the Hanusa group, our mechanochemical infrastructure has evolved over time, the greater control of which has facilitated the pursuit of even more challenging targets. Though some groups are investigating other bulk mechanochemical techniques such as resonant acoustic mixing (RAM), we have always been focused on ball milling. Initially, reagents were added to a glass round bottom flask with stainless steel ball bearings that was rotated slowly on a rotary evaporator in a glovebox. This resulted in our first mechanochemical success, a long-sought after base-free tris-allyl aluminum.[44] The next piece of equipment acquired was a tube disperser, which is designed to grind or homogenize samples. As the name suggests, it is a small machine similar to a vortexer that shakes a tube with steel or glass balls. There were many benefits to moving to a more advanced setup. First, reactions could be done outside of the box since the tubes were somewhat airtight. The reactions were also much faster than with the makeshift rotary evaporator mill, since speed did not need to be limited to avoid fracturing of glass vessels. With the results from this equipment in hand, the Hanusa group was able to secure funding for a planetary ball mill, which drastically increased our capabilities. Most synthetic groups use some sort of planetary or mixer mill, though there is work being done with bench-scale twin screw extruders, which allow continuous/flow synthesis.

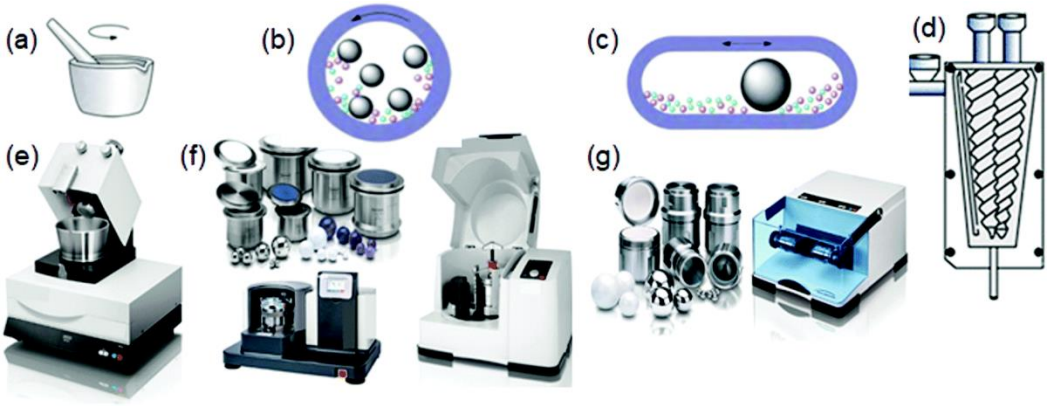

Figure 1. Schematic illustration of mechanochemical equipment. (a) mortar and pestle, (b) planetary mill, (c) shaker and (d) extruder. Images of the instruments for mechanochemical synthesis: (e) mortar grinder, (f) planetary mills with equipment and (g) mixer mill with equipment (reproduced with permission of the RSC)

In the work discussed in the following chapters, a planetary mill was used in almost all cases. There are a variety of reasons this mill was used, as there is also a mixer mill available, which theoretically allows for higher throughput (two reactions at once, as opposed to one with the Retsch PM100). In our hands, the mixer mills allow for a higher ball-to-reagent loading (BRR, the effects of which have been discussed in a recent paper),[45] and the use of larger ball bearings. Though there has not been systematic study on this phenomenon, in our hands, the mixer mill is better suited to reactions that are challenging, as fewer, larger ball bearings will impart more energy per impact, while an equivalent mass of smaller ball bearings in a planetary mill provides a larger number of less forceful impacts. Most of the reactions discussed occur through salt metathesis, which are partially driven by the elimination of a halide salt in the case of metal halide precursors. Because of this, the reactions have a strong intrinsic driving force that does not require harsh milling conditions. In most cases, a change in yield or product is not seen upon increasing milling time past 15 minutes. In fact, increasing milling time is potentially detrimental for a variety of reasons. One is the potential for heat buildup, as the reactions themselves are exothermic. This can alter selectivity and induce decomposition; in solution, many of these reactions must be done at low temperatures (standard conditions -78 °C). In many cases, even for a ~100 mg scale reaction, a successful reaction can be predicted before workup simply by touching the jar and feeling how warm it is, as a productive salt metathesis will generate heat. Another reason is the increased potential for side reactions, since all of the reagents and products continue to mix with each other and experience forces that may lead to reaction. Normally, for salt metathesis, the salt byproduct precipitates out and is functionally removed from the system. Under mechanochemical conditions, there is no phase separation in this case and halide salts or other “insoluble” byproducts are able to react or be incorporated into products. An example of this is the mechanochemical synthesis of ferrocene, where it was found after extended milling, the reaction actually

starts to go in the reverse direction (i.e., 2 CpTl + $FeCl_2$ ⇄ Cp_2Fe + 2 TlCl).[46] Essentially, some reactions for which equilibrium may not be a concern have to be reconsidered under mechanochemical conditions. Finally, the longer a reaction is milling, the longer it is potentially exposed to oxygen and moisture, as our mills are on the benchtop.

In the literature, there are reports of the stainless steel surfaces of jars and ball bearings acting as reducing agents.[47] Despite the metal reagents being reducible (especially by the potassium allyl itself), stainless steel ball bearings and jars have been used without incident in the systems discussed in this thesis. It is possible some of the failed reactions that displayed reductive coupling could be due to the stainless steel, but in almost all cases the analogous solution reactions also resulted in coupling products.

A certain portion of our understanding has come from the development of *in-situ* monitoring techniques, including PXRD and Raman spectroscopy.[48–50] Molecular dynamics calculations have also proven relevant to the microscopic phenomena at play. However, the detailed analysis of model reactions provides the most practically useful information. For instance, recent work studying the mechanochemical Knoevenagel condensation of vanillin and barbituric acid suggests that an entire spectrum of cohesive states of matter can have drastic effects on the kinetics and outcomes of mechanochemical reactions.[51] From this study, it was found that an induction period was associated with a dry, powdery phase, the sigmoidal portion of the reaction was related to a transition from the dry powder to a rubbery mass that encapsulated the ball bearing, and then back to a powder. Though this is not necessarily relevant for every single mechanochemical system, it illustrates that there is an often-complex confluence of physical and chemical properties that the average solution-phase chemist can ignore.

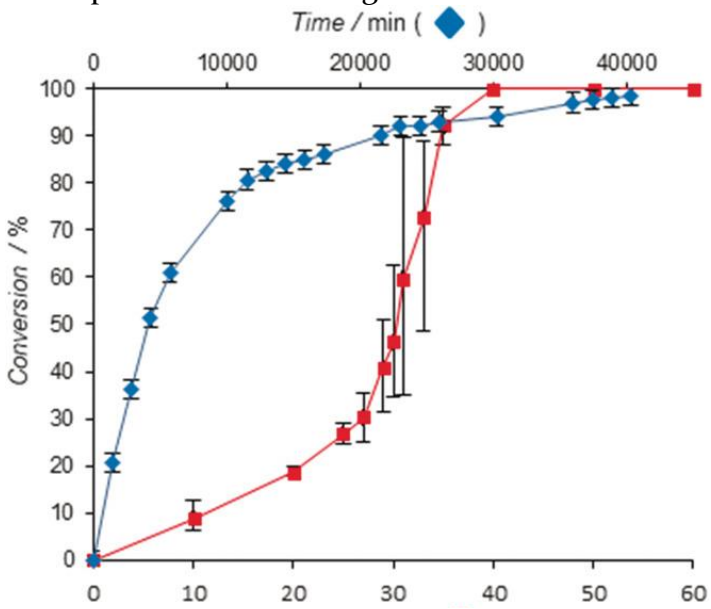

Figure 2. Comparison of conversion versus time for the Knoevenagel reaction in solution (DMSO-d_6) and under mechanochemical conditions (mixer mill, 25 Hz with added water 10 % wt). Error bars were calculated from three standard deviations from the mean of each dataset for each time point. (Reproduced with permission)

1.1.1 Mechanochemistry as a synthetic technique

A common question posed by newcomers to ball milling is, how are these reactions actually occurring? What are the fundamental phenomena that facilitate reactivity? For reactions requiring thermal energy, solvents facilitate collisions and transfer of thermal energy to or from the reagents. Under mechanochemistry, milling action allows mixing of reagents, and kinetic energy from the ball bearings is transferred to the reagents, as opposed to thermal energy under solution conditions. However, the resulting thermal energy or lack thereof cannot be transferred as effectively as in solution, with the balls and jars acting as heat sinks. The exact mechanism of mechanochemical reactivity is hotly contested, and likely varies depending on the reaction and reagents used. It has been hypothesized that at the ball-jar interface, localized hot spots up to 2000 °C may be generated, in a similar fashion to how ultrasonic cavitation is proposed to generate localized sites of very high pressure and temperature. In the field of mechanochemistry, this was initially used to explain occasionally highly divergent reactivity.[52,53] However, work studying the effects of temperature on reactivity rate essentially discredited this theory. In work by the Užarević group in Croatia, a 45 °C increase in reaction temperature results in a six-fold reduction in reaction time.[54] If the reaction was occurring through the production of hot spots >1000 °C, a 45 °C temperature difference should have little or no effect. Additionally, ball milling reactions with reagents and products that would decompose under these harsh conditions have contributed to the invalidation of hot spot theory for general synthesis, though it is invoked for metal and metal-alloy reactivity.[38] In addition, the bulk temperature of mixer mill vessels only slightly increases even after milling for hours, which would not be the case if enough ~2000 °C events were occurring for all chemicals to react. Furthermore, calculations and systematic studies show that at least in most cases, this is extremely unlikely to be relevant.[55–57] A more realistic hypothesis is the comminution or reduction of materials and reagents to generate very small particles. These can be on the nanometer scale and have high surface energy, rendering them extremely reactive. Another potential theory is the cracking of crystals upon deformation and size reduction results in dangling bonds and atoms that are very reactive, without even mentioning the localized electric field generated. It is also possible that crystalline compounds may be converted into a more reactive polymorph during grinding, which facilitates reactivity.[58]

The ball milling reaction variable of milling frequency has frequently been compared to temperature in solution reactions. Analogously to temperature, the milling speed of a ball mill should vary the speed of the ball bearings and therefore their force, and energy upon collision. A variety of papers, specifically from the Mack group, focus on deconvoluting the effect of milling frequency on yield and reaction selectivity. In one case, this was done for reactions where the effect of temperature is well understood (Diels-Alder cycloadditions) and calculations to investigate reaction barrier height can be completed.[59] In this specific case, the mechanochemical reaction outcome can be predicted based on the calculated reaction barrier height, with higher barriers requiring harder jar materials and higher milling frequency. Additionally, the Mack group has milling apparatus that can have its temperature modulated.

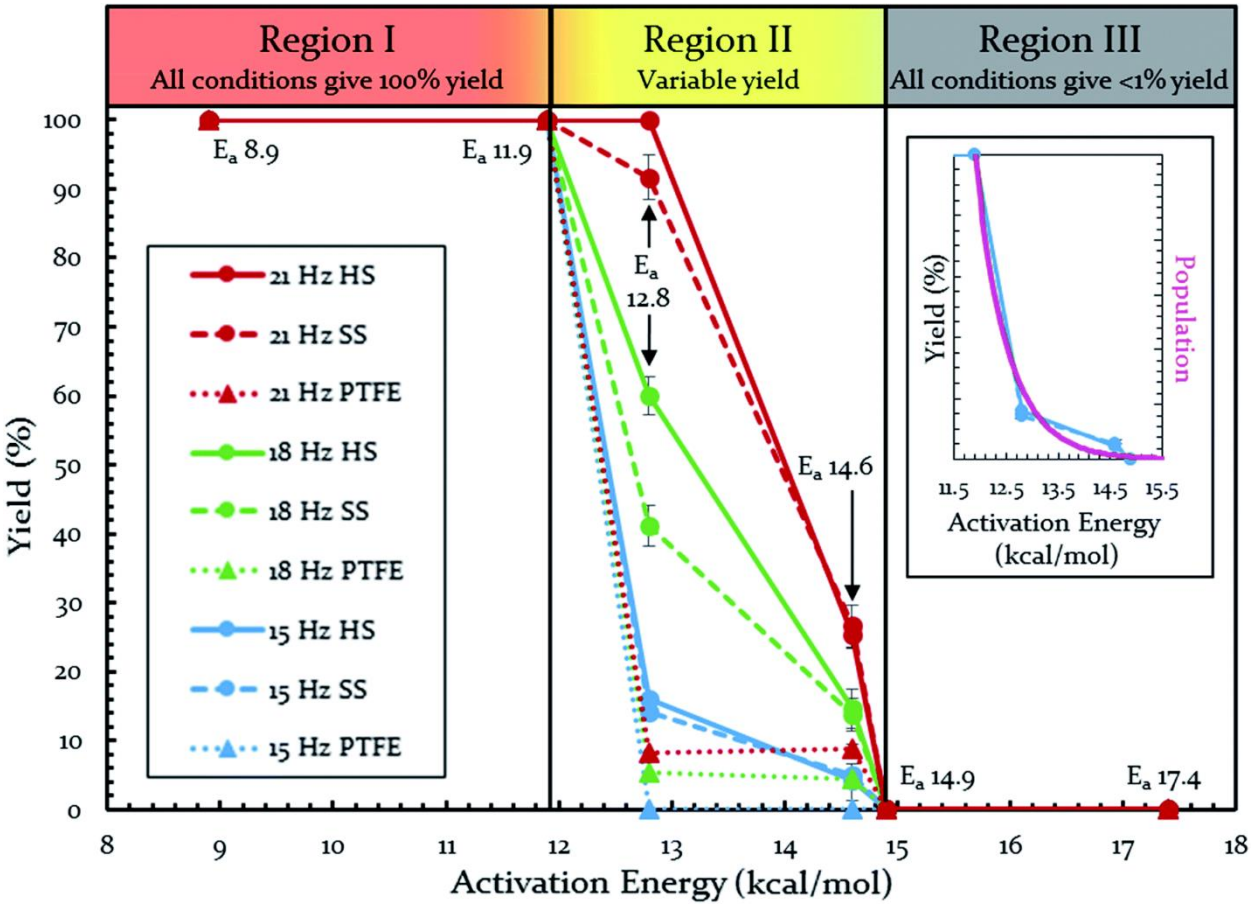

Figure 3. Yields of Diels–Alder reactions under various ball-milling conditions. Note: all nine conditions produce overlapping yields for E_a 8.9, 11.9, 14.9, and 17.4 kcal mol^{-1}. Teflon (PTFE), stainless steel (SS), and hardened steel (HS). Inset: population of energies determined by Boltzmann distribution overlaid on top of yield data. (Reproduced with permission from *Chem. Sci.* **2017**, *8* (8), 5447–5453.)

When the milling jar was cooled from the peak operating temperature of 38 °C to 22 °C, the reaction between benzoquinone and 9,10-dimethylanthracene yield dropped from 92% to 12%. This indicates there is some type of synergistic effect or link between milling frequency and reaction vessel temperature and how they modulate reactivity. Though milling frequency may act as a mechanochemical temperature surrogate in some cases, frequency and temperature can also be used in tandem. In the paper, this is described as fine control (milling frequency) and coarse control (temperature). However, this work assumes that milling simply facilitates molecular collisions, which based on the changes in yield and reaction outcome when jar and ball materials are changed, is an oversimplification.[60] Though this was not investigated in the work described in this thesis, the development and application of temperature-controlled milling will be necessary to continue the dramatic rate of advancement mechanochemistry is experiencing. Additionally, more investigation on the effect of jar materials, ball bearing quantity, mass, and size, and milling frequency is necessary, as these are all inherently related (milling frequency is assumed to modulate ball bearing collision speed, assuming ideal conditions) and are challenging to deconvolute.

In many reported examples of mechanochemistry, some aspect of the reaction is often dramatically improved. Some of these potential benefits are shown in figure below.

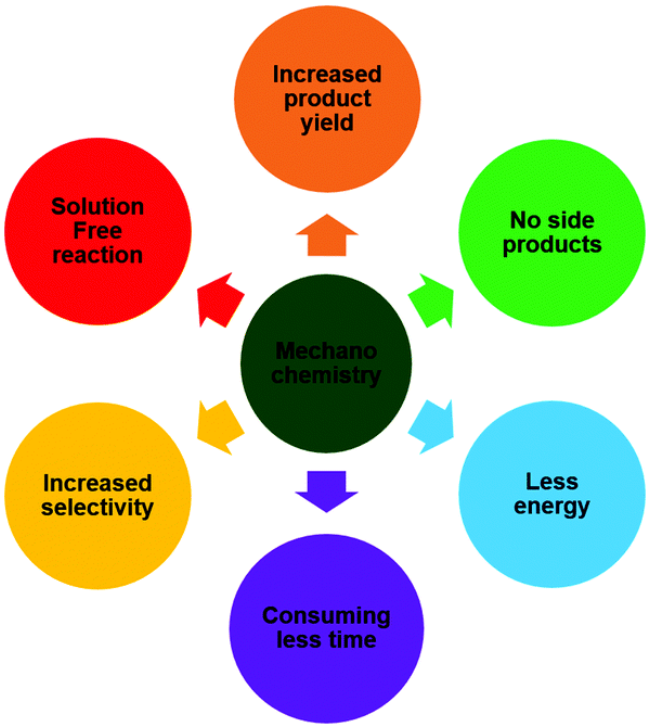

Figure 4: Advantages of mechanochemistry over solution-based chemistry (Reproduced with permission)

1.1.2 Inorganic and organometallic mechanochemistry

Inorganic and organometallic mechanochemistry has been developed by a small vanguard of intrepid researchers across the globe. Notable groups include those led by Ito,[26,61,62] Borchardt,[9,25,63] Browne,[64–67] Stolle,[68] Garcia,[12,13,69–71] Blair/Jurca,[72] Bolm/Hernandez,[73–76] Lamaty,[14,17,77] Friščić,[20,60,78,79] Užarević[80] and Mack,[81,82] who have focused on investigating either the synthesis of molecular metal-containing species or their use in catalysis under mechanochemical conditions. A few groups specializing in lanthanide chemistry[16,83] have also experimented in mechanochemistry, although this is rare due to the cost of commercially manufactured mechanochemical equipment (~$10,000 for a Retsch MM400). From this combined work, we see that mechanochemistry is a feasible alternative to conventional solution routes in many cases. It has a variety of benefits (reaction speed, selectivity, less harsh or stringent reaction conditions) and also provides access to new compounds and types of reactivity. A notable example of this is the use of piezoelectric perovskites under mechanochemical conditions as electron transfer reagents,[84] where traditionally photoredox or transition metal catalysts are used (Figure 5).[85,86] The perovskite-mediated reactions can be done under air and are complete in as little as one hour, unlike the traditional methods which can take over 24 hours and must be done under an inert atmosphere. Though ball mills are specialized equipment, some of these reactions can actually be done by hand using a mortar and pestle or other manual equipment.[84]

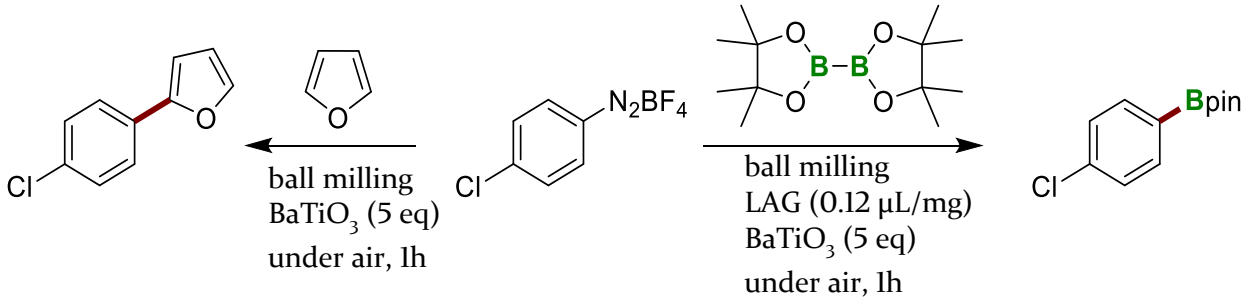

Figure 5. Perovskite-mediated borylation and arylation of aryldiazonium salts under mechanochemical conditions. The LAG solvent used for borylation is MeCN.

For organometallic synthesis, mechanochemistry has a few notable differences from solution reactions. A comparison of common considerations for solution phase vs mechanochemical reactions is shown below. Reactions can be stopped and started as quickly as the mill can stop or start, though some reactions are known to initiate by grinding and continue thereafter (accelerated ageing). Many compounds are sensitive to coordinating solvent, and mechanochemistry allows these to be avoided. Additionally, solubility of reagents is not so intrinsically linked to reactivity, though it may be relevant for workup procedures if the reaction does not go to completion or if there are byproducts.

In practice, there are few truly "solvent-free" reactions, especially when the synthesis of commercially available reagents is considered.

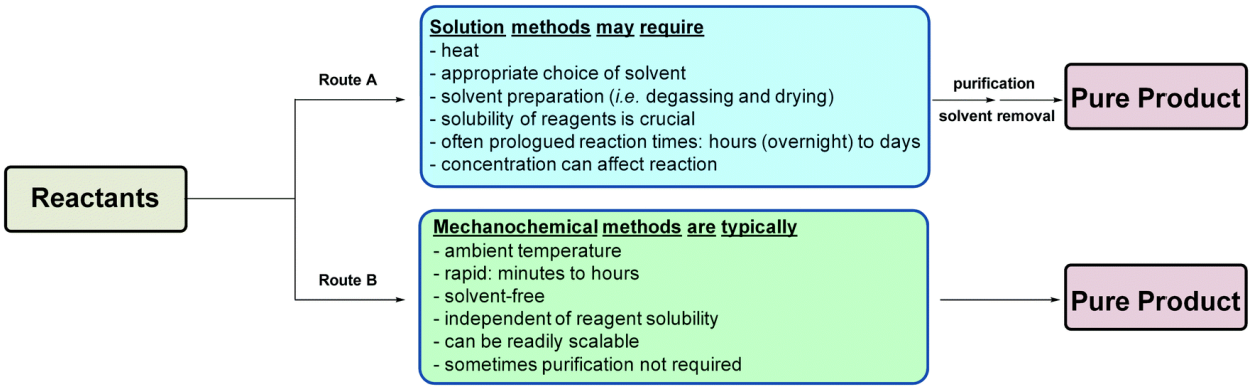

Figure 6. Variables associated with solvent-based and mechanochemical methodologies via route A and route B, respectively. (Reproduced with permission from Chem. Soc. Rev., 2019,48, 2274-2292, published by The Royal Society of Chemistry)

In terms of synthetic inorganic and organometallic chemistry, the recently released book chapter by Leon and Garcia[87] provides an up-to-date summary of advances, though other reviews focused on similar material exist.[11,29,88,89] Though the work in the following chapters is mostly based on salt metathesis reactions (which under mechanochemical conditions can be quite unpredictable, as will be discussed in later chapters), it is worth briefly showing that mechanochemistry is also amenable to systems that are more complex. A prime example is the mechanochemical formation of a Noels-type Ru-NHC species, where alkylation to form the ligand, metalation with silver, and transmetalation to ruthenium are all accomplished by ball milling. This product has so far only been formed mechanochemically, though it has not been attempted in solution.

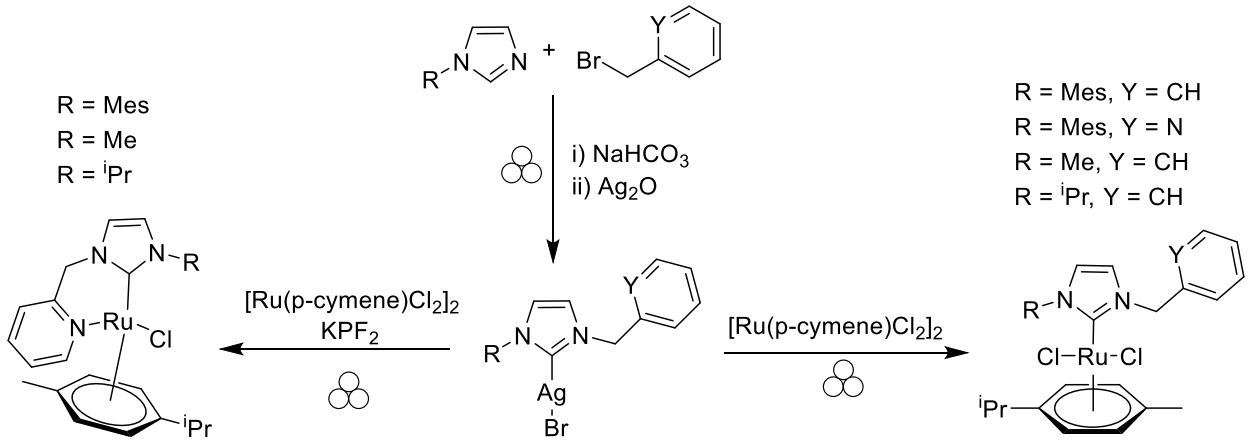

Figure 7. Lamaty's mechanochemical synthesis of Ru-NHC Noel complexes; note the use of the 3 ball symbol to represent ball milling

Though the type of work discussed is of great interest, the fundamental main-group mechanochemistry that is reported in this thesis has much less precedent.[90,91] In terms of s-block mechanochemistry, there are few examples. The closest example to our work is a report from the Blair group on the large-scale synthesis of Cp_2Sr analogs for chemical vapor deposition (CVD) that has only been published as conference proceedings in the Faraday Transactions.[92] There are other reports of s-block mechanochemistry, often focused on materials discovery or synthesis optimization.[93–95] An illustrative example of mechanochemistry's potential is the *in-situ* formation of $LiBH_4$ from $NaBH_4$ and LiCl, producing a much more powerful reagent from relatively inert starting materials.[96]

A seminal example of mechanochemistry's power to expand the available main group chemistry is the isodesmic rearrangement of a bulky phosphazane, shown below. In solution, with isopropyl groups, the reaction takes 12 days at 160 °C. For the *tert*-butyl substituted form, even 24 days at a similar temperature does not result in desired reactivity. In fact, this had previously been considered a sterically inaccessible compound. However, by simply grinding for 90 minutes with a salt additive (LiCl) at 30 Hz, the desired product is formed.[12]

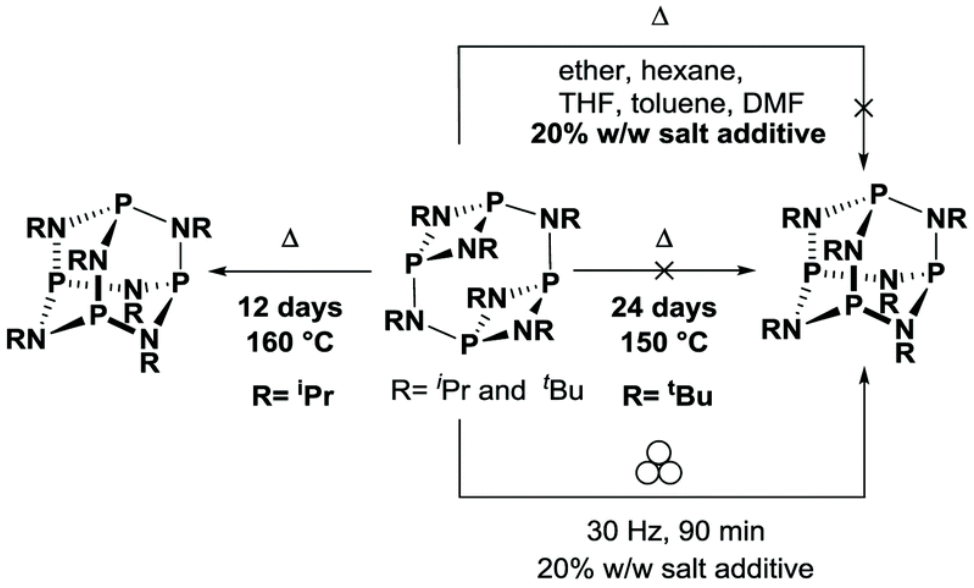

Figure 8. Isodesmic rearrangement of the tert-butyl macrocyclic bis-cyclodiphosphazane into its adamantoid structure, enabled only by ball milling. (Reused from *Chem. Soc. Rev.*, **2019**, *48*, 2274 with permission from RSC)

1.2 Modern computational methods (density functional theory)

Like many techniques, computational chemistry has gone from a specialist field to being so commonplace that most synthetic publications are expected to have some amount of computational work to rationalize or back up experimental results. Modern software and the exponential growth in computational resources ("Moore's Law") have made challenging calculations from 1-2 decades ago seem trivial today. A consequence of the growth of computational chemistry is the increase in breadth of available methods and ease of use. The amount of functionals available continues to grow, and quantum mechanical calculations using Hartree-Fock (HF) or density functional theory (DFT) no longer require supercomputers or clusters; publication-quality calculations can be easily run on personal computers. This can be intimidating to novices and must be approached cautiously, as most methods are relatively simple to run, but do not necessarily provide a physically relevant or trustworthy result when treated as a black box, especially for complicated systems. For the Hanusa group, computational investigation greatly contributes to our understanding of these often-complex systems, and for that reason my work often involves a significant computational component.

Density functional theory and Hartree-Fock are electronic structure (quantum mechanical) methods that attempt to solve the Schrödinger equation, but in different ways. In either case, the goal is to predict electronic properties based on electrons. The Schrödinger equation can only be solved exactly for 1-electron systems (H_2^+, He^+, etc), and must be approximated numerically otherwise. For Hartree-Fock, the exact Hamiltonian for the Schrödinger equation is known, but the wave function is approximated. Electron exchange is handled perfectly, but electron-electron repulsion is averaged for the whole system, and functionally cancels out. The HF wave function accounts for 99% of the total energy, but the last 1% (correlation energy) is very important, and the basis for chemical phenomena.

A variety of methods have been developed to recover this correlation energy. Unfortunately, these become extremely computationally expensive as the size of the system increases and each have their own flaws, rendering them impractical in many cases. A general problem with these so-called wave function theory (WFT) methods is the rapid scaling of variables. A wave function with N electrons has $3N$ variables ($4N$ if spin is accounted for). Thankfully, in 1964, Hohenberg and Kohn demonstrated in a proof that the ground state energy of a system is determined completely by its corresponding electron density ρ. The practical outcome is that for each calculated electron density ρ, there is a unique ground state energy, and it only depends on 3 variables, the x, y, and z coordinates of the electron density. However, we do not know the exact functional that connects the electron density and the ground state energy. For this thesis, the details are not appropriate, merely that DFT is capable of much more accurately predicting correlation energy, which HF cannot. Using the Kohn-Sham theory (application of MOs and splitting of kinetic energy into an exact and a corrected component), DFT becomes practically

analogous to HF. Unfortunately, the addition of orbitals moves DFT from a 3-variable back to a 3*N* variable system, making the initial computational cost also analogous to HF. Just like HF, Kohn-Sham DFT ignores the electron-electron interaction. However, Kohn-Sham DFT allows the correlation energy to be recovered using an exchange-correlation functional (part of the overall energy functional). So, for decades, theoretical and computational chemists have taken a variety of approaches to developing exchange and correlation functionals that will either approach the "true functional" and work for all systems, or give very accurate results for certain systems. A DFT method generally consists of separate exchange and correlation functionals, which can be mixed and matched but should be done carefully, with certain combinations found to be particularly accurate. Generally, functionals should meet some physically relevant specifications but may be heavily parameterized to match experimental values in the hopes of developing highly accurate functionals for systems that are similar to the training sets.

1.2.1 Dispersion-corrected DFT and the recognition of dispersion in inorganic and organometallic chemistry

A major theme in inorganic and organometallic chemistry is the use of bulky, sterically encumbered ligands to stabilize reactive species. This is especially important for main group chemistry, where the goal is often to isolate unique and unstable species. This stabilization was attributed primarily to the steric shielding, physically blocking the metal center from reacting and providing kinetic stabilization. It is now understood that in many cases, part of this stabilization is due to the attractive London dispersion forces (LDF) that arise from inter- and intra-ligand dispersion interactions.[97–102] In empirical terms, dispersion is the long-range electron correlation interactions that are not based on polarity or wave function overlap. It is based on dipole polarizability and atomic ionization potential.[103] It is a non-covalent interaction. It contributes to stability and bonding in chemical systems, and accurately modelling it is quite important for chemical accuracy.

We have already discussed that density functionals are designed to model correlation, but do not do this perfectly and often give poor agreement at long ranges, where dispersion is relevant. To remedy this, there are computational/theoretical chemists who focus on developing dispersion corrections that can be integrated into computational methods like DFT. Because dispersion is based on atomic properties, not on wave functions or any complex electronic structure, it should be easy to integrate into existing systems. Grimme and coworkers are leaders in this effort. The group's D3 correction is the standard in terms of accuracy and computational expedience. It is based on atomic properties (pairwise interactions of the polarizability and ionization potentials) that have already been calculated using time-dependent DFT for each atom pair, adding a negligible amount of computational time. This correction only slightly deviates (~5%) from the "gold standard" wave function method that models dispersion well, CCSD(T) with complete basis set (CBS) extrapolations.[104,105]

The main goal of Grimme's correction is to take functionals that do most things well, and add a correction that helps them model dispersion, to increase the accuracy for all systems, and especially for those that involve non-covalent interactions. Since many functionals already take some amount of dispersion into account and incorrectly model dispersion at different distance regimes, Grimme's correction must be tailored for each. This is done using 2 parameters that empirically smooth short-range (that DFT handles well by itself) and long-range (that DFT handles poorly) dispersion into the medium-range. Everything else for the correction is built from first principles. Though higher level dispersion corrections are available, they are not necessarily available in computational software, do not offer much improvement in accuracy over Grimme's D3 correction, ironically often have a more empirical basis, and are not fully integrable into existing computational software.[106] For these reasons, the DFT-D3 method remains the standard for dispersion-corrected DFT. As is discussed in further chapters, accurately modeling dispersion is extremely important for some of the main group complexes investigated, as their bonding is often highly polar and easily interrupted or affected by what would normally be considered "weak" interactions.

The large ligands used to stabilize reactive species often have many methyl groups and hydrogens that can interact with each other and contribute dispersion stabilization. In fact, ligands containing many methyl groups (trimethylsilyl, *tert*-butyl, etc.) are occasionally described as "dispersion donors" based on their propensity to contribute to dispersion. In some cases, the use of these bulky ligands with many C-H bonds result in structures and geometries that cannot explained solely by steric repulsion. In these cases, attractive dispersion interactions are often the explanation. Though intermolecular contacts with distances less than the sum of corresponding van der Waals radii were often noted in crystal structures,[107] van der Waals forces themselves were not often invoked (except in some notable examples).[108] In some cases, crystal packing was used to describe these unexpected geometries, though it is possible many of these can be explained using dispersion. Like hydrogen bonds, dispersion interactions are individually weak but when a large number are present, can significantly contribute to stability and alter systems. As an example, the C–H···H–C interaction of a methane dimer has been calculated to be about 0.31 kcal/mol.[109] This phenomenon is given as at least a partial explanation for the increase in melting point of linear hydrocarbons with increase in chain length.

An illustrative example of the role of dispersion in stability is the so-called hexaphenylethane riddle.[110] Hexaphenylethane was claimed to be synthesized from triphenylmethyl radicals,[111] but cannot be synthesized despite seeming quite straightforward. In fact, the actual product, a methylenecyclohexadiene resulting from dimerization, was not settled upon until 1968.[112]

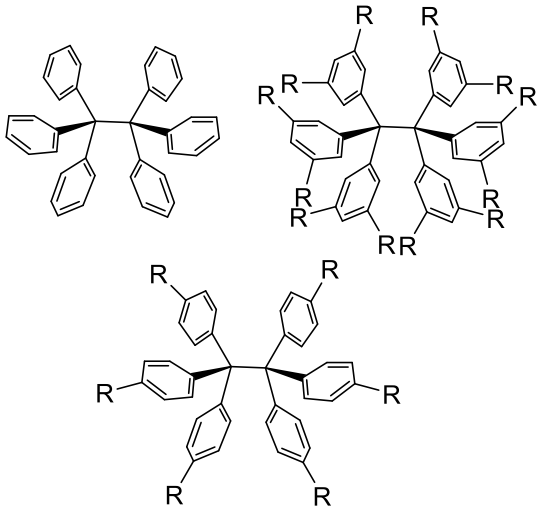

Figure 9. Clockwise from top left: hexaphenylethane, its all-*meta* and all-*para* ^{t}Bu-substituted analogs R = ^{t}Bu.

The tri(4-tert-butylphenyl)methyl radical also does not dimerize to give the *para*-substituted hexaphenylethane shown above. The instability of these two hexaphenylethanes was attributed to steric congestion, but a physical model does not show them to have a large amount of steric clash at all. In fact, the *more* congested *meta*-substituted form is quite easy to synthesize, melts at 214 °C, and has been crystallographically characterized.[113] The Grimme group[97] used dispersion-corrected DFT calculations to show that the C-H···H-C interactions of the *meta*-substituted significantly stabilizes the compound (~60 kcal/mol), enough to make dissociation endothermic.

Similarly, for some inorganic and organometallic systems, dispersion interactions can significantly stabilize compounds.[98,100,102,114,115] A good example is that of transition metal norbornyls, specifically $M(nor)_4$.[116] These are unique because the +4 oxidation state is not commonly accessible, let alone stable, for many transition metals. However, these compounds are generally quite stable and for most of the first-row transition metals, high-valent norbornyl complexes can be prepared. A large proportion of this stabilization is attributed to inter-ligand dispersion. As can be seen in the figure below, there are many C-H···H-C interactions that overall contribute as much as 45.9 kcal/mol (M = Fe) according to dispersion-corrected calculations.[101]

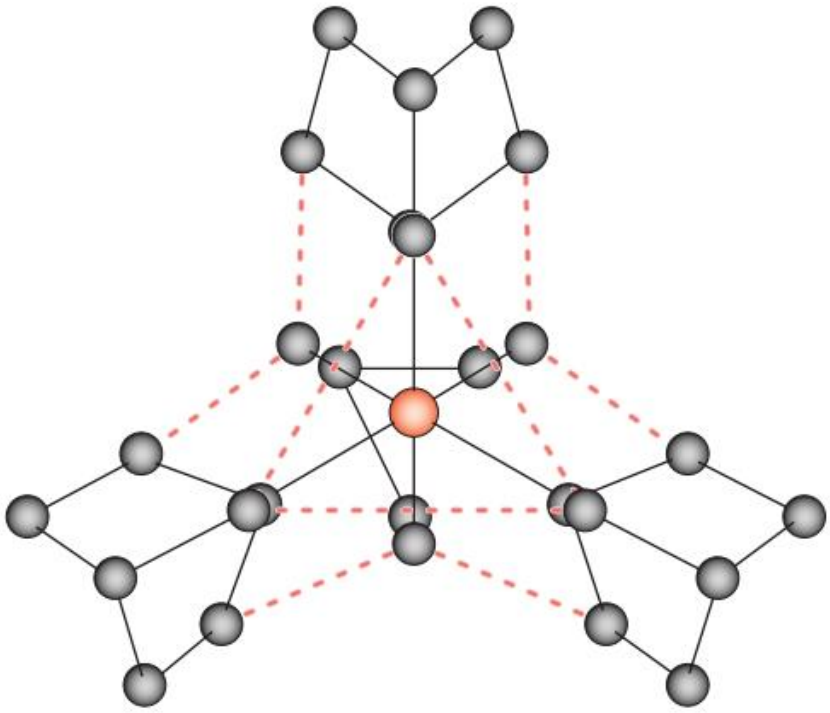

Figure 10. Crystal structure of Fe(1-norbornyl)$_4$ with probable $CH_2\cdots CH_2$ London dispersion interactions denoted by dotted red lines (hydrogens omitted for clarity)

A program frequently used to evaluate steric crowding is Solid-G,[117] which calculates the steric shielding a metal atom experiences, based on experimental or calculated structures. This is reported as the $G_{complex}$ value, with 100% denoting 100% coverage of the metal atom coordination sphere by ligands. Just like in solution, we hypothesize that under mechanochemical conditions, sterically unsaturated compounds react easily. However, under mechanochemical conditions, there are generally no solvents to shield the metal center temporarily or permanently, leading us to believe that understanding steric effects under mechanochemical conditions is doubly important. For that reason, as will be discussed in further chapters, we often use Solid-G to understand the involvement of steric influences in known compounds, and in theoretical compounds we are surprisingly unable to isolate. In general, for electropositive/oxophilic elements, we hypothesize that a compound with low steric saturation may not be isolable from solution routes because the metal center is accessible to coordinating solvents. Unfortunately, it may also continue to react under mechanochemical conditions, but with careful reaction screening may be isolated or intercepted. In many cases, this continued reactivity provides access to compounds with unexpected stoichiometry, which we have been investigating and is discussed in further chapters.

1.3 The chemistry of metal-allyl complexes

As the smallest delocalized anion, the allyl ($C_3H_5^-$) ligand has been studied frequently since the 1960s. A variety of metal-allyl compounds were made with transition metals by Wilke and Bogdanovic in the 1960s.[118–120] Work with the parent allyl showed that these compounds are often extremely unstable at room temperatures for 1st-row transition metals, and in some cases are pyrophoric or decompose explosively. Allyl complexes made with 2nd or 3rd row transition metals are much more stable, which has resulted in metal-allyl complexes being used as starting materials for or involved as intermediates in catalytic reactions.[121–123] While transition metals favor η^3-coordinated allyls because of d-orbital interactions in almost all cases[124], the structural allyl chemistry of main-group elements is much more varied. In fact, just for the parent allyl coordinated to main-group elements, there are more than 13 crystallographically characterized bonding motifs as of 2013.[125]

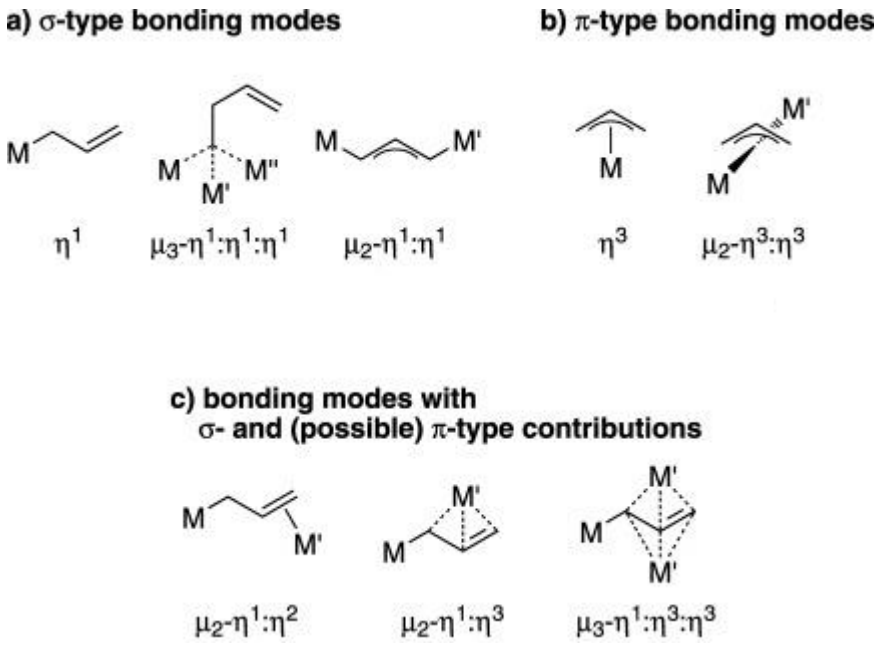

Figure 11. Structurally authenticated bonding modes of the parent allyl with main group elements ca. 2013 (Reprinted from *Angew. Chem. Int. Ed.*, **2013**, *52*: 5228-5246 with permission from Wiley)

Of particular relevance to this thesis is the continuum of bonding between η^1- or σ-bound and η^3-bound allyls. In some cases η^3-coordination is described as π-coordinated, but this is a less specific description, as η^2-coordination also involves the π-system. As is discussed in further detail in the following chapters, the factors that affect whether η^1- or η^3-coordination is favored is complicated and depends on a variety of factors depending on the element. As shown above, the bonding can be quite complicated. However even these figures are a gross simplification, with many examples not simply fitting neatly into η^1- or η^3. For example, the allyllithium pentamethyldiethylenetriamine (PMDTA) complex has an unsymmetrical bonding situation where the allyl is almost completely delocalized (C1-C2 and C2-C3 bonds similar length) but the C1-Li distance is much shorter than C2-Li.[126]

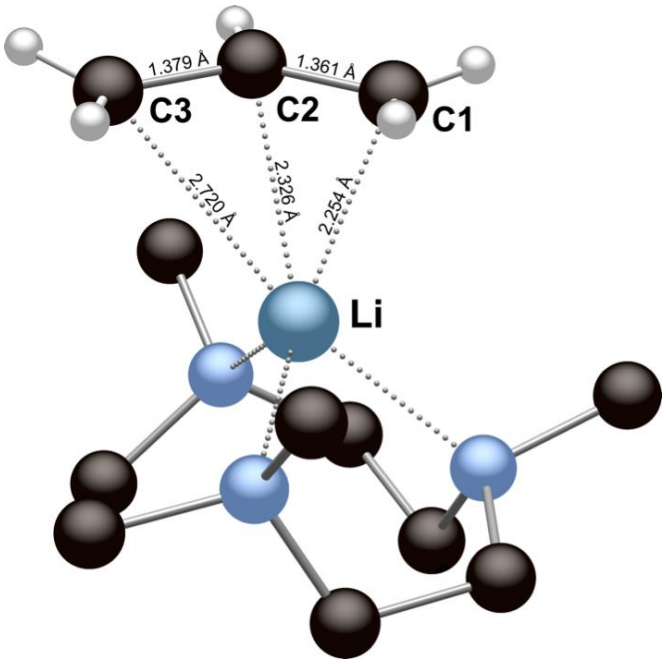

Figure 12. Crystal structure of (pmdta)Li(C_3H_5) showing unsymmetrical allyl coordination to Li. Hydrogens on PMDTA ligand are removed for clarity.

Some elements favor a specific bonding mode except under extreme situations. For instance, calcium, prefers η^3-coordinated allyls in almost all cases.[127] A notable exception is the 18-crown-6 supported allylcalcium monocation, whose structure also contains the tris-allyl zincate anion.[128] In general, main-group elements (and group 12) that can support covalent bonds to carbon will favor η^1- allyls, while elements with more ionic M-C bonding character favor η^3-allyls. As will be discussed, for group 2 elements, this is often confounded by changes in size and propensity for interaction with Lewis basic solvent.

There is a surprising lack of information about some basic metal-allyl systems. Though the homoleptic metal allyl complexes seem simple, many of their structures are unknown or disputed. For example, recent reinvestigation of the bis-allyl zinc system revealed new structural motifs.[129] This holds true for many of the alkaline earth elements. Though one would expect the homoleptic bis-allyl magnesium and calcium to be well studied during the early years of organometallic chemistry, the first crystallographically characterized calcium-allyl bond was reported by our group in 1999.[130] $M(C_3H_5)_2$ (M = Mg, Ca) are assumed to be insoluble extended coordination polymers. The patent literature reports synthesis of essentially uncharacterized [$Ca(C_3H_5)_2$] by transmetallation with mercury or tin allyls,[131,132] but very little was known about this species until work by the Okuda group in 2009.[127] They reported that [$Ca(C_3H_5)_2$] is in fact quite soluble, and obtained a crystal structure of the triglyme adduct. The literature on homoleptic calcium

allyls is essentially nonexistent except for this paper and our report of $Ca(SiMe_3C_3H_3)_2$•2THF. Given this dearth of knowledge, the Hanusa group has been focused on the fundamental organometallic chemistry of metal-allyl systems, specifically with main-group elements. We hope that a stronger understanding of bonding and structure will allow us to exploit these compounds as catalysts and polymerization initiators, and to design more useful systems. To do this, we employ the trimethylsilyl-substituted allyl anion 1,3-$(SiMe_3)_2C_3H_3$ $[A']^-$ as a ligand. This was initially developed to study allyllithium structures in solution, which is described as "chameleon-like".[133] The trimethylsilyl groups play a number of roles: increasing solubility of resulting compounds, providing steric shielding (and dispersion), and stabilizing the anion itself. The lithium allyl form is extremely soluble, which complicates purification. [LiA′] is transmetallated with KO^{t}Bu, yielding [KA′]. This reagent is insoluble in hexanes and when used for salt metathesis results in the much less soluble and recalcitrant KX. The overall synthetic scheme for [KA′] is shown below. The mono- and tri-substituted allyls are also known, but in our experience provide insufficient steric shielding or inhibit reactivity.[134] As mentioned with respect to the calcium allyl, the Hanusa group has used this ligand to great effect, synthesizing compounds whose analogs with the parent allyl are extremely stable or completely unknown.

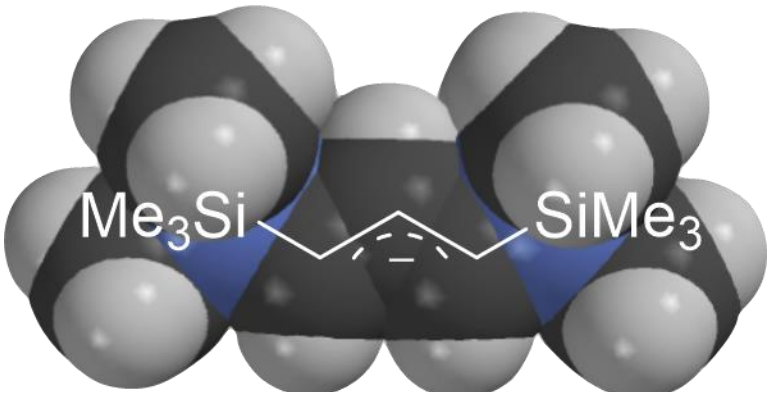

Figure 13. Space filling model of $[A']^-$, which is ~2.5x bulkier than the parent allyl

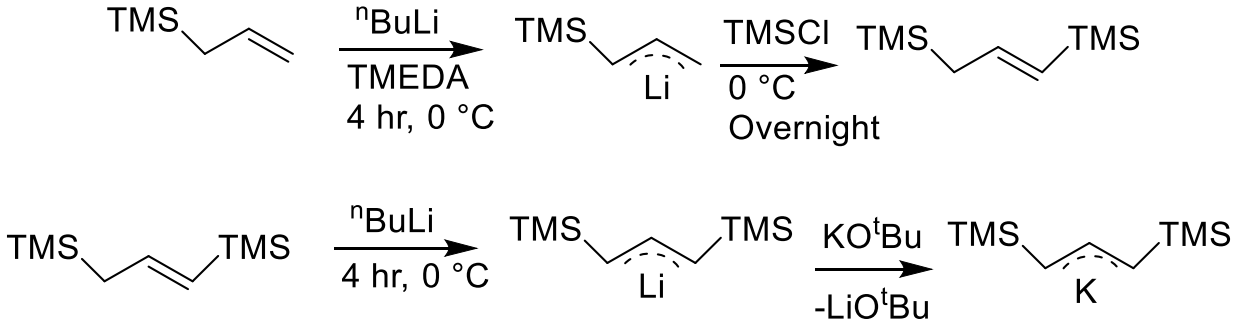

Figure 14. Synthetic scheme for the synthesis of [KA′]

A peculiarity of many electropositive organometallic complexes is the high degree of fluxionality. This is especially true for allyl complexes, and one of the reasons for Fraenkel's "chameleon-like" description. The NMR spectra at low-, room-, and high-temperature can vary significantly, and in some cases, none are particularly representative of the crystal structure, if any are known. This can complicate combined interpretation of solution and solid-state data. For example, initial mechanochemical studies on the Ca-A′ system yielded a crystal structure that had 2 unique allyl environments. ^{1}H NMR also showed 2 allyl environments, but further reaction optimization (shown in chapter 6) revealed that these belong to two unique complexes. In some cases, ligands are fluxional at all experimentally accessible temperatures (~ -80 °C in toluene-d_8), such the beryllium indenyl complex described in Chapter 7. This is one of the reasons the Hanusa group relies on computational chemistry to provide more data and insight into these complicated systems.

1.4 Conclusion

In this chapter, I have attempted to give a brief overview of three themes; mechanochemistry, computational chemistry, and metal allyls (though much is extendible to other forms of delocalized ligands). The following chapters are an account of my work grappling with these topics and attempting to use each of them to understand more about the others. One of the group's goals is to show that mechanochemistry is a surprisingly useful tool for making unique and sensitive compounds, despite at first glance appearing to be a harsh synthetic technique, having a relatively high barrier to entry due to the cost of equipment, and having little work dedicated to synthetic inorganic and organometallic chemistry.

1.5 References

(1) Ying, P.; Yu, J.; Su, W. Liquid-Assisted Grinding Mechanochemistry in the Synthesis of Pharmaceuticals. *Adv. Synth. Catal.* **2021**, *363*, 1246..

(2) Huskić, I.; Lennox, C. B.; Friščić, T. Accelerated Ageing Reactions: Towards Simpler, Solvent-Free, Low Energy Chemistry. *Green Chem.* **2020**, *22* (18), 5881–5901.

(3) Andersen, J.; Brunemann, J.; Mack, J. Exploring Stable, Sub-Ambient Temperatures in Mechanochemistry via a Diverse Set of Enantioselective Reactions. *React. Chem. Eng.* **2019**, *4* (7), 1229–1236.

(4) James, S. L.; Adams, C. J.; Bolm, C.; Braga, D.; Collier, P.; Friščić, T.; Grepioni, F.; Harris, K. D. M.; Hyett, G.; Jones, W.; Krebs, A.; Mack, J.; Maini, L.; Orpen, A. G.; Parkin, I. P.; Shearouse, W. C.; Steed, J. W.; Waddell, D. C. Mechanochemistry: Opportunities for New and Cleaner Synthesis. *Chem. Soc. Rev.* **2012**, *41* (1), 413–447.

(5) Ostwald, W.; Drucker, C.; Walden, P. *Handbuch Der Allgemeinen Chem.: JP Kuenen. Die Eigenschaften Der Gase*; Akademische Verlagsgesellschaft mb H., 1919; Vol. 3.

(6) Amrute, A. P.; De Bellis, J.; Felderhoff, M.; Schüth, F. Mechanochemical Synthesis of Catalytic Materials. *Chem.—Eur. J.* **2021**, *27*, 6819.

(7) Tetzlaff, D.; Pellumbi, K.; Baier, D. M.; Hoof, L.; Shastry Barkur, H.; Smialkowski, M.; Amin, H. M. A.; Grätz, S.; Siegmund, D.; Borchardt, L.; Apfel, U.-P. Sustainable and Rapid Preparation of Nanosized Fe/Ni-Pentlandite Particles by Mechanochemistry. *Chem. Sci.* **2020**, *11* (47), 12835–12842.

(8) Braga, D.; Maini, L.; Grepioni, F. Mechanochemical Preparation of Co-Crystals. *Chem. Soc. Rev.* **2013**, *42* (18), 7638–7648.

(9) Krusenbaum, A.; Grätz, S.; Bimmermann, S.; Hutsch, S.; Borchardt, L. The Mechanochemical Scholl Reaction as a Versatile Synthesis Tool for the Solvent-Free Generation of Microporous Polymers. *RSC Adv.* **2020**, *10* (43), 25509–25516.

(10) Chen, C.-H.; Gaillard, E.; Mentink-Vigier, F.; Chen, K.; Gan, Z.; Gaveau, P.; Rebière, B.; Berthelot, R.; Florian, P.; Bonhomme, C.; Smith, M. E.; Métro, T.-X.; Alonso, B.; Laurencin, D. Direct 17O Isotopic Labeling of Oxides Using Mechanochemistry. *Inorg. Chem.* **2020**, *59* (18), 13050–13066.

(11) Tan, D.; García, F. Main Group Mechanochemistry: From Curiosity to Established Protocols. *Chem. Soc. Rev.* **2019**, *48*, 2274-2292.

(12) Shi, Y. X.; Xu, K.; Clegg, J. K.; Ganguly, R.; Hirao, H.; Friščić, T.; García, F. The First Synthesis of the Sterically Encumbered Adamantoid Phosphazane $P_4(N^tBu)_6$: Enabled by Mechanochemistry. *Angew. Chem. Int. Ed.* **2016**, *55* (41), 12736–12740.

(13) Gečiauskaitė, A. A.; García, F. Main Group Mechanochemistry. *Beilstein J. Org. Chem.*. **2017**, pp 2068–2077.

(14) Beillard, A.; Quintin, F.; Gatignol, J.; Retailleau, P.; Renaud, J.-L.; Gaillard, S.; Métro, T.-X.; Lamaty, F.; Bantreil, X. Solving the Challenging Synthesis of Highly Cytotoxic Silver Complexes Bearing Sterically Hindered NHC Ligands with Mechanochemistry. *Dalton Trans.* **2020**, *49* (36), 12592–12598.

(15) Mukherjee, N.; Marczyk, A.; Szczepaniak, G.; Sytniczuk, A.; Kajetanowicz, A.; Grela, K. A Gentler Touch: Synthesis of Modern Ruthenium Olefin Metathesis Catalysts Sustained by Mechanical Force. *ChemCatChem* **2019**, *11*, 5362-5369.

(16) Fetrow, T. V; Bhowmick, R.; Achazi, A. J.; Blake, A. V; Eckstrom, F. D.; Vlaisavljevich, B.; Daly, S. R. Chelating Borohydrides for Lanthanides and Actinides: Structures, Mechanochemistry, and Case Studies with Phosphinodiboranates. *Inorg. Chem.* **2020**, *59* (1), 48–61.

(17) Beillard, A.; Bantreil, X.; Métro, T.-X.; Martinez, J.; Lamaty, F. A More Sustainable and Efficient Access to IMes·HCl and IPr·HCl by Ball-Milling. *Green Chem.* **2018**, *20* (5), 964–968.
(18) Eguaogie, O.; Vyle, J. S.; Conlon, P. F.; Gîlea, M. A.; Liang, Y. Mechanochemistry of Nucleosides, Nucleotides and Related Materials. *Beilstein J. Org. Chem.* **2018**, *14*, 955–970.
(19) Tan, D.; Loots, L.; Friščić, T. Towards Medicinal Mechanochemistry: Evolution of Milling from Pharmaceutical Solid Form Screening to the Synthesis of Active Pharmaceutical Ingredients (APIs). *Chem. Commun.* **2016**, *52* (50), 7760–7781.
(20) Do, J.-L.; Mottillo, C.; Tan, D.; Štrukil, V.; Friščić, T. Mechanochemical Ruthenium-Catalyzed Olefin Metathesis. *J. Am. Chem. Soc.* **2015**, *137* (7), 2476–2479.
(21) Achar, T. K.; Bose, A.; Mal, P. Mechanochemical Synthesis of Small Organic Molecules. *Beilstein J. Org. Chem.* **2017**, *13*, 1907–1931.
(22) Canale, V.; Frisi, V.; Bantreil, X.; Lamaty, F.; Zajdel, P. Sustainable Synthesis of a Potent and Selective 5-HT7 Receptor Antagonist Using a Mechanochemical Approach. *J. Org. Chem.* **2020**, *85* (16), 10958–10965.
(23) Yeboue, Y.; Gallard, B.; Le Moigne, N.; Jean, M.; Lamaty, F.; Martinez, J.; Métro, T.-X. Peptide Couplings by Reactive Extrusion: Solid-Tolerant and Free from Carcinogenic, Mutagenic and Reprotoxic Chemicals. *ACS Sustain. Chem. Eng.* **2018**, *6* (12), 16001–16004.
(24) Andersen, J. M.; Starbuck, H. F. Rate and Yield Enhancements in Nucleophilic Aromatic Substitution Reactions via Mechanochemistry. *J. Org. Chem.* **2021**. https://doi.org/10.1021/acs.joc.0c02996
(25) Vogt, C.; Graetz, S.; Lukin, S.; Halasz, I.; Etter, M.; Evans, J. D.; Borchardt, L. "Direct Mechanocatalysis" – Palladium as Milling Media and Catalyst in the Mechanochemical Suzuki Polymerization. *Angew. Chem. Int. Ed.* **2019**, *58*, 18942-18947.
(26) Kubota, K.; Ito, H. Mechanochemical Cross-Coupling Reactions. *Trends Chem.* **2020**, *2* (12), 1066–1081.
(27) Seo, T.; Ishiyama, T.; Kubota, K.; Ito, H. Solid-State Suzuki–Miyaura Cross-Coupling Reactions: Olefin-Accelerated C–C Coupling Using Mechanochemistry. *Chem. Sci.* **2019**, *10* (35), 8202–8210.
(28) Nicholson, W. I.; Seastram, A. C.; Iqbal, S. A.; Reed-Berendt, B. G.; Morrill, L. C.; Browne, D. L. N-Heterocyclic Carbene Acyl Anion Organocatalysis by Ball-Milling. *ChemSusChem* **2020**, *13* (1), 131–135.
(29) Porcheddu, A.; Colacino, E.; De Luca, L.; Delogu, F. Metal-Mediated and Metal-Catalyzed Reactions Under Mechanochemical Conditions. *ACS Catal.* **2020**, *10* (15), 8344–8394.
(30) Doerr, A. M.; Burroughs, J. M.; Gitter, S. R.; Yang, X.; Boydston, A. J.; Long, B. K. Advances in Polymerizations Modulated by External Stimuli. *ACS Catal.* **2020**, *10* (24), 14457–14515.
(31) Piermattei, A.; Karthikeyan, S.; Sijbesma, R. P. Activating Catalysts with Mechanical Force. *Nat. Chem.* **2009**, *1* (2), 133–137.
(32) Naumov, P.; Chizhik, S.; Panda, M. K.; Nath, N. K.; Boldyreva, E. Mechanically Responsive Molecular Crystals. *Chem. Rev.* **2015**, *115* (22), 12440–12490.
(33) Brown, C. L.; Bowser, B. H.; Meisner, J.; Kouznetsova, T. B.; Seritan, S.; Martinez, T. J.; Craig, S. L. Substituent Effects in Mechanochemical Allowed and Forbidden Cyclobutene Ring-Opening Reactions. *J. Am. Chem. Soc.* **2021**.
(34) Crawford, D. E.; James, S. L.; McNally, T. Use of Batch Mixing To Investigate the Continuous Solvent-Free Mechanical Synthesis of OLED Materials by Twin-Screw Extrusion (TSE). *ACS Sustain. Chem. Eng.* **2018**, *6* (1), 193–201.
(35) Takacs, L. The Historical Development of Mechanochemistry. *Chem. Soc. Rev.* **2013**, *42* (18), 7649–7659.

(36) Takacs, L. Two Important Periods in the History of Mechanochemistry. *J. Mater. Sci.* **2018**, *53* (19), 13324–13330.
(37) Takacs, L. M. Carey Lea, the Father of Mechanochemistry. *Bull. Hist. Chem* **2003**, *28* (1), 26–34.
(38) Takacs, L. The Mechanochemical Reduction of AgCl with Metals. *J. Therm. Anal. Calorim.* **2007**, *90* (1), 81–84.
(39) Caley, E. R.; Richards, J. F. C. *Theophrastus on Stones: Introduction, Greek Text, English Translation, and Commentary*; The Ohio State University Press, 1956.
(40) Faraday, M. On the Decomposition of Chloride of Silver, by Hydrogen, and by $ZnCl_2$. *Q. J. Sci., Lit., Arts*. **1820**, 8, 374-375.
(41) Parker, L. H. No Title. *J. Chem. Soc. Abstr.* 1914, p 1504.
(42) Lea, M. C. ART. LV.--On Endothermic Decompositions Obtained by Pressure. Second Part. Transformations of Energy by Shearing Stress;: (I) (II). *Am. J. Sci.* **1893**, *46* (276), 413.
(43) Lea, M. C. ART. LXVII.--Disruption of the Silver Haloid Molecule by Mechanical Force. *Am. J. Sci.* **1892**, *43* (258), 527.
(44) Rightmire, N. R.; Hanusa, T. P.; Rheingold, A. L. Mechanochemical Synthesis of [1,3-$(SiMe_3)_2C_3H_3]_3$(Al,Sc), a Base-Free Tris(Allyl)Aluminum Complex and Its Scandium Analogue. *Organometallics* **2014**, *33* (21), 5952–5955.
(45) Kulla, H.; Fischer, F.; Benemann, S.; Rademann, K.; Emmerling, F. The Effect of the Ball to Reactant Ratio on Mechanochemical Reaction Times Studied by in Situ PXRD. *CrystEngComm* **2017**, *19* (28), 3902–3907.
(46) Belenguer, A. M.; Friščić, T.; Day, G. M.; Sanders, J. K. M. Solid-State Dynamic Combinatorial Chemistry: Reversibility and Thermodynamic Product Selection in Covalent Mechanosynthesis. *Chem. Sci.* **2011**, *2* (4), 696–700.
(47) Rak, M. J.; Saade, N. K.; Friscic, T.; Moores, A. Mechanosynthesis of Ultra-Small Monodisperse Amine-Stabilized Gold Nanoparticles with Controllable Size. *Green Chem.* **2014**, *16* (1), 86–89.
(48) Kulla, H.; Haferkamp, S.; Akhmetova, I.; Röllig, M.; Maierhofer, C.; Rademann, K.; Emmerling, F. In Situ Investigations of Mechanochemical One-Pot Syntheses. *Angew. Chem. Int. Ed.* **2018**, *57* (20), 5930–5933.
(49) Užarević, K.; Halasz, I.; Friščić, T. Real-Time and In Situ Monitoring of Mechanochemical Reactions: A New Playground for All Chemists. *J. Phys. Chem. Lett.* **2015**, *6* (20), 4129–4140.
(50) Ardila-Fierro, K. J.; Lukin, S.; Etter, M.; Užarević, K.; Halasz, I.; Bolm, C.; Hernández, J. G. Direct Visualization of a Mechanochemically Induced Molecular Rearrangement. *Angew. Chem. Int. Ed.* **2020**, *59*, 13458.
(51) Hutchings, B. P.; Crawford, D. E.; Gao, L.; Hu, P.; James, S. L. Feedback Kinetics in Mechanochemistry: The Importance of Cohesive States. *Angew. Chem. Int. Ed.* **2017**, *56* (48), 15252–15256.
(52) Urakaev, F. K.; Boldyrev, V. V. Mechanism and Kinetics of Mechanochemical Processes in Comminuting Devices: 2. Applications of the Theory. Experiment. *Powder Technol.* **2000**, *107* (3), 197–206.
(53) Urakaev, F. K.; Boldyrev, V. V. Mechanism and Kinetics of Mechanochemical Processes in Comminuting Devices: 1. Theory. *Powder Technol.* **2000**, *107* (1), 93–107.
(54) Užarević, K.; Štrukil, V.; Mottillo, C.; Julien, P. A.; Puškarić, A.; Friščić, T.; Halasz, I. Exploring the Effect of Temperature on a Mechanochemical Reaction by in Situ Synchrotron Powder X-Ray Diffraction. *Cryst. Growth Des.* **2016**, *16* (4), 2342–2347.
(55) Užarević, K.; Ferdelji, N.; Mrla, T.; Julien, P. A.; Halasz, B.; Friščić, T.; Halasz, I. Enthalpy vs. Friction: Heat Flow Modelling of Unexpected Temperature Profiles in Mechanochemistry of

Metal–Organic Frameworks. *Chem. Sci.* **2018**, *9* (9), 2525–2532.
(56) Kulla, H.; Wilke, M.; Fischer, F.; Röllig, M.; Maierhofer, C.; Emmerling, F. Warming up for Mechanosynthesis – Temperature Development in Ball Mills during Synthesis. *Chem. Commun.* **2017**, *53* (10), 1664–1667.
(57) Ferguson, M.; Moyano, M. S.; Tribello, G. A.; Crawford, D. E.; Bringa, E. M.; James, S. L.; Kohanoff, J.; Del Pópolo, M. G. Insights into Mechanochemical Reactions at the Molecular Level: Simulated Indentations of Aspirin and Meloxicam Crystals. *Chem. Sci.* **2019**, *10* (10), 2924–2929.
(58) Belenguer, A. M.; Lampronti, G. I.; Cruz-Cabeza, A. J.; Hunter, C. A.; Sanders, J. K. M. Solvation and Surface Effects on Polymorph Stabilities at the Nanoscale. *Chem. Sci.* **2016**, *7* (11), 6617–6627.
(59) Andersen, J. M.; Mack, J. Decoupling the Arrhenius Equation via Mechanochemistry. *Chem. Sci.* **2017**, *8* (8), 5447–5453.
(60) Hernández, J. G.; Butler, I. S.; Friščić, T. Multi-Step and Multi-Component Organometallic Synthesis in One Pot Using Orthogonal Mechanochemical Reactions. *Chem. Sci.* **2014**, *5* (9), 3576–3582.
(61) Kubota, K.; Seo, T.; Koide, K.; Hasegawa, Y.; Ito, H. Olefin-Accelerated Solid-State C–N Cross-Coupling Reactions Using Mechanochemistry. *Nat. Commun.* **2019**, *10* (1), 111.
(62) Seo, T.; Kubota, K.; Ito, H. Selective Mechanochemical Monoarylation of Unbiased Dibromoarenes by in Situ Crystallization. *J. Am. Chem. Soc.* **2020**, *142* (22), 9884–9889.
(63) Pickhardt, W.; Grätz, S.; Borchardt, L. Direct Mechanocatalysis: Using Milling Balls as Catalysts. *Chem.—Eur. J.* **2020**, *26* (57), 12903–12911.
(64) Howard, J. L.; Brand, M. C.; Browne, D. L. Switching Chemoselectivity: Using Mechanochemistry to Alter Reaction Kinetics. *Angew. Chem. Int. Ed.* **2018**, *57* (49), 16104–16108.
(65) Howard, J. L.; Cao, Q.; Browne, D. L. Mechanochemistry as an Emerging Tool for Molecular Synthesis: What Can It Offer? *Chem. Sci.* **2018**, *9* (12), 3080–3094.
(66) Cao, Q.; Nicholson, W. I.; Jones, A. C.; Browne, D. L. Robust Buchwald–Hartwig Amination Enabled by Ball-Milling. *Org. Biomol. Chem.* **2018**.
(67) Yin, J.; Stark, R. T.; Fallis, I. A.; Browne, D. L. A Mechanochemical Zinc-Mediated Barbier-Type Allylation Reaction under Ball-Milling Conditions. *J. Org. Chem.* **2020**, *85* (4), 2347–2354.
(68) Zille, M.; Stolle, A.; Wild, A.; Schubert, U. S. $ZnBr_2$-Mediated Synthesis of Indoles in a Ball Mill by Intramolecular Hydroamination of 2-Alkynylanilines. *RSC Adv.* **2014**, *4* (25), 13126–13133.
(69) Wang, J.; Ganguly, R.; Yongxin, L.; Díaz, J.; Soo, H. Sen; García, F. A Multi-Step Solvent-Free Mechanochemical Route to Indium(Iii) Complexes. *Dalton Trans.* **2016**, *45* (19), 7941–7946.
(70) Wang, J.; Soo, H. Sen; Garcia, F. Synthesis, Properties, and Catalysis of p-Block Complexes Supported by Bis(Arylimino)Acenaphthene Ligands. *Commun. Chem.* **2020**, *3* (1), 113.
(71) Singh, V. K.; Chamberlain-Clay, A.; Ong, H. C.; León, F.; Hum, G.; Par, M. Y.; Daley-Dee, P.; García, F. Multigram Mechanochemical Synthesis of a Salophen Complex: A Comparative Analysis. *ACS Sustain. Chem. Eng.* **2021**, *9* (3), 1152–1160.
(72) Shaw, T. E.; Mathivathanan, L.; Jurca, T. One-Pot, One-Step Precatalysts through Mechanochemistry. *Organometallics* **2019**, *38* (21), 4066–4070.
(73) Hermann, G. N.; Bolm, C. Mechanochemical Rhodium(III)-Catalyzed C–H Bond Amidation of Arenes with Dioxazolones under Solventless Conditions in a Ball Mill. *ACS Catal.* **2017**, *7* (7), 4592–4596.
(74) Staleva, P.; Hernández, J. G.; Bolm, C. Mechanochemical Copper-Catalyzed Asymmetric

Michael-Type Friedel–Crafts Alkylation of Indoles with Arylidene Malonates. *Chem.—Eur. J.* **2019**, *25* (39), 9202–9205.
(75) Cheng, H.; Hernández, J. G.; Bolm, C. Mechanochemical Ruthenium-Catalyzed Hydroarylations of Alkynes under Ball-Milling Conditions. *Org. Lett.* **2017**, *19* (23), 6284–6287.
(76) Hermann, G. N.; Jung, C. L.; Bolm, C. Mechanochemical Indole Synthesis by Rhodium-Catalysed Oxidative Coupling of Acetanilides and Alkynes under Solventless Conditions in a Ball Mill. *Green Chem.* **2017**, *19* (11), 2520–2523.
(77) Quintin, F.; Pinaud, J.; Lamaty, F.; Bantreil, X. Mechanosynthesis of Noels-Type NHC–Ruthenium Complexes and Applications in Ring-Opening Metathesis Polymerization. *Organometallics* **2020**, *39* (5), 636–639.
(78) Hernández, J. G.; Macdonald, N. A. J.; Mottillo, C.; Butler, I. S.; Friščić, T. A Mechanochemical Strategy for Oxidative Addition: Remarkable Yields and Stereoselectivity in the Halogenation of Organometallic Re(i) Complexes. *Green Chem.* **2014**, *16* (3), 1087–1092.
(79) Garci, A.; Castor, K. J.; Fakhoury, J.; Do, J.-L.; Di Trani, J.; Chidchob, P.; Stein, R. S.; Mittermaier, A. K.; Friščić, T.; Sleiman, H. Efficient and Rapid Mechanochemical Assembly of Platinum(II) Squares for Guanine Quadruplex Targeting. *J. Am. Chem. Soc.* **2017**, *139* (46), 16913–16922.
(80) Juribašić, M.; Užarević, K.; Gracin, D.; Ćurić, M. Mechanochemical C–H Bond Activation: Rapid and Regioselective Double Cyclopalladation Monitored by in Situ Raman Spectroscopy. *Chem. Commun.* **2014**, *50* (71), 10287–10290.
(81) Cook, T. L.; Walker, J. A.; Mack, J. Scratching the Catalytic Surface of Mechanochemistry: A Multi-Component CuAAC Reaction Using a Copper Reaction Vial. *Green Chem.* **2013**, *15* (3), 617–619.
(82) Fulmer, D. A.; Shearouse, W. C.; Medonza, S. T.; Mack, J. Solvent-Free Sonogashira Coupling Reaction Viahigh Speed Ball Milling. *Green Chem.* **2009**, *11* (11), 1821–1825.
(83) Woen, D. H.; White, J. R. K.; Ziller, J. W.; Evans, W. J. Mechanochemical C–H Bond Activation: Synthesis of the Tuckover Hydrides, $(C_5Me_5)_2Ln(\mu\text{-}H)(\mu\text{-}H1{:}H5\text{-}CH_2C_5Me_4)Ln(C_5Me_5)$ from Solvent-Free Reactions of $(C_5Me_5)_2Ln(\mu\text{-}Ph)_2BPh_2$ with KC_5Me_5. *J. Organomet. Chem.* **2019**, *899*, 120885.
(84) Kubota, K.; Pang, Y.; Miura, A.; Ito, H. Redox Reactions of Small Organic Molecules Using Ball Milling and Piezoelectric Materials. *Science (80-.).* **2019**, *366* (6472), 1500 LP – 1504.
(85) Yu, J.; Zhang, L.; Yan, G. Metal-Free, Visible Light-Induced Borylation of Aryldiazonium Salts: A Simple and Green Synthetic Route to Arylboronates. *Adv. Synth. Catal.* **2012**, *354* (14-15), 2625–2628.
(86) Hari, D. P.; Schroll, P.; König, B. Metal-Free, Visible-Light-Mediated Direct C–H Arylation of Heteroarenes with Aryl Diazonium Salts. *J. Am. Chem. Soc.* **2012**, *134* (6), 2958–2961.
(87) Leon, F.; Garcia Molecular Sciences and Chemical Engineering, F. B. T.-R. M. in C. Metal Complexes in Mechanochemistry; Elsevier, 2021.
(88) Beillard, A.; Bantreil, X.; Métro, T.-X.; Martinez, J.; Lamaty, F. Alternative Technologies That Facilitate Access to Discrete Metal Complexes. *Chem. Rev.* **2019**, *119* (12), 7529–7609.
(89) Rightmire, N. R.; Hanusa, T. P. Advances in Organometallic Synthesis with Mechanochemical Methods. *Dalton Trans.* **2016**, *45* (6), 2352–2362.
(90) Braga, D.; Grepioni, F.; Maini, L.; Brescello, R.; Cotarca, L. Simple and Quantitative Mechanochemical Preparation of the First Zinc and Copper Complexes of the Neuroleptic Drug Gabapentin. *CrystEngComm* **2008**, *10* (5), 469–471.
(91) Wang, J.; Ganguly, R.; Yongxin, L.; Díaz, J.; Soo, H. Sen; García, F. Synthesis and the Optical and Electrochemical Properties of Indium(III) Bis(Arylimino)Acenaphthene Complexes.

Inorg. Chem. **2017**, *56* (14), 7811–7820.
(92) Peters, D. W.; Blair, R. G. Mechanochemical Synthesis of an Organometallic Compound: A High Volume Manufacturing Method. *Faraday Discuss.* **2014**, *170* (0), 83–91.
(93) Li, Z.; Zhang, J.; Wang, S.; Jiang, L.; Latroche, M.; Du, J.; Cuevas, F. Mechanochemistry of Lithium Nitride under Hydrogen Gas. *Phys. Chem. Chem. Phys.* **2015**, *17* (34), 21927–21934.
(94) Ravnsbæk, D. B.; Sørensen, L. H.; Filinchuk, Y.; Besenbacher, F.; Jensen, T. R. Screening of Metal Borohydrides by Mechanochemistry and Diffraction. *Angew. Chem. Int. Ed.* **2012**, *51* (15), 3582–3586.
(95) Soiron, S.; Rougier, A.; Aymard, L.; Tarascon, J.-M. Mechanochemical Synthesis of Li–Mn–O Spinels: Positive Electrode for Lithium Batteries. *J. Power Sources* **2001**, *97–98*, 402–405.
(96) Mack, J.; Fulmer, D.; Stofel, S.; Santos, N. The First Solvent-Free Method for the Reduction of Esters. *Green Chem.* **2007**, *9* (10), 1041–1043.
(97) Grimme, S.; Schreiner, P. R. Steric Crowding Can Stabilize a Labile Molecule: Solving the Hexaphenylethane Riddle. *Angew. Chem. Int. Ed.* **2011**, *50* (52), 12639–12642.
(98) Li, H.; Hu, Y.; Wan, D.; Zhang, Z.; Fan, Q.; King, R. B.; Schaefer, H. F. Dispersion Effects in Stabilizing Organometallic Compounds: Tetra-1-Norbornyl Derivatives of the First-Row Transition Metals as Exceptional Examples. *J. Phys. Chem. A* **2019**, *123* (44), 9514–9519.
(99) Grimme, S. Density Functional Theory with London Dispersion Corrections. *Wiley Interdiscip. Rev. Comput. Mol. Sci.* **2011**, *1* (2), 211–228.
(100) Jung, J.; Löffler, S. T.; Langmann, J.; Heinemann, F. W.; Bill, E.; Bistoni, G.; Scherer, W.; Atanasov, M.; Meyer, K.; Neese, F. Dispersion Forces Drive the Formation of Uranium–Alkane Adducts. *J. Am. Chem. Soc.* **2020**, *142* (4), 1864–1870
(101) Liptrot, D. J.; Guo, J.-D.; Nagase, S.; Power, P. P. Dispersion Forces, Disproportionation, and Stable High-Valent Late Transition Metal Alkyls. *Angew. Chem.* **2016**, *128* (47), 14986–14989.
(102) Rekken, B. D.; Brown, T. M.; Fettinger, J. C.; Lips, F.; Tuononen, H. M.; Herber, R. H.; Power, P. P. Dispersion Forces and Counterintuitive Steric Effects in Main Group Molecules: Heavier Group 14 (Si–Pb) Dichalcogenolate Carbene Analogues with Sub-90° Interligand Bond Angles. *J. Am. Chem. Soc.* **2013**, *135* (27), 10134–10148.
(103) London, F. Zur Theorie Und Systematik Der Molekularkräfte. *Z. Phys.* **1930**, *63* (3), 245–279.
(104) Tschumper, G. S. Reliable Electronic Structure Computations for Weak Noncovalent Interactions in Clusters. *Reviews in Computational Chemistry*. October 20, 2008, pp 39–90.
(105) Sherrill, C. D. Computations of Noncovalent π Interactions. *Rev. Comput. Chem*. October 20, 2008, pp 1–38.
(106) Hujo, W.; Grimme, S. Performance of Non-Local and Atom-Pairwise Dispersion Corrections to DFT for Structural Parameters of Molecules with Noncovalent Interactions. *J. Chem. Theory Comput.* **2013**, *9* (1), 308–315.
(107) Evans, W. J.; Hughes, L. A.; Hanusa, T. P. Synthesis and Crystallographic Characterization of an Unsolvated, Monomeric Samarium Bis(Pentamethylcyclopentadienyl) Organolanthanide Complex, $(C_5Me_5)_2Sm$. *J. Am. Chem. Soc.* **1984**, *106* (15), 4270–4272.
(108) Ghotra, J. S.; Hursthouse, M. B.; Welch, A. J. Three-Co-Ordinate Scandium(III) and Europium(III); Crystal and Molecular Structures of Their Trishexamethyldisilylamides. *J. Chem. Soc. Chem. Commun.* **1973**, No. 18, 669–670.
(109) Novoa, J. J.; Whangbo, M.; Williams, J. M. Interactions Energies Associated with Short Intermolecular Contacts of C–H Bonds. II. Ab Initio Computational Study of the C–H···H–C Interactions in Methane Dimer. *J. Chem. Phys.* **1991**, *94* (7), 4835–4841.
(110) McBride, J. M. The Hexaphenylethane Riddle. *Tetrahedron* **1974**, *30* (14), 2009–2022.
(111) Gomberg, M. Triphenylmethyl, Ein Fall von Dreiwerthigem Kohlenstoff. *Ber. Dtsch. Chem. Gesell.* **1900**, *33* (3), 3150–3163.

(112) Lankamp, H.; Nauta, W. T.; MacLean, C. A New Interpretation of the Monomer-Dimer Equilibrium of Triphenylmethyl- and Alkylsubstituted-Diphenyl Methyl-Radicals in Solution. *Tetrahedron Lett.* **1968**, *9* (2), 249–254.
(113) Selwood, P. W.; Dobres, R. M. The Diamagnetic Correction for Free Radicals. *J. Am. Chem. Soc.* **1950**, *72* (9), 3860–3863.
(114) Song, L.; Schoening, J.; Wölper, C.; Schulz, S.; Schreiner, P. R. Role of London Dispersion Interactions in Ga-Substituted Dipnictenes. *Organometallics* **2019**.
(115) Bursch, M.; Caldeweyher, E.; Hansen, A.; Neugebauer, H.; Ehlert, S.; Grimme, S. Understanding and Quantifying London Dispersion Effects in Organometallic Complexes. *Acc. Chem. Res.* **2019**, *52* (1), 258–266.
(116) Bower, B. K.; Tennent, H. G. Transition Metal Bicyclo[2.2.1]Hept-1-Yls. *J. Am. Chem. Soc.* **1972**, *94* (7), 2512–2514.
(117) Guzei, I. A.; Wendt, M. An Improved Method for the Computation of Ligand Steric Effects Based on Solid Angles. *Dalton Trans.* **2006**, No. 33, 3991–3999.
(118) Wilke, G.; Bogdanovic, B. Bis(π-Allyl)Nickel. *Angew. Chem.* **1961**, *73*, 756.
(119) Wilke, G.; Bogdanović, B.; Hardt, P.; Heimbach, P.; Keim, W.; Kröner, M.; Oberkirch, W.; Tanaka, K.; Steinrücke, E.; Walter, D.; Zimmermann, H. Allyl-Transition Metal Systems. *Angew. Chem. Int. Ed. English* **1966**, *5* (2), 151–164.
(120) Wilke, G.; Bogdanovič, B.; Borner, P.; Breil, H.; Hardt, P.; Heimbach, P.; Herrmann, G.; Kaminsky, H.-J.; Keim, W.; Kröner, M.; Müller, H.; Müller, E. W.; Oberkirch, W.; Schneider, J.; Stedefeder, J.; Tanaka, K.; Weyer, K. Cyclooligomerization of Butadiene and Transition Metal π-Complexes. *Angew. Chem. Int. Ed. English* **1963**, *2* (3), 105–115.
(121) Tsuji, J. 25 Years in the Organic Chemistry of Palladium. *J. Organomet. Chem.* **1986**, *300* (1), 281–305.
(122) Trost, B. M. Transition Metals and Olefins. A Promising Land: A Personal Account. *J. Organomet. Chem.* **1986**, *300* (1), 263–280.
(123) John, K. D.; Salazar, K. V; Scott, B. L.; Baker, R. T.; Sattelberger, A. P. Comparison of the Reactivity of $M(Allyl)_3$ (M = Rh, Ir) with Donor Ligands. *Organometallics* **2001**, *20* (2), 296–304.
(124) Erker, G.; Berg, K.; Angermund, K.; Krueger, C. $CpZr(Allyl)_3$: The Molecular Structure of a .Pi.- and .Sigma.-Dynamic Allyl Transition Metal Complex. *Organometallics* **1987**, *6* (12), 2620–2621.
(125) Lichtenberg, C.; Okuda, J. Structurally Defined Allyl Compounds of Main Group Metals: Coordination and Reactivity. *Angew. Chem. Int. Ed.* **2013**, *52* (20), 5228–5246.
(126) Schümann, U.; Weiss, E.; Dietrich, H.; Mahdi, W. Über Metallalkyl- Und Aryl-Verbindungen: XXXV. Zur Struktur von Allyllithium. Darstellung Und Kristallstruktur Einer Monomeren Allyllithium-Verbindung, Allyl(Pentamethyldiethylentriamin)Lithium, $LiC_3H_5(Me_2NC_2H_4N(Me)C_2H_4NMe_2)$. *J. Organomet. Chem.* **1987**, *322* (3), 299–307.
(127) Jochmann, P.; Dols, T. S.; Spaniol, T. P.; Perrin, L.; Maron, L.; Okuda, J. Bis(Allyl)Calcium. *Angew. Chem. Int. Ed.* **2009**, *48* (31), 5715–5719.
(128) Lichtenberg, C.; Jochmann, P.; Spaniol, T. P.; Okuda, J. The Allylcalcium Monocation: A Bridging Allyl Ligand with a Non-Bent Coordination Geometry. *Angew. Chem. Int. Ed.* **2011**, *50* (25), 5753–5756.
(129) Lichtenberg, C.; Engel, J.; Spaniol, T. P.; Englert, U.; Raabe, G.; Okuda, J. Bis(Allyl)Zinc Revisited: Sigma versus Pi Bonding of Allyl Coordination. *J. Am. Chem. Soc.* **2012**, *134* (23), 9805–9811.
(130) Harvey, M. J.; Hanusa, T. P.; Young Victor G., J. Synthesis and Crystal Structure of the Bis(Allyl)Calcium Complex $[Ca\{C_3(SiMe_3)_2H_3\}_2\cdot(THF)_2]$. *Angew. Chem. Int. Ed.* **1999**, *38* (1-2),

217–219.
(131) West, P.; Woodville, M. C. US P. 3766281, 1972. *Chem. Abs* **1973**, *79*, 137274.
(132) West, P, Woodville, M. US P. US3766281A, 1972. US3766281A, 1972.
(133) Fraenkel, G.; Chow, A.; Winchester, W. R. Dynamics of Solvated Li^+ within Exo,Exo- [1 ,3 - Bis(Trimethylsilyl)Ally]Lithium *N*,*N*,*N*',*N*'-Tetramethylethylenediamine Complex. *J. Am. Chem. Soc.* **1990**, *112*, 1382–1386.
(134) Smith, J. D.; Hanusa, T. P.; Young, V. G. Steric Stabilization of Homoleptic Bis(π-Allyl) Complexes of Chromium(II) and Iron(II). *J. Am. Chem. Soc.* **2001**, *123* (26), 6455–6456.

Chapter 2

Dispersion and Distortion in Heavy Group 2 and Lanthanide Decamethylmetallocenes: the $(C_5Me_5)_2$(Sr,Sm) Connection

Reprinted with permission from Ross F. Koby and Timothy P. Hanusa. *J. Organomet. Chem.* **2018**, *857*.

2.1 Introduction

The highly electropositive lanthanide (Ln) metals and the related heavy group 2 (Ae) elements calcium, strontium, and barium are characterized by metal–ligand (Ln–L or Ae–L) interactions that are strongly polar. Lacking metal valence electrons (or in the case of the lanthanides, possessing "core-like" 4f valence electrons) that could influence the orientation of ligands, a simple electrostatic analysis of the bonding in LnL_2 or AeL_2 compounds predicts that their geometries should be linear, and that LnL_3 or $[AeL_3]^-$ species should be trigonal planar, i.e., that the ligands should be as far from each other as is possible.[1] Nevertheless, it has long been known, for example, that heavy Ae difluorides (Ae = Ca–Ba) are bent in the gas phase,[2] that the unsolvated 2-coordinate dialkyl compound $Ca[C(SiMe_3)_3]_2$ is nonlinear,[3,4] and that, with the exception of species with extremely bulky rings,[5–9] almost all Cp'_2Ae complexes[10,11] (and the comparable organolanthanide metallocenes Cp'_2Sm, Cp'_2Eu, and Cp'_2Yb)[12,13] possess non-parallel cyclopentadienyl rings (Figure 15, for the case of $Cp' = C_5Me_5$).

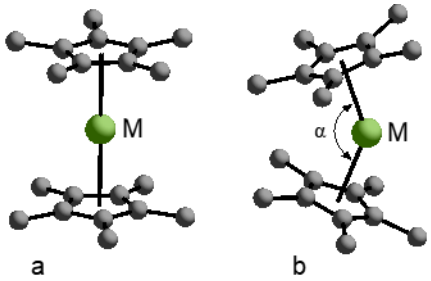

Figure 15. Geometries of bis(pentamethylcyclopentadienyl)metal complexes: (a) parallel rings; (b) nonparallel rings (bent metallocene); α is the ring centroid–metal–ring centroid angle.

Reconciliation of an electrostatically-based bonding scheme for AeL_2 or LnL_2 compounds with their nonlinear structures has proven to be difficult, especially as the molecules are geometrically "floppy" (in some cases, "quasilinear"),[14] with the energy required to bend the bonds from linearity or planarity to the observed values being small (generally $\lesssim$2 kcal mol^{-1}); this can challenge computational accuracy with heavy metal compounds.[2] It is not surprising, therefore, that a range of explanations (not necessarily mutually exclusive)[15] have been proposed for the phenomena, including: 1) reverse (core) polarization of the metal cation by the ligands; i.e., perturbation of the core electrons by

the ligands that induces a dipole moment, resulting in a non-uniform distribution of electrons to counteract it;[1,16] 2) for the group 2 elements, participation of (n – 1)d orbitals of the cation; 3) pseudo-Jahn Teller effect-induced distortions;[17] and 4) in appropriate complexes, attractive van der Waals (dispersion) interactions between the ligands.[18] The latter explanation has been proposed as an explanation for the bending in the decamethylmetallocenes of Ca–Ba and Sm, Eu, and Yb, and has been supported with the use of molecular mechanics calculations that reproduce the bending angles (ring centroid–metal–ring centroid) angles observed in the gas-phase structures.[19,20] Intriguingly, this explanation was considered but then rejected for the bending in $(C_5Me_5)_2Yb$ and $(C_5Me_5)_2No$.[21] The reason was that the dispersion force explanation implies that the existence of the metal is irrelevant to the bent geometries. In a density functional theory (DFT) study, two $[C_5Me_5]^-$ rings sandwiching a dummy atom were found to prefer a linear (parallel ring) orientation, contrary to the result expected from the operation of interligand van der Waals attractions.[21]

The potential role of dispersion interactions in the bending of Group 2 and lanthanide metallocenes has been explored more recently for the particular cases of $(C_5Me_5)_2Sr$ and $(C_5Me_5)_2Sm$,[22] especially as computational disentanglement of the explanations for bending has become feasible with the development of density functionals with additive empirical terms that capture the effects of dispersion interactions.[23] Such functionals allow dispersion corrections to be turned "on" or "off", and thus provide a means to distinguish between various bending forces in the molecules.

We have had a long-standing interest in compounds of the group 2 elements and the lanthanides, and in particular with issues of bonding and geometry for which unique explanations are not always evident. In some cases, this may take the form of structural resemblances between compounds that have no obvious reason to be similar, e.g., the comparable bending angles in stannocenes (Cp'_2Sn) and calcocenes (Cp'_2Ca), even though the former have a metal-centered lone pair of electrons that is usually cited as being responsible for the bending, and the latter do not.[24] In other cases, interligand steric effects from bulky ligands can force distortions on molecular geometries, thereby obscuring other metal-ligand interactions. Thus the structural anomalies found in various $M(E(SiMe_3)_2)_3$ complexes (M = f-element; E = N, CH) can be reproduced in calculations using orbital-free molecular mechanics methods, even though agostic M···(CH) interactions are also present that could produce similar effects.[3]

We wondered whether a related situation existed with the group 2 metallocenes, i.e., whether the fact that molecular mechanics calculations or the use of dispersion-corrected functionals reproduced the bending in the complexes might have masked other influences on their bonding. We therefore reexamined the computed geometry of $(C_5Me_5)_2Sr$, and compared it to that of $(C_5Me_5)_2Sm$. As Nief, et al., has noted,[22] these two metallocenes provide a convenient pair for evaluation, as the ionic radii of Sr^{2+} and Sm^{2+} are nearly identical (1.18 Å and 1.17 Å, respectively).[25] even though the electronic structures of the ions are markedly different ([Kr] and [Xe]$4f^6$, respectively).

2.2 Methods

2.2.1 Basis set requirements'

The electronic structures of the group 2 elements and their common ions ([NG]ns^2 and $[NG]^{2+}$, respectively) create distinctive challenges for their computational chemistry.[26] In particular, there is poor spatial separation between the valence *n*s and subvalent ("semi-core", (*n*-1)s,p) orbitals in these metals.[15] Consequently, polarization of either the valence or subvalent orbitals will influence the other, and semi-core electrons must be explicitly described in the metal basis sets used for calculations to yield calculations with meaningful results (if a pseudopotential (ECP) is used to replace some of the inner electrons, it must be "small core").[27] Another consequence is that in the heavier group 2 metals, particular care must be used in construction of the (*n*-1)d orbitals,[28] as they are formally unoccupied but have been considered "virtual states of the core".[29]

In the design of basis sets for Sr, in particular, several features must be considered. One is relativistic effects, potentially a concern in a 4th row metal such as strontium. Sadlej has argued that although relativistic effects are important in accurate polarizability calculations with the neutral Sr atom, and to a lesser extent, with the Sr^+ cation, they become "negligible" compared to electron correlation effects in the Sr^{2+} cation.[30] The small effect of relativistic corrections for calculations on molecular strontium species has been noted as well.[31] Nevertheless, relativistically corrected basis sets, either all-electron or containing ECPs that replace some of the core electrons, are available that can account for major scalar effects.

In view of the overlap between semi-core, valence, and (n-1)d orbitals of the group 2 metals, highly flexible valence functions must be present in the basis sets for accurate results with strontium compounds.[14] In studies of the quasilinear molecule $SrCl_2$, for example, it was shown that the use of the standard small-core Stuttgart/Dresden SDD basis set for Sr[32], which is constructed around a pseudopotential and is accompanied by a valence basis set with a 3,2 contraction of the "d" space ((6s,6p,5d) → [4s,4p,2d]), led to a linear molecule at the RHF level of theory.[28] Simply uncontracting the d shell allowed the molecule to bend (167.3°), although higher levels of theory and further elaboration of the valence basis set, including the addition of f functions, was necessary to model the experimentally determined bent structure adequately.[14]

Basis sets for Sr with more flexible valence spaces than the standard one originally developed for the SDD ECP are now available, and were used in the present study. Among them are the "dhf-" segmented contracted basis sets of Weigend and Baldes.[33] These are available in split (double zeta) valence to quadruple zeta valence quality, which allows for a systematic exploration of the effect of the basis set size on the resultant geometries. The valence sets are matched with a small-core, ten-valence electron energy-consistent

pseudopotential, which includes corrections for scalar relativistic effects.[34] The pseudopotential is an updated version of the original SDD ECP.

2.2.2 Density functional requirements

The development of density functionals designed to model dispersion interactions accurately has been one of the most actively developed areas of recent computational design, and the various approaches taken to address the issue have been reviewed.[23] For the present study, we were particularly interested in the use of specifically designed "dispersion-free" functionals, and their dispersion-corrected forms.[35–37] The rationale behind their development is not only that commonly used functionals do not describe long-range dispersion interactions correctly (e.g., with R^{-6} dependence on the interatomic distance R), but they may also display non-physical attractive or repulsive interactions that vary with R. This anomaly occurs with many commonly used functionals, including B3LYP, B3PW91, TPSS, PBE1PBE, M06-2X, and B2PLYP (figure 16).[37] Empirical semiclassical corrections that patch conventional functionals (e.g., with the DFT-D*n* approach) do not correct the underlying over/underbinding, and in some cases, can worsen it.[38,39]

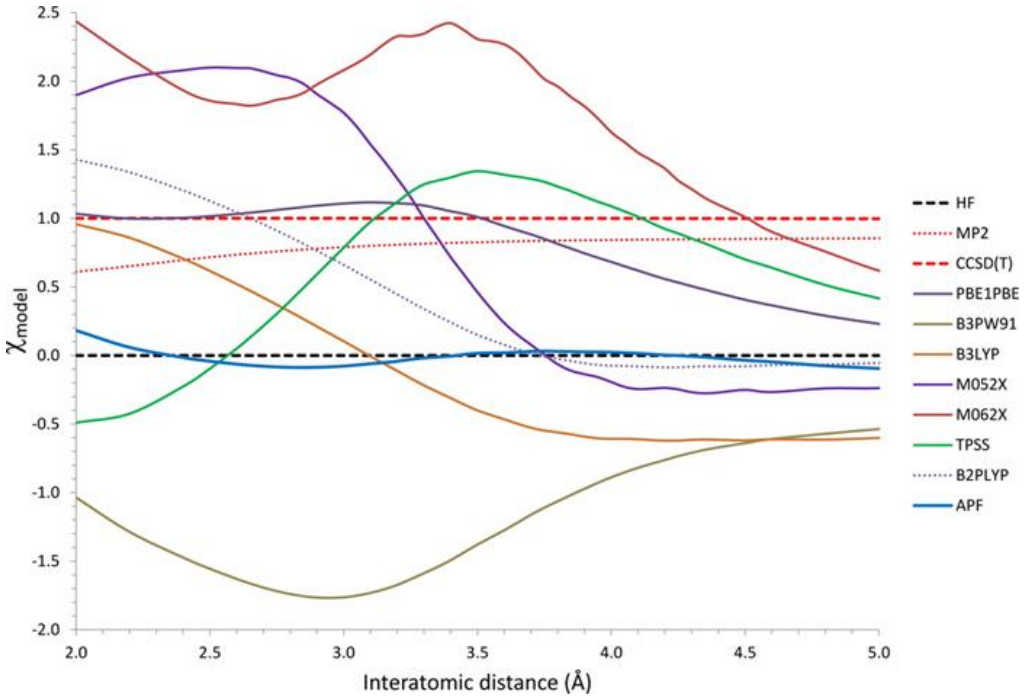

Figure 16: Plot of χ(R), the relative error in the dispersion energy for the case of Ne_2. χ(R) will approach a constant value at long interatomic distances with a functional that includes the proper R^{-6} dependence for dispersion. Standard DFT functionals produce χ(R) that goes to 0, either from above (attractive interactions at shorter R) or from below (repulsive interactions at shorter R). APF provides minimal error in this regard. Reprinted with permission from A. Austin, G.A. Petersson, M.J. Frisch, F.J. Dobek, G. Scalmani, K. Throssell, J. Chem. Theory Comp., 8(12) (2012), 4989–5007. Copyright 2012 American Chemical Society.

The dispersion-free functional used in this study is APF, an empirical combination of the well-established B3PW91 and PBE1PBE functionals (with approximately 23% HF admixture) that is designed to minimize spurious dispersion interactions. The APF-D modification has a spherical atomic model for dispersion forces.[37] APF-D approximates dispersion forces with an accuracy comparable to the CCSD(T)/aug-cc-PVTZ level of theory, and its modeling of electron density is also among the very best provided by current density functionals. It provides results similar to those from *ab initio* methods such as CCSD(T) or MP2.[40]

2.2.3 Computational details

All geometry optimizations and energy calculations were performed with the Gaussian 09 suite of programs.[41] The majority of calculations employed the APF or APF-D functionals, described above.[37] The dhf-ECP basis sets were used for Sr.[33,34] For Sm, the small core Stuttgart-Dresden relativistic effective core potential (SDD) was used, along with its standard valence set ((12s,11p,9d,8f)/[5s,5p,4d,3f]). For comparison, the Stuttgart ECP ANO valence basis set for Sm was also tested.[42] For C and H, the def2-SVP basis sets were generally used; trial calculations with other basis sets of polarized double zeta or better quality indicated that there were only small effects on the geometry. An ultrafine integration grid (99,590) was used during all geometry optimizations, which were conducted without imposed symmetry. Based on the final structures obtained when the starting geometries were changed, the error in the calculated centroid-metal-centroid angles in the metallocenes (α) was placed at ±4°. AIM and Mulliken analyses of the molecular topology were conducted with the Multiwfn package (v. 3.3.9).[43]

2.3 Results and discussion

2.3.1 Calibration calculations

Several calculations were performed to establish the reliability of the basis sets for Sr and the APF functional to describe the geometries of the systems under investigation (Table 1, see next page). Where possible, these results were compared with experimentally determined values and various high-level *ab initio* approaches.

Table 1: Calculated geometries of Sr_2, SrO, and strontium halides.

Entry	Complex	Method	Sr basis set	other basis	Sr–X (Å)	Angle (°)	ref.
1	Sr_2	exper. (gas phase)		n/a	4.672	n/a	44
2	Sr_2	CCSD(T)	CBS (extrap.)	n/a	4.710	n/a	45
3	Sr_2	CASPT2	ANO–RCC	n/a	4.772	n/a	46
4	Sr_2	APF	def2-TZVP	n/a	4.642	n/a	a
5	Sr_2	B3LYP	def2-TZVP	n/a	4.838	n/a	a
6	Sr_2	M06	def2-TZVP	n/a	4.528	n/a	a
7	SrO	exper. (gas phase)			1.920	n/a	47
8	SrO	CISD	Sadlej pVTZ	cc-pVTZ	1.917	n/a	48
9	SrO	APF	def2-TZVP	def2-TZVP	1.915	n/a	a
10	SrO	B3LYP	def2-TZVP	def2-TZVP	1.937	n/a	a
11	SrO	M06	def2-TZVP	def2-TZVP	1.911	n/a	a
12	SrF_2	exper. (Kr matrix–IR)			2.20	108	49
13	SrF_2	CCSD(T)	SDD(uc)+f[b]	cc-pVTZ	2.142	136.9	17
14	SrF_2	CISD	SDD(uc)+f[b]	SDD	2.161	138.8	28
15	SrF_2	B3LYP	SDD(uc)+f[b]	cc-pVTZ	2.119	128.5	50
16	SrF_2	APF	SDD	def2-TZVP	2.124	130.6	a
17	SrF_2	APF	cc-pwCVTZ-PP	def2-TZVP	2.116	131.0	a
18	SrF_2	APF	ANO-RCC(full)	def2-TZVP	2.110	130.8	a
19	$SrCl_2$	exper. (ED, equil. values)			2.607(13)	143.3(3.4)	14
20	$SrCl_2$	CCSD(T)	SDD(uc)+f[b]	cc-pVTZ	2.634	167.3	17
21	$SrCl_2$	CISD	SDD(uc)+f[b]	SDD	2.640	159.5	28
22	$SrCl_2$	B3LYP	SDD(uc)+f[b]	cc-pVTZ	2.632	155.5	50
23	$SrCl_2$	APF	SDD	def2-TZVP	2.612	151.6	a
24	$SrCl_2$	APF	cc-pwCVTZ-PP	def2-TZVP	2.603	148.7	a
25	$SrCl_2$	APF	ANO-RCC(full)	def2-TZVP	2.598	148.0	a

[a] This work; [b] The valence d orbitals were uncontracted and a single f orbital was added

The Sr_2 molecule in its ground state ($X_1\Sigma g^+$) is not covalently bound, and its binding energy (1081.6 cm^{-1}, 3.09 kcal mol^{-1})[44] is reflective of a van der Waals dimer.[51] Nevertheless, the bond length is captured about as well with the APF functional (entry 4) as with several *ab initio* techniques (entries 2,3).[37] Note that the reproduction of the equilibrium bond length in the dimer does not mean that its potential energy curve is accurately accounted for.[52] Strontium monoxide (SrO), in contrast, is more representative of a typical strontium compound, and its bond length is readily reproduced with a variety of DFT functionals, including APF (entry 9).

Molecules of greater relevance to the metallocene systems are the strontium dihalides. Strontium fluoride is known to be a bent molecule, but the actual angle is poorly determined. The results of krypton matrix isolation studies provide a value of 108°,[49] but this is almost certainly strongly distorted by interaction with the krypton matrix. CCSD(T) calculations put the bending angle at 136.9°, and DFT calculations with the B3LYP functional reduce this to 128.5° (entry 15).[50] The value from an APF/dhf-TZVP calculation is 131.1° (entry 17), in line with the B3LYP results.

The best available estimate for the equilibrium bending angle of the quasilinear molecule $SrCl_2$ is from electron diffraction measurements coupled with corrections for anharmonic vibrations.[14] This is a difficult value to reproduce computationally (see a full discussion of the issue),[14] although the APF/dhf-TZVP combination gets within 6° of the angle (entry 23).

2.3.2 Calculations on $(C_5H_5)_2$(Sr,Sm)

Both $(C_5H_5)_2Sr$ and $(C_5H_5)_2Sm$ have long been known, although the structure of neither has been experimentally determined. They are presumed to be polymeric in the solid state.[53,54] The parent $(C_5H_5)_2Sr$ molecule has been studied computationally several times, and both bent[55] and linear[56–58] forms have been found as the lowest energy configuration. The energy difference between the conformations is consistently found to be small, and not surprisingly, the results are sensitive to the level of calculation employed. As an example, an early calculation reported that $(C_5H_5)_2Sr$ optimized to a bent structure (α = 145°) with the use of the BP86 functional and DFT-optimized all-electron DGDZVP basis set.[55] We repeated the calculation with the same functional and basis set, and also found a bent geometry (Table 2, entry 1), although the angle is larger (α = 164°), perhaps because we conducted a full optimization (no imposed symmetry) rather than a limited one (only ring rotation and the bending angle were varied in the original study). A reinvestigation of this system by the same authors[58] using a triple-ζ Slater-type orbital with a frozen core (3d and below) and the BP86 functional found that $(C_5H_5)_2Sr$ optimized to a linear structure; the previous bent structure was ascribed to deficiencies in the DGDZVP basis. Actually, issues with the functional need to be considered as well, as we find that the combination of the APF functional and the DGDZVP basis set also optimizes to a linear structure (entry 2). This suggests that it is the BP86/DGDZVP *combination* that overbinds the molecule. Several additional test calculations were then performed on $(C_5H_5)_2Sr$ to

ensure that there were no spurious effects on the geometries induced by the APF(-D) functional (entries 3–5).

Table 2: Geometry of $(C_5H_5)_2M$ optimized with various functional/basis set combinations.

Entry	Complex	Functional	M basis set[a]	M–centroid (Å)	Angle (deg)
1	$(C_5H_5)_2Sr$	BP86	DGDZVP[b]	2.537	164.1
2	$(C_5H_5)_2Sr$	APF	DGDZVP[b]	2.532	180
3	$(C_5H_5)_2Sr$	APF	SDD	2.539	180
4	$(C_5H_5)_2Sr$	APF-D	SDD	2.533	180
5	$(C_5H_5)_2Sr$	B3LYP-D3	SDD[c]	2.550	180
6	$(C_5H_5)_2Sr$	APF	ANO(full)	2.509	162.6
7	$(C_5H_5)_2Sm$	APF	SDD	2.495	147.7
8	$(C_5H_5)_2Sm$	APF	ANO/ECP	2.494	141.9

[a]def2-SVP is used on C, H in all calculations using the APF(-D) functionals; [b]the corresponding DGDZVP basis was also used on C, H; [c]6-31G(d,p) on C, H.

With the SDD basis set on Sr and the APF functional, a linear geometry is again obtained for $(C_5H_5)_2Sr$ (entry 3). This is the same result found with the BP86 functional and the SDD basis set on Sr.[57] Adding dispersion corrections with APF-D does not change the result (entry 4). With the larger dhf-TZVP valence set on Sr, $(C_5H_5)_2Sr$ still stays linear (entry 5). As a check with one of the functional/basis set combinations previously used to study the decamethylmetallocenes,[22] $(C_5H_5)_2Sr$ also remains unbent with the B3LYP-D3/SDD combination (entry 6). With the exception of the problematic entry 1, all these DFT results support conclusions from previous CCSD(T) calculations; i.e., that to a high level of approximation, $(C_5H_5)_2Sr$ has a linear or quasilinear geometry.[57]

A different situation exists with the samarium analogue, $(C_5H_5)_2Sm$; it also has been the subject of previous studies, where it is always found to be bent at levels of theory above Hartree-Fock.[56,59] With the use of the standard double-ζ valence set on the SDD ECP, $(C_5H_5)_2Sm$ bends with an angle of 147.7° (entry 7). With the use of the larger Stuttgart ANO/ECP basis set, used in a previous study of the bending angle of $(C_5Me_5)_2Sm$,[22] the bending angle of $(C_5H_5)_2Sm$ (141.9°, entry 8) is not far from that found in the crystal structure ($\alpha = 140.1°$),[12] which supports the conclusion that dispersive interactions between the methyl groups are comparatively unimportant contributors to its bending.

2.3.3 $(C_5Me_5)_2Sr$ calculations

The determination of how well various methods reproduce the geometry of $(C_5Me_5)_2Sr$ is tempered by the fact that its structure is known only from gas-phase electron diffraction measurements. To the best of our knowledge, the crystal structure of $(C_5Me_5)_2Sr$ has not been reported in the open literature; the Cambridge Structure Database (v. 5.38, November, 2016) has no entry for the compound. The reference cited for this,[22] which purportedly describes the solid state structure, is actually for the gas-phase structure determined by Blom, et al.[11] Hence the values for the solid state bond distances and angles of $(C_5Me_5)_2Sr$ listed[22] cannot be used as reference numbers. The thermal average ring centroid–Sr–centroid angle of 149° has an estimated error of ±3°.[11] In contrast to the experimental structure, and as previously found with the SDD basis set and various functionals without explicit dispersion corrections, $(C_5Me_5)_2Sr$ optimizes to a linear geometry with the APF functional (Table 3, entry 1). Addition of the SAM dispersion correction leads to a bent molecule with a centroid–Sr–centroid angle of 146.6° (entry 2). This is consistent with the values of 145–153° previously found with the SDD basis and other commonly used functionals, including B3LYP-D3, M05, M05-2X, M06, and wB97X-D.[22]

Table 3: Geometry of $(Me_5C_5)_2Sr$ optimized with various functional/basis set combinations.

Entry	Method	Sr basis set	C, H basis sets	Sr–centr (Å)	Angle (α, deg)
1	APF	SDD	def2-SVP	2.517	180
2	APF-D	SDD	def2-SVP	2.486	146.6
3	APF	def2-TZVP	def2-SVP	2.509	163.2
4	APF	def2-TZVP	6-31G(d,p)	2.507	161.4
5	APF	def2-TZVP	def2-TZVP	2.505	159.6
6	APF	def2-QZVPP	def2-SVP	2.496	165.3
7	APF	ANO-VDZ	def2-SVP	2.559	180
8	APF-D	ANO-VDZ	def2-SVP	2.546	163.3
7	APF	ANO-VDZP	def2-SVP	2.481	166.4
8	APF-D	ANO-VDZP	def2-SVP	2.464	151.3
9	APF	ANO-VTZP	def2-SVP	2.498	157.1
10	APF-D	ANO-VTZP	def2-SVP	2.475	146.1
11	APF	ANO-VQZP	def2-SVP	2.463	154.6
12	APF-D	ANO-VQZP	def2-SVP	2.437	147.0
13	APF	ANO(full)	def2-SVP	2.481	151.2
14	APF	ANO(full)	def2-TZVP	2.504	146.3
15	B3LYP	ANO(full)	def2-SVP	2.509	150.8
16	APF-D	ANO(full)	def2-SVP	2.460	144.4
			exper. (ED)[11]	2.469(6)	149(3)

Exchanging the Sr SDD basis set for the dhf-SVP + ECP basis combination replaces both the ECP and the valence functions; for the latter, the p and d functions are contracted differently, and a single f function has been added.[33] Nevertheless, $(C_5Me_5)_2Sr$ remains unbent at this level with the APF functional (entry 3). With the APF-D functional, the molecule again strongly bends (α = 147.9°, entry 4).

Compared with the def-SVP basis for Sr, dhf-TZVP adds extra s and p functions, and supplies a different contraction pattern for the d polarization functions ((8s,8p,5d,1f) → [6s,5p,3d,1f]). With the APF functional, this change results in a very slightly bent $(C_5Me_5)_2Sr$ (α = 174.8°, entry 5). This amount of bending is barely outside the error limit of a significant difference from 180°, but bending persisted even using tighter convergence criteria (10^{-4} au in maximum force), and we take it as real effect. Application of the dispersion correction not surprisingly led to a much more strongly bent molecule, with a centroid–Sr–centroid angle of 147.2° (entry 6).

Finally, use of the def-QZVP basis ((9s,9p,6d,2f,1g) → [7s,6p,4d,2f,1g]) with the APF functional led to an unambiguously bent molecule (α = 160.6°, entry 7). The angle is relatively unaffected by the basis sets on C and H, as long as they are polarized double zeta or better (entries 8, 9). The bent structure is a minimum on the potential energy surface (N_{imag} = 0), and forcing the molecule to remain linear during optimization with imposed D_5 symmetry resulted in the generation of 2 imaginary frequencies (–23 cm^{-1}). These results indicate that bending of $(C_5Me_5)_2Sr$ is possible even with the use of a functional that is explicitly designed not to capture dispersion interactions. Using the SAM dispersion correction resulted in further bending to 146.2° (entry 10). It should be noted that the energy difference ($\Delta H°$) between the bent structure of entry 10 and that of the linear counterpart (D_5 symmetry) is only 0.51 kcal mol^{-1}, in line with other estimates of the bending force.[57] It is also a testament to the very small amounts of energy that are involved in these calculations. The results with the dhf-basis sets and APF(-D) functional are summarized in Table 3, entries 3–10, and are depicted in Figure 18.

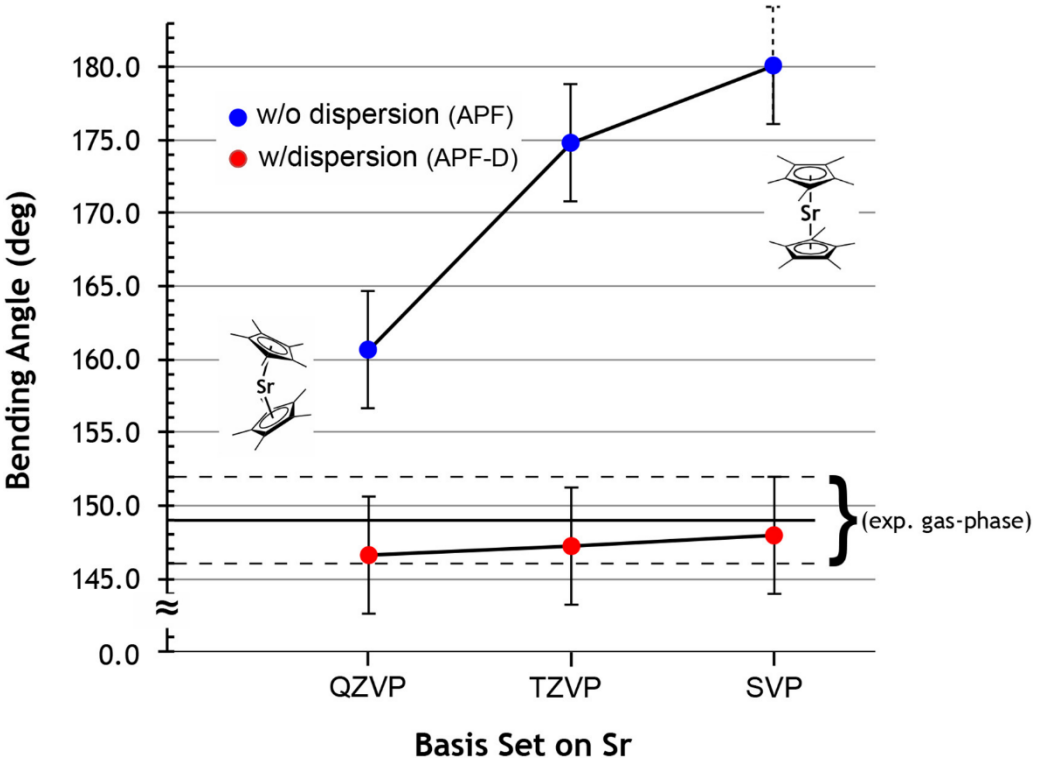

Figure 17. Ring centroid-Sr-centroid angles for $(C_5Me_5)_2Sr$ as a function of basis set size. The dhf-basis sets are used with Sr; the def2SVP basis was used on C, H. The error bars are set at ±4°.

2.3.4 Covalency in the bonding in $(C_5Me_5)_2Sr$

Given the low electronegativity of the heavy group 2 metals—(that for Sr is ~1.0)[60] —there is no question that the bonding in their organometallic complexes, and in $(C_5Me_5)_2Sr$ in the present case, is highly polar, even if not actually electrostatic. The quantification of the polarity is difficult, as is determining how different computational treatments affect such measures. Detailed orbital analysis have been made for bonding in the group 2 metallocenes,[55,57,58] and it is not the intent to repeat such information here. Rather, we wish to highlight the effect on indicators of covalency caused by the addition of methyl groups to the metallocenes, and of the use of highly flexible basis sets in the optimization of the compounds. One such indicator is the calculated charge(s) on the metal centers. Natural population charges (NPA) are relatively insensitive to basis set composition,[61] and of note is that NPA charges reported for Sr in $(C_5H_5)_2Sr$ have clustered near +1.8 (i.e., +1.867[56], +1.77[57], +1.80[58]), despite the use of different basis sets and computational methods. Interestingly, the NPA charge previously reported for the Sr center in $(C_5Me_5)_2Sr$, +1.53[22] is similar to that calculated with the dhf-QZVP basis set and the APF functional, +1.60 (entry 7 Table 3). The difference in average metal charge (Δq = 0.25) between the two molecules is large enough that it likely reflects the better

donor properties of the pentamethylcyclopentadienyl ring compared to the unsubstituted ligand.

An alternative investigation of the possible importance of covalent interactions was conducted with Bader's atoms in molecules (AIM) theory.[62] When examined at the B3LYP-D3/SDD level, the structure of $(C_5Me_5)_2Sr$ was found to have only three bond-critical paths between the Sr atom and the ring carbons, providing little evidence for covalence between the metal and ligands, and an additional three bond-critical paths between the methyl groups on the bent side of the molecule, taken as representing the stabilizing effect of van der Waals forces.[22] For the present study, bond-critical points and paths were calculated for $(C_5Me_5)_2Sr$ with the APF-D/dhf-QZVP optimized structure (entry 10, Table 3). Fig. 19 illustrates that bond critical paths are now clearly evident between the metal and the 10 carbon atoms in the ring, and additional ring critical points, indicative of delocalization in space, are also present. There are also three bond-critical paths found between hydrogen atoms on the methyl groups on the bent side. The average electron density (in au) at the bond critical points along the paths from Sr to the ring carbons is 0.029, over six times the value for the points along the paths that represent van der Waals interactions between the methyl groups (avg. 0.0043). Of course, even the Sr···C interactions involve only a fraction of the electron density found in the ring bonds (e.g., the average for the bond critical paths between the ring carbons is 0.29). Nevertheless, the analysis provides evidence for both an orbital-based and a dispersion contribution to the bending.

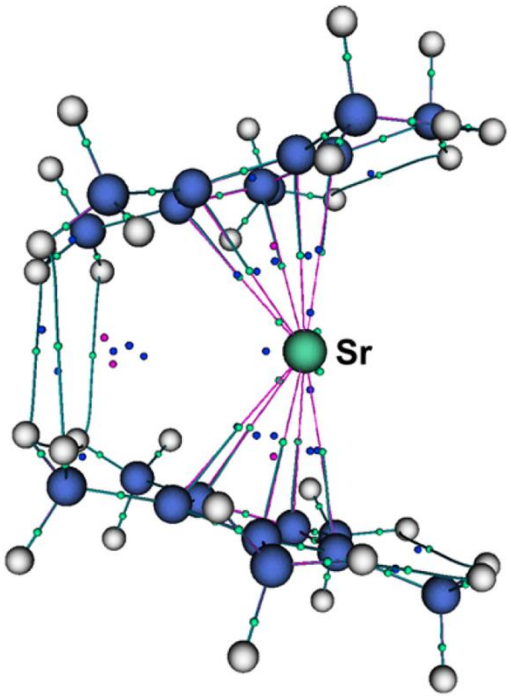

Figure 18. AIM representation for $(C_5Me_5)_2Sr$; bond critical points are in green, ring critical points are in blue and cage critical points are in magenta.

In an analysis of the orbitals of $(C_5Me_5)_2Sm$,[22] it was noted that they fell into three different categories: one of pure metal orbitals, one of pure ligand orbitals, and one of mixed metal-ligand character (*ca*. 5% 4f and 10% 5d per orbital). Critically, it was also observed that the set of mixed metal-ligand orbitals was missing in $(C_5Me_5)_2Sr$, a sign of the higher ionic character in the bonding. In this context, it is noteworthy that with the dhf-QZVP basis set, evidence for mixed metal–ligand orbitals is in fact present. Fig. 20 presents the six highest occupied orbitals of $(C_5Me_5)_2Sr$. Whereas 75, 76, 79, and 80 (HOMO-5, HOMO-4, HOMO-1, and HOMO, respectively) are evidently largely ligand-based, Mulliken orbital analysis indicates that 77 (HOMO-4) contains 9.4% of Sr d character, and 78 (HOMO-2) has 7.4% d character. The mixing is not as extensive as in $(C_5Me_5)_2Sm$, but it does give an indication that the flexibility of the valence representation on the metal center can alter the calculated percentage of metal-ligand interactions.

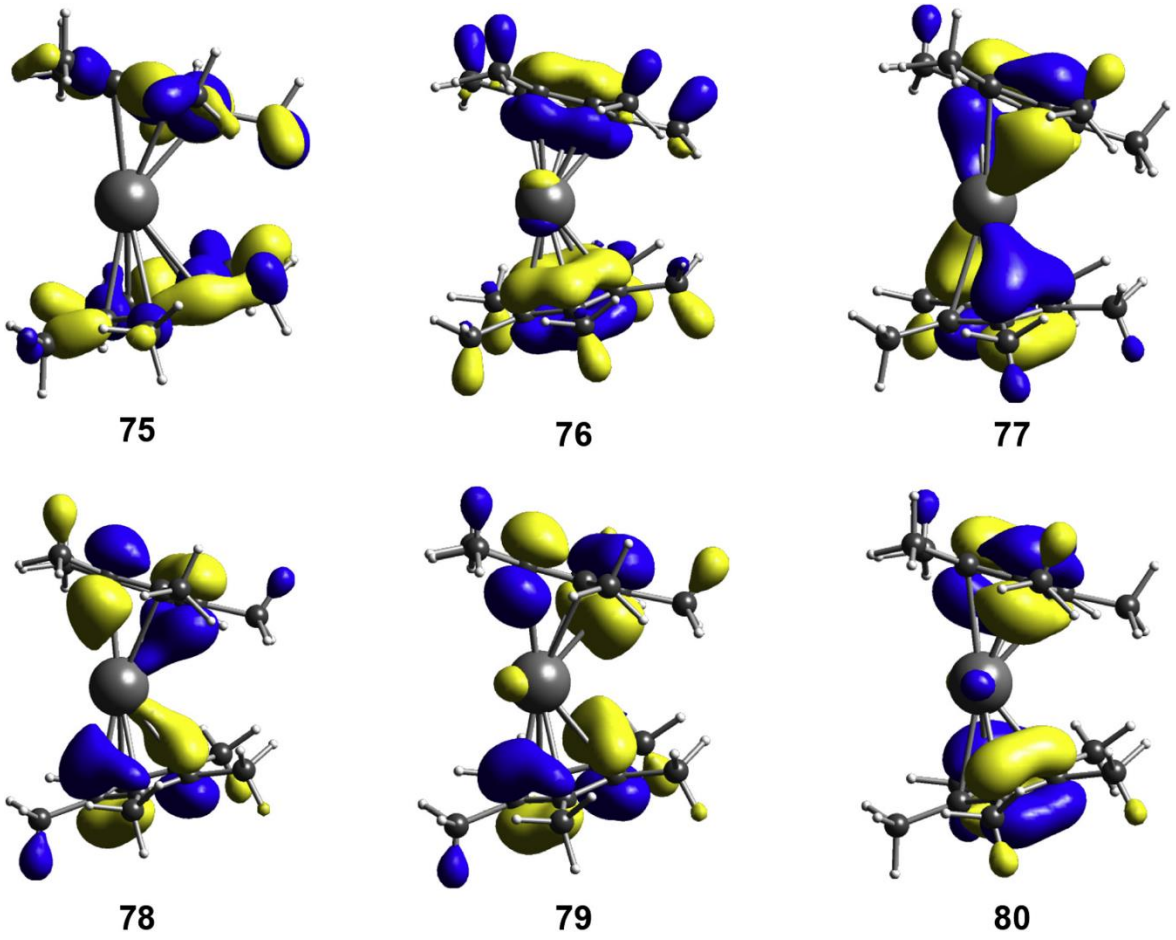

Figure 19. Highest energy occupied orbitals of $(C_5Me_5)_2Sr$, optimized with the APF-D functional, dhf-QZVP basis set on Sr. Isodensity surfaces are drawn at the 0.40 level.

2.4 Conclusion

By using the "dispersion-free" functional APF and its accompanying dispersion correction (APF-D), we have found that, provided a sufficiently flexible basis set is used on strontium, the bent structure of the heavy alkaline earth metallocene $(C_5Me_5)_2Sr$ can be shown to be bent, even without the application of dispersion corrections. However, dispersion effects do bring the bending of the metallocene into conformity with the experimentally determined structure. The methyl groups both provide the possibility for dispersion interactions and slightly increase the covalency in the metal-ring bonding, so that orbital and dispersion effects contribute together to the bending. Dispersion corrections alone can cause bending, however, and in a structurally floppy molecule such as $(C_5Me_5)_2Sr$, can mask deficiencies in the basis sets and/or density functionals used. An additional consequence of these findings is that $(C_5H_5)_2Sr$, whose linearity has been reconfirmed in this study, should not be used as a surrogate for the decamethylated species.[55] The contribution of the methyl groups to the geometry of $(C_5Me_5)_2Sr$ cannot be ignored.

Although the covalent contribution to the bonding in $(C_5Me_5)_2Sr$ is certainly less than in the lanthanide counterpart $(C_5Me_5)_2Sm$, it is not completely negligible. These results leave the door open to orbitally based explanations of the bending, such as pseudo-Jahn Teller effect-induced distortions.[17]

2.5 Appendix

2.5.1. Coordinates of Optimized Structures 1 2 3 4 5 6 7 8 9 10 1 2 3 4 5 6

2
Sr2; APF/def2TZVP; ΔG° = -61.420796 au
Sr 0.000000 0.000000 2.321026
Sr 0.000000 0.000000 -2.321026

2
Sr2; B3LYP/def2TZVP; ΔG° = -61.436620 au
Sr 0.000000 0.000000 2.418795
Sr 0.000000 0.000000 -2.418795

2
Sr2; M06/def2TZVP; ΔG° = -61.338315 au
Sr 0.000000 0.000000 2.264070
Sr 0.000000 0.000000 -2.264070

2
SrO; APF/def2TZVP; ΔG° = -105.904094 au
Sr 0.000000 0.000000 0.333019
O 0.000000 0.000000 -1.581840

2
SrO; B3LYP/def2TZVP; ΔG° = -105.969752 au
Sr 0.000000 0.000000 0.336895
O 0.000000 0.000000 -1.600253

2
SrO; M06/def2TZVP; ΔG° = -105.881993 au
Sr 0.000000 0.000000 0.332336
O 0.000000 0.000000 -1.578598

3
SrF2; APF/SDD(Sr),def2TZVP(F); ΔG° = -230.511369 au
Sr 0.000000 1.930015 -0.602441
F 0.000000 -1.930015 -0.602441
F 0.000000 0.000000 0.285367

3
SrF2; APF/cc-pwCVTZ-PP(Sr),def2TZVP(F); ΔG° = -230.523904 au
Sr 0.000000 1.925463 -0.595644
F 0.000000 -1.925463 -0.595644
F 0.000000 0.000000 0.282147

3

SrF2; APF/ANO(full)(Sr),def2TZVP(F); ΔG° = -3298.666971 au
Sr 0.000000 1.919208 -0.595687
F 0.000000 -1.919208 -0.595687
F 0.000000 0.000000 0.282168

3
SrCl2; APF/SDD(Sr),def2TZVP(F); ΔG° = -951.130036 au
Sr 0.000000 2.531878 0.337749
Cl 0.000000 -2.531878 0.337749
Cl 0.000000 0.000000 -0.302196

3
SrCl2; APF/cc-pwCVTZ-PP(Sr),def2TZVP(F); ΔG° = -951.139932 au
Sr 0.000000 2.506334 -0.370941
Cl 0.000000 -2.506334 -0.370941
Cl 0.000000 0.000000 0.331895

3
SrCl2; APF/ANO-RCC(full) (Sr),def2TZVP(F); ΔG° = -4019.279904 au
Sr 0.000000 2.497424 -0.377508
Cl 0.000000 -2.497424 -0.377508
Cl 0.000000 0.000000 0.337770

21
Cp2Sr; BP86/DGDZVP(Sr),DGDZVP(C,H); ΔG° = -3520.324180 au
C -1.883695 2.428115 -0.414131
C -2.798342 3.516317 -0.570838
C -4.126778 2.991074 -0.501110
C -4.033570 1.577785 -0.301588
C -2.646868 1.229548 -0.248067
H -0.792710 2.507143 -0.370780
H -2.529527 4.572182 -0.673882
H -5.051335 3.575756 -0.538697
H -4.874723 0.892884 -0.153023
H -2.241795 0.231918 -0.049489
Sr -3.089448 1.998384 -2.920012
C -2.098004 3.059685 -5.328880
C -2.092727 1.643366 -5.528526
C -3.459766 3.493247 -5.272921
H -1.215828 3.705895 -5.281855
C -3.451869 1.201467 -5.595817
H -1.205405 1.017332 -5.667892
C -4.296546 2.345286 -5.438185
H -3.800874 4.528375 -5.173355
H -3.785998 0.178597 -5.798015
H -5.389890 2.349866 -5.492939

21

Cp2Sr; APF/DGDZVP(Sr),DGDZVP(C,H); ΔG° = -3519.493820 au

C	-1.891930	2.377492	-0.383704
C	-2.764850	3.494878	-0.387534
C	-4.097282	3.009954	-0.391697
C	-4.047869	1.592873	-0.390487
C	-2.684857	1.201986	-0.385552
H	-0.807965	2.415392	-0.327945
H	-2.465993	4.537699	-0.335221
H	-4.996781	3.616649	-0.343203
H	-4.902887	0.925037	-0.340782
H	-2.314041	0.182627	-0.331363
Sr	-3.088862	2.333588	-2.920002
C	-2.129196	3.077323	-5.448414
C	-2.080969	1.660200	-5.449263
C	-3.491855	3.469390	-5.452799
H	-1.273605	3.744503	-5.497044
C	-3.413832	1.176431	-5.454173
H	-1.181990	1.052813	-5.498705
C	-4.285794	2.294576	-5.456377
H	-3.861782	4.489151	-5.505414
H	-3.713573	0.133943	-5.508098
H	-5.369790	2.257717	-5.512222

21

Cp2Sr; APF/SDD(Sr),def2SVP(C,H); ΔG° = -417.126062 au

C	2.541135	-0.211181	-1.185529
C	2.539740	1.064087	-0.566031
C	2.536931	0.868923	0.838249
C	2.536538	-0.526931	1.086568
C	2.539155	-1.194497	-0.164175
H	2.597462	-0.402254	-2.259257
H	2.594779	2.026326	-1.079478
H	2.589375	1.654687	1.594809
H	2.588559	-1.003541	2.067737
H	2.593556	-2.274827	-0.314149
Sr	-0.000032	-0.000141	-0.003354
C	-2.540379	-0.870186	-0.833216
C	-2.537606	-1.063002	0.571393
C	-2.540778	0.525324	-1.083826
H	-2.595982	-1.657204	-1.588255
C	-2.536322	0.213299	1.188781
H	-2.590703	-2.024406	1.086602
C	-2.538246	1.194933	0.165832
H	-2.596762	1.000368	-2.065541
H	-2.588200	0.406100	2.262415
H	-2.591895	2.275508	0.314296

21

Cp2Sr; APF-D/SDD(Sr),def2SVP(C,H); ΔG° = -417.134556 au

C	2.534165	1.148104	0.368059
C	2.533759	0.004204	1.205941
C	2.532918	-1.146155	0.376952
C	2.532791	-0.713223	-0.973277
C	2.533564	0.704709	-0.978773
H	2.587414	2.187084	0.701189
H	2.586637	0.008404	2.297029
H	2.585000	-2.182580	0.718132
H	2.584720	-1.358014	-1.853523
H	2.586234	1.342602	-1.863992
Sr	0.000000	0.000865	0.000392
C	-2.533946	1.145154	-0.377584
C	-2.533166	-0.005351	-1.206362
C	-2.534022	0.712462	0.972728
H	-2.586969	2.181463	-0.718975
C	-2.532768	-1.149095	-0.368274
H	-2.585460	-0.009810	-2.297477
C	-2.533296	-0.705464	0.978480
H	-2.587121	1.357353	1.852832
H	-2.584698	-2.188190	-0.701245
H	-2.585749	-1.343257	1.863782

21

Cp2Sr; B3LYP-D3/SDD(Sr),6-31G(d,p)(C,H); ΔG° = -417.748190 au

C	-1.896411	2.384099	-0.363368
C	-2.775970	3.498839	-0.375323
C	-4.107964	3.006650	-0.380346
C	-4.051580	1.587674	-0.371576
C	-2.684685	1.202928	-0.361111
H	-0.814774	2.427563	-0.303104
H	-2.482874	4.541480	-0.325899
H	-5.008904	3.608098	-0.335435
H	-4.901923	0.917164	-0.318541
H	-2.309686	0.187571	-0.298574
Sr	-3.088161	2.321116	-2.919999
C	-2.118330	3.074063	-5.460158
C	-2.076918	1.654630	-5.468263
C	-3.481032	3.473448	-5.465148
H	-1.260895	3.736024	-5.505593
C	-3.414101	1.176713	-5.478275
H	-1.182438	1.044237	-5.521182
C	-4.281793	2.300832	-5.476401
H	-3.845101	4.493456	-5.514969
H	-3.718291	0.137911	-5.540287
H	-5.363868	2.269727	-5.536449

21

Cp2Sr; APF/ANO(full),def2SVP(C,H); ΔG° = -3485.280479 au

C	-1.889765	2.409105	-0.447986
C	-2.778166	3.499008	-0.618763
C	-4.102149	3.001219	-0.542715
C	-4.032588	1.603080	-0.325117
C	-2.664789	1.236774	-0.266874
H	-0.800231	2.470426	-0.408020
H	-2.492881	4.545925	-0.738885
H	-5.014946	3.598392	-0.591127
H	-4.882791	0.935422	-0.169717
H	-2.276870	0.237725	-0.056361
Sr	-3.090498	1.969706	-2.920029
C	-2.123261	3.068214	-5.285513
C	-2.095117	1.668674	-5.503185
C	-3.478819	3.474951	-5.225665
H	-1.253746	3.725864	-5.225885
C	-3.434069	1.210312	-5.577755
H	-1.199732	1.060259	-5.647633
C	-4.289061	2.327291	-5.406445
H	-3.835946	4.500085	-5.109744
H	-3.750592	0.187306	-5.792625
H	-5.379685	2.314485	-5.459956

21

Cp2Sm; APF/SDD,def2SVP(C,H); ΔG° = -1044.476230 au

C	-2.060640	2.773527	-0.603950
C	-3.236453	3.514892	-0.878102
C	-4.348631	2.663503	-0.664778
C	-3.860403	1.397208	-0.257857
C	-2.446129	1.465347	-0.220100
H	-1.039379	3.157705	-0.638442
H	-3.279353	4.567127	-1.163269
H	-5.398856	2.948226	-0.753349
H	-4.468928	0.536416	0.026925
H	-1.773719	0.666009	0.098173
Sr	-3.091893	1.669150	-2.920067
C	-1.854396	2.738507	-5.150282
C	-2.249441	1.442160	-5.563521
C	-3.024466	3.515749	-4.965259
H	-0.827386	3.091466	-5.038593
C	-3.663926	1.417280	-5.633072
H	-1.579582	0.622341	-5.831021
C	-4.142719	2.698378	-5.263021
H	-3.056770	4.569173	-4.683114
H	-4.275165	0.575014	-5.963745
H	-5.187465	3.015046	-5.253557

21

Cp2Sm; APF/ANO(full),def2SVP(C,H); ΔG° = -1044.476476 au

C	-1.897041	2.448349	-0.585405
C	-2.806204	3.469701	-0.953358
C	-4.120241	2.968840	-0.781354
C	-4.022983	1.637288	-0.306425
C	-2.648523	1.314377	-0.186762
H	-0.808779	2.535079	-0.570165
H	-2.542265	4.476690	-1.279578
H	-5.043786	3.526786	-0.945776
H	-4.859731	0.991222	-0.032548
H	-2.240377	0.377496	0.198220
Sm	-3.088563	1.553690	-2.919947
C	-2.103836	3.033407	-5.035322
C	-2.103682	1.698829	-5.511543
C	-3.451280	3.448096	-4.894557
H	-1.222453	3.649673	-4.849485
C	-3.451191	1.287540	-5.662722
H	-1.220669	1.108438	-5.765077
C	-4.283542	2.370180	-5.282591
H	-3.787260	4.435849	-4.575766
H	-3.788778	0.326475	-6.056322
H	-5.374517	2.386221	-5.323519

2.6 References

(1) Guido, M.; Gigli, G. Ion Model and Equilibrium Configuration of the Gaseous Alkaline-earth Dihalides. *J. Chem. Phys.* **1976**, *65* (4), 1397–1402.

(2) Hargittai, M. Molecular Structure of Metal Halides. *Chem. Rev.* **2000**, *100* (6), 2233–2302.

(3) Boyde, N. C.; Chmely, S. C.; Hanusa, T. P.; Rheingold, A. L.; Brennessel, W. W. Structural Distortions in $M[E(SiMe_3)_2]_3$ Complexes (M = Group 15, f-Element; E = N, CH): Is Three a Crowd? *Inorg. Chem.* **2014**, *53* (18), 9703–9714.

(4) Goodwin, C. A. P.; Chilton, N. F.; Natrajan, L. S.; Boulon, M.-E.; Ziller, J. W.; Evans, W. J.; Mills, D. P. Investigation into the Effects of a Trigonal-Planar Ligand Field on the Electronic Properties of Lanthanide(II) Tris(Silylamide) Complexes (Ln = Sm, Eu, Tm, Yb). *Inorg. Chem.* **2017**, *56* (10), 5959–5970.

(5) Sitzmann, H.; Dezember, T.; Ruck, M. Synthesis of Symmetric Metallocenes from Metallic Calcium, Strontium, or Barium and Pentaisopropylcyclopentadienyl Radicals. *Angew. Chem. Int. Ed.* **1998**, *37* (22), 3113–3116.

(6) Zuniga, M. F.; Deacon, G. B.; Ruhlandt-Senge, K. Developments in Heterobimetallic S-Block Systems: Synthesis and Structural Survey of Molecular M/Ae (M = Li, Na, K, Cs; Ae = Ca, Sr) Aryloxo Complexes. *Inorg. Chem.* **2008**, *47* (11), 4669–4681.

(7) Orzechowski, L.; Piesik, D. F.-J.; Ruspic, C.; Harder, S. Superbulky Metallocene Complexes of the Heavier Alkaline-Earth Metals Strontium and Barium. *Dalton Trans.* **2008**, No. 35, 4742–4746.

(8) Kuchenbecker, D.; Harder, S.; Jansen, G. Insight in Structures of Superbulky Metallocenes with the CpBIG Ligand: Theoretical Considerations of Decaphenyl Metallocenes. *Z. Anorg. Allg. Chem,* **2010**, *636* (12), 2257–2261.

(9) Kelly, R. P.; Bell, T. D. M.; Cox, R. P.; Daniels, D. P.; Deacon, G. B.; Jaroschik, F.; Junk, P. C.; Le Goff, X. F.; Lemercier, G.; Martinez, A.; Wang, J.; Werner, D. Divalent Tetra- and Penta-Phenylcyclopentadienyl Europium and Samarium Sandwich and Half-Sandwich Complexes: Synthesis, Characterization, and Remarkable Luminescence Properties. *Organometallics* **2015**, *34* (23), 5624–5636.

(10) R. Anderson, R. Blom, J. M. Boncella, C. J. Burns, H. V. V. The Thermal Average Molecular Structures of Bis (Pentamethylcyclopentadienyl) Magnesium (II),-Calcium (II) and-Ytterbium (II) in the Gas Phase. *Acta Chem. Scand.* **1986**, *41a*, 24–35.

(11) Andersen, R. A.; Blom, R.; Burns, C. J.; Volden, H. V. Synthesis and Thermal Average Gas Phase Molecular Structures of Bis(Pentamethylcyclopentadienyl)-Strontium and -Barium; the First Organo-Strontium and -Barium Structures. *J. Chem. Soc. Chem. Commun.* **1987**, No. 10, 768–769.

(12) Evans, W. J.; Hughes, L. A.; Hanusa, T. P. Synthesis and X-Ray Crystal Structure of Bis(Pentamethylcyclopentadienyl) Complexes of Samarium and Europium: $(C_5Me_5)_2Sm$ and $(C_5Me_5)_2Eu$. *Organometallics* **1986**, *5* (7), 1285–1291.

(13) Andersen, R. A.; Boncella, J. M.; Burns, C. J.; Blom, R.; Haaland, A.; Volden, H. V. The Molecular Structures of Bis(Pentamethylcyclopentadienyl)-Calcium and -Ytterbium in the Gas Phase; Two Bent Metallocenes. *J. Organomet. Chem.* **1986**, *312* (3), C49–C52.

(14) Varga, Z.; Lanza, G.; Minichino, C.; Hargittai, M. Quasilinear Molecule Par Excellence, SrCl2: Structure from High-Temperature Gas-Phase Electron Diffraction and Quantum-Chemical Calculations—Computed Structures of $SrCl_2$·Argon Complexes. *Chem.—Eur. J.* **2006**, *12* (32), 8345–8357.

(15) Kaupp, M. "Non-VSEPR" Structures and Bonding in D^0 Systems. *Angew. Chem. Int. Ed.* **2001**, *40* (19), 3534–3565.

(16) Hassett, D. M.; Marsden, C. J. The Shapes and Bending Potentials of Monomeric MgF_2 and

CaF_2. *J. Mol. Struct.* **1995**, *346*, 249–263.
(17) Garcia-Fernandez, P.; Bersuker, I. B.; Boggs, J. E. Why Are Some ML_2 Molecules (M = Ca, Sr, Ba; L = H, F, Cl, Br) Bent While Others Are Linear? Implications of the Pseudo Jahn–Teller Effect. *J. Phys. Chem. A* **2007**, *111* (41), 10409–10415.
(18) Sapunov, V. N.; Kirchner, K.; Schmid, R. Revisiting the Main Group Cyclopentadienyl Metal Complexes in Terms of the Through-Space Coupling Concept. *Coord. Chem. Rev.* **2001**, *214* (1), 143–185.
(19) Keith Hollis, T.; Burdett, J. K.; Bosnich, B. Why Are Bis(Pentamethylcyclopentadienyl) Complexes, [MCp^*_2], of Calcium, Strontium, Barium, Samarium, Europium, and Ytterbium Bent? *Organometallics* **1993**, *12* (9), 3385–3386.
(20) Timofeeva, T. V; Lii, J.-H.; Allinger, N. L. Molecular Mechanics Explanation of the Metallocene Bent Sandwich Structure. *J. Am. Chem. Soc.* **1995**, *117* (28), 7452–7459.
(21) Kaltsoyannis, N.; Russo, M. R. Are $YbCp^*_2$ and $NoCp^*_2$ Bent? *J. Nucl. Sci. Technol.* **2002**, *39* (sup3), 393–399.
(22) Labouille, S.; Clavaguéra, C.; Nief, F. Theoretical Insights into the Nature of Divalent Lanthanide-Ligand Interactions. *Organometallics* **2013**, *32* (5), 1265–1271.
(23) Klimeš, J.; Michaelides, A. Perspective: Advances and Challenges in Treating van Der Waals Dispersion Forces in Density Functional Theory. *J. Chem. Phys.* **2012**, *137* (12), 120901.
(24) Hanusa, T. P.; Burkey, D. J. Structural Lessons from Main-Group Metallocenes. *Comm. Inorg. Chem.* **1995**, *17* (1), 41–77.
(25) Shannon, R. Revised Effective Ionic Radii and Systematic Studies of Interatomic Distances in Halides and Chalcogenides. *Acta Crystallogr. Sect. A* **1976**, *32* (5), 751–767.
(26) Dyall, K. G. Relativistic Double-Zeta, Triple-Zeta, and Quadruple-Zeta Basis Sets for the 4s, 5s, 6s, and 7s Elements. *J. Phys. Chem. A* **2009**, *113* (45), 12638–12644.
(27) Minenkov, Y.; Bistoni, G.; Riplinger, C.; Auer, A. A.; Neese, F.; Cavallo, L. Pair Natural Orbital and Canonical Coupled Cluster Reaction Enthalpies Involving Light to Heavy Alkali and Alkaline Earth Metals: The Importance of Sub-Valence Correlation. *Phys. Chem. Chem. Phys.* **2017**, *19* (14), 9374–9391.
(28) Kaupp, M.; Schleyer, P. v. R.; Stoll, H.; Preuss, H. The Question of Bending of the Alkaline Earth Dihalides MX_2 (M = Beryllium, Magnesium, Calcium, Strontium, Barium; X = Fluorine, Chlorine, Bromine, Iodine). An Ab Initio Pseudopotential Study. *J. Am. Chem. Soc.* **1991**, *113* (16), 6012–6020.
(29) von Szentpály, L.; Schwerdtfeger, P. Which Double-Octet ABC Molecules Are Bent? CI Calculations on CaF2, and a Softness Criterion to Predict Bending. *Chem. Phys. Lett.* **1990**, *170* (5–6), 555–560.
(30) Sadlej, A. J.; Urban, M. Medium-Size Polarized Basis Sets for High-Level-Correlated Calculations of Molecular Electric Properties. III. Alkali (Li, Na, K, Rb) and Alkaline-Earth (Be, Mg, Ca, Sr) Atoms. *J. Mol. Struct. THEOCHEM* **1991**, *234* (C), 147–171.
(31) Fromm, K. M.; Gueneau, E. D.; Bernardinelli, G.; Goesmann, H.; Weber, J.; Mayor-López, M.-J.; Boulet, P.; Chermette, H. Understanding the Formation of New Clusters of Alkali and Alkaline Earth Metals: A New Synthetic Approach, Single-Crystal Structures, and Theoretical Calculations. *J. Am. Chem. Soc.* **2003**, *125* (12), 3593–3604.
(32) Kaupp, M.; Schleyer, P. v. R.; Stoll, H.; Preuss, H. Pseudopotential Approaches to Ca, Sr, and Ba Hydrides. Why Are Some Alkaline Earth MX_2 Compounds Bent? *J. Chem. Phys.* **1991**, *94* (2), 1360–1366.
(33) Weigend, F.; Baldes, A. Segmented Contracted Basis Sets for One- and Two-Component Dirac–Fock Effective Core Potentials. *J. Chem. Phys.* **2010**, *133* (17), 174102.
(34) Lim, I. S.; Stoll, H.; Schwerdtfeger, P. Relativistic Small-Core Energy-Consistent

Pseudopotentials for the Alkaline-Earth Elements from Ca to Ra. *J. Chem. Phys.* **2006**, *124* (3), 34107.
(35) Pernal, K.; Podeszwa, R.; Patkowski, K.; Szalewicz, K. Dispersionless Density Functional Theory. *Phys. Rev. Lett.* **2009**, *103* (26), 263201.
(36) Podeszwa, R.; Szalewicz, K. Communication: Density Functional Theory Overcomes the Failure of Predicting Intermolecular Interaction Energies. *J. Chem. Phys.* **2012**, *136* (16), 161102.
(37) Austin, A.; Petersson, G. A.; Frisch, M. J.; Dobek, F. J.; Scalmani, G.; Throssell, K. A Density Functional with Spherical Atom Dispersion Terms. In *J. Chem. Theor. Comput.,* **2012**, *8*, 4989–5007.
(38) Grimme, S.; Antony, J.; Ehrlich, S.; Krieg, H. A Consistent and Accurate Ab Initio Parametrization of Density Functional Dispersion Correction (DFT-D) for the 94 Elements H-Pu. *J. Chem. Phys.* **2010**, *132* (15), 154104.
(39) Grimme, S.; Ehrlich, S.; Goerigk, L. Effect of the Damping Function in Dispersion Corrected Density Functional Theory. *J. Comput. Chem.* **2011**, *32* (7), 1456–1465.
(40) Medvedev, M. G.; Bushmarinov, I. S.; Sun, J.; Perdew, J. P.; Lyssenko, K. A. Density Functional Theory Is Straying from the Path toward the Exact Functional. *Science (80-.).* **2017**, *355* (6320), 49 LP – 52.
(41) M. J. Frisch, G. W. Trucks, H. B. Schlegel, G. E. Scuseria, M.; A. Robb, J. R. Cheeseman, G. Scalmani, V. Barone, B. Mennucci, G. A. Petersson, H.; Nakatsuji, M. Caricato, X. Li, H. P. Hratchian, A. F. Izmaylov, J. Bloino, G. Zheng, J. L.; Sonnenberg, M. Hada, M. Ehara, K. Toyota, R. Fukuda, J. Hasegawa, M. Ishida, T.; Nakajima, Y. Honda, O. Kitao, H. Nakai, T. Vreven, J. A. Montgomery, Jr., J. E. Peralta, F.; Ogliaro, M. Bearpark, J. J. Heyd, E. Brothers, K. N. Kudin, V. N. Staroverov, R.; Kobayashi, J. Normand, K. Raghavachari, A. Rendell, J. C. Burant, S. S. Iyengar, J.; Tomasi, M. Cossi, N. Rega, J. M. Millam, M. Klene, J. E. Knox, J. B. Cross, V. Bakken, C.; Adamo, J. Jaramillo, R. Gomperts, R. E. Stratmann, O. Yazyev, A. J. Austin, R. Cammi, C.; Pomelli, J. W. Ochterski, R. L. Martin, K. Morokuma, V. G. Zakrzewski, G. A. Voth, P.; Salvador, J. J. Dannenberg, S. Dapprich, A. D. Daniels, Ö. Farkas, J. B. Foresman, J. V.; Ortiz, J. Cioslowski, and D. J. Fox, Gaussian, Inc., Wallingford CT, 2009. Gaussian16 Revision D.01. *http//www. gaussian. com/* **2009**.
(42) Schuchardt, K. L.; Didier, B. T.; Elsethagen, T.; Sun, L.; Gurumoorthi, V.; Chase, J.; Li, J.; Windus, T. L. Basis Set Exchange: A Community Database for Computational Sciences. *J. Chem. Inf. Model.* **2007**, *47* (3), 1045–1052.
(43) Lu, T.; Chen, F. Multiwfn: A Multifunctional Wavefunction Analyzer. *J. Comput. Chem.* **2012**, *33* (5), 580–592.
(44) Stein, A.; Knöckel, H.; Tiemann, E. The 1S+1S Asymptote of Sr_2 Studied by Fourier-Transform Spectroscopy. *Eur. Phys. J. D* **2010**, *57* (2), 171–177.
(45) Li, H.; Feng, H.; Sun, W.; Zhang, Y.; Fan, Q.; Peterson, K. A.; Xie, Y.; Schaefer, H. F. The Alkaline Earth Dimer Cations (Be^{2+}, Mg^{2+}, Ca^{2+}, Sr^{2+}, and Ba^{2+}). Coupled Cluster and Full Configuration Interaction Studies†. *Mol. Phys.* **2013**, *111* (14–15), 2292–2298.
(46) Roos, B. O.; Veryazov, V.; Widmark, P.-O. Relativistic Atomic Natural Orbital Type Basis Sets for the Alkaline and Alkaline-Earth Atoms Applied to the Ground-State Potentials for the Corresponding Dimers. *Theor. Chem. Acc.* **2004**, *111* (2), 345–351.
(47) Kaufman, M.; Wharton, L.; Klemperer, W. Electronic Structure of SrO. *J. Chem. Phys.* **1965**, *43* (3), 943–952.
(48) Buenker, R. J.; Liebermann, H.-P. Ab Initio Study of the Positronation of the CaO and SrO Molecules Including Calculation of Annihilation Rates. *J. Comput. Chem.* **2012**, *33* (19), 1594–1602.

(49) Calder, V.; Mann, D. E.; Seshadri, K. S.; Allavena, M.; White, D. Geometry and Vibrational Spectra of Alkaline-Earth Dihalides. II. CaF_2, SrF_2, and BaF_2. *J. Chem. Phys.* **1969**, *51* (5), 2093–2099.
(50) Levy, J. B.; Hargittai, M. Unusual Dimer Structures of the Heavier Alkaline Earth Dihalides: A Density Functional Study. *J. Phys. Chem. A* **2000**, *104* (9), 1950–1958.
(51) Skomorowski, W.; Pawłowski, F.; Koch, C. P.; Moszynski, R. Rovibrational Dynamics of the Strontium Molecule in the $A^1\Sigma u^+$, $c^3\Pi_u$, and $a^3\Sigma^+_u$ Manifold from State-of-the-Art Ab Initio Calculations. *J. Chem. Phys.* **2012**, *136* (19), 194306.
(52) Gerber, I. C.; Ángyán, J. G. Potential Curves for Alkaline-Earth Dimers by Density Functional Theory with Long-Range Correlation Corrections. *Chem. Phys. Lett.* **2005**, *416* (4), 370–375.
(53) Jutzi, P.; Burford, N. Structurally Diverse π-Cyclopentadienyl Complexes of the Main Group Elements. *Chem. Rev.* **1999**, *99* (4), 969–990.
(54) Deacon, G. B.; Stellfeldt, D.; Meyer, G. The Solubility of Bis(Cyclopentadienyl)Samarium(II) and Implications for the Reaction of Samarium Metal with Bis(Cyclopentadienyl)Mercury(II). *Z. Anorg. Allg. Chem.* **2000**, *626* (3), 623–624.
(55) J. Bridgeman, A. The Shapes of Bis(Cyclopentadienyl) Complexes of the s-Block Metals. *J. Chem. Soc. Dalton Trans.* **1997**, No. 17, 2887–2894.
(56) Kaupp, M.; Schleyer, P. v. R.; Dolg, M.; Stoll, H. The Equilibrium Structures of Monomeric Group 2 and Lanthanide(II) Metallocenes MCp_2 (M = Calcium, Strontium, Barium, Samarium, Europium, Ytterbium) Studied by Ab Initio Calculations. *J. Am. Chem. Soc.* **1992**, *114* (21), 8202–8208.
(57) Rayón, V. M.; Frenking, G. Structures, Bond Energies, Heats of Formation, and Quantitative Bonding Analysis of Main-Group Metallocenes $[E(Cp)_2]$ (E=Be–Ba, Zn, Si–Pb) and [E(Cp)] (E=Li–Cs, B–Tl). *Chem.—Eur. J.* **2002**, *8* (20), 4693–4707.
(58) Bridgeman, A. J.; Empson, C. J. Bond Orders between Molecular Fragments. *Chem.—Eur. J.* **2006**, *12* (8), 2252–2262.
(59) Tatsumi, K. Extended Hückel MO Study on Electronic Structures of Samarocene Complexes. Kidorui, **1996**, No. 28, 272–273.
(60) Suresh, C. H.; Koga, N. A Molecular Electrostatic Potential Bond Critical Point Model for Atomic and Group Electronegativities. *J. Am. Chem. Soc.* **2002**, *124* (8), 1790–1797.
(61) Reed, A. E.; Weinstock, R. B.; Weinhold, F. Natural Population Analysis. *J. Chem. Phys.* **1985**, *83* (2), 735–746.
(62) Bader, R. F. W. *Atoms in Molecules : A Quantum Theory*; Oxford University Press: New York, 1994.

Chapter 3

Mechanochemically Driven Transformations in Organotin Chemistry: Stereochemical Rearrangement, Redox Behavior, and Dispersion-Stabilized Complexes

Reprinted with permission from Ross F. Koby, Nathan D. Schley, and Timothy P. Hanusa. *J. Am. Chem. Soc*. 2018, 140, 15934–15942

3.1 Introduction

Mechanochemistry, especially in the form of grinding and ball milling, is a technique that has experienced a resurgence in modern preparative chemistry, encompassing the synthesis of organic,[1–3] organometallic,[4–11] coordination compounds,[12–15] and the generation of new nanomaterials.[16,17] In the broadest sense, a mechanochemical reaction is one induced by the direct absorption of mechanical energy. Such energy can be supplied in various forms, including that from surface friction (tribology), sound (sonochemistry), shock waves, bond stretching (in macromolecular systems), and trituration (grinding and milling). The last form is under consideration here.

In most cases, reactions performed mechanochemically require little to no solvent, use less energy, and proceed more quickly than conventional solvent-based reactions. Besides being compatible with the philosophy and practice of green chemistry,[18–21] mechanochemistry can significantly alter reaction outcomes. Kinetics and mechanisms can be drastically changed,[2] providing access to new products in higher yields and shorter reaction times than otherwise possible.[3] Most intriguingly, mechanochemistry has been used to form a variety of organic and organometallic compounds not available through solution methods, revealing pathways to compounds that are unique to the solid-state approach.

The reasons that mechanochemically promoted syntheses can differ from solution-based reactions are varied. For example, the solvents required to dissolve starting materials might also attack the product; this is the reason that only a mechanochemical approach was successful in producing the unsolvated tris(allyl) aluminum complex [AlA′$_3$] {[A′] = [1,3-(SiMe$_3$)$_2$C$_3$H$_3$]$^-$} (Figure 2la).[4] Alternatively, usable solvents, even at their boiling points, may not provide enough energy input to overcome the reaction barrier, preventing a molecule from being assembled, as with the sterically encumbered adamantoid phosphazane P$_4$(N^{t}Bu)$_6$ (Figure 2lb).[22] In a third case, owing to different reaction rates and effective concentrations of reagents, solution-based and mechanochemical reactions may reach different end points, as in the reaction of C_{60} with KCN. In solution, the reaction stops with the hydrocyanation product [C_{60}(CN)]$^-$, whereas in the solid state, the cyano anion reacts with additional C_{60} to form the fullerene dimer, C_{120} (Figure 2lc).[23,24] These

examples do not exhaust the ways that solvent removal combined with mechanochemical activation can facilitate the synthesis of new compounds. We describe here the formation through mechanochemical synthesis of sterically bulky allyl compounds that exist because of a disproportionation reaction involving tin. The redox process is not observed when the reaction is conducted in solution.

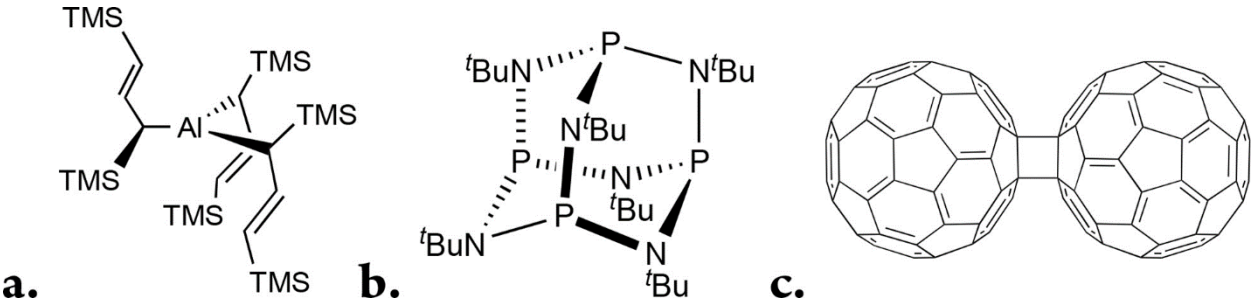

Figure 20. Compounds formed exclusively through mechanochemical methods: (a) an unsolvated tris(allyl) complex, [Al{1,3-$(SiMe_3)_2C_3H_3$}$_3$]; (b) a ^{t}Bu-substituted phosphazane; and (c) the fullerene dimer, C_{120}.

It should be noted that many organotin(IV) species display considerable thermal, hydrolytic, and oxidative stability, which in general is a result of kinetic factors and not especially strong Sn–C bonds. For example, [$SnMe_4$] decomposes above 400 °C, for example, but its mean bond enthalpy [$\overline{D}$(Sn–C)] is only 52 kcal mol^{-1}.[25] The corresponding neutral tin(II) alkyl and aryl complexes (stannylenes, [:SnR_2]) in contrast, are generally more reactive and unless stabilized with sterically bulky groups[26] or cyclopentadienyl ligands,[27] commonly occur only as transient reaction intermediates.[28] Sterically enhanced allyl ligands[29–32] have been used to suppress oligomerization and enhance kinetic stability in a wide range of metal complexes and offer a way to generate stabilized tin(II) allyl species. Layfield et al. explored the use of the trimethylsilylated allyl ligand A′ with tin, demonstrating that the reaction of 3 equiv of K[A′] with $SnCl_2$ in THF leads to the stannate [SnA'_3K(THF)], in which the THF-coordinated potassium ion also interacts in a cation-π fashion with the double bonds of the three allyl ligands (Figure 22a).[33] The same structural motif is found in isostructural beryllium[34] and zinc[35] complexes (Figure 22b). These compounds have no counterparts with unsubstituted allyl ligands.

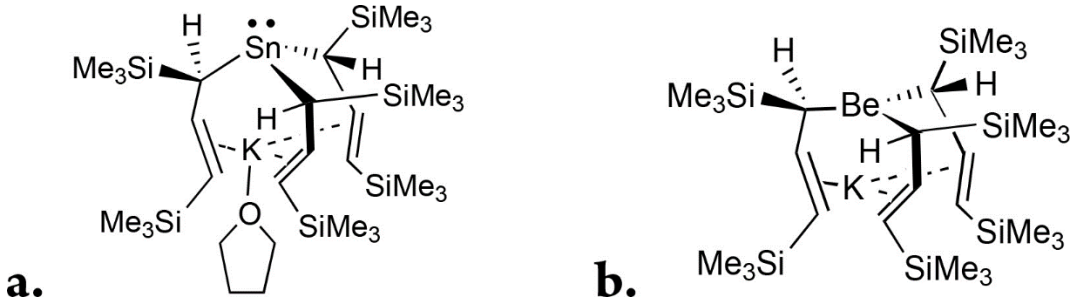

Figure 21. (a) Schematic of [SnA′$_3$K(THF)]; the coordination around Sn is pyramidal, with the sum of C–Sn–C′ angles = 288.5°. (b) Schematic of [BeA′$_3$K]; Be is in a near planar environment, with the sum of C–Be–C′ angles = 357.6°.Similar trigonal planar coordination is found in the [ZnA′$_3$M] (M = Li, Na, K) complexes.

All the [M^{II}A′$_3M^I$(THF)$_n$] metallates are found in a C_3-symmetric *R*,*R*,*R* (or *S*,*S*,*S*) configuration, with the stereodescriptors referring to the attachment site of the allyls to the metal centers. In contrast, the related neutral MA′$_3$ (M = As, Sb, Bi) complexes exist in two diastereomeric forms, with *R*,*R*,*R* (equivalently, *S*,*S*,*S*) and *R*,*R*,*S* (or *S*,*S*,*R*) arrangements.[36] It is likely that the alkali metal counterions in the anionic complexes serve to template the arrangement of the allyl ligands around the central element.[34]

3.2 Results

Even though the unsubstituted di(allyl)tin [Sn(C_3H_5)$_2$] is unknown, it seemed possible that the use of only 2 equiv of K[A′] and the avoidance of a coordinating reaction solvent could lead to the isolation of the substituted analogue, [SnA′$_2$]. Monomeric [SnA′$_2$] is calculated to be a minimum on its potential energy surface at the B3PW91-D3BJ/def2-TZVPD level. The dissociation step SnA′$_2$ → •SnA′ + •A′ is estimated as 36.8 kcal mol^{-1} ($\Delta H°$; $\Delta G°$ = 22.1 kcal mol^{-1}). Of course, were [SnA′$_2$] to be generated, it might well exist in the form of a coordination polymer with different energetics. See the appendix for geometry-optimized coordinates.

As a check to ensure that mechanochemical activation was actually needed, stirring a mixture of K[A′] and $SnCl_2$ in hexanes produced no reaction, but grinding the same solids together in a 2:1 ratio for 5 min in a planetary ball mill generated a brown powder that was partially hexanes-soluble. Filtration of a hexanes extract to remove insoluble matter, evaporation of the filtrate, and subsequent crystallization from hexanes led to the isolation of canary yellow crystals of **1**, the ^{1}H NMR spectrum of which shows five resonances characteristic of σ-bound A′ ligands [two singlets for the trimethylsilyl groups and three allylic signals; details in the appendix]. This data and the observation of a singlet in the ^{119}Sn NMR spectrum at δ –138.7 ppm, not far from the δ –132.9 ppm resonance reported for [SnA′$_3$K(THF)],[33] suggested that a similar structure might be involved, despite the suboptimal ratio of reagents in the mechanochemical reaction. It should be noted that **1** is evidently the most stable (and the most easily generated) product of the

K[A′]:$SnCl_2$ system, as it can be formed under a range of mechanochemical conditions, including changes of scale and reaction stoichiometry (from 1:1 to 5:1), although its purity and yield varies with the specific reaction parameters used (see additional examples in the appendix).

A single-crystal X-ray structure of **1** revealed that the compound was in fact the stannate [SnA'_3K], with three σ-bound allyl ligands on tin and the K^+ counterion coordinated to the π-bonds of the allyl ligand (Figure 23). The core structure, with its $\mu:\eta^2:\eta^1$-bonding arrangement to K and Sn, is thus isostructural with the THF-solvated Sn species and with the Zn and Be counterparts. Owing to the lack of coordinated THF in **1**, the K^+ is located more deeply inside the "umbrella" formed by the three allyl ligands than is the case in the THF-solvated species. This is reflected in the $K^+\cdots$Sn separation of 3.537(1) Å in **1**, notably shorter than the corresponding 3.666(3) Å distance in the solvate.[33] As a result, two of the α-carbons are found at the same distances from the K^+ (3.01, 3.07 Å) as are the olefinic carbons (average distance of 3.06 Å), even though the α-carbons are saturated and not similarly basic. The $[SnA'_3]^-$ framework distorts enough that the third $K^+\cdots$α carbon contact ($K^+\cdots$C10) is moved away to 3.20 Å.

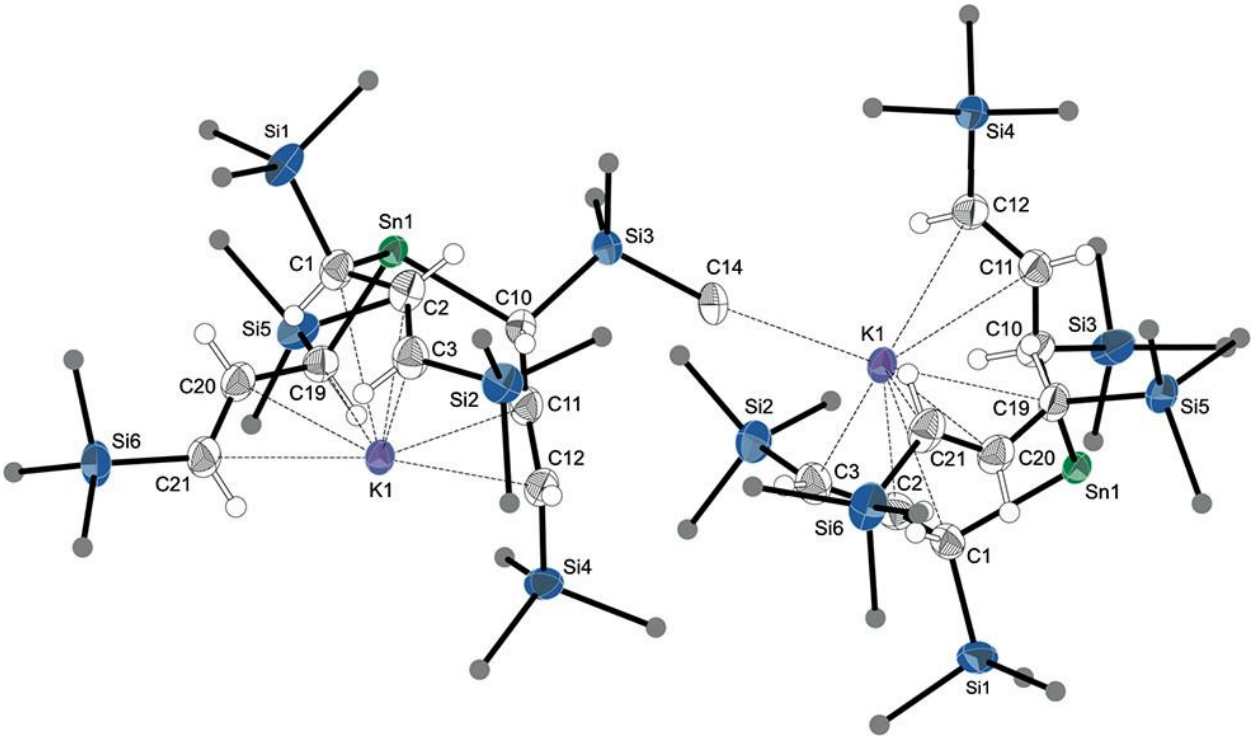

Figure 22. Thermal ellipsoid plot (50% level) of two molecules of **1**. For clarity, hydrogens have been removed from trimethylsilyl groups, and with the exception of C14, their carbon atoms have been replaced with gray circles. Selected bond distances (Å) and angles (deg): Sn1–C1, 2.324(5); Sn1–C10, 2.346(5); Sn1–C19, 2.310(5); K1–C1, 3.073(7); K1–C2, 3.090(6); K1–C3, 2.979(6); K1–C10, 3.204(5); K1–C11, 3.126(5); K1–C12, 3.007(5); K1–C19, 3.010(6); K1–C20, 3.069(6); K1–C21, 3.062(5); K1···C14, 3.198(8); C1–Sn1–C10, 97.47(19); C1–Sn1–C19, 96.77(19); C10–Sn1–C19, 95.45(18).

A notable difference of **1** from its Be, Zn, and solvated-Sn precedents is that it exists in the solid state as a coordination polymer, with the K^+ ion interacting with a methyl group on a neighboring molecule at a distance of 3.198(8) Å. This distance is about 0.1 Å longer than that of K^+ to the olefinic carbons of the allyl groups, but it is similar to the $K^+\cdots CH_3$ linkage found in the coordination polymer $[K(18\text{-}C\text{-}6)SnMe_3]_\infty$ [3.181(3) Å], for example, or in the discrete anion $[(Me_2SnCH_3)K(18\text{-}C\text{-}6)SnMe_3]^-$ anion [3.237(2) Å].[37] DFT calculations on the latter provided a $K^+\cdots CH_3$ force constant (k) of 16–17 N m^{-1}, in the range of hydrogen bonds.[37] The unit cell of **1** ($P2_1/n$, $Z = 4$) comprises parts of two chains; all of the stannate units in a single chain possess the same arrangement of allyl ligands around the tin (*R*,*R*,*R* or *S*,*S*,*S*, with the latter shown in Figure 23). The other chain displays the opposite configuration, so that a racemic mixture of chains is present.

The weakness of the intermolecular interaction in **1** explains its facile disruption, as happens due to the presence of the coordinated THF ligand in $[SnA'_3K(THF)]$.[33] The ease of such disruption was also demonstrated from one particular recrystallization attempt of **1**, in which trace adventitious water, evidently from the solvent, was found to be bound to the K^+ ion, interrupting the $K^+\cdots CH_3$ linkage and converting the stannate into discrete solvated monomers, $[SnA'_3K(OH_2)]$, **2** (Figure 24). The near absence of other evidence of hydrolysis products (e.g., HA′ in ^{1}H NMR) is a testament to the minute amount of water involved, to the greater Lewis acidity of K^+ relative to the tin center, and to the relatively low polarity of the Sn–C bonds. Like $[SnA'_3K(THF)]$, **2** has crystallographically imposed 3-fold symmetry (the H atoms on water are disordered), and the water is associated with an increase in the effective coordination number of K^+. The average distance of the K^+ to the olefinic carbons lengthens from 3.06 Å in **1** to 3.13 Å in **2**, a change that tracks with the difference between the ionic radii of six- and seven-coordinate K^+ (0.08 Å).[38]

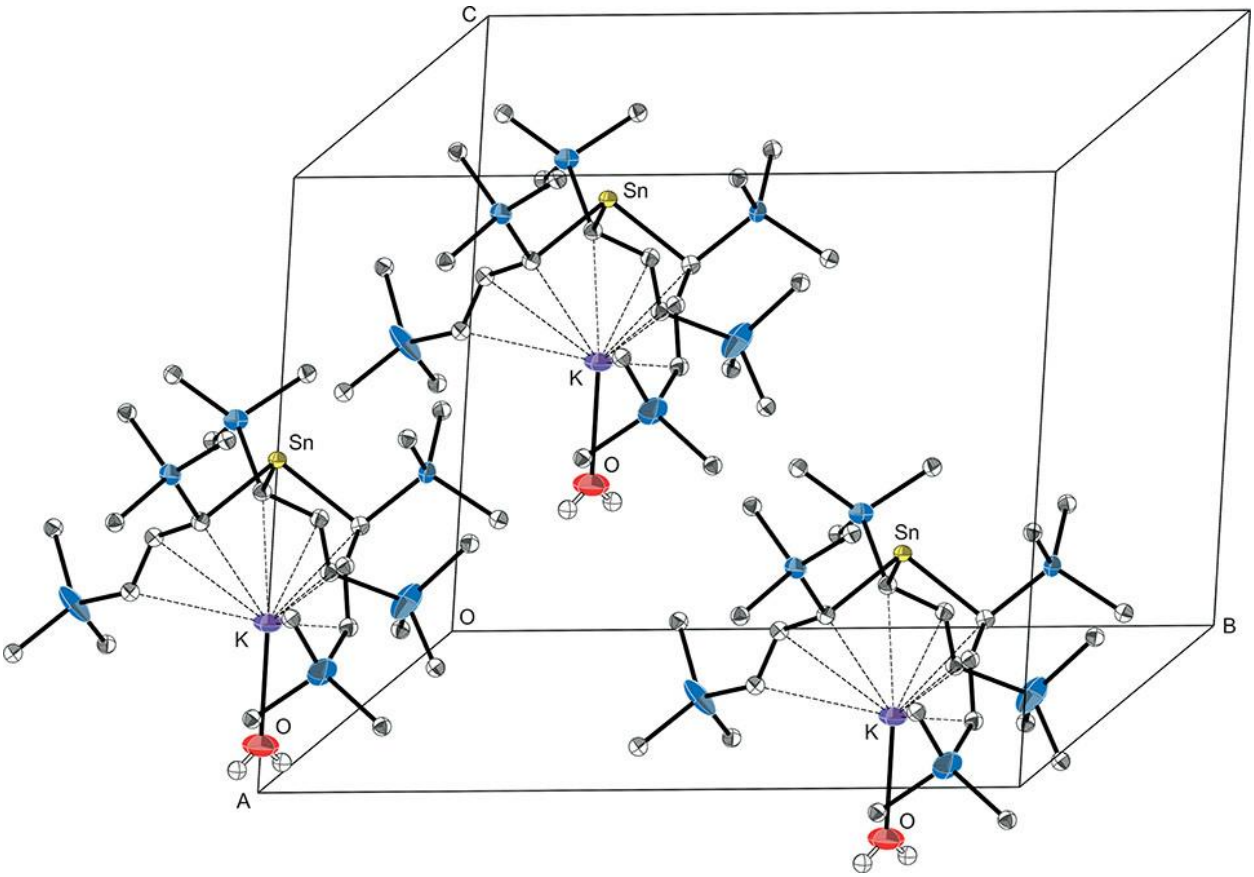

Figure 23. Thermal ellipsoid plot (50% level) of the unit cell of **2** (space group *R*3*m*, *Z* = 3). For clarity, all hydrogens have been removed except from the water molecules, and carbon atoms have been assigned arbitrary isotropic radii. Crystallographically imposed disorder in the allyl ligands has also been removed. Selected bond distances (Å) and angles (deg): Sn–C, 2.338(7); K–O, 2.729(14); K···C, 3.09–3.17 Å; C–Sn–C′, 96.6(2).

The possibility that the unsolvated **1** might be usable as a six-e⁻ donor ligand, isoelectronic with Cp^-, and a tripodal synthon for heterobimetallic allyl complexes[33] prompted a more thorough examination of its preparation. As a first step, the reagent stoichiometry of K[A′] and $SnCl_2$ was adjusted from 2:1 to 3:1, in order to improve the yield of the original reaction; this was also the ratio originally used to produce [$SnA'_3K(THF)$] in THF.[33] Now, however, milling the two reagents for 5 min left an oily residue. Extracting the solid with hexanes left an insoluble heterogeneous mixture of light bluish-gray and dark gray powders, assigned to potassium chloride and tin metal, respectively. Milled KCl typically has a pale bluish-gray appearance, visibly distinct from the tin remaining after the formation of the Sn(IV)-containing **3**. As a check on the presence of other tin species, a ^{119}Sn NMR spectrum was taken of the powder placed in C_6D_6; no signal was observed from δ +500 to –2000 ppm

Filtration of the hexanes extract followed by removal of solvent from the filtrate left a beige solid (**3**). It quickly became evident that **3** was a substance considerably different from the intended **1**.

A striking feature of **3** is its instability in solution. In the solid state at room temperature under an inert atmosphere, **3** is sufficiently stable to obtain combustion analysis and to confirm the bulk purity of the freshly prepared material. Even a 6-month-old sample was only partially decomposed and contained crystals of satisfactory quality to allow a redetermination of its X-ray structure (see below). However, when dissolved in hexanes, only about 1 h of working time is available before visible decomposition is evident, which is accompanied by the formation of a precipitate. One of the species present in the aged solution is tetrakis(trimethylsilyl)-1,5-hexadiene {A'_2}, a product of allyl radical coupling.[39] Nevertheless, rapid recrystallization is possible from freshly prepared hexanes solutions, and although crystals suitable for X-ray analysis could be obtained this way (see below), such attempts often resulted in the formation of oily solids. When dissolved in C_6D_6 at room temperature for the purpose of NMR studies, the onset of decomposition is even more rapid, with the initial amber solution beginning to turn brown after *ca.* 10 min and eventually yielding a dark precipitate. This had the consequence of making clean NMR spectra difficult to obtain. Even with the additional step of freezing the sample in liquid nitrogen immediately after preparation and thawing it just before signal collection, decomposition products were invariably detectable in NMR spectra.

Despite difficulties with sample stability, a ^{119}Sn NMR spectrum of **3** was eventually obtained that displayed a single peak at δ –36.6 ppm, a roughly 100 ppm downfield shift from that for [SnA'_3K]. If all else were equal, the decrease in shielding would suggest a reduction in metal coordination number, but given the broad chemical shift range for ^{119}Sn in complexes with hydrocarbyl ligands (over 1000 ppm)[40] and the high sensitivity of the shift to minor structural changes, this alone was not diagnostic of the structural differences from [SnA'_3K]. The ^{1}H NMR spectrum contains resonances consistent with σ-bonded allyl ligands, but these are also not determinative of structure. The identity of **3** was eventually established from the results of a single-crystal X-ray study, performed on a crystal obtained from a rapidly evaporated hexanes solution. It proved to be the tetra(allyl)tin(IV) species, [SnA'_4] (Figure 25), which represents the first crystal structure of a homoleptic tin allyl complex. Its formation, discussed below, also represents the first example of a mechanochemically driven organometallic disproportionation reaction, occurring without the benefit of added external oxidants.[9,41]

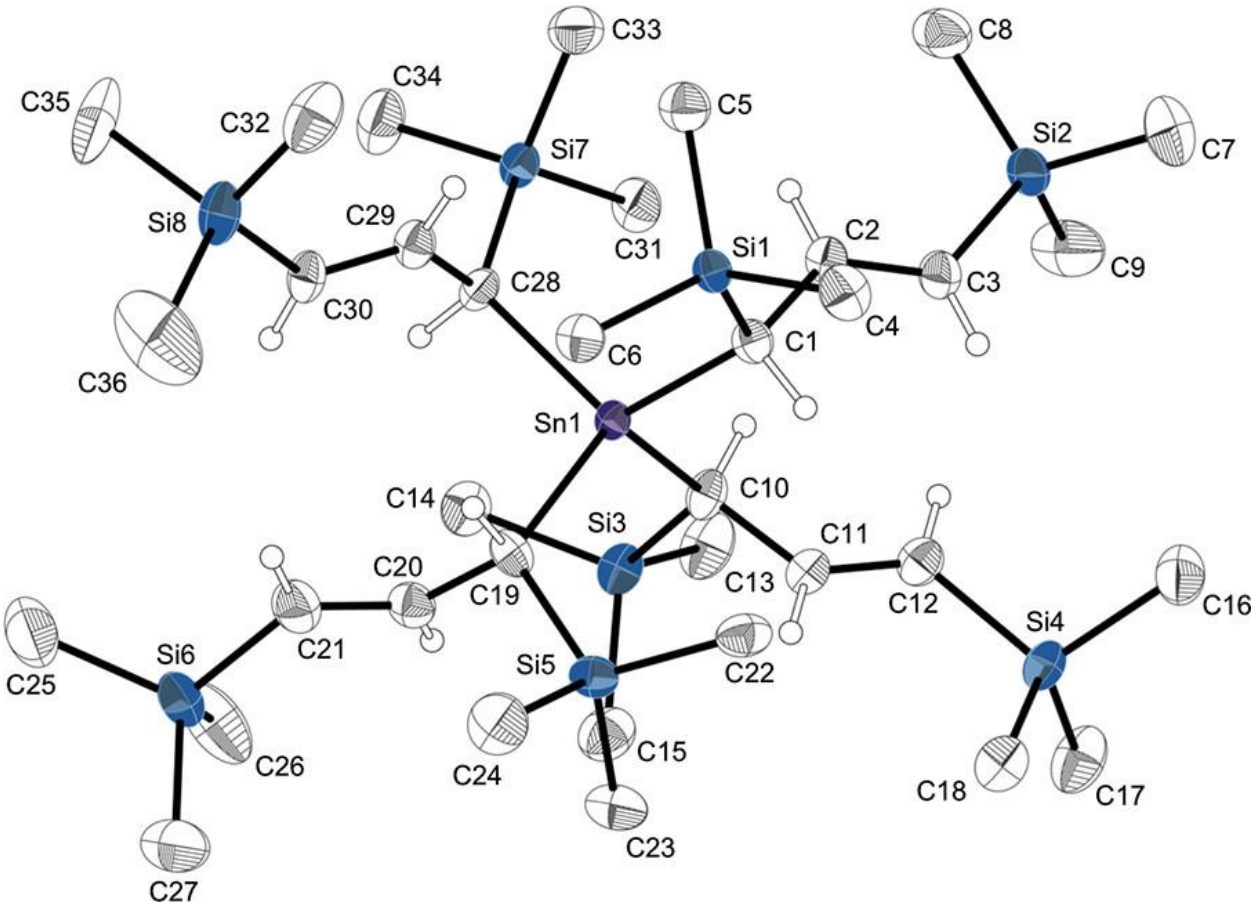

Figure 24. Thermal ellipsoid plot (50% level) of **3**. For clarity, hydrogens have been removed from trimethylsilyl groups and the others assigned an arbitrary radius. Selected bond distances (Å) and angles (deg): Sn1–C1, 2.195(6); Sn1–C11, 2.203(5); Sn1–C19, 2.206(5); Sn1–C28, 2.195(6); C1–C2, 1.493(8); C2–C3, 1.337(8); C10–C11, 1.490(8); C10–C11, 1.490(8); C19–C20, 1.495(10); C20–C21, 1.334(9); C28–C29, 1.484(8); C29–C30, 1.333(9); C1–Sn1–C10, 105.2(2); C1–Sn1–C19, 110.0(3); C1–Sn1–C28, 112.7(2); Sn1–C1–C2–C3, 111.5(5); Sn1–C10–C11–C12, 126.4(4); Sn1–C19–C20–C21, 123.6(5); Sn1–C28–C29–C30, 101.7(5)

Around the central tin atom of **3**, four σ-bound allyls are arranged in a distorted tetrahedral fashion, all of which are attached with the same relative stereochemistry, generating a chiral center. (In the crystal selected for analysis, the orientation is *S*,*S*,*S*,*S*, although under a microscope with polarizing filters, crystals that rotated light with the opposite orientation were also observed.) The combined effect is to give the molecule approximate D_2 symmetry, although this is not crystallographically imposed. The average Sn–C bond length of 2.200(11) Å is on the long end of known Sn–C(allyl) distances in Sn(IV) compounds, but it is similar to that found for the Sn–allyl bond in the trimethylsilylated compound $Sn(CH_2Ph)_2[C(SiMe_3)_3][CH_2CH{=}C(SiMe_3)_2]$ [2.19(1) Å].[42] The Sn–C–C=C torsion angles range from 101.7° to 126.4°, averaging 115.8°. The angles are larger than typical values observed in Sn-allyl compounds (100° ± 10°; see below), but they can be

influenced by steric crowding {the value in $Sn(CH_2Ph)_2[C(SiMe_3)_3][CH_2CH = C(SiMe_3)_2]$ is 128.5°}.[42]

To gain further insight into the origins of both **1** and **3**, both of which involve sub-stoichiometric ratios of reagents, a wider range of reagent ratios and grinding times (up to 60 min) was studied. With a 2:1 ratio of K[A′]:$SnCl_2$ and a 15 min grinding time, a more complex mixture of products was observed, including **1**, **3**, and a small amount of a new substance (**4**) that displayed a single peak in its ^{119}Sn NMR spectrum at δ –32.5 ppm, close to but distinctly different from the δ –36.6 ppm shift for **3**. It yielded crystals following the standard workup with hexanes, but the best X-ray diffraction data that could be obtained was from a crystal that proved to be twinned and from which almost no high-angle information was obtained, so that the resulting structure was essentially of connectivity only quality. Nevertheless, the space group ($P\bar{1}$, Z = 2) was clearly different from that for **3** ($P2_1$), and the heavy atom connectively is not in doubt. It proved to be a diastereomer of **3**; specifically, the connectivity of the allyl ligands to the tin has *R*,*S*,*R*,*S* stereochemistry, so that the molecule has *meso* symmetry (Figure 26). The idealized symmetry of **4** is S_4, rather than the D_2 of **3**.

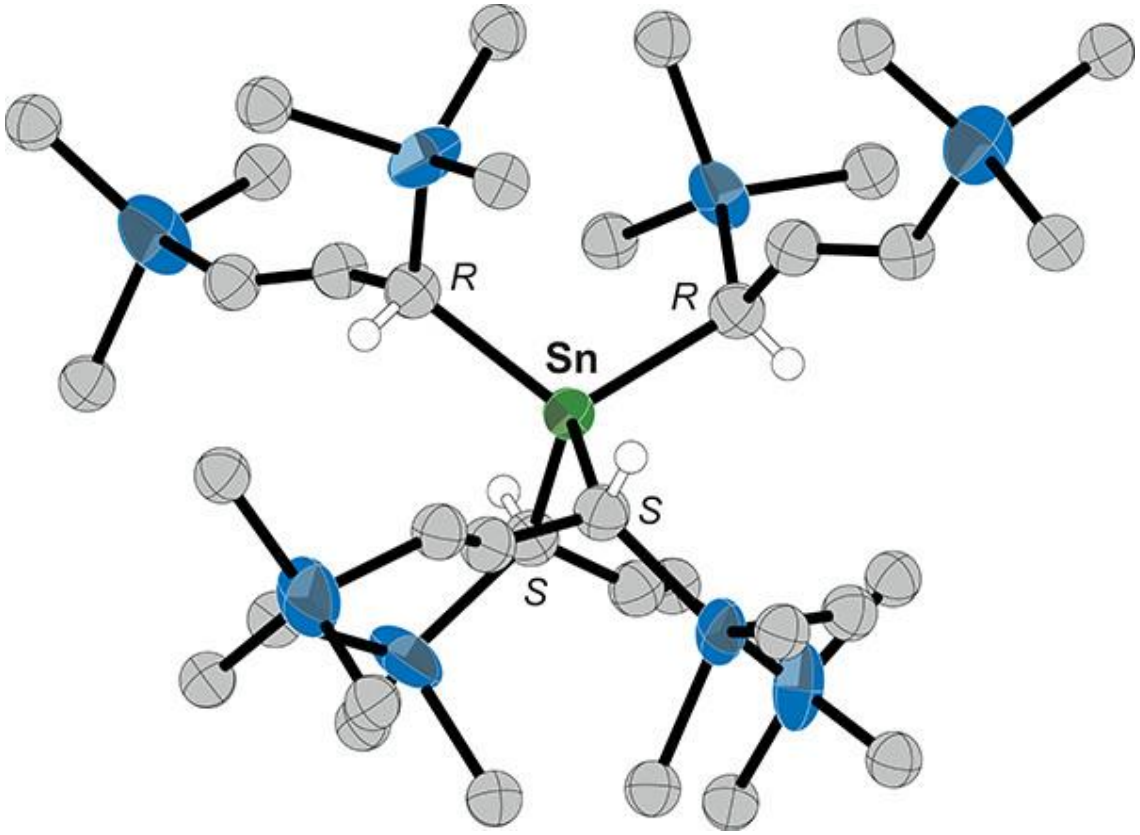

Figure 25. Connectivity of **4**. Thermal ellipsoids of Sn and Si are at 50% probability; carbon atoms are given arbitrary radii, and all hydrogens have been removed except for those required to illustrate the stereochemistry at the α-carbon positions.

Milling the 3:1 mixture of starting materials for 15 min led to a mixture similar to that observed with the 2:1 ratio; i.e., not only was **3** present, but also **1**, **4**, and K[A′]. Extending the grinding time to 60 min did not reveal any other identifiable tin-containing species (search conducted from δ +500 to –2000 ppm).

3.3 Discussion

Determining the course of mechanochemically activated reactions is challenging, and although substantial progress has been made in recent years by employing synchrotron radiation[43–45] or ex-situ Raman spectroscopy,[46–49] such experimental setups are not yet common or universally applicable.[50,51] In the present case, despite the complex inter-relationships between the various compounds produced from $SnCl_2$ with K[A′], a plausible scheme for the reactions with a 2:1 ratio of reagents that captures the nonstoichiometric origin of the compounds can be constructed (Figure 27). The nonstoichiometric formation of **1** and **3** has precedent in beryllium chemistry, where [KBeA′$_3$] is formed from the milling of a 2:1 mixture of K[A′] and $BeCl_2$.[34] There is also related nonstoichiometric behavior known in (solution-based) tin chemistry, as the reaction of a 3:1 ratio of Li[^{i}Pr] and $SnCl_4$ does not produce the expected [Sn^{i}Pr$_3$Cl] but rather gives rise to a mixture of [Sn^{i}Pr$_4$], [Sn^{i}PrCl$_3$], and [Sn^{i}Pr$_2$Cl$_2$] in roughly equal amounts.[52] The rapid formation of **1** is also paralleled in the formation of [KBeA′$_3$], which is assembled within 15 min of the start of milling. The slower conversion of the starting materials into **3** and **4** is understandable based on the need for redox reactions to intervene and the ensuing steric congestion around the metal center.

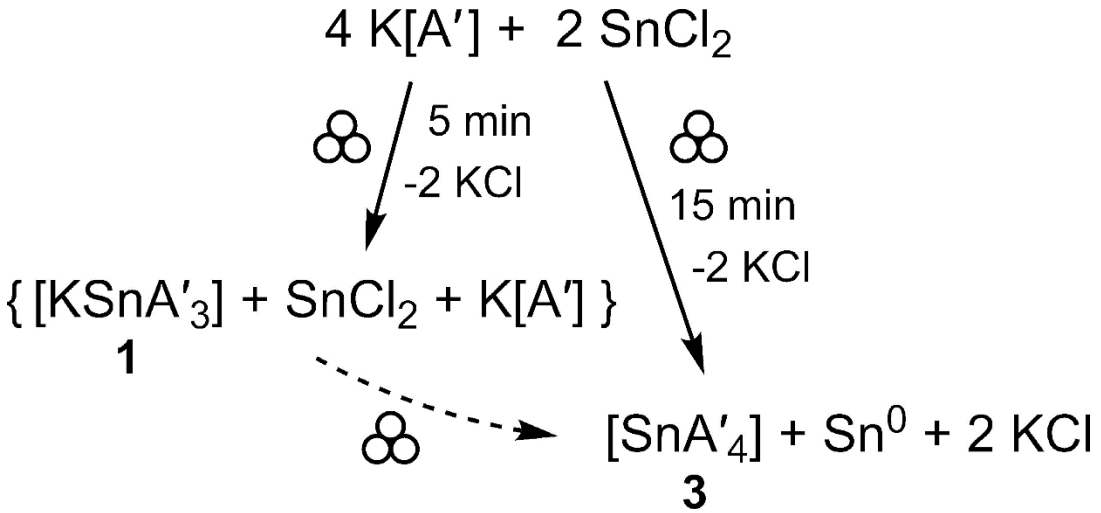

Figure 26. Possible Formation of **1** and **3** from a 2:1 Ratio of K[A′] and $SnCl_2$

Computational investigations were performed to provide insight into the properties of **3** and its relationship to **1** and **4**. DFT calculations were conducted with the B3PW91 hybrid functional[53,54] with additional dispersion correction provided by Grimme's D3 dispersion correction[55] and Becke–Johnson dampening (D3-BJ)[56] (see computational details in appendix).

3.3.1 Instability of [SnA′$_4$]

The solution instability of **3** was unanticipated, as the parent tetra(allyl)tin is an air- and H_2O-stable oil (bp 87–88 °C/4 mmHg),[57] and the addition of trimethylsilyl groups to the allyl ligands was, if anything, expected to enhance the stability of the complex. It has of course long been known that organotin complexes with unsaturated ligands (e.g., vinyl, phenyl, allyl) are more labile than the corresponding saturated counterparts, which is the source of their usefulness in synthetic chemistry.[58] In particular, the R_3Sn–allyl bond has been estimated as being *ca*. 10 kcal mol^{-1} weaker than an analogous R_3Sn–alkyl bond, although this number has not been experimentally verified.[59] The source of the weakening has been assigned to the so-called β-tin effect, which involves a hyperconjugative interaction between $\sigma_{M\text{-}X}$ and $(\pi_{C=C})^*$ orbitals.[60–63] This effect is maximized when the Sn–allyl bond is roughly orthogonal to the plane of the C=C group (in practice, the Sn–C–C=C torsional angle is usually found to be in the range of 100° ± 10°). The delocalization of the π-electrons has the consequence of weakening the Sn–C(allyl) and C=C bonds and greatly elevating the reactivity of allylstannanes with electrophiles. A simplified depiction of the interaction is provided in Figure 28a,b. A semiquantitative indication of the bonding changes is reflected in the Mayer bond orders[64,65] for the model complex [Me_3Sn–A′] (Figure 28c). Whereas the Sn–C(methyl) bond orders are all close to unity (average value of 1.02), that for Sn–C(A′) is 0.81, a 20% decrease. The formal double bond of the allyl ligand is weakened slightly (BO = 1.78), although the BO of the formal C–C single bond does not reflect any strengthening (0.98). Despite these changes in bond strength, something more than the normal β-tin effect must be contributing to the extreme lability of **3**.

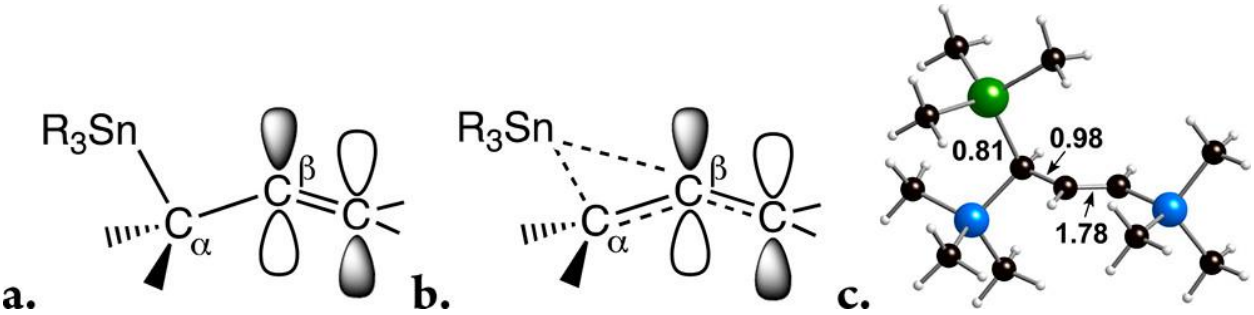

Figure 27. Consequences of hyperconjugative interaction of $\sigma_{Sn\text{-}X}$ and $(\pi_{C=C})^*$ orbitals in allyl–tin species. (a) The formal bonding arrangement without hyperconjugation. (b) The Sn–C(allyl) and C=C bonds are weakened. (c) Mayer bond orders in the allyl ligand of [Me_3Sn–A′] (green = Sn, blue = Si).

A series of calculations was completed to determine whether there were special consequences associated with the hyperconjugation in **3**, beginning with a calibration of the energy of methyl group dissociation from $SnMe_4$ ($SnMe_4 \rightarrow \bullet SnMe_3 + \bullet Me$), for which an experimental value is available [$\Delta H° = 69 \pm 2$ kcal mol^{-1};[66]note that this number is for the first methyl group cleavage, not the mean bond dissociation enthalpy, $\overline{D}$(Sn–C)]. Note

that the first dissociation energy is typically appreciably higher than the second and subsequent steps for many main group homoleptic alkyls.[25] The calculated value, 69.0 kcal mol^{-1} ($\Delta H°$), is in excellent agreement with the experimental figure (Table 4, entry 1). The free energy of dissociation is about 12 kcal mol^{-1} lower than this. For the more relevant reaction involving tetra(allyl)tin [i.e., $Sn(C_3H_5)_4 \rightarrow \bullet Sn(C_3H_5)_3 + \bullet C_3H_5$], both the enthalpy and free energy of dissociation are lowered relative to that of tetramethyltin (entry 2). Notably, the $\Delta G°$ value is 16.2 kcal mol^{-1} less, reflecting a bond weakening consistent with the operation of the β-tin effect.

Table 4: Energies of ligand dissociation (B3PW91-D3BJ, kcal mol^{-1})

No.	Reaction[a]	Energy ($\Delta H°$, $\Delta G°$)
1	$SnMe_4 \rightarrow \bullet SnMe_3 + \bullet CH_3$	+69.0[a], +56.9
2	$Sn(C_3H_5)_4 \rightarrow \bullet Sn(C_3H_5)_3 + \bullet C_3H_5$	+53.0, +40.7
3	$Sn[(1,3\text{-}SiH_3)_2C_3H_3)]_4 \rightarrow Sn[(1,3\text{-}SiH_3)_2C_3H_3)]_3 + \bullet(1,3\text{-}SiH_3)_2C_3H_3$	+59.7, +40.9
4	SnA'_4 (D_2) $\rightarrow \bullet SnA'_3 + \bullet A'$	+70.6, +52.9
5	SnA'_4 (D_2) $\rightarrow \bullet SnA'_3 + \bullet A'$	+41.1, +30.9[b]

[a]Experimental value ($\Delta H°$) = 69±2 kcal mol–1.63 [b]Both $\Delta H°$ and $\Delta G°$ are calculated without dispersion corrections.

Adding silyl (SiH_3) groups to the 1- and 3-positions of the allyls leaves the free energy of dissociation essentially unaffected compared to that of the unsubstituted allyl (Table 4, entry 3). For the full model of **3** ($SnA'_4 \rightarrow \bullet SnA'_3 + \bullet A'$), however, the free energy value actually *increases* by 12 kcal mol^{-1} (Table 4, entry 4), a result that was initially unexpected in view of the substantial increase in the steric bulk of the ligands and the anticipated bond weakening that would occur through inter-ligand Pauli repulsion.

The steric congestion that is present in **3** and **4** can be visualized in the encapsulation of the metal coordination sphere. As estimated with the program Solid-G,[67] and specifically by the value of $G_{complex}$, the net percentage of coordination sphere covered by the ligands, the value for [$SnMe_4$] is low (60.5%) and increases only to 69.7% for [$Sn(C_3H_5)_4$] (Figure 29a). For **3** and **4**, however, the $G_{complex}$ values rise to 97.1% and 96.2%, respectively (Figure 29b,c). Note that values of $G_{complex}$ that approach 100% are associated with molecules that display structural evidence of steric strain, including bond lengthening (and presumably weakening).[67]

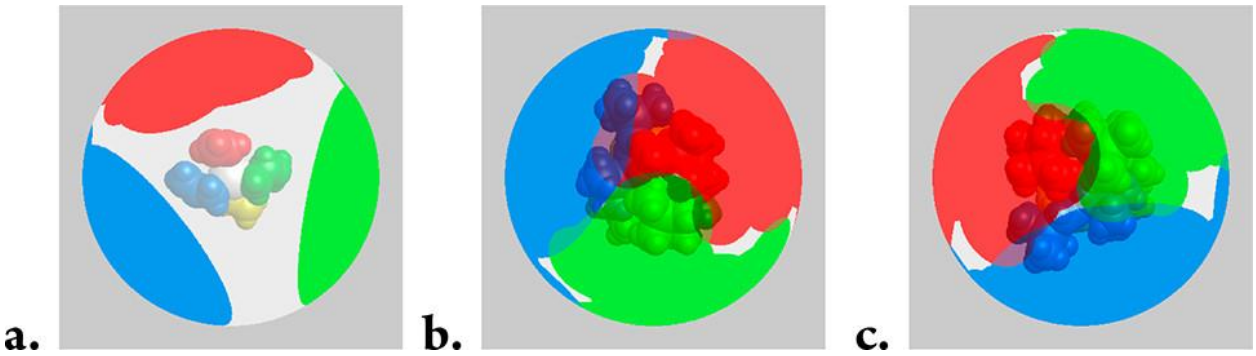

Figure 28. Visualization of the extent of coordination sphere coverage ($G_{complex}$) of (a) $[Sn(C_3H_5)_4]$, 69.7%; (b) **3** (D_2 symmetry), 97.1%; and (c) **4** (S_4 symmetry), 96.2%. Optimized coordinates [B3PW91-D3BJ/def2-TZVP(Sn,Si),def2-SVP(C,H)] and the program Solid-G were used. The $G_{complex}$ value represents the net coverage, so that regions of the coordination sphere where the projections of the ligands overlap are counted only once.

A counteracting consequence of the proximity of the many $-SiMe_3$ groups is that they can serve to stabilize the molecule through the operation of London dispersion forces (LDF). The ability of bulky groups such as *tert*-butyl or $SiMe_3$ to function as "dispensers" of attractive dispersion energy, and not simply as centers of repulsive force, has been computationally demonstrated by Grimme et al.[68] and used to explain the stability of the heavily substituted hexakis(3,5-di-*tert*-butylphenyl)ethane,[69] even though the ostensibly less crowded parent molecule hexaphenylethane cannot be isolated.[70] It has now been recognized that a range of inorganic and organometallic molecules owe their existence to the operation of LDF provided by groups such as terphenyl, $-C(SiMe_3)_3$, $-N(SiMe_3)_2$, and norbornyl.[71]

One of the distinctive structural markers of these LDF-stabilized molecules is the presence of multiple inter-ligand H···H′ contacts that are at or below the sum of the van der Waals radii ($2r_H$ = 2.40 Å).[72] Not surprisingly, both **3** and **4** display numerous such contacts (Figure 30), and significantly, there are no analogous distances in the calculated structures of $[Sn(C_3H_5)_4]$ or $[Sn\{(1,3\text{-}SiH_3)_2C_3H_3\}_4]$.

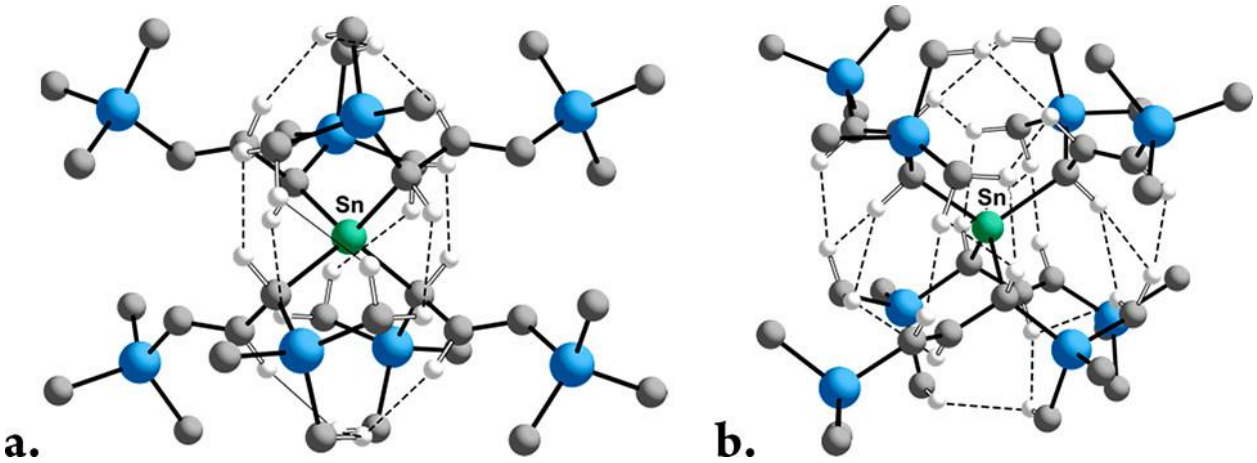

Figure 29. Frameworks of **3** (a) and **4** (b), illustrating H···H′ contacts that are less than the sum of the van der Waals' radii (≤2.4 Å). The contacts range from 2.07 to 2.30 Å in **3** and from 2.01 to 2.29 Å in **4**. Contacts are calculated from the geometry-optimized structures; for contacts from the X-ray data of **3**, see the appendix

Computational support for the importance of LDF in stabilizing **3** was gathered by examining the dissociation reaction ($SnA'_4 \rightarrow \bullet SnA'_3 + \bullet A'$) without explicit dispersion corrections, i.e., using only the unmodified B3PW91 functional (Table 4, entry 5). Both $\Delta H°$ and $\Delta G°$ fall by 42% and are well below the values found for the complex with SiH_3-substituted allyls. This both quantifies the role that LDF plays in stabilizing the molecules and indicates that the $-SiMe_3$ groups would in fact be weakening the bonding owing to steric repulsions if the dispersion forces were not opposing their effects.

Solvent interactions, even from alkanes, can interfere with the action of LDFs,[70] and cyclohexane was found to do so with hexakis(3,5-di-*tert*-butylphenyl)ethane to the extent that $\bullet C_6H_3(3,5\text{-}{}^tBu)_2$ radicals are formed in solution.[70] It is appears that hexanes and toluene exert the same effect on **3**, accounting for its rapid degradation in solution. The presence of $\{A'_2\}$ in the solution spectra of **3** is consistent with the disruption of the inter-ligand LDF and the release of $\bullet A'$ radicals, followed by their subsequent coupling.

3.3.2 Formation of $[SnA'_4]$

Starting from $SnCl_2$ and K[A′], the formation of **3** and **4** obviously involves multiple steps, including the stereoregular assembly of the ligands around the metal and the oxidation of Sn(II) to Sn(IV). It is most likely that the stannate **1** is the precursor to the tetra(allyl)tins (see below), yet given the low yields of **3** (*ca.* 20%), we considered the possibility that it is formed independently of **1**. That is, some of the unreacted $SnCl_2$ remaining after the formation of **1** (see the products of the 5 min grind in Figure 27) could potentially undergo disproportionation to elemental tin and $SnCl_4$, with the latter then reacting with the residual K[A′] to form **3**. Using standard thermodynamic values,[73] the reaction in eq 1 below is in fact slightly favorable.

$$2SnCl_2\ (s) \rightarrow SnCl_4\ (l) + Sn(s) \quad (\Delta G° = -5.6\ kcal\ mol^{-1}) \qquad (1)$$

This reaction can occur thermally, but at most to the extent of ca. 10% and then only above temperatures of 500 °C.[74] In test grinds of $SnCl_2$ alone (with times up to 2 h at 600 rpm in a planetary mill under N_2), we found no evidence for the formation of $SnCl_4$, suggesting that the reaction is kinetically inhibited. $SnCl_2$ is a white, air-stable solid (mp 246 °C); $SnCl_4$ is a hygroscopic liquid (mp –33 °C) that fumes on contact with air. The ground sample of $SnCl_2$ was unchanged in appearance: there was no darkening, as would be the case if elemental tin had formed; no liquid was present; and the solid was not noticeably clumped together, as might have occurred as a result of partial formation of $SnCl_4$. There was no visible evidence of any fuming when the ground powder was exposed to air.

Since the testing conditions were considerably more energetic than those present during the formation of **3**, it seems safe to discount this route as the source of Sn(IV). It is consequently much more likely that the tin that becomes oxidized is that in the stannate itself, given that the tin center is more electron rich in **1** than in $SnCl_2$ and that the stereochemical attachment is already set for the three allyl ligands. Only a single ligand needs to attach in the same conformation as the first three to generate **3**. The interchange of the ligands and the electron transfer are sketched in a schematic (Figure 30).

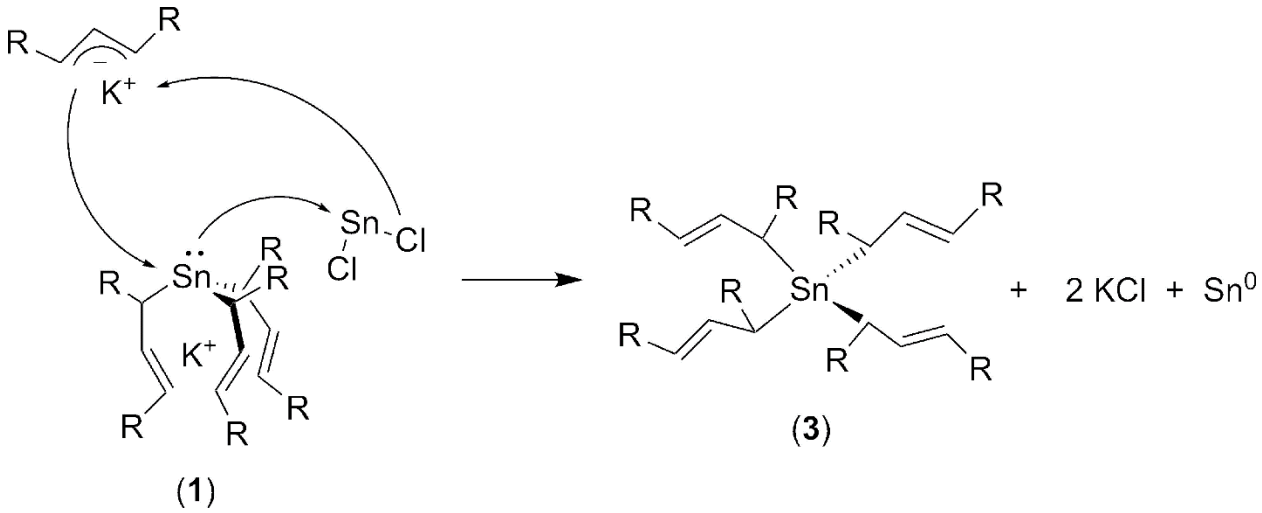

Figure 30. Proposed formation of **3** from **1**(R = $SiMe_3$). This is a schematic to account for the reconnection of the various molecular fragments, not a detailed mechanism.

Compound **4** never appears apart from **3** and then only at longer grinding times, suggesting that its formation is more difficult and takes additional steps. To compare the two energetically, both **3** and **4** were optimized under their idealized symmetry, i.e., D_2 and S_4, respectively. At the level of theory employed here, both are minima on their respective potential energy surfaces, and **4** is higher in energy by 7.8 kcal mol^{-1} ($\Delta G°$). This is consistent with the faster formation of **3**, but it also speaks to the more complicated route required to synthesize **4**. Formation of **4** from **3** would require a loss of two allyl ligands and their reattachment with the opposite stereoconfiguration. Starting with **3** with a (*S*,*S*,*S*,*S*) configuration, for example, loss of a ligand and then reattachment with inverted stereochemistry would lead to an (*R*,*S*,*S*,*S*) intermediate, found to be 11.8 kcal mol^{-1} higher in energy than **3**. Repetition of the process with another *S*-bound allyl would generate the S_4 form, 4.0 kcal mol^{-1} ($\Delta G°$) lower in energy than the intermediate. The three relevant forms are compared in Figure 32

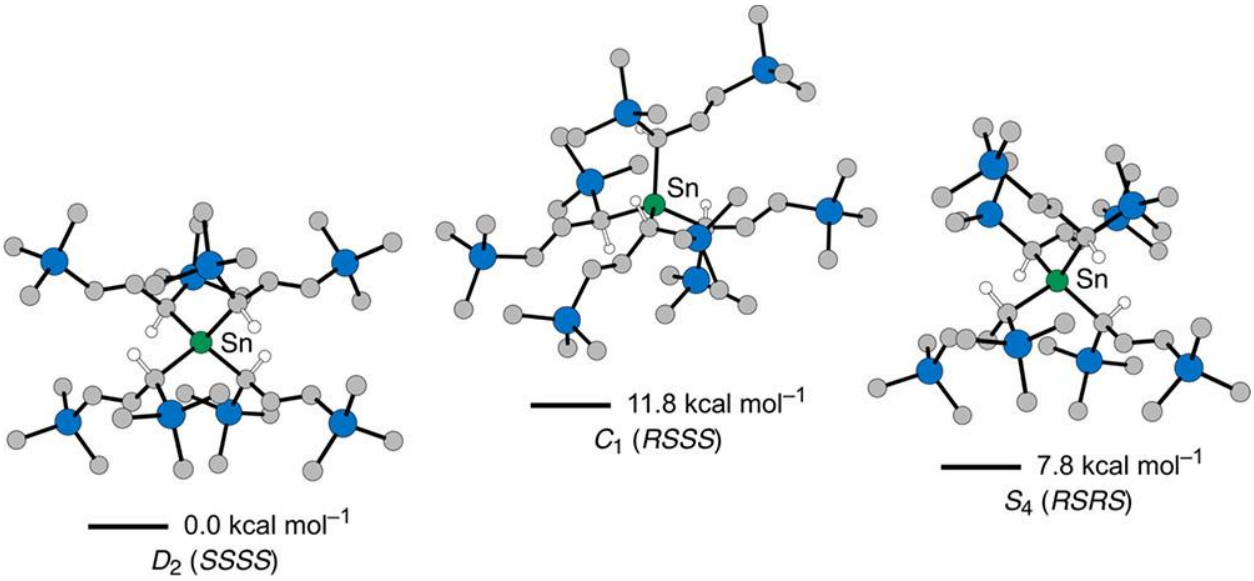

Figure 31. Relative energies of **3**, a nonsymmetric intermediate, and **4**, with conformations of (*S*,*S*,*S*,*S*), (*R*,*S*,*S*,*S*), and (*R*,*S*,*R*,*S*), respectively. Geometries were calculated at the B3PW91-D3BJ/def2-TZVP(Sn, Si), def2-SVP(C,H) level.

3.3 Conclusion

In summary, we have established that the nonstoichiometric reactions observed in beryllium and zinc chemistry with a sterically bulky allyl ligand occur also with tin under mechanochemical conditions, producing a stannate, [SnA′$_3$K], from a 2:1 mixture of the potassium allyl K[A′] and $SnCl_2$. Furthermore, extended grinding initiates a redox reaction, from which tetra(allyl)tins, in both chiral and *meso* forms, can be isolated. The work demonstrates that even in the absence of solvent, stereochemical control can be maintained during the assembly of compounds, from the *R*,*R*,*R*/*S*,*S*,*S* chains of the allyl stannate to the fully *R*,*R*,*R*,*R*/*S*,*S*,*S*,*S* forms of the tetra(allyl)tin [SnA′$_4$].

Both **3** and **4** evidently owe their solid-state stability to the operation of London dispersion forces provided by their $SiMe_3$ groups, which compensate for their otherwise sterically congested ligand environments. Considering that neither the unsolvated stannate **1** nor the solution-unstable tetra(allyl)tins are isolable from solvent-based reactions, these results exemplify unique characteristics of mechanochemical activation. A high probability exists that related transformative organometallic chemistry is to be found with other redox-active elements.

3.3 Appendix

Experimental Details

General Considerations. All manipulations were performed with the exclusion of air and moisture using Schlenk or glovebox techniques. Proton and carbon ($^{13}C\{^1H\}$) NMR spectra were obtained on a DRX-500 spectrometer at 500 (^1H) and 125 (^{13}C) MHz or an AV-400 spectrometer at 400 (^1H) and 100 (^{13}C) MHz and were referenced to the residual proton and ^{13}C resonances of C_6D_6. Tin (^{119}Sn) NMR spectra were obtained at 186.5 MHz and were externally referenced to $SnMe_4$. Elemental analysis was performed by ALS, Tucson, AZ and the CENTC Elemental Analysis Facility at the University of Rochester.

Materials. $SnCl_2$ was purchased from commercial suppliers and used as received. The potassium allyl K[A′] = K[(1,3-$SiMe_3$)C_3H_3] was synthesized by transmetalation of Li[A′][75] with potassium *tert*-butoxide in hexanes solution. Toluene was degassed with argon and dried over activated alumina using a solvent purification system, then stored over 4 Å molecular sieves in a glovebox. Hexanes were distilled under nitrogen over NaK/benzophenone radical,[76] then stored over 4 Å molecular sieves in a glovebox. Benzene-d_6 was obtained from Cambridge Isotopes and stored over 4 Å molecular sieves.

Mechanochemical protocol. Ball milling reactions used 50 stainless steel (440 grade) ball bearings ($^3/_{16}$ in (5 mm), 0.44 g) that were thoroughly cleaned with detergent and water, then washed with acetone, and dried in a 125 °C oven prior to use. Planetary milling was performed with a Retsch PM100 mill, 50 mL stainless steel grinding jar type C, and a safety clamp for air-sensitive grinding. A typical reaction involved 300 mg total sample weight, sealed under an inert atmosphere. The ground mixture was extracted with minimal hexanes (<100 mL) and filtered through a medium porosity ground glass frit. The extraction is designed to dissolve the complex, and the filtration removes traces of KCl (and in the case of disproportionation reactions, tin metal). The filtrate was then dried under vacuum prior to NMR analysis.

K[Sn{1,3-($SiMe_3$)$_2C_3H_3$}$_3$] (1). Although originally conducted with a 1 $SnCl_2$: 2 K[A′] ratio, details for a 1:1 reaction are given here. Inside a glovebox, $SnCl_2$ (94.8 mg, 0.50 mmol) and K[A′] (112 mg, 0.50 mmol) were added to a 50 mL stainless steel milling jar with fifty 5 mm stainless steel ball bearings. The jar was closed tightly with the appropriate safety clamp,

brought out of the glovebox, and milled for 5 min at 600 RPM. The jar, still clamped, was returned to the glovebox. When opened, the inside of the jar and balls were coated in a dark brown powder that when extracted with hexanes and filtered through a medium-porosity ground glass frit, yielded an orange filtrate. Removal of solvent under vacuum yielded a brown oil (71 mg, 60% yield) from which crystals grew. Upon standing for an extended period of time (> 1 wk), the oil solidifies and leaves transparent yellow crystals. **^{1}H NMR** (δ/ppm, 500 MHz, C_6D_6, *J*/Hz, atom labels are in the order of proximity to Sn, starting with 1): 6.25 (dd, 3H, H2, ^{3}J(H2-H3) = 18.1, ^{3}J(H2-H1) = 14.4 Hz; 4.25 (d, 3H, H3); 1.04 (d, 3H, H1, ^{3}J(H2-H1) = 14.4 Hz); 0.34 (27H, $SiMe_3$); 0.20 (27H, $SiMe_3$). **^{13}C{^{1}H} NMR** (δ/ppm, 100 MHz, C_6D_6, Hz) δ 159.60, C2, 112.68, C2, 39.73, C1, 1.07, $SiMe_3$, -0.28, $SiMe_3$. **^{119}Sn NMR** (δ/ppm, 186.5 MHz, C_6D_6 Hz): δ -138.70 (s). Accurate elemental analysis was difficult to obtain, owing to the compound's extreme tendency to scavenge trace amounts of solvents present in the glovebox atmosphere while it was being manipulated. Such solvents could be detected when the compound was dissolved for ^{1}H NMR analysis, although they were obviously not present in the crystalline compound. The best fit to the analytical data was obtained by assuming that one molecule of THF was adsorbed per each stannate, although almost as good a match was found using 0.5 mole of hexane (both were solvents present in the glovebox atmosphere). Anal. Calcd for $C_{27}H_{63}KSi_6Sn$: C, 45.41; H, 8.89; calcd for $C_{27}H_{63}KSi_6Sn(C_4H_8O)$: C, 47.36; H, 9.10. Found: C, 47.57; H, 9.03.

[Sn{1,3-(SiMe$_3$)$_2$C$_3$H$_3$}$_4$] (3). Inside a glovebox, $SnCl_2$ (70 mg, 0.37 mmol) and K[A′] (250 mg, 1.11 mmol) were added to a 50 mL stainless steel milling jar with fifty 5 mm stainless steel ball bearings. The jar was clamped closed tightly with the appropriate safety clamp, brought out of the glovebox, and milled for 5 min at 600 RPM. The jar, still clamped, was returned to the glovebox. When opened, both the inside of the jar and balls were coated in a dark grey powder that when extracted with hexanes and filtered through a medium-porosity ground glass frit yielded a green-tinted filtrate. Removal of solvent under vacuum yielded 54.3 mg (23% yield) of a dark brown/green oil containing microcrystals. (In some cases, depending on the sample of the K[A′] used, both the residue in the jar and the resulting oil and compound could be a lighter color.) In hexanes, decomposition could be seen in as little as 30 min; the lightly colored solution would become darker and a dark precipitate would form. However, in the solid state, a crystal structure was obtained from a sample more than 6 months after initial removal of solvent, indicating reasonable stability in the absence of solvent (though mostly a yellow oil with dark grey residue, presumably precipitated tin metal).

Interpretation and assignment of the ^{1}H NMR spectrum is extremely difficult due to the invariable presence of decomposition products when SnA′$_4$ is in C_6D_6 for more than a few minutes; these resonances, which include signals from tetrakis(trimethylsilyl)-1,5-hexadiene [A′$_2$], are interspersed and overlap with the product peaks. **^{1}H NMR** (δ/ppm, 500 MHz, C_6D_6, *J*/Hz,^{1}H NMR): Multiple peaks centered at 6.3 (6.24–6.39, unintegrable, uninterpretable via multiplet analysis); 5.55 (dt, 0.8 H, ^{2}J(H-Sn) = 1.3 Hz, ^{3}J(H-H) = 18.3 Hz); 2.22 (dd, 1.5 H, ^{1}J(H-H) = 11.63, ^{2}J(H-H) = 10.40 Hz); 0.24–0.28 (multiple singlets, ca.

45 H, $SiMe_3$), 0.15 (s, ca. 27 H, $SiMe_3$). **^{119}Sn NMR** (δ/ppm, 186.5 MHz, C_6D_6 Hz): -36.6. A $^{13}C\{^1H\}$ NMR spectrum was unobtainable owing to rapid decomposition in solution. Anal. Calcd for $C_{36}H_{84}Si_8Sn$: C, 50.25; H, 9.84. Found: C, 50.17; H, 9.93.

Table 5: Products from Additional Ratios of K[A′] : $SnCl_2$ [a]

Ratio\Time	5 min	15 min	60 min
1:1	1 (60%) (see page S2)		
2:1	K[A′]:1 (1:2.5) Total starting mass: 318.8 mg; recov.: 78.3 mg	1:3:4 (13.1:2.6:1) Total starting mass: 318.8 mg; recov.: 125.2 mg	
3:1	See manuscript for details.	1:3:4 (25.0:1.8:1) Total starting mass: 320 mg; recov.: 62.4 mg	
4:1		K[A′]:1:3:4 (15:3:4.6:1.13:1) Total starting mass: 326.3 mg; recov.: 36.7 mg	K[A′]:1:3 (1:0.2:4) Total starting mass: 271.9 mg; recov.: 96.7 mg
5:1		K[A′]:1 (1:0.34) Total starting mass: 328.1 mg; recov.: 10.9 mg	

[a] molar ratios of products in parentheses

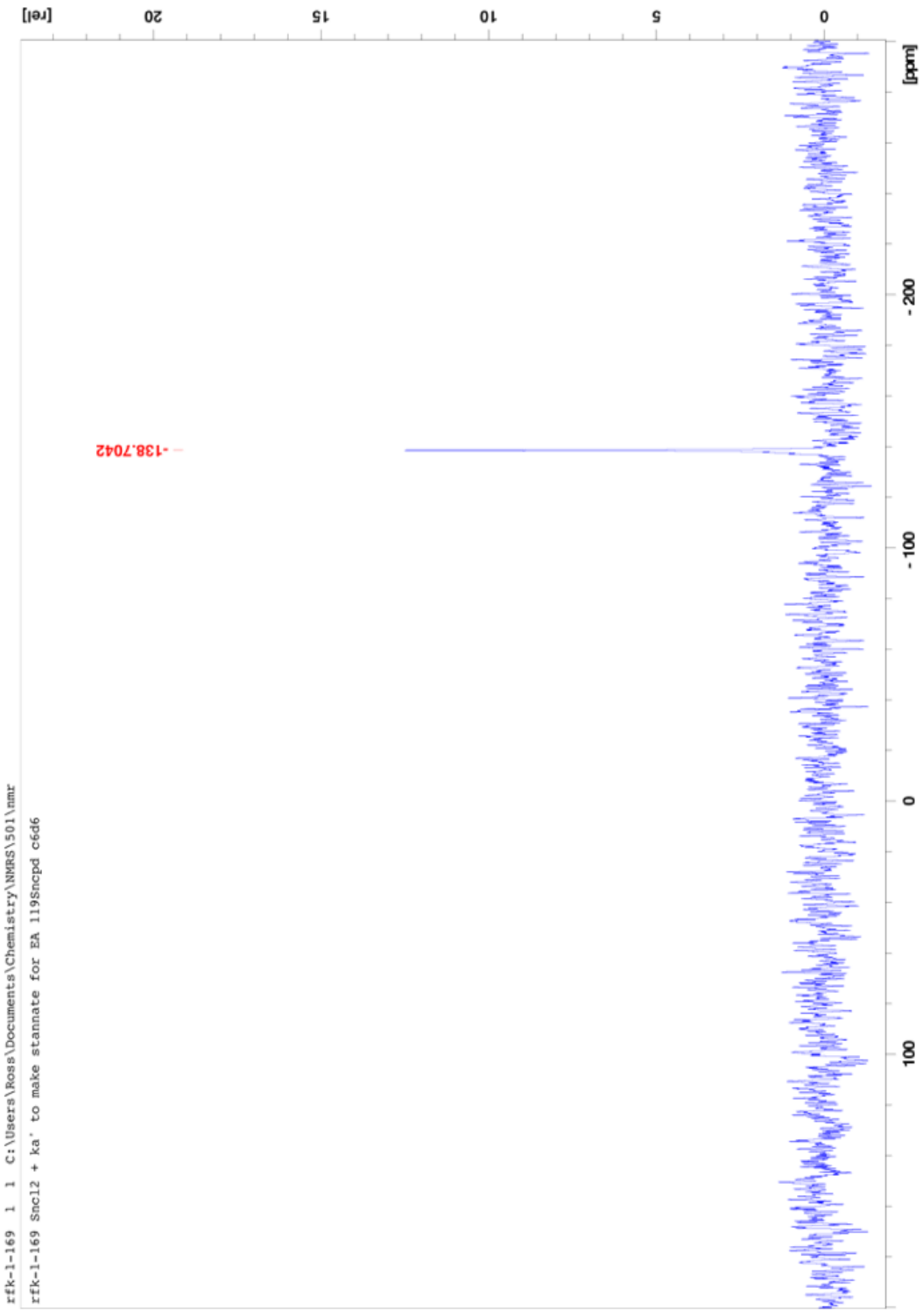

Figure 32. ^{119}Sn NMR of [SnA′$_3$K] (**1**)

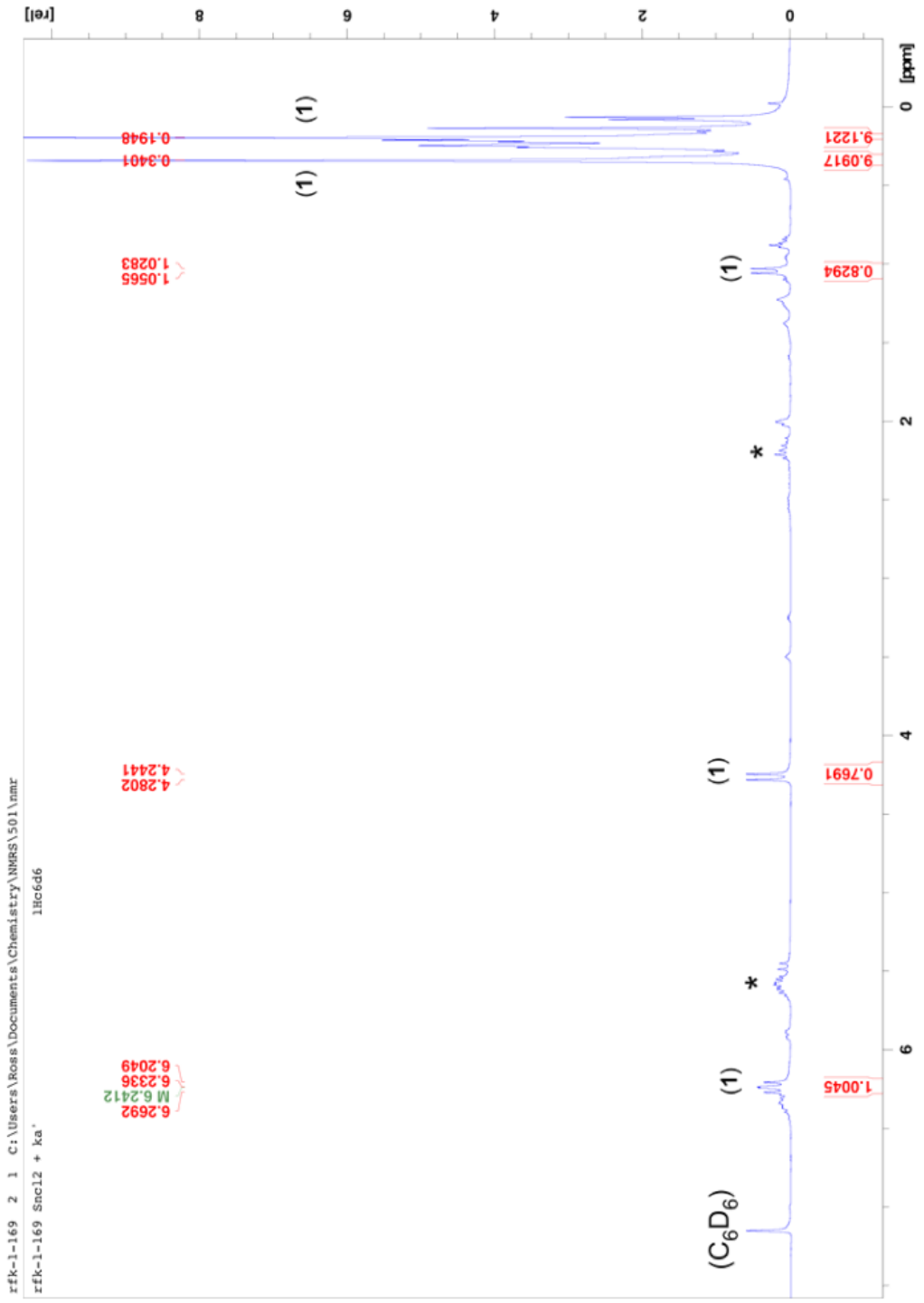

Figure 33. ^{1}H NMR of [SnA′$_3$K] (**1**)

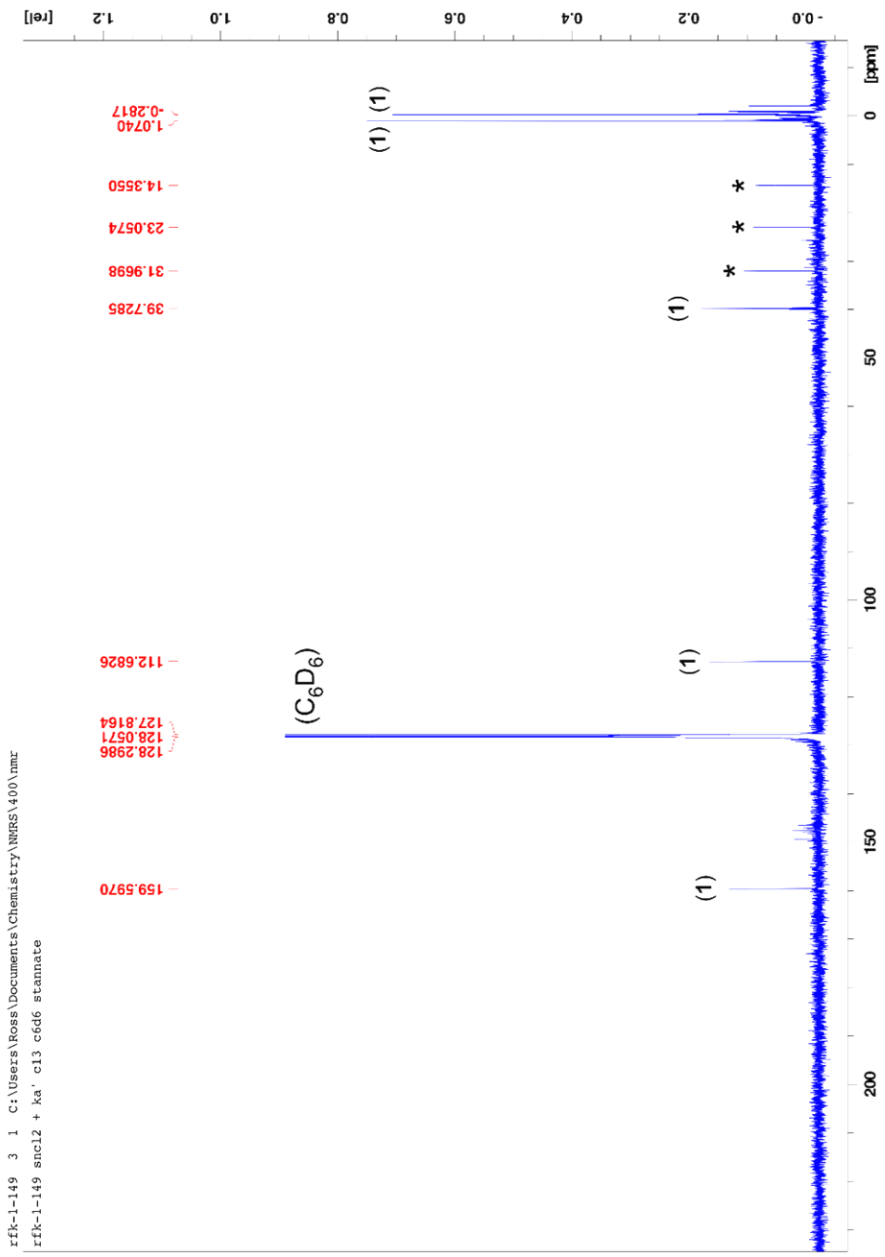

Figure 34. ^{13}C NMR of [SnA′$_3$K] (**1**) (* hexanes)

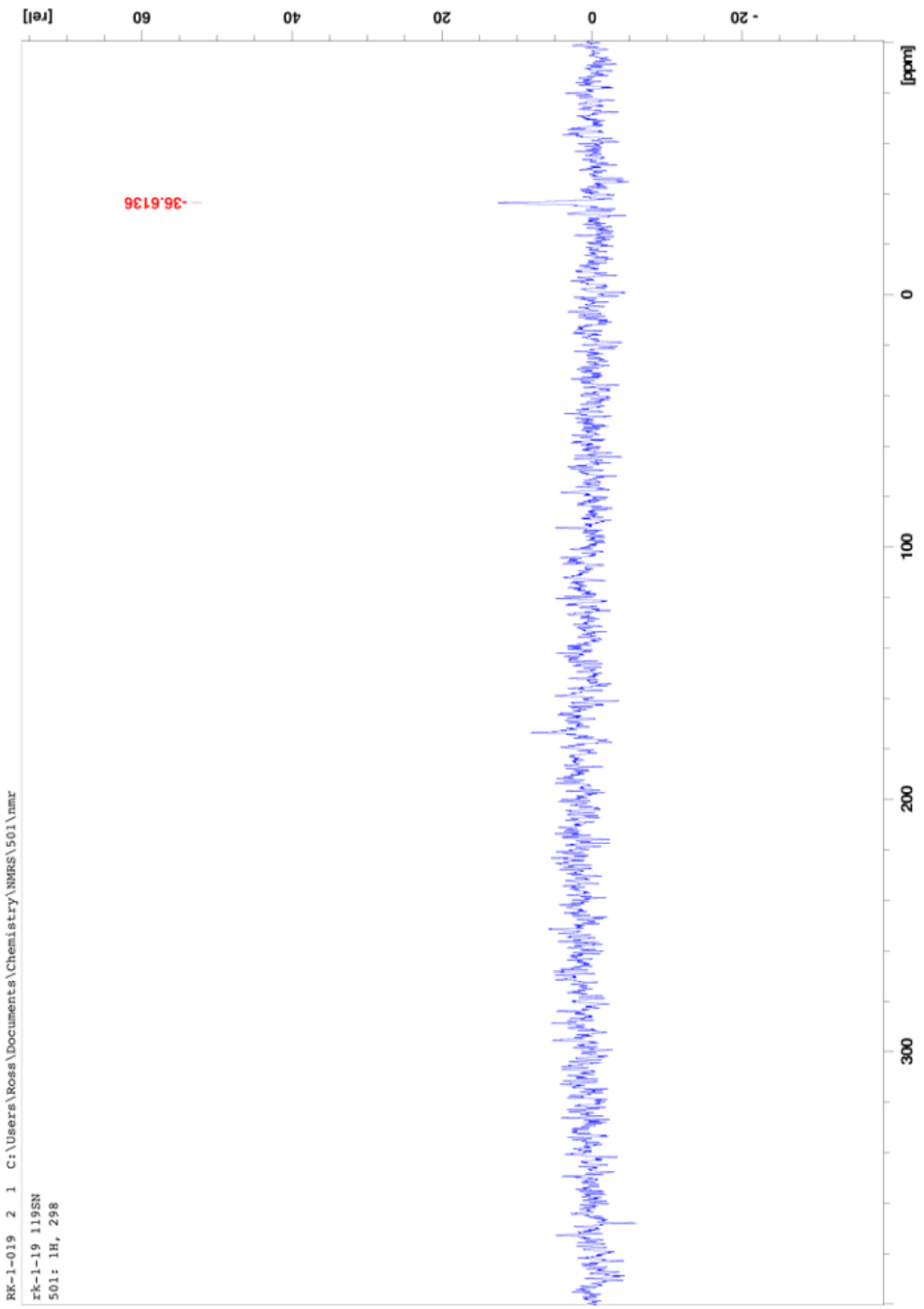

Figure 35. ^{119}Sn NMR of [SnA′$_4$] (**3**)

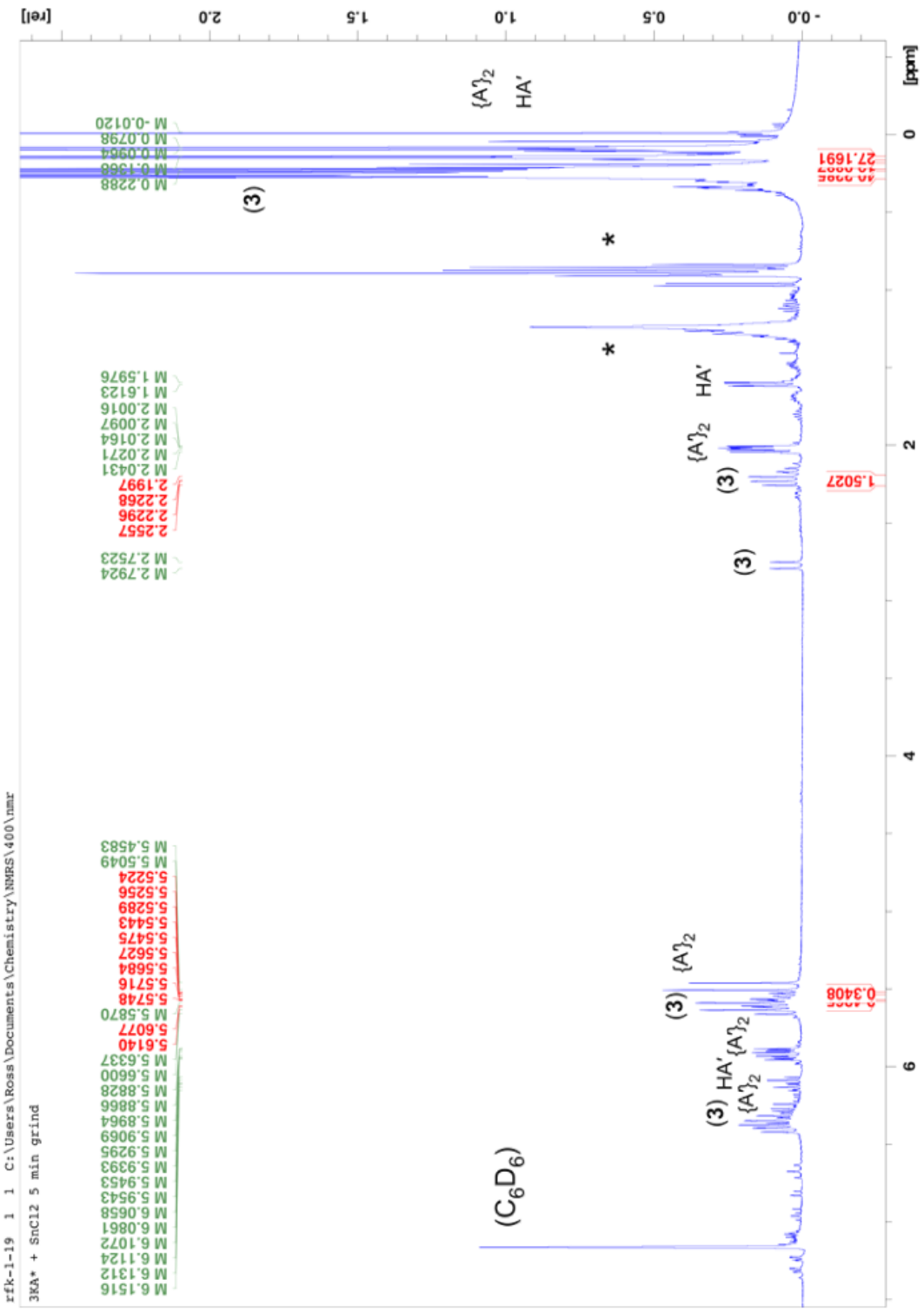

Figure 36. ^{1}H NMR of [SnA′$_4$] (**3**) (* hexanes)

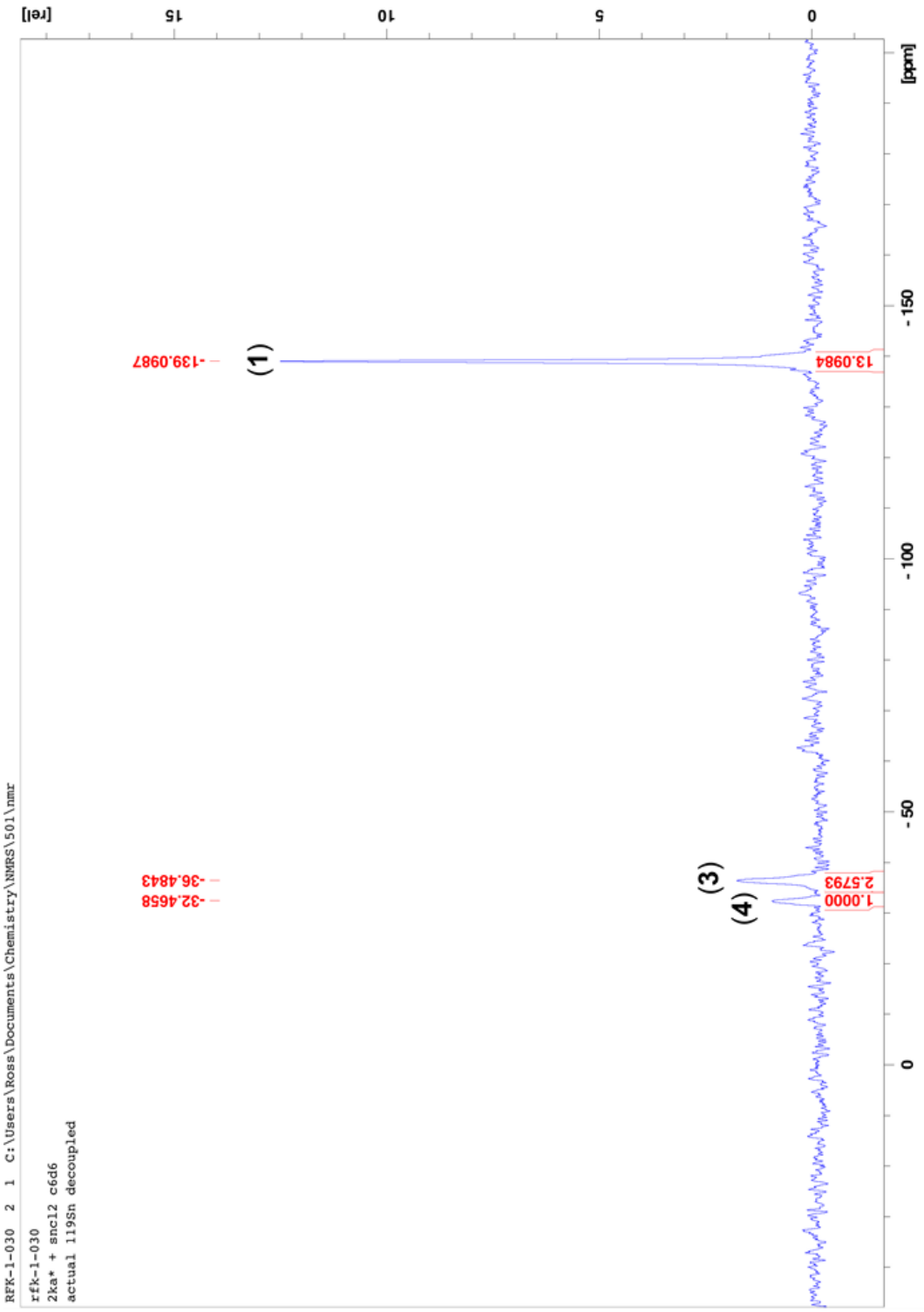

Figure 37. ^{119}Sn of [SnA′$_3$K] (**1**), chiral-[SnA′$_4$] (**3**). *meso*-[SnA′$_4$] (**4**), From a 2:1 ratio of K[A′] and $SnCl_2$, 15 min, planetary mill

General Procedures for X-Ray Crystallography

X-ray crystallographic data were collected on a Rigaku Oxford Diffraction Supernova diffractometer. Crystal samples were handled under immersion oil and quickly transferred to a cold nitrogen stream. The crystals were kept at 100 K during data collection. Under Olex2,[77] the structure was solved with the SHELXT[78] structure solution program using direct methods and refined with the SHELXL[79] refinement package using least squares minimization. All non-hydrogen atoms were refined with anisotropic displacement parameters.

Crystallographic data for the structures reported in this paper have been deposited with the Cambridge Crystallographic Data Centre as CCDC 1857435 (1), 1857436 (2), 1857437 (3), and 1857438 (4). Copies of the data can be obtained free of charge on application to CCDC, 12 Union Road, Cambridge CB2 1EZ, UK [fax: (+44)1223-336-033; e-mail: deposit@ccdc.cam.ac.uk]

General Procedures for Calculations

All calculations were performed with the Gaussian 09W[80] or Gaussian 16 (Linux) suite of programs.[81] The B3PW91 functional, which incorporates Becke's three-parameter exchange functional[54] with the 1991 gradient-corrected correlation functional of Perdew and Wang, was used. This hybrid functional has previously been shown to provide realistic geometries for organometallic species, and in our testing with a variety of other hybrid functionals, provided the best geometry and dissociation energy for $SnMe_4$. For dispersion-corrected calculations, Grimme's D3 correction[55] with additional Becke-Johnson damping was used[56] (Gaussian keyword: empiricaldispersion=GD3BJ). For bond dissociation enthalpy calculations, the def2SVPD basis set was used on C and H atoms, and the def2TZVPD basis on Sn and Si with the accompanying ECP used for Sn.[82] (For the reaction SnA'_2 (C_2) → $\bullet SnA'_3$ + $\bullet A'$, the def2TZVPD basis set was used on all atoms). An ultrafine grid was used for all calculations (Gaussian keyword: int=ultrafine). For comparing the relative energies of the D_2, S_4, and proposed *RSSS* form of the SnA'_4 molecules, the def2SVP basis set was used on C and H atoms, and the def2TZVP basis on Si and Sn, with the corresponding ECP used for Sn. Calculation of Mayer bond orders in the model complex [Me_3Sn–A′] was performed with the Multiwfn program (3.3.9).[83]

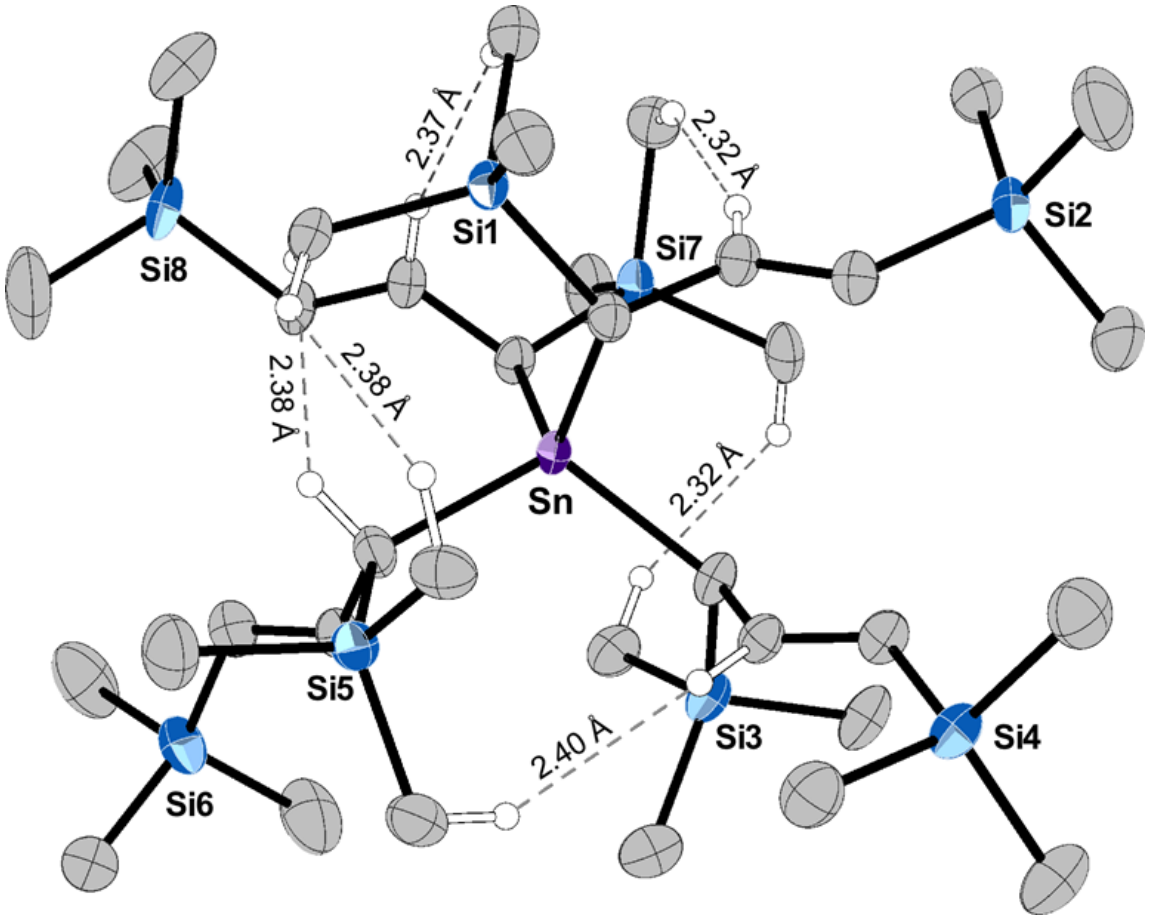

Figure 38. Framework of **3**, illustrating H···H contacts that are less than or equal to the sum of the van der Waals' radii (≤ 2.4 Å). Contacts are calculated from the X-ray data of **3** (exp. C–H distances 0.93–0.98 Å), and are consequently not identical to those calculated from the geometry-optimized structure (calc. C–H distances 1.098–1.101 Å).

Table 6: Crystal Data and Summary of X–ray Data Collection

Compound	**[Sn{1,3-(SiMe$_3$)$_2$C$_3$H$_3$}$_3$K] (1)**	**[Sn{1,3-(SiMe$_3$)$_2$C$_3$H$_3$}$_3$-K(OH$_2$)] (2)**	**[Sn{1,3-(SiMe$_3$)$_2$C$_3$H$_3$}$_4$] (*chiral*) (3)**	**[Sn{1,3-(SiMe$_3$)$_2$C$_3$H$_3$}$_4$] (*meso*) (4)**
Empirical formula	$C_{27}H_{63}KSi_6Sn$	$C_{27}H_{65}KOSi_6Sn$	$C_{36}H_{84}Si_8Sn$	$C_{36}H_{84}Si_8Sn$
Formula weight	714.10	732.10	860.44	860.44
Color of compound	yellow	yellow	colorless	colorless
Temperature/K	99.9(4)	100.0(3)	100	100.0(3)
Crystal system	monoclinic	trigonal	monoclinic	triclinic
Space group	$P2_1/n$	R3m	$P2_1$	$P\bar{1}$
a/Å	12.5863(3)	17.1821(4)	11.3719(2)	11.4372(6)
b/Å	16.2257(4)	17.1821(4)	19.8321(4)	11.5112(7)
c/Å	20.9657(6)	13.6991(6)	12.1517(2)	20.7806(17)
α/°	90	90	90	95.647(6)
β/°	100.864(3)	90	107.788(2)	103.837(6)
γ/°	90	120	90	90.081(5)
Volume/Å^3	4204.92(19)	3502.5(2)	2609.54(9)	2642.7(3)
Z	4	3	2	2
ρ_{calc} g/cm^3	1.128	1.041	1.095	1.081
μ/mm^{-1}	7.447	0.805	5.798	5.725
F(000)	1512.0	1644.0	924.0	924.0
Crystal size/mm^3	0.25 × 0.195 × 0.027	0.197 × 0.144 × 0.109	0.123 × 0.049 × 0.021	0.104 × 0.081 × 0.023
Radiation	CuKα (λ = 1.54184)	MoKα (λ = 0.71073)	CuKα (λ = 1.54184)	CuKα (λ = 1.54184)
2Θ range for data collect/°	6.936 to 147.06	6.232 to 60.406	7.64 to 145.664	7.72 to 143.284
Index ranges	$-15 \le h \le 14$, $-19 \le k \le 19$, $-24 \le l \le 25$	$-23 \le h \le 22$, $-23 \le k \le 24$, $-19 \le l \le 19$	$-13 \le h \le 13$, $-24 \le k \le 24$, $-15 \le l \le 15$	$-8 \le h \le 8$, $-14 \le k \le 14$, $-16 \le l \le 16$
Reflections collected	39 298	27 543	11 540	4288
Independent reflections	8332 [R_{int} = 0.0632, R_{sigma} = 0.0428]	2407 [R_{int} = 0.0463, R_{sigma} = 0.0231]	11 540 [R_{sigma} = 0.0342]	4288 [R_{sigma} = 0.0212]
Data/restraints/parameters	8332/33/365	2407/5/91	11540/1/433	4288/866/551
Goodness-of-fit on F^2	1.045	1.121	1.036	1.053
Final *R* indexes [$I > 2\sigma(I)$]	R_1 = 0.0577, wR_2 = 0.1308	R_1 = 0.0408, wR_2 = 0.0992	R_1 = 0.0342, wR_2 = 0.0871	R1 = 0.0554, wR2 = 0.1401
Final *R* indexes [all data]	R1 = 0.0678, wR2 = 0.1381	R_1 = 0.0415, wR_2 = 0.1003	R1 = 0.0359, wR2 = 0.0879	R1 = 0.0583, wR2 = 0.1420
Largest diff. peak/hole/e Å^{-3}	1.88/-1.88	1.27/-0.60	0.76/-0.73	0.56/-0.35
Flack parameter	N/A	0.34(5)	0.008(4)	N/A

Optimized coordinates of all structures in XYZ format

65

[SnA_2], C_2; B3PW91-D3BJ/def2TZVPD; ΔG°= -2083.340663 au

C	-1.199787	1.555046	-0.074671
C	0.000000	2.376255	-0.039165
C	0.574755	2.916829	1.074132
H	0.569490	2.424313	-0.965448
C	-0.574755	-2.916829	1.074132
C	0.000000	-2.376255	-0.039165
C	1.199787	-1.555046	-0.074671
H	-0.569490	-2.424313	-0.965448
H	-0.013556	2.890171	1.994446
H	-1.892340	1.801788	0.737230
H	1.892340	-1.801788	0.737230
H	0.013556	-2.890171	1.994446
Si	2.230692	3.761259	1.123671
Si	-2.103264	1.289715	-1.682777
Si	2.103264	-1.289715	-1.682777
Si	-2.230692	-3.761259	1.123671
C	-2.779743	-0.452775	-1.811605
C	2.779743	0.452775	-1.811605
C	-3.555509	2.479398	-1.755306
C	3.555509	-2.479398	-1.755306
C	-0.958553	1.655930	-3.123531
C	0.958553	-1.655930	-3.123531
C	2.081770	5.330995	2.140358
C	-2.081770	-5.330995	2.140358
C	3.485836	2.625439	1.937589
C	-3.485836	-2.625439	1.937589
C	2.789482	4.179649	-0.615492
C	-2.789482	-4.179649	-0.615492
H	-4.258887	2.289164	-0.940213
H	-3.216722	3.514662	-1.668066
H	-4.102988	2.381011	-2.696645
H	-3.430239	-0.562232	-2.682975
H	-1.975018	-1.183014	-1.899443
H	-3.363065	-0.707357	-0.923466
H	-0.708983	2.719363	-3.156509
H	-0.024723	1.095155	-3.070687
H	-1.443049	1.400259	-4.069321
H	1.732121	5.110473	3.152337
H	3.046159	5.838667	2.224866

H	1.372272	6.026613	1.685920
H	2.061878	4.820417	-1.119233
H	3.742464	4.714439	-0.586082
H	2.933786	3.284654	-1.223396
H	3.162928	2.351540	2.945154
H	3.596764	1.702534	1.363335
H	4.468294	3.098960	2.014480
H	-4.468294	-3.098960	2.014480
H	-3.162928	-2.351540	2.945154
H	-3.596764	-1.702534	1.363335
H	-2.933786	-3.284654	-1.223396
H	-2.061878	-4.820417	-1.119233
H	-3.742464	-4.714439	-0.586082
H	4.102988	-2.381011	-2.696645
H	4.258887	-2.289164	-0.940213
H	3.216722	-3.514662	-1.668066
H	1.975018	1.183014	-1.899443
H	3.363065	0.707357	-0.923466
H	3.430239	0.562232	-2.682975
H	0.024723	-1.095155	-3.070687
H	1.443049	-1.400259	-4.069321
H	0.708983	-2.719363	-3.156509
H	-3.046159	-5.838667	2.224866
H	-1.372272	-6.026613	1.685920
H	-1.732121	-5.110473	3.152337
Sn	0.000000	0.000000	1.212694

33

[•SnA_3], C_1; B3PW91-D3BJ/def2TZVPD; ΔG°= -1148.882341 au

C	-1.249861	0.349432	-0.801921
C	0.000001	0.753877	-0.285755
Sn	-0.000001	-1.624790	0.005392
H	-1.251092	0.042797	-1.849132
C	1.249862	0.349425	-0.801920
H	1.251093	0.042795	-1.849132
H	0.000002	1.212137	0.702223
Si	2.881894	0.772198	-0.013343
Si	-2.881894	0.772199	-0.013343
C	2.590202	1.188545	1.790995
H	2.071282	0.374557	2.303976
H	3.541725	1.354850	2.302390
H	1.992842	2.096368	1.906086
C	4.030775	-0.701884	-0.156789
H	5.030266	-0.464251	0.216717
H	3.648048	-1.550208	0.416069
H	4.129777	-1.020033	-1.197905
C	3.658424	2.241199	-0.886932
C	-4.030773	-0.701881	-0.156820

H	-4.129712	-1.020054	-1.197935
H	-3.648081	-1.550193	0.416080
H	-5.030286	-0.464239	0.216621
C	-2.590206	1.188517	1.791003
H	-3.541731	1.354839	2.302392
H	-2.071310	0.374511	2.303978
H	-1.992827	2.096325	1.906110
C	-3.658419	2.241217	-0.886907
H	-3.011060	3.119385	-0.825056
H	-3.825948	2.024180	-1.945015
H	-4.623185	2.499992	-0.442004
H	4.623203	2.499963	-0.442051
H	3.011080	3.119378	-0.825073
H	3.825927	2.024152	-1.945042

32

[•A'], C_1; B3PW91-D3BJ/def2TZVPD; ΔG°= -934.423068 au

C	1.233671	-0.868631	-0.000926
C	-0.000001	-0.236409	-0.000398
C	-1.233673	-0.868632	-0.000986
C	3.846794	-0.525452	-1.527994
C	2.631330	1.844460	0.001950
C	3.846661	-0.528820	1.526934
C	-3.847351	-0.526556	-1.527292
C	-2.631334	1.844460	0.000586
C	-3.846097	-0.527718	1.527645
H	1.209894	-1.959616	-0.001899
H	-0.000002	0.852970	0.000561
H	-1.209896	-1.959616	-0.001980
H	4.838380	-0.064739	-1.537057
H	3.324993	-0.225347	-2.439681
H	3.981500	-1.609592	-1.560800
H	2.079739	2.172066	0.886481
H	2.079872	2.173891	-0.881989
H	3.595714	2.358992	0.002545
H	3.324858	-0.230592	2.439236
H	4.838327	-0.068302	1.537043
H	3.981177	-1.613053	1.557416
H	-3.326085	-0.226768	-2.439390
H	-4.839094	-0.066176	-1.536129
H	-3.981719	-1.610758	-1.559456
H	-2.079638	2.172676	0.884827
H	-3.595717	2.358992	0.000958
H	-2.079981	2.173280	-0.883644
H	-3.980667	-1.611920	1.558950
H	-4.837727	-0.067124	1.537835
H	-3.323897	-0.228879	2.439521
Si	2.883740	-0.012878	-0.000004

Si -2.883742 -0.012879 -0.000029

17
[$SnMe_4$], *T* symm; B3PW91-D3BJ/def2TZVPD(Sn);def2SVPD(C,H); ΔG°= -373.827236 au
Sn 0.000000 0.000000 0.000000
C -1.239585 1.239585 1.239585
H -1.881424 0.619068 1.879791
H -0.619068 1.879791 1.881424
H -1.879791 1.881424 0.619068
C 1.239585 -1.239585 1.239585
H 0.619068 -1.879791 1.881424
H 1.879791 -1.881424 0.619068
H 1.881424 -0.619068 1.879791
C -1.239585 -1.239585 -1.239585
H -1.881424 -0.619068 -1.879791
H -0.619068 -1.879791 -1.881424
H -1.879791 -1.881424 -0.619068
C 1.239585 1.239585 -1.239585
H 1.879791 1.881424 -0.619068
H 1.881424 0.619068 -1.879791
H 0.619068 1.879791 -1.881424

13
[•$SnMe_3$], C_1; B3PW91-D3BJ/def2TZVPD(Sn);def2SVPD(C,H); Δ= -333.948505 au
Sn 0.000000 0.000000 0.295936
C -0.663955 1.903487 -0.498402
H -1.688833 2.124096 -0.173177
H 0.000000 2.714052 -0.171370
H -0.642442 1.845316 -1.597314
C -1.316490 -1.526746 -0.498402
H -1.276869 -1.479029 -1.597314
H -0.995105 -2.524620 -0.173177
H -2.350438 -1.357026 -0.171370
C 1.980446 -0.376741 -0.498402
H 2.683937 0.400524 -0.173177
H 2.350438 -1.357026 -0.171370
H 1.919311 -0.366287 -1.597314

4
[•CH_3], D_{3h}; B3PW91-D3BJ/def2SVPD(C,H); ΔG° = -39.787990 au
C 0.000000 0.000000 0.000000
H 0.000000 1.088990 0.000000
H 0.943093 -0.544495 0.000000
H -0.943093 -0.544495 0.000000

33
[$Sn(C_3H_5)_4$], D_2; B3PW91-D3BJ/def2TZVPD(Sn);def2SVPD(C,H); ΔG°= -682.992897 au
C 1.307825 1.255625 1.190657

C	1.951950	2.235886	0.282936
C	3.169524	2.122723	-0.265604
C	1.307825	-1.255625	-1.190657
C	1.951950	-2.235886	-0.282936
C	3.169524	-2.122723	0.265604
C	-1.307825	-1.255625	1.190657
C	-1.951950	-2.235886	0.282936
C	-3.169524	-2.122723	-0.265604
C	-1.307825	1.255625	-1.190657
C	-1.951950	2.235886	-0.282936
C	-3.169524	2.122723	0.265604
H	2.034099	0.584301	1.668117
H	1.345740	3.108097	0.012185
H	3.823077	1.278900	-0.032962
H	2.034099	-0.584301	-1.668117
H	1.345740	-3.108097	-0.012185
H	3.823077	-1.278900	0.032962
H	-2.034099	-0.584301	1.668117
H	-1.345740	-3.108097	0.012185
H	-3.823077	-1.278900	-0.032962
H	-2.034099	0.584301	-1.668117
H	-1.345740	3.108097	-0.012185
H	-3.823077	1.278900	0.032962
Sn	0.000000	0.000000	0.000000
H	-3.552125	2.875218	0.955862
H	3.552125	2.875218	-0.955862
H	3.552125	-2.875218	0.955862
H	-3.552125	-2.875218	-0.955862
H	0.695265	1.737577	1.963933
H	0.695265	-1.737577	-1.963933
H	-0.695265	-1.737577	1.963933
H	-0.695265	1.737577	-1.963933

25

[•Sn(C_3H_5)$_3$], C_1; B3PW91-D3BJ/def2TZVPD(Sn);def2SVPD(C,H); ΔG°= -565.824339 au

C	1.843111	-0.306770	1.054461
C	2.983910	0.330403	0.361565
C	4.092930	-0.287597	-0.068805
C	-0.313458	1.339564	-1.224986
C	-0.088575	2.324563	-0.150142
C	-1.011717	2.781573	0.714518
C	-1.632538	-0.940389	1.003542
C	-2.866835	-1.090231	0.204441
C	-3.777088	-0.134959	-0.034988
H	2.102291	-1.283991	1.482851
H	2.885968	1.403617	0.163493
H	4.252447	-1.356020	0.096966
H	-1.361660	1.274091	-1.544764

H	0.941153	2.677335	-0.030091
H	-2.055980	2.470567	0.649856
H	-1.646428	-0.046244	1.644287
H	-3.020614	-2.071969	-0.258558
H	-3.689062	0.862873	0.400260
Sn	0.127541	-0.628738	-0.307391
H	-4.646077	-0.326999	-0.665376
H	4.876334	0.257763	-0.596448
H	-0.748060	3.490446	1.499871
H	1.422437	0.334020	1.844293
H	0.343288	1.479408	-2.090948
H	-1.411523	-1.824916	1.616223

8

[•C_3H_5], C_2; B3PW91-D3BJ/def2SVPD(C,H); ΔG°= -117.103765 au

C	0.000000	1.229904	-0.196654
C	0.000000	0.000000	0.443313
C	0.000000	-1.229904	-0.196654
H	-0.000387	1.296675	-1.286752
H	0.000000	0.000000	1.538932
H	0.000387	-1.296675	-1.286752
H	0.000076	-2.162974	0.367271
H	-0.000076	2.162974	0.367271

57

[$Sn((SiH_3)_2C_3H_3)_4$], D_2; B3PW91-D3BJ/def2TZVPD(Sn,Si);def2SVPD(C,H); ΔG°= -3008.367353 au

C	1.315695	1.244738	1.200852
C	1.915582	2.197328	0.232793
C	3.076558	2.039972	-0.436025
C	1.315695	-1.244738	-1.200852
C	1.915582	-2.197328	-0.232793
C	3.076558	-2.039972	0.436025
C	-1.315695	-1.244738	1.200852
C	-1.915582	-2.197328	0.232793
C	-3.076558	-2.039972	-0.436025
C	-1.315695	1.244738	-1.200852
C	-1.915582	2.197328	-0.232793
C	-3.076558	2.039972	0.436025
H	2.056581	0.513743	1.558475
H	1.315881	3.090605	0.018247
H	3.673804	1.146727	-0.219515
H	2.056581	-0.513743	-1.558475
H	1.315881	-3.090605	-0.018247
H	3.673804	-1.146727	0.219515
H	-2.056581	-0.513743	1.558475
H	-1.315881	-3.090605	0.018247
H	-3.673804	-1.146727	-0.219515
H	-2.056581	0.513743	-1.558475

H	-1.315881	3.090605	-0.018247
H	-3.673804	1.146727	0.219515
Si	0.412297	2.022702	2.648780
Si	3.667435	3.238144	-1.716586
Si	0.412297	-2.022702	-2.648780
Si	3.667435	-3.238144	1.716586
Si	-0.412297	-2.022702	2.648780
Si	-3.667435	-3.238144	-1.716586
Si	-0.412297	2.022702	-2.648780
Si	-3.667435	3.238144	1.716586
Sn	0.000000	0.000000	0.000000
H	2.741296	4.401045	-1.751903
H	2.741296	-4.401045	1.751903
H	-2.741296	-4.401045	-1.751903
H	-2.741296	4.401045	1.751903
H	5.046474	3.714888	-1.419112
H	5.046474	-3.714888	1.419112
H	-5.046474	-3.714888	-1.419112
H	-5.046474	3.714888	1.419112
H	3.698151	2.602305	-3.064424
H	3.698151	-2.602305	3.064424
H	-3.698151	-2.602305	-3.064424
H	-3.698151	2.602305	3.064424
H	0.138156	3.333250	-2.216669
H	-0.138156	3.333250	2.216669
H	-0.138156	-3.333250	-2.216669
H	0.138156	-3.333250	2.216669
H	0.717429	1.172393	-3.109254
H	-0.717429	1.172393	3.109254
H	-0.717429	-1.172393	-3.109254
H	0.717429	-1.172393	3.109254
H	-1.331912	2.239920	-3.797383
H	1.331912	2.239920	3.797383
H	1.331912	-2.239920	-3.797383
H	-1.331912	-2.239920	3.797383

43

[•Sn($(SiH_3)_2C_3H_3)_3$], C_1; B3PW91-D3BJ/def2TZVPD(Sn,Si);def2SVPD(C,H); ΔG°= -2309.856621 au

C	1.701213	-1.183438	0.818471
C	2.882441	-0.459953	0.291054
C	3.873413	-0.972727	-0.466618
C	-0.054743	1.354173	-1.012364
C	0.171883	1.918507	0.328992
C	-0.783111	2.199364	1.248888
C	-1.887588	-1.189584	0.432346
C	-2.972786	-0.774166	-0.477665
C	-3.777061	0.300453	-0.330932
H	-3.645100	0.917313	0.565360

H	0.868276	3.295059	-2.770955
H	1.841524	-2.272565	0.745869
H	2.920174	0.610493	0.527467
H	3.834650	-2.041751	-0.708757
H	-1.107661	1.446238	-1.321503
H	1.218599	2.100057	0.602115
H	-1.822851	2.012111	0.960437
H	-1.817074	-0.533798	1.313593
H	-3.114680	-1.405839	-1.365180
H	1.645894	0.684799	2.825950
H	2.514348	1.759436	-1.897071
H	-0.632300	-3.360944	1.584774
H	-0.172594	-0.900898	2.892249
H	0.921704	1.008479	-3.561383
H	-3.025333	-3.263300	1.914493
H	2.038897	-1.592058	3.532314
H	5.097000	1.454063	-0.607829
H	1.013070	3.250723	3.019625
H	-5.066092	-0.230035	-2.668480
H	6.581994	-0.461337	-0.724750
H	-1.242068	4.139433	3.141265
H	-6.435629	0.783634	-0.938924
H	5.226947	0.109723	-2.620781
H	-0.782078	1.946734	4.001813
H	-4.831783	2.120112	-2.120154
H	-2.117070	-3.832599	-0.257062
Si	1.271401	-0.732001	2.589644
Si	5.250472	0.069461	-1.130984
Si	1.112120	1.880956	-2.372313
Si	-0.430522	2.910259	2.920524
Si	-1.926605	-2.984263	0.951230
Si	-5.081444	0.761933	-1.558851
Sn	0.048627	-0.831758	-0.612940

l4

[•$(SiH_3)_2C_3H_3$)], C_S; B3PW91-D3BJ/def2TZVPD(Si);def2SVPD(C,H); ΔG°= -698.445588 au

C	0.000003	-0.634087	1.237522
H	0.000042	-1.730932	1.225631
C	-0.000025	0.006529	0.000000
H	-0.000078	1.103964	0.000000
C	0.000003	-0.634087	-1.237522
H	0.000042	-1.730932	-1.225631
Si	0.000003	0.248888	2.864989
H	-1.200592	-0.118962	3.667191
H	1.201008	-0.118333	3.666870
H	-0.000395	1.716742	2.624878
Si	0.000003	0.248888	-2.864989
H	-0.000395	1.716742	-2.624878

H	1.201008	-0.118333	-3.666870
H	-1.200592	-0.118962	-3.667191

129

[SnA′$_4$], D_2; B3PW91-D3BJ/def2TZVPD(Sn,Si);def2SVPD(C,H); ΔG°= -3950.784831 au

C	1.336347	1.197612	1.220244
C	2.245783	1.938410	0.309630
C	3.567009	1.725621	0.152471
C	1.898090	2.406698	3.913301
C	0.321029	4.039679	1.897381
C	-0.997591	1.670656	3.271142
C	6.205634	3.194413	-0.198939
C	3.733103	4.087355	-1.777768
C	5.124571	1.432869	-2.438823
C	1.336347	-1.197612	-1.220244
C	2.245783	-1.938410	-0.309630
C	3.567009	-1.725621	-0.152471
C	1.898090	-2.406698	-3.913301
C	-0.997591	-1.670656	-3.271142
C	0.321029	-4.039679	-1.897381
C	5.124571	-1.432869	2.438823
C	6.205634	-3.194413	0.198939
C	3.733103	-4.087355	1.777768
C	-1.336347	-1.197612	1.220244
C	-2.245783	-1.938410	0.309630
C	-3.567009	-1.725621	0.152471
C	0.997591	-1.670656	3.271142
C	-0.321029	-4.039679	1.897381
C	-1.898090	-2.406698	3.913301
C	-5.124571	-1.432869	-2.438823
C	-3.733103	-4.087355	-1.777768
C	-6.205634	-3.194413	-0.198939
C	-1.336347	1.197612	-1.220244
C	-2.245783	1.938410	-0.309630
C	-3.567009	1.725621	-0.152471
C	0.997591	1.670656	-3.271142
C	-1.898090	2.406698	-3.913301
C	-0.321029	4.039679	-1.897381
C	-3.733103	4.087355	1.777768
C	-6.205634	3.194413	0.198939
C	-5.124571	1.432869	2.438823
H	1.917437	0.424380	1.746435
H	1.775548	2.728988	-0.289133
H	4.014056	0.933488	0.767209
H	1.917437	-0.424380	-1.746435
H	1.775548	-2.728988	0.289133
H	4.014056	-0.933488	-0.767209
H	-1.917437	-0.424380	1.746435

H	-1.775548	-2.728988	-0.289133
H	-4.014056	-0.933488	0.767209
H	-1.917437	0.424380	-1.746435
H	-1.775548	2.728988	0.289133
H	-4.014056	0.933488	-0.767209
H	2.062239	-1.423008	-4.379466
H	1.602749	-3.112062	-4.705824
H	2.860808	-2.743012	-3.497356
H	-1.787064	-1.619182	-2.507846
H	-1.344310	-2.349489	-4.065970
H	-0.888055	-0.671476	-3.714512
H	1.258374	-4.486588	-1.533135
H	-0.068191	-4.683912	-2.701245
H	-0.406805	-4.065136	-1.075002
H	5.673639	-0.566296	2.037704
H	5.772294	-1.924102	3.182371
H	4.234612	-1.051298	2.962119
H	5.971408	-3.910564	-0.604004
H	6.895765	-3.685318	0.903240
H	6.739257	-2.344715	-0.255902
H	2.832416	-3.783234	2.329776
H	4.381830	-4.636836	2.477963
H	3.424763	-4.787104	0.985523
H	1.787064	-1.619182	2.507846
H	1.344310	-2.349489	4.065970
H	0.888055	-0.671476	3.714512
H	-1.258374	-4.486588	1.533135
H	0.068191	-4.683912	2.701245
H	0.406805	-4.065136	1.075002
H	-2.062239	-1.423008	4.379466
H	-1.602749	-3.112062	4.705824
H	-2.860808	-2.743012	3.497356
H	-5.673639	-0.566296	-2.037704
H	-5.772294	-1.924102	-3.182371
H	-4.234612	-1.051298	-2.962119
H	-2.832416	-3.783234	-2.329776
H	-4.381830	-4.636836	-2.477963
H	-3.424763	-4.787104	-0.985523
H	-5.971408	-3.910564	0.604004
H	-6.895765	-3.685318	-0.903240
H	-6.739257	-2.344715	0.255902
H	1.787064	1.619182	-2.507846
H	1.344310	2.349489	-4.065970
H	0.888055	0.671476	-3.714512
H	-2.062239	1.423008	-4.379466
H	-1.602749	3.112062	-4.705824
H	-2.860808	2.743012	-3.497356
H	-1.258374	4.486588	-1.533135

H	0.068191	4.683912	-2.701245
H	0.406805	4.065136	-1.075002
H	-2.832416	3.783234	2.329776
H	-4.381830	4.636836	2.477963
H	-3.424763	4.787104	0.985523
H	-5.971408	3.910564	-0.604004
H	-6.895765	3.685318	0.903240
H	-6.739257	2.344715	-0.255902
H	-5.673639	0.566296	2.037704
H	-5.772294	1.924102	3.182371
H	-4.234612	1.051298	2.962119
H	1.602749	3.112062	4.705824
H	2.860808	2.743012	3.497356
H	2.062239	1.423008	4.379466
H	-0.406805	4.065136	1.075002
H	1.258374	4.486588	1.533135
H	-0.068191	4.683912	2.701245
H	-1.787064	1.619182	2.507846
H	-1.344310	2.349489	4.065970
H	-0.888055	0.671476	3.714512
H	5.971408	3.910564	0.604004
H	6.895765	3.685318	-0.903240
H	6.739257	2.344715	0.255902
H	2.832416	3.783234	-2.329776
H	4.381830	4.636836	-2.477963
H	3.424763	4.787104	-0.985523
H	5.673639	0.566296	-2.037704
H	5.772294	1.924102	-3.182371
H	4.234612	1.051298	-2.962119
Si	0.610733	2.311771	2.556262
Si	4.645801	2.616251	-1.062559
Si	0.610733	-2.311771	-2.556262
Si	4.645801	-2.616251	1.062559
Si	-0.610733	-2.311771	2.556262
Si	-4.645801	-2.616251	-1.062559
Si	-0.610733	2.311771	-2.556262
Si	-4.645801	2.616251	1.062559
Sn	0.000000	0.000000	0.000000

97

[•SnA′$_3$], from D_2, C_1; B3PW91-D3BJ/def2TZVPD(Sn,Si);def2SVPD(C,H); ΔG°= -3016.720277 au

C	-0.153242	-1.173813	-1.175284
C	-0.681977	-1.791652	0.058806
C	-3.675472	0.713178	-0.383832
C	4.337023	0.965667	0.001502
H	-0.976603	-0.991963	-1.883951
H	0.06822	-2.071528	0.804946
H	-3.738732	0.39844	0.664252

H	4.350189	2.05578	0.129012
C	-1.452954	1.761242	0.161113
C	1.978028	0.916561	0.929485
C	-2.567882	1.391759	-0.740244
C	3.213245	0.319384	0.368911
C	-1.980165	-2.038892	0.334534
H	-1.594245	1.292573	1.144278
H	2.126607	1.997207	1.071967
H	-2.471374	1.721832	-1.782162
H	3.186537	-0.767474	0.241966
H	-2.704987	-1.738236	-0.426748
Sn	0.412901	0.884923	-0.616998
Si	-2.627633	-2.84626	1.870385
Si	1.17752	-2.168527	-2.058752
Si	5.830158	0.122107	-0.711425
Si	1.592852	0.21527	2.641421
Si	-1.336332	3.618454	0.40758
Si	-5.062299	0.258265	-1.525179
C	-4.633964	0.773283	-3.27373
H	-4.490475	1.860763	-3.346831
H	-3.711207	0.282533	-3.615129
H	-5.440602	0.493715	-3.965639
C	-5.339294	-1.597055	-1.459729
H	-4.4806	-2.148405	-1.867373
H	-5.491931	-1.930921	-0.423528
H	-6.229746	-1.880737	-2.0384
C	-6.636922	1.111504	-0.97132
H	-6.523335	2.204148	-1.012142
H	-7.488734	0.830354	-1.607826
H	-6.883713	0.837169	0.064748
C	-1.292711	4.466458	-1.259833
H	-1.183469	5.553809	-1.14109
H	-0.448505	4.104796	-1.864984
H	-2.218762	4.280597	-1.821372
C	0.205937	4.070671	1.37337
H	0.31236	3.459894	2.280107
H	1.113603	3.944003	0.767289
H	0.159605	5.12426	1.683331
C	-2.852003	4.15693	1.36271
H	-3.762294	3.817527	0.848593
H	-2.853245	3.718937	2.371465
H	-2.899274	5.250472	1.465316
C	-3.646197	-4.341621	1.380986
H	-4.097382	-4.822656	2.26109
H	-4.457725	-4.053333	0.69797
H	-3.021854	-5.085207	0.865387
C	-3.735232	-1.648989	2.799512
H	-3.186431	-0.744372	3.0948

H	-4.58623	-1.341256	2.175623
H	-4.138258	-2.116712	3.70934
C	-1.207163	-3.380443	2.966647
H	-1.588127	-3.891524	3.861829
H	-0.540613	-4.076329	2.438156
H	-0.607698	-2.524116	3.298877
C	2.076746	-3.260356	-0.832195
H	2.862234	-3.83803	-1.337842
H	2.552387	-2.694711	-0.023165
H	1.375112	-3.971831	-0.375333
C	0.308021	-3.271678	-3.297613
H	-0.211202	-2.673657	-4.06036
H	1.017926	-3.935485	-3.811886
H	-0.44021	-3.898034	-2.790581
C	2.376987	-1.049531	-2.960664
H	3.11263	-1.641546	-3.523884
H	1.845384	-0.405162	-3.675317
H	2.925437	-0.397542	-2.267207
C	6.114915	0.724654	-2.464018
H	5.255517	0.480644	-3.103914
H	6.25389	1.815298	-2.486306
H	7.01141	0.260288	-2.900809
C	5.559493	-1.730335	-0.724803
H	5.367448	-2.118044	0.285528
H	4.708705	-2.00418	-1.361481
H	6.450459	-2.239462	-1.118041
C	7.334271	0.53479	0.3286
H	7.208676	0.170379	1.358262
H	8.242414	0.075906	-0.089026
H	7.494939	1.621839	0.372391
C	2.167099	-1.562917	2.756133
H	3.253098	-1.625811	2.60529
H	1.941067	-1.963807	3.753705
H	1.687204	-2.218969	2.02144
C	-0.211605	0.325712	3.124341
H	-0.345256	-0.084959	4.13506
H	-0.562785	1.365434	3.141242
H	-0.85188	-0.244585	2.440179
C	2.598826	1.237276	3.846464
H	2.512187	0.848365	4.871367
H	3.660604	1.222018	3.561636
H	2.263992	2.284392	3.850244

32

[•A′], C_2; B3PW91-D3BJ/def2SVPD(C,H); ΔG°= -934.061376 au

C	0.000022	1.241995	0.885825
C	0.000000	0.000000	0.254374
C	-0.000022	-1.241995	0.885825

C	1.525166	3.851290	0.514785
C	-1.525725	3.850838	0.513974
C	0.000506	2.608444	-1.838484
C	-1.525166	-3.851290	0.514785
C	1.525725	-3.850838	0.513974
C	-0.000506	-2.608444	-1.838484
H	0.000030	1.225602	1.983409
H	0.000000	0.000000	-0.842189
H	-0.000030	-1.225602	1.983409
H	1.555472	3.999121	1.604072
H	1.531914	4.842819	0.038211
H	2.442068	3.321966	0.219106
H	-2.442306	3.321179	0.217901
H	-1.532570	4.842319	0.037298
H	-1.556604	3.998764	1.603231
H	0.890645	2.049262	-2.160582
H	0.000690	3.573188	-2.365106
H	-0.889501	2.049338	-2.161080
H	-1.555472	-3.999121	1.604072
H	-1.531914	-4.842819	0.038211
H	-2.442068	-3.321966	0.219106
H	2.442306	-3.321179	0.217901
H	1.532570	-4.842319	0.037298
H	1.556604	-3.998764	1.603231
H	-0.890645	-2.049262	-2.160582
H	-0.000690	-3.573188	-2.365106
H	0.889501	-2.049338	-2.161080
Si	0.000000	2.883228	0.013208
Si	0.000000	-2.883228	0.013208

129

[SnA′$_4$], D_2; B3PW91/def2TZVPD(Sn,Si);def2SVPD(C,H); ΔG°= -3950.512982 au

C	-1.358486	1.215529	1.232538
C	1.358486	-1.215529	1.232538
C	-2.291323	1.992127	0.364686
C	2.291323	-1.992127	0.364686
C	-3.628172	-1.833817	-0.268704
C	3.628172	1.833817	-0.268704
H	-1.935759	0.433726	1.751244
H	1.935759	-0.433726	1.751244
H	-1.828997	2.796572	-0.218728
H	1.828997	-2.796572	-0.218728
H	-4.067610	-1.025470	-0.867203
H	4.067610	1.025470	-0.867203
C	-1.358486	-1.215529	-1.232538
C	1.358486	1.215529	-1.232538
C	-2.291323	-1.992127	-0.364686
C	2.291323	1.992127	-0.364686

C	-3.628172	1.833817	0.268704
C	3.628172	-1.833817	0.268704
H	-1.935759	-0.433726	-1.751244
H	1.935759	0.433726	-1.751244
H	-1.828997	-2.796572	0.218728
H	1.828997	2.796572	0.218728
H	-4.067610	1.025470	0.867203
H	4.067610	-1.025470	0.867203
Si	-4.793455	2.882062	-0.741890
Si	0.691562	2.345293	-2.611563
Si	4.793455	2.882062	0.741890
Si	4.793455	-2.882062	-0.741890
Si	0.691562	-2.345293	2.611563
Si	-4.793455	-2.882062	0.741890
Si	-0.691562	-2.345293	-2.611563
Si	-0.691562	2.345293	2.611563
Sn	0.000000	0.000000	0.000000
C	-6.162633	3.512249	0.380800
H	-6.898421	4.101842	-0.186163
H	-6.698494	2.678258	0.857522
H	-5.758606	4.151293	1.179283
C	-5.570951	1.848589	-2.107363
H	-4.810337	1.478411	-2.809435
H	-6.099891	0.977518	-1.694050
H	-6.300229	2.440922	-2.679703
C	-3.888562	4.339967	-1.502530
H	-3.452635	4.990394	-0.730789
H	-3.079650	4.018156	-2.172814
H	-4.587325	4.947390	-2.095661
C	-2.000912	2.384949	3.957730
H	-1.731258	3.104812	4.744581
H	-2.973351	2.686305	3.542541
H	-2.128261	1.401384	4.431959
C	-0.448043	4.100969	1.992043
H	-1.393757	4.538800	1.645033
H	-0.073905	4.726600	2.815418
H	0.277300	4.169653	1.171614
C	0.930843	1.771932	3.365655
H	0.861362	0.770283	3.807753
H	1.746869	1.764295	2.630731
H	1.213839	2.466313	4.170583
C	5.570951	1.848589	2.107363
H	4.810337	1.478411	2.809435
H	6.099891	0.977518	1.694050
H	6.300229	2.440922	2.679703
C	6.162633	3.512249	-0.380800
H	5.758606	4.151293	-1.179283
H	6.898421	4.101842	0.186163

H	6.698494	2.678258	-0.857522
C	3.888562	4.339967	1.502530
H	3.452635	4.990394	0.730789
H	3.079650	4.018156	2.172814
H	4.587325	4.947390	2.095661
C	-0.930843	1.771932	-3.365655
H	-0.861362	0.770283	-3.807753
H	-1.746869	1.764295	-2.630731
H	-1.213839	2.466313	-4.170583
C	0.448043	4.100969	-1.992043
H	0.073905	4.726600	-2.815418
H	-0.277300	4.169653	-1.171614
H	1.393757	4.538800	-1.645033
C	2.000912	2.384949	-3.957730
H	1.731258	3.104812	-4.744581
H	2.973351	2.686305	-3.542541
H	2.128261	1.401384	-4.431959
C	-3.888562	-4.339967	1.502530
H	-3.452635	-4.990394	0.730789
H	-3.079650	-4.018156	2.172814
H	-4.587325	-4.947390	2.095661
C	-6.162633	-3.512249	-0.380800
H	-6.898421	-4.101842	0.186163
H	-6.698494	-2.678258	-0.857522
H	-5.758606	-4.151293	-1.179283
C	-5.570951	-1.848589	2.107363
H	-4.810337	-1.478411	2.809435
H	-6.099891	-0.977518	1.694050
H	-6.300229	-2.440922	2.679703
C	-0.448043	-4.100969	-1.992043
H	-1.393757	-4.538800	-1.645033
H	-0.073905	-4.726600	-2.815418
H	0.277300	-4.169653	-1.171614
C	-2.000912	-2.384949	-3.957730
H	-2.128261	-1.401384	-4.431959
H	-1.731258	-3.104812	-4.744581
H	-2.973351	-2.686305	-3.542541
C	0.930843	-1.771932	-3.365655
H	0.861362	-0.770283	-3.807753
H	1.746869	-1.764295	-2.630731
H	1.213839	-2.466313	-4.170583
C	3.888562	-4.339967	-1.502530
H	3.452635	-4.990394	-0.730789
H	3.079650	-4.018156	-2.172814
H	4.587325	-4.947390	-2.095661
C	0.448043	-4.100969	1.992043
H	0.073905	-4.726600	2.815418
H	-0.277300	-4.169653	1.171614

H	1.393757	-4.538800	1.645033
C	2.000912	-2.384949	3.957730
H	2.128261	-1.401384	4.431959
H	1.731258	-3.104812	4.744581
H	2.973351	-2.686305	3.542541
C	-0.930843	-1.771932	3.365655
H	-0.861362	-0.770283	3.807753
H	-1.746869	-1.764295	2.630731
H	-1.213839	-2.466313	4.170583
C	6.162633	-3.512249	0.380800
H	5.758606	-4.151293	1.179283
H	6.898421	-4.101842	-0.186163
H	6.698494	-2.678258	0.857522
C	5.570951	-1.848589	-2.107363
H	4.810337	-1.478411	-2.809435
H	6.099891	-0.977518	-1.694050
H	6.300229	-2.440922	-2.679703

97

[•SnA′$_3$], from D_2, C_1; B3PW91/def2TZVPD(Sn,Si);def2SVPD(C,H); ΔG°= -3016.457011 au

C	-0.153242	-1.173813	-1.175284
C	-0.681977	-1.791652	0.058806
C	-3.675472	0.713178	-0.383832
C	4.337 023	0.965667	0.001502
H	-0.976603	-0.991963	-1.883951
H	0.06822	-2.071528	0.804946
H	-3.738732	0.39844	0.664252
H	4.350189	2.05578	0.129012
C	-1.452954	1.761242	0.161113
C	1.978028	0.916561	0.929485
C	-2.567882	1.391759	-0.740244
C	3.213245	0.319384	0.368911
C	-1.980165	-2.038892	0.334534
H	-1.594245	1.292573	1.144278
H	2.126607	1.997207	1.071967
H	-2.471374	1.721832	-1.782162
H	3.186537	-0.767474	0.241966
H	-2.704987	-1.738236	-0.426748
Sn	0.412901	0.884923	-0.616998
Si	-2.627633	-2.84626	1.870385
Si	1.17752	-2.168527	-2.058752
Si	5.830158	0.122107	-0.711425
Si	1.592852	0.21527	2.641421
Si	-1.336332	3.618454	0.40758
Si	-5.062299	0.258265	-1.525179
C	-4.633964	0.773283	-3.27373
H	-4.490475	1 .860763	-3.346831
H	-3.711207	0.282533	-3.615129

H	-5.440602	0.493715	-3.965639
C	-5.339294	-1.597055	-1.459729
H	-4.4806	-2.148405	-1.867373
H	-5.491931	-1.930921	-0.423528
H	-6.229746	-1.880737	-2.0384
C	-6.636922	1.111504	-0.97132
H	-6.523335	2.204148	-1.012142
H	-7.488734	0.830354	-1.607826
H	-6.883713	0.837169	0.064748
C	-1.292711	4.466458	-1.259833
H	-1.183469	5.553809	-1.14109
H	-0.448505	4.104796	-1.864984
H	-2.218762	4.280597	-1.821372
C	0.205937	4.070671	1.37337
H	0.31236	3.459894	2.280107
H	1.113603	3.944003	0.767289
H	0.159605	5.12426	1.683331
C	-2.852003	4.15693	1.36271
H	-3.762294	3.817527	0.848593
H	-2.853245	3.718937	2.371465
H	-2.899274	5.250472	1.465316
C	-3.646197	-4.341621	1.380986
H	-4.097382	-4.822656	2.26109
H	-4.457725	-4.053333	0.69797
H	-3.021854	-5.085207	0.865387
C	-3.735232	-1.648989	2.799512
H	-3.186431	-0.744372	3.0948
H	-4.58623	-1.341256	2.175623
H	-4.138258	-2.116712	3.70934
C	-1.207163	-3.380443	2.966647
H	-1.588127	-3.891524	3.861829
H	-0.540613	-4.076329	2.438156
H	-0.607698	-2.524116	3.298877
C	2.076746	-3.260356	-0.832195
H	2.862234	-3.83803	-1.337842
H	2.552387	-2.694711	-0.023165
H	1.375112	-3.971831	-0.375333
C	0.308021	-3.271678	-3.297613
H	-0.211202	-2.673657	-4.06036
H	1.017926	-3.935485	-3.811886
H	-0.44021	-3.898034	-2.790581
C	2.376987	-1.049531	-2.960664
H	3.11263	-1.641546	-3.523884
H	1.845384	-0.405162	-3.675317
H	2.925437	-0.397542	-2.267207
C	6.114915	0.724654	-2.464018
H	5.255517	0.480644	-3.103914
H	6.25389	1.815298	-2.486306

H	7.01141	0.260288	-2.900809
C	5.559493	-1.730335	-0.724803
H	5.367448	-2.118044	0.285528
H	4.708705	-2.00418	-1.361481
H	6.450459	-2.239462	-1.118041
C	7.334271	0.53479	0.3286
H	7.208676	0.170379	1.358262
H	8.242414	0.075906	-0.089026
H	7.494939	1.621839	0.372391
C	2.167099	-1.562917	2.756133
H	3.253098	-1.625811	2.60529
H	1.941067	-1.963807	3.753705
H	1.687204	-2.218969	2.02144
C	-0.211605	0.325712	3.124341
H	-0.345256	-0.084959	4.13506
H	-0.562785	1.365434	3.141242
H	-0.85188	-0.244585	2.440179
C	2.598826	1.237276	3.846464
H	2.512187	0.848365	4.871367
H	3.660604	1.222018	3.561636
H	2.263992	2.284392	3.850244

32

[•A′], C_2; B3PW91/def2SVPD; ΔG°= -934.006739 au

C	0.000035	1.242378	0.844073
C	0.000000	0.000000	0.209292
C	-0.000035	-1.242378	0.844073
C	1.527654	3.865585	0.547194
C	-1.528496	3.864952	0.545940
C	0.000770	2.704817	-1.853451
C	-1.527654	-3.865585	0.547194
C	1.528496	-3.864952	0.545940
C	-0.000770	-2.704817	-1.853451
H	0.000048	1.216092	1.942352
H	0.000000	0.000000	-0.887886
H	-0.000048	-1.216092	1.942352
H	1.559496	3.978590	1.640927
H	1.534602	4.873244	0.104876
H	2.447565	3.350260	0.235352
H	-2.447930	3.349196	0.233407
H	-1.535535	4.872574	0.103538
H	-1.561253	3.978023	1.639639
H	0.890846	2.159902	-2.200303
H	0.000873	3.689259	-2.343372
H	-0.888932	2.159745	-2.201019
H	-1.559496	-3.978590	1.640927
H	-1.534602	-4.873244	0.104876
H	-2.447565	-3.350260	0.235352

H	2.447930	-3.349196	0.233407
H	1.535535	-4.872574	0.103538
H	1.561253	-3.978023	1.639639
H	-0.890846	-2.159902	-2.200303
H	-0.000873	-3.689259	-2.343372
H	0.888932	-2.159745	-2.201019
Si	0.000000	2.911090	0.011295
Si	0.000000	-2.911090	0.011295

45

[Me_3SnA'], C_1; B3PW91-D3BJ/def2TZVP(Sn,Si);def2SVP(C,H); $\Delta G°$= -1268.055070 au

C	0.246770	-2.815345	-0.073610
C	0.419828	0.590902	-0.579728
C	-0.956993	0.394512	-0.063465
C	-2.072579	0.148693	-0.779378
C	0.282778	3.602722	-0.962774
C	2.994689	2.266573	-0.493998
C	0.964802	2.482517	1.790098
C	-4.319900	-1.882041	-0.508568
C	-4.977838	1.090582	-0.685115
C	-3.639457	-0.030733	1.832086
C	2.432727	-0.979489	1.948159
C	3.165989	-1.413878	-1.466202
H	-0.488451	-2.722232	0.737968
H	0.418753	0.563430	-1.684031
H	-1.051842	0.439798	1.031304
H	-1.965967	0.100086	-1.873314
H	2.962031	-1.907827	2.208295
H	3.888098	-0.588378	-1.405507
H	0.436727	3.521728	-2.050376
H	0.633799	4.596926	-0.644315
H	-0.800662	3.545234	-0.774510
H	3.572736	1.534829	0.091049
H	3.421739	3.261798	-0.293639
H	3.150990	2.044532	-1.561251
H	-0.099160	2.536491	2.067148
H	1.435838	3.429222	2.098736
H	1.427367	1.673107	2.373029
H	-4.371849	-1.993068	-1.603330
H	-5.321327	-2.095198	-0.101746
H	-3.625786	-2.647499	-0.128016
H	-4.687516	2.114746	-0.403364
H	-5.987156	0.899995	-0.286728
H	-5.038027	1.050656	-1.784328
H	-2.941189	-0.772031	2.251054
H	-4.627885	-0.212367	2.282848
H	-3.306177	0.969313	2.150574
Si	1.172792	2.229057	-0.053623

Si	-3.741609	-0.161205	-0.034867
Sn	1.599501	-1.153505	-0.022837
H	-0.298760	-2.822935	-1.027866
H	0.785929	-3.766811	0.039764
H	3.695942	-2.360204	-1.284646
H	2.744624	-1.438341	-2.481468
H	1.636129	-0.815377	2.687632
H	3.144559	-0.144413	2.004738

3.4 References

(1) Tan, D.; Loots, L.; Friščić, T. Towards Medicinal Mechanochemistry: Evolution of Milling from Pharmaceutical Solid Form Screening to the Synthesis of Active Pharmaceutical Ingredients (APIs). *Chem. Commun.* **2016**, *52* (50), 7760–7781.

(2) Andersen, J. M.; Mack, J. Decoupling the Arrhenius Equation via Mechanochemistry. *Chem. Sci.* **2017**, *8* (8), 5447–5453.

(3) Hernández, J. G.; Bolm, C. Altering Product Selectivity by Mechanochemistry. *J. Org. Chem.* **2017**, *82* (8), 4007–4019.

(4) Rightmire, N. R.; Hanusa, T. P.; Rheingold, A. L. Mechanochemical Synthesis of [1,3-$(SiMe_3)_2C_3H_3]_3$(Al,Sc), a Base-Free Tris(Allyl)Aluminum Complex and Its Scandium Analogue. *Organometallics* **2014**, *33* (21), 5952–5955.

(5) Leon, F.; Garcia Molecular Sciences and Chemical Engineering, F. B. T.-R. M. in C. Metal Complexes in Mechanochemistry; Elsevier, 2021.

(6) Gečiauskaitė, A. A.; García, F. Main Group Mechanochemistry. *Beilstein Journal of Organic Chemistry*. 2017, pp 2068–2077.

(7) Tan, D.; García, F. Main Group Mechanochemistry: From Curiosity to Established Protocols. *Chemical Society Reviews*. 2019.

(8) Wang, J.; Ganguly, R.; Yongxin, L.; Díaz, J.; Soo, H. Sen; García, F. A Multi-Step Solvent-Free Mechanochemical Route to Indium(III) Complexes. *Dalt. Trans.* **2016**, *45* (19), 7941–7946.

(9) Hernández, J. G.; Butler, I. S.; Friščić, T. Multi-Step and Multi-Component Organometallic Synthesis in One Pot Using Orthogonal Mechanochemical Reactions. *Chem. Sci.* **2014**, *5* (9), 3576–3582.

(10) Glavinović, M.; Krause, M.; Yang, L.; McLeod, J. A.; Liu, L.; Baines, K. M.; Friščić, T.; Lumb, J.-P. A Chlorine-Free Protocol for Processing Germanium. *Sci. Adv.* **2017**, *3*, e1700149.

(11) Aleksanyan, D. V; Churusova, S. G.; Aysin, R. R.; Klemenkova, Z. S.; Nelyubina, Y. V; Kozlov, V. A. The First Example of Mechanochemical Synthesis of Organometallic Pincer Complexes. *Inorg. Chem. Commun.* **2017**, *76*, 33.

(12) Jobbágy, C.; Tunyogi, T.; Pálinkás, G.; Deák, A. A Versatile Solvent-Free Mechanochemical Route to the Synthesis of Heterometallic Dicyanoaurate-Based Coordination Polymers. *Inorg. Chem.* **2011**, *50*, 7301.

(13) Jobbágy, C.; Molnar, M.; Baranyai, P.; Deák, A. Mechanochemical Synthesis of Crystalline and Amorphous Digold(I) Helicates Exhibiting Anion- and Phase-Switchable Luminescence Properties. *Dalt. Trans* **2014**, *43*, 11807.

(14) Bowmaker, G. A.; Hanna, J. V; Hart, R. D.; Healy, P. C.; King, S. P.; Marchetti, F.; Pettinari, C.; Skelton, B. W.; Tabacaru, A.; White, A. H. Mechanochemical and Solution Synthesis, X-Ray Structure and IR and 31P Solid State NMR Spectroscopic Studies of Copper(I) Thiocyanate Adducts with Bulky Monodentate Tertiary Phosphine Ligands. *Dalt. Trans* **2012**, *41*, 7513.

(15) Garay, A. L.; Pichon, A.; James, S. L. Solvent-Free Synthesis of Metal Complexes. *Chem. Soc. Rev.* **2007**, *36*, 846.

(16) Balaz, P.; Achimovicova, M.; Balaz, M.; Billik, P.; Cherkezova-Zheleva, Z.; Criado, J. M.; Delogu, F.; Dutkova, E.; Gaffet, E.; Gotor, F. J.; Kumar, R.; Mitov, I.; Rojac, T.; Senna, M.; Streletskii, A.; Wieczorek-Ciurowa, K. Hallmarks of Mechanochemistry: From Nanoparticles to Technology. *Chem. Soc. Rev.* **2013**, *42*, 7571.

(17) Baláž, P. *Mechanochemistry in Nanoscience and Minerals Engineering*; 2008.

(18) Anastas, P. T.; Warner, J. C. *Green Chemistry: Theory and Practice*; 1998.

(19) Anastas, P.; Eghbali, N. Green Chemistry: Principles and Practice. *Chem. Soc. Rev.* **2010**, *39*

(1), 301–312.
(20) Erythropel, H. C.; Zimmerman, J. B.; de Winter, T. M.; Petitjean, L.; Melnikov, F.; Lam, C. H.; Lounsbury, A. W.; Mellor, K. E.; Janković, N. Z.; Tu, Q.; Pincus, L. N.; Falinski, M. M.; Shi, W.; Coish, P.; Plata, D. L.; Anastas, P. T. The Green ChemisTREE: 20 Years after Taking Root with the 12 Principles. *Green Chem.* **2018**, *20* (9), 1929–1961.
(21) Ardila-Fierro, K. J.; Hernández, J. G. Sustainability Assessment of Mechanochemistry Using the Twelve Principles of Green Chemistry. *ChemSusChem* **2021**,
(22) Shi, Y. X.; Xu, K.; Clegg, J. K.; Ganguly, R.; Hirao, H.; Friščić, T.; García, F. The First Synthesis of the Sterically Encumbered Adamantoid Phosphazane P4(NtBu)6: Enabled by Mechanochemistry. *Angew. Chemie Int. Ed.* **2016**, *55* (41), 12736–12740.
(23) Komatsu, K.; Wang, G.-W.; Murata, Y.; Tanaka, T.; Fujiwara, K.; Yamamoto, K.; Saunders, M. Mechanochemical Synthesis and Characterization of the Fullerene Dimer C120. *J. Org. Chem.* **1998**, *63*, 9358.
(24) Zhu, S.-E.; Li, F.; Wang, G.-W. Mechanochemistry of Fullerenes and Related Materials. *Chem. Soc. Rev.* **2013**, *42*, 7535.
(25) Elschenbroich, C. *Organometallics*; 3, Ed.; 2006.
(26) Davidson, P. J.; Harris, D. H.; Lappert, M. F. The Synthesis and Physical Properties of Kinetically Stable Bis(Bistrimethsilylmethyl)Ge(II), Sn(II), and Pb(II). *J. Chem. Soc., Dalt. Trans.* **1976**, 2268.
(27) Jutzi, P.; Burford, N. Structurally Diverse π-Cyclopentadienyl Complexes of the Main Group Elements. *Chem. Rev.* **1999**, *99* (4), 969–990.
(28) Becerra, R.; Gaspar, P. P.; Harrington, C. R.; Leigh, W. J.; Vargas-Baca, I.; Walsh, R.; Zhou, D. Direct Detection of Dimethylstannylene and Tetramethyldistannene in Solution and the Gas Phase by Laser Flash Photolysis of 1,1-Dimethylstannacyclopent-3-Enes. *J. Am. Chem. Soc.* **2005**, *127*, 17469.
(29) Chmely, S. C.; Hanusa, T. P. Complexes with Sterically Bulky Allyl Ligands: Insights into Structure and Bonding. *Eur. J. Inorg. Chem.* 2010, pp 1321–1337.
(30) Chmely, S. C.; Hanusa, T. P. D- and f-Block Transition Metal Complexes with Bulky Allyl Ligands. *Encyclopedia of Inorganic and Bioinorganic Chemistry*. December 15, 2011.
(31) Hanusa, T. P.; Carlson, C. N. Transition Metal Complexes with Bulky Allyl Ligands. *Encyclopedia of Inorganic and Bioinorganic Chemistry*. December 15, 2011.
(32) Solomon, S. a; Layfield, R. a. The Coordination Chemistry of Silyl-Substituted Allyl Ligands. *Dalton Trans.* **2010**, *39*, 2469–2483.
(33) Layfield, R. A.; García, F.; Hannauer, J.; Humphrey, S. M. Ansa-Tris(Allyl) Complexes of Alkali Metals: Tripodal Analogues of Cyclopentadienyl and Ansa-Metallocene Ligands. *Chem. Commun.* **2007**, *499* (47), 5081–5083.
(34) Boyde, C. N.; Rightmire, R. N.; Hanusa, P. T.; Brennessel, W. W. Symmetric Assembly of a Sterically Encumbered Allyl Complex: Mechanochemical and Solution Synthesis of the Tris(Allyl)Beryllate, K[BeA′$_3$] (A′ = 1,3-(SiMe$_3$)$_2$C$_3$H$_3$). *Inorganics* **2017**, *5* (2), 36.
(35) Gren, C. K.; Hanusa, T. P.; Rheingold, A. L. Threefold Cation-π Bonding in Trimethylsilylated Allyl Complexes. *Organometallics* **2007**, *26* (7), 1643–1649.
(36) Rightmire, N. R.; Bruns, D. L.; Hanusa, T. P.; Brennessel, W. W. Mechanochemical Influence on the Stereoselectivity of Halide Metathesis: Synthesis of Group 15 Tris(Allyl) Complexes. *Organometallics* **2016**, *35* (11), 1698–1706.
(37) Kleeberg, C.; Grunenberg, J.; Xie, X. K–H3C and K–Sn Interactions in Potassium Trimethylstannyl Complexes: A Structural, Mechanochemical, and NMR Study. *Inorg. Chem.* **2014**, *53* (9), 4400–4410.
(38) Shannon, R. Revised Effective Ionic Radii and Systematic Studies of Interatomic Distances

in Halides and Chalcogenides. *Acta Crystallogr. Sect. A* **1976**, *32* (5), 751–767.
(39) Quisenberry, K. T.; Smith, J. D.; Voehler, M.; Stec, D. F.; Hanusa, T. P.; Brennessel, W. W. Trimethylsilylated Allyl Complexes of Nickel. The Stabilized Bis(Pi-Allyl)Nickel Complex $[\eta^3$-1,3-$(SiMe_3)_2C_3H_3]_2Ni$ and Its Mono(π-Allyl)NiX (X=Br, I) Derivatives. *J. Am. Chem. Soc.* **2005**, *127* (12), 4376–4387.
(40) Davies, A. G.; Gielen, M.; Pannell, K. H.; Tiekink, E. R. T. *Tin Chemistry: Fundamentals, Frontiers, and Applications*; 2008.
(41) Hernández, J. G.; Macdonald, N. A. J.; Mottillo, C.; Butler, I. S.; Friščić, T. A Mechanochemical Strategy for Oxidative Addition: Remarkable Yields and Stereoselectivity in the Halogenation of Organometallic Re(i) Complexes. *Green Chem.* **2014**, *16* (3), 1087–1092.
(42) Brown, P.; Mahon, M. F.; Molloy, K. C. Sterically Hindered Organotin Compounds. Part 1. Synthesis and Reaction Chemistry of Tris(Trimethylsilyl)Methyltin(IV) Derivatives. X-Ray Crystal Structures of $Sn(CH_2Ph)_2[C(SiMe_3)_3](OSiMe_3)$ and $Sn(CH_2Ph)_2[C(SiMe_3)_3][CH_2CH = C(SiMe_3)_2]$. *J. Chem. Soc., Dalt. Trans.* **1990**, 2643.
(43) Friščić, T.; Halasz, I.; Beldon, P. J.; Belenguer, A. M.; Adams, F.; Kimber, S. A. J.; Honkimäki, V.; Dinnebier, R. E. Real-Time and in Situ Monitoring of Mechanochemical Milling Reactions. *Nat. Chem.* **2013**, *5*, 66.
(44) Halasz, I.; Kimber, S. A. J.; Beldon, P. J.; Belenguer, A. M.; Adams, F.; Honkimäki, V.; Nightingale, R. C.; Dinnebier, R. E.; Friščić, T. In Situ and Real-Time Monitoring of Mechanochemical Milling Reactions Using Synchrotron X-Ray Diffraction. *Nat. Protoc.* **2013**, *8*, 1718.
(45) Kulla, H.; Fischer, F.; Benemann, S.; Rademann, K.; Emmerling, F. The Effect of the Ball to Reactant Ratio on Mechanochemical Reaction Times Studied by in Situ PXRD. *CrystEngComm* **2017**, *19* (28), 3902–3907.
(46) Gracin, D.; Štrukil, V.; Friščić, T.; Halasz, I.; Užarević, K. Laboratory Real-Time and In Situ Monitoring of Mechanochemical Milling Reactions by Raman Spectroscopy. *Angew. Chem., Int. Ed.* **2014**, *53*, 6193.
(47) Juribašić, M.; Užarević, K.; Gracin, D.; Ćurić, M. Mechanochemical C–H Bond Activation: Rapid and Regioselective Double Cyclopalladation Monitored by in Situ Raman Spectroscopy. *Chem. Commun.* **2014**, *50* (71), 10287–10290.
(48) Štrukil, V.; Gracin, D.; Magdysyuk, O. V; Dinnebier, R. E.; Friščić, T. Trapping Reactive Intermediates by Mechanochemistry: Elusive Aryl N-Thiocarbamoylbenzotriazoles as Bench-Stable Reagents. *Angew. Chem., Int. Ed.* **2015**, *54*, 8440.
(49) Fischer, F.; Fendel, N.; Greiser, S.; Rademann, K.; Emmerling, F. Impact Is Important—Systematic Investigation of the Influence of Milling Balls in Mechanochemical Reactions. *Org. Process Res. Dev.* **2017**, *21*, 655.
(50) Užarević, K.; Halasz, I.; Friščić, T. Real-Time and In Situ Monitoring of Mechanochemical Reactions: A New Playground for All Chemists. *J. Phys. Chem. Lett.* **2015**, *6* (20), 4129–4140.
(51) Lukin, S.; Stolar, T.; Tireli, M.; Blanco, M. V; Babić, D.; Friščić, T.; Užarević, K.; Halasz, I. Tandem In Situ Monitoring for Quantitative Assessment of Mechanochemical Reactions Involving Structurally Unknown Phases. *Chem. - Eur. J.* **2017**, *23*, 13941.
(52) Prince, R. H. Reaction Mechanism in Organometallic Compounds. Comparative Solvolyses of Organotin and Organosilicon Chlorides. *J. Chem. Soc.* **1959**, 1783.
(53) Burke, K.; Perdew, J. P.; Wang, Y. Derivation of a Generalized Gradient Approximation: The PW91 Density Functional BT - Electronic Density Functional Theory: Recent Progress and New Directions; Dobson, J. F., Vignale, G., Das, M. P., Eds.; Springer US: Boston, MA, 1998; pp 81–111.
(54) Becke, A. D. Density-functional Thermochemistry. III. The Role of Exact Exchange. *J. Chem.*

Phys. **1993**, *98* (7), 5648–5652.
(55) Grimme, S.; Antony, J.; Ehrlich, S.; Krieg, H. A Consistent and Accurate Ab Initio Parametrization of Density Functional Dispersion Correction (DFT-D) for the 94 Elements H-Pu. *J. Chem. Phys.* **2010**, *132* (15), 154104.
(56) Grimme, S.; Ehrlich, S.; Goerigk, L. Effect of the Damping Function in Dispersion Corrected Density Functional Theory. *J. Comput. Chem.* **2011**, *32* (7), 1456–1465.
(57) Scott, W. J.; Moretto, A. F. Tetraallylstannane. *Encyclopedia of Reagents for Organic Synthesis*. April 15, 2001.
(58) Pereyre, M.; Quintard, J.-P.; Rahm, A. *Tin in Organic Synthesis*; 1987.
(59) Alwyn, D. Allyl-, Allenyl-, Propargyl-, and Cyclopentadienyl-Stannanes. *Organotin Chemistry*. March 11, 2004, pp 133–155.
(60) Kawakami, K.; Kuivila, H. G. Preparation and Spectral Characteristics of Some Allyltins. *J. Org. Chem.* **1969**, *34*, 1502.
(61) Weidner, U.; Schweig, A. Nature of the "Silicon β-Effect" in Allyltrimethylsilane. *Angew. Chemie Int. Ed. English* **1972**, *11* (2), 146–147.
(62) Burshtein, K. Y.; Isaev, A. N.; Shorygin, P. P. σ-π Interaction in Some σ-Bonded Allyl Compounds. A MNDO Study. *J. Organomet. Chem.* **1989**, *361*, 21.
(63) Bach, R. D.; Scherr, P. A. Extended Hückel Calculations on Group IV Allyl Compounds Evidence for σ-π Conjugation. *Tetrahedron Lett.* **1973**, *14*, 1099.
(64) Mayer, I. Charge, Bond Order and Valence in the AB Initio SCF Theory. *Chem. Phys. Lett.* **1983**, *97*, 270.
(65) Bridgeman, A. J.; Cavigliasso, G.; Ireland, L. R.; Rothery, J. The Mayer Bond Order as a Tool in Inorganic Chemistry. *J. Chem. Soc. Dalt. Trans.* **2001**, No. 14, 2095–2108.
(66) Simões, J. A. M.; Linstrom, P. J.; Mallard, W. G. *NIST Chemistry WebBook, NIST Standard Reference Database Number 69*; 2018.
(67) Guzei, I. A.; Wendt, M. An Improved Method for the Computation of Ligand Steric Effects Based on Solid Angles. *Dalt. Trans.* **2006**, No. 33, 3991–3999.
(68) Grimme, S.; Huenerbein, R.; Ehrlich, S. On the Importance of the Dispersion Energy for the Thermodynamic Stability of Molecules. *ChemPhysChem* **2011**, *12*, 1258.
(69) Kahr, B.; Van Engen, D.; Mislow, K. Length of the Ethane Bond in Hexaphenylethane and Its Derivatives. *J. Am. Chem. Soc.* **1986**, *108* (26), 8305–8307.
(70) Grimme, S.; Schreiner, P. R. Steric Crowding Can Stabilize a Labile Molecule: Solving the Hexaphenylethane Riddle. *Angew. Chem. Int. Ed.* **2011**, *50* (52), 12639–12642.
(71) Liptrot, D. J.; Power, P. P. London Dispersion Forces in Sterically Crowded Inorganic and Organometallic Molecules. *Nat. Rev. Chem.* **2017**, *1*, 4.
(72) Bondi, A. Van Der Waals Volumes and Radii. *J. Phys. Chem.* **1964**, *68*, 441.
(73) Gamsjäger, H.; Gajda, T. S.; Saxena, S. K.; Sangster, J.; Voigt, W. *Chemical Thermodynamics of Tin*; 2012; Vol. 12.
(74) Čerič, B.; Bukovec, P. Thermal Decomposition of the Mixture of Antimony(III) Oxide and Tin(II) Chloride. *Thermochim. Acta* **1992**, *195*, 73.
(75) Fraenkel, G.; Chow, A.; Winchester, W. R. Dynamics of Solvated Li+ within Exo,Exo- [1 ,3 - Bis(Trimethylsilyl)Ally]Lithium N,N,N',N'-Tetramethylethylenediamine Complex. *J. Am. Chem. Soc.* **1990**, *112*, 1382–1386.
(76) Armarego, W. L. F.; Chai, C. L. L. Chapter 1 - Common Physical Techniques Used in Purification; Armarego, W. L. F., Chai,(Sixth E., Eds.; Butterworth-Heinemann: Oxford, 2009; pp 1–60.
(77) Dolomanov, O. V; Bourhis, L. J.; Gildea, R. J.; Howard, J. A. K.; Puschmann, H. OLEX2: A Complete Structure Solution, Refinement and Analysis Program. *J. Appl. Crystallogr.* **2009**,

42 (2), 339–341.
(78) Sheldrick, G. SHELXT - Integrated Space-Group and Crystal-Structure Determination. *Acta Crystallogr. Sect. A* **2015**, *71* (1), 3–8.
(79) Sheldrick, G. Crystal Structure Refinement with SHELXL. *Acta Crystallogr. Sect. C* **2015**, *71* (1), 3–8.
(80) M. J. Frisch, G. W. Trucks, H. B. Schlegel, G. E. Scuseria, M.; A. Robb, J. R. Cheeseman, G. Scalmani, V. Barone, B. Mennucci, G. A. Petersson, H.; Nakatsuji, M. Caricato, X. Li, H. P. Hratchian, A. F. Izmaylov, J. Bloino, G. Zheng, J. L.; Sonnenberg, M. Hada, M. Ehara, K. Toyota, R. Fukuda, J. Hasegawa, M. Ishida, T.; Nakajima, Y. Honda, O. Kitao, H. Nakai, T. Vreven, J. A. Montgomery, Jr., J. E. Peralta, F.; Ogliaro, M. Bearpark, J. J. Heyd, E. Brothers, K. N. Kudin, V. N. Staroverov, R.; Kobayashi, J. Normand, K. Raghavachari, A. Rendell, J. C. Burant, S. S. Iyengar, J.; Tomasi, M. Cossi, N. Rega, J. M. Millam, M. Klene, J. E. Knox, J. B. Cross, V. Bakken, C.; Adamo, J. Jaramillo, R. Gomperts, R. E. Stratmann, O. Yazyev, A. J. Austin, R. Cammi, C.; Pomelli, J. W. Ochterski, R. L. Martin, K. Morokuma, V. G. Zakrzewski, G. A. Voth, P.; Salvador, J. J. Dannenberg, S. Dapprich, A. D. Daniels, Ö. Farkas, J. B. Foresman, J. V.; Ortiz, J. Cioslowski, and D. J. Fox, Gaussian, Inc., Wallingford CT, 2009. Gaussian16 Revision D.01. *http//www. gaussian. com/* **2009**.
(81) Frisch, M. J.; Trucks, G. W.; Schlegel, H. B.; Scuseria, G. E.; Robb, M. a.; Cheeseman, J. R.; Scalmani, G.; Barone, V.; Petersson, G. a.; Nakatsuji, H.; Li, X.; Caricato, M.; Marenich, a. V.; Bloino, J.; Janesko, B. G.; Gomperts, R.; Mennucci, B.; Hratchian, H. P.; Ortiz, J. V.; Izmaylov, a. F.; Sonnenberg, J. L.; Williams; Ding, F.; Lipparini, F.; Egidi, F.; Goings, J.; Peng, B.; Petrone, A.; Henderson, T.; Ranasinghe, D.; Zakrzewski, V. G.; Gao, J.; Rega, N.; Zheng, G.; Liang, W.; Hada, M.; Ehara, M.; Toyota, K.; Fukuda, R.; Hasegawa, J.; Ishida, M.; Nakajima, T.; Honda, Y.; Kitao, O.; Nakai, H.; Vreven, T.; Throssell, K.; Montgomery Jr., J. a.; Peralta, J. E.; Ogliaro, F.; Bearpark, M. J.; Heyd, J. J.; Brothers, E. N.; Kudin, K. N.; Staroverov, V. N.; Keith, T. a.; Kobayashi, R.; Normand, J.; Raghavachari, K.; Rendell, a. P.; Burant, J. C.; Iyengar, S. S.; Tomasi, J.; Cossi, M.; Millam, J. M.; Klene, M.; Adamo, C.; Cammi, R.; Ochterski, J. W.; Martin, R. L.; Morokuma, K.; Farkas, O.; Foresman, J. B.; Fox, D. J. Gaussian16 B01. 2016, p Gaussian 16, Revision C.01, Gaussian, Inc., Wallin.
(82) Rappoport, D.; Furche, F. Property-Optimized Gaussian Basis Sets for Molecular Response Calculations. *J. Chem. Phys.* **2010**, *133* (13), 134105.
(83) Lu, T.; Chen, F. Multiwfn: A Multifunctional Wavefunction Analyzer. *J. Comput. Chem.* **2012**, *33* (5), 580–592.

Chapter 4

Halide metathesis in overdrive: mechanochemical synthesis of a heterometallic group 1 allyl complex

Reprinted with permission from Ross F. Koby, Nicholas R. Rightmire, Nathan D. Schley, Timothy P. Hanusa and William W.Brennessel *Beilstein J. Org. Chem.* **2019,** *15,* 1856–1863

4.1 Introduction

Halide (or 'salt') metathesis is a broadly useful synthetic technique in organometallic chemistry, applicable to elements across the entire periodic table. A typical instance involves the reaction of a metal halide ($M'X_n$) with an organoalkali metal compound (RM; M = Li, Na, K) (Equation 1).[1]

$$n\ RM + M'X_n \rightarrow R_nM' + n\ MX \quad (1)$$

As the generation of MX normally provides a substantial portion of the energy for the exchange, M should be more electropositive than M', in order to maximize hard–soft acid–base interactions.[2] The reaction will proceed without solvent, and mechanochemical activation, which promotes reactions through grinding or milling with no, or minimal, use of solvents, has been used in conjunction with halide metathesis to form organometallic compounds of the transition metals[3–7] and both s-[8,9] and p-block[10,11] main group elements.

The extent to which the exchange represented in Equation 1 is complete varies widely with the system. In general, the larger the value of *n*, and the correspondingly increased amount of MX that is formed, the greater the driving force. Consequently, exchange will be assisted with higher valent $M'X_n$ halides. Furthermore, although in general a solvent is not required, in solution environments the formation of products is assisted if the solubility of MX or R_nM' is limited, as their precipitation helps shift the equilibrium toward the product side. If ethers are used as solvents, for example, the low solubility of MX can be reduced further by choosing M to be potassium rather than lithium; as an added benefit, the resulting potassium halides are less likely to contaminate the desired product.

Without a solvent present and if M and M' are both univalent metals with similar electronegativity, complete exchange becomes difficult, and the extent of even partial exchange is hard to predict. For the alkali metals, all electronegativity scales indicate that cesium is the most electropositive, but they also indicate that there is comparatively little variation in this metric.[12] What happens when the energy difference between M'X and MX becomes particularly small? Here we describe the application of mechanochemistry in an organometallic context to examine alkali metal halide exchange unassisted by solvents. The

organic group used is the bulky 1,3-bis(trimethylsilyl)allyl anion, [1,3-$(SiMe_3)_2C_3H_3]^-$ ($[A']^-$),[13,14] for which alkali metal complexes are known, including those of Li,[15] Na,[16] K,[17,18] and Cs[18]. These have been formed via traditional solvent-based routes, by deprotonation of the substituted propene precursor with a metal alkyl or hydride (Equation 2) or with the metal itself (Equation 3).[18] Intra-alkali metal exchange (although not specifically halide metathesis) has been conducted with the $[A']^-$ anion, but always in the presence of a solvent to help drive the process (Equation 4).[19]

$$\text{Li}(n\text{-Bu}) + \text{HA}' \xrightarrow{\text{hexanes}} \text{LiA}' + \text{H}(n\text{-Bu}) \uparrow \quad (2)$$

$$\text{Cs} + \text{HA}' \xrightarrow{\text{THF}} [(\text{thf})\text{CsA}'] + \tfrac{1}{2}\,\text{H}_2 \uparrow \quad (3)$$

$$[\text{LiA}'] + [\text{KO}^t\text{Bu}] \xrightarrow{\text{hexanes}} [\text{KA}'] \downarrow + [\text{LiO}^t\text{Bu}] \quad (4)$$

4.2 Results and Discussion

4.2.1 Conditions for halide exchange

Apart from thermodynamic considerations, practical concerns place limits on the combinations of halides and alkali metals that could be feasibly studied in intra-alkali exchange experiments. For example, the fluorides have the largest heats of formation of the alkali halides, regardless of metal, but their high lattice energies make them typically unreactive, even under mechanochemical conditions.[20] However note that alkali metal fluorides can be useful as reagents if the thermodynamics of the system are appropriately configured. For example, the reaction of $[LiN(SiMe_3)_2]$ with CsF works to produce the products $[CsN(SiMe_3)_2]$ with LiF in high yield because the relative heats of formation ($\Delta H°_f$) of CsF and LiF (–554 and –616 kJ mol^{-1}, respectively) provide a net driving force of –62 kJ mol^{-1}.[21] The iodides, in contrast, have the smallest lattice energies and thus should be the most easily disrupted and liable to exchange. Although several metal compounds of the allyl anion $[A']^-$ were potential candidates for the present study, the need for a base-free, unsolvated complex that preferably had been crystallographically characterized limited the choice to the potassium complex $[KA']_\infty$. In that form,[17] as well as when crystallized from THF,[18] DME,[22] or as described below, arenes, $[KA']_\infty$ retains the structure of an undulating or helical coordination polymer. Within these experimental parameters, the general reaction in Equation 5 was examined. When n = 1, a reaction carried to completion would result in full metal exchange, with partial exchange the outcome for any larger values of n.

$$[\text{KA}'] + \text{M}'\text{I} \rightarrow [\text{MK}_{n-1}\text{A}'_n] + \text{KI} \quad (5)$$

The experimental protocol involved grinding various ratios of [KA'] and alkali metal iodides, extracting the ground mixtures with hydrocarbon solvents, and then attempting crystallization of the extracts. This is necessarily an imperfect route to sampling the product space, as definitive characterization of any product(s) depended critically on the crystallizing process. In particular, NMR spectra were not expected to be highly diagnostic, as in all its group 1 complexes the resonances from the $[A']^-$ anion provide a characteristic spectrum of similar chemical shifts with singlet (-$SiMe_3$), doublet ($C_{1,3}$-H), and triplet (C_2-H) patterns that result from a π-bound allyl with *syn*,*syn*-trimethylsilyl arrangements.[22]

Grinding [KA'] in a mixer or planetary mill in a 1:1 or 2:1 ratio with LiI, NaI, or RbI left the solids visibly unchanged. Only unreacted [KA'] could be extracted with toluene from the ground mixtures, and the allyl could be crystallized as its toluene solvate (see below). As a check on the consequences of halide identity, a 1:1 grind of [KA'] with LiCl was also investigated, but there was no evidence of reaction.

The grinds with CsI behaved differently from the others. A 1:1 grind for 5 min in a planetary mill left a pale orange solid that could be extracted with hexanes. When filtered and dried, the orange-brown residue displayed resonances in its ^{1}H NMR spectrum corresponding to a single type of π-bonded allyl ligand, all shifted slightly (by 0.09-0.4 ppm) from those for [KA'].[22] The material could not be purified, and repeating the grind for 10 min did not help. After grinding a 3:1 mixture of [KA']:CsI for 15 min, however, a pale yellow-orange solid was generated that could be extracted with hexanes. After being filtered, the yellow filtrate was evaporated to yield a yellow solid in low yield. Recrystallization from hexanes produced crystals that were yellow-orange; they were highly soluble in C_6D_6, giving a bright red solution. Single crystal X-ray analysis identified the crystals as the heterometallic complex [$KCsA'_2$] (see below). The ^{1}H NMR spectrum of the products from the 1:1 and 3:1 grinds were identical. It should be noted that both [KA'] and CsI are insoluble in hexanes, and the grinding clearly initiated a reaction that occurred before the first hexanes extraction.

4.2.3 Structure of [$CsKA'_2$]

Small blocks grown from hexanes were identified from a single crystal X-ray study as the coordination polymer $[CsKA'_2]_\infty$. A depiction of a single chain is provided in Figure 40, and a partial packing diagram is given in Figure 41. The asymmetric unit contains three alkali metal cations and three substituted allyl anions, all in general positions. Each of the three metal sites is modeled as a site disorder of atoms types K and Cs. Two distinct peaks were found in the difference Fourier map for the site containing atoms Cs1 and K1, and their positions were refined freely, but their anisotropic displacement parameters were constrained to be equivalent. For the other two site disorders (atom pairs Cs2/K2 and Cs3/K3), the atoms were constrained to be isopositional and their anisotropic displacement parameters were constrained to be equivalent. The ratios of Cs to K in the three sites refined to 0.60:0.40, 0.29:0.71, and 0.61:0.39 for atom pairs Cs1/K1, Cs2/K2, and Cs3/K3, respectively.

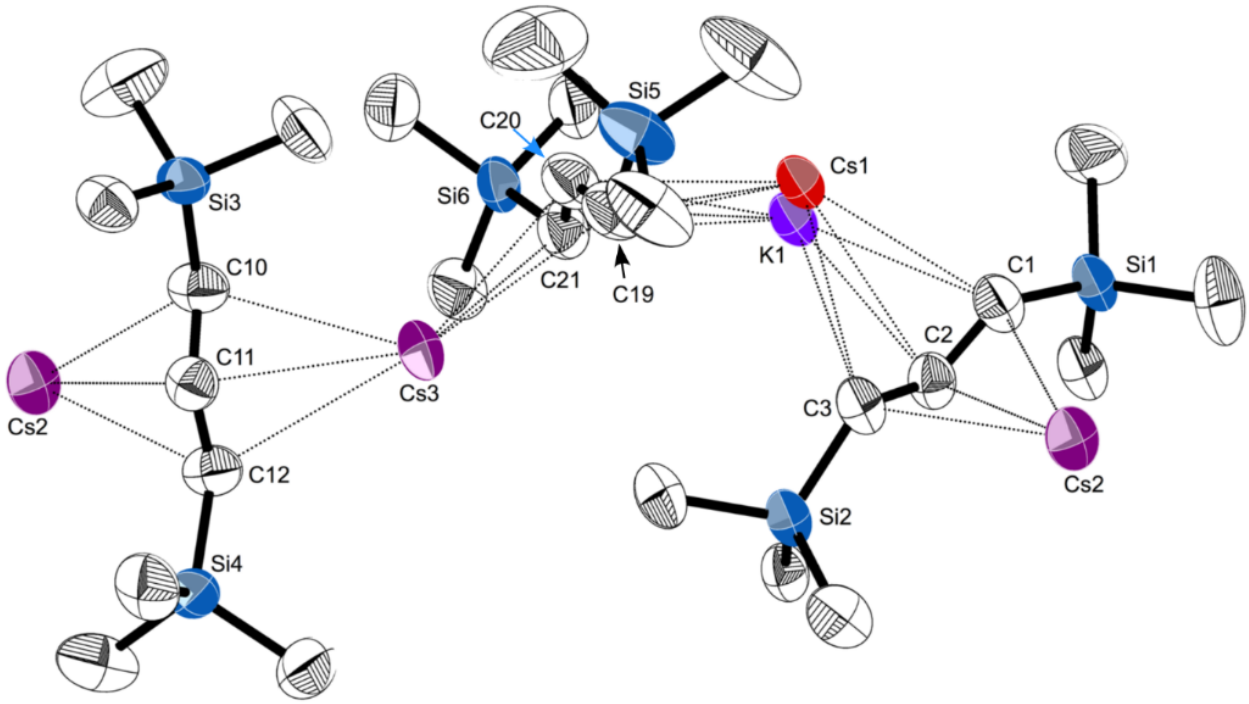

Figure 39. Portion of the polymeric chain of [CsKA'$_2$], with thermal ellipsoids drawn at the 50% level. Hydrogen atoms have been removed for clarity. Atoms marked "Cs2" and "Cs3" are site disorders of Cs and K, with relative occupancies of 0.29:0.71 and 0.61:0.39, respectively. Selected distances (Å) and angles (deg): Cs2–C1, 3.099(4); Cs2–C2, 3.058(4); Cs2–C3, 3.198(4); Cs2–C10, 3.072(4); Cs2–C11, 2.990(4); Cs2–C12, 3.066(4); Cs1–C1, 3.242(4); Cs1–C2, 3.329(4); Cs1–C3, 3.562(4); K1–C1, 3.135(5); K1–C2, 3.026(5); Cs1–C19, 3.149(5); Cs1–C20, 3.197(4); Cs1–C21, 3.364(4); K1–C19, 3.127(6); K1–C20, 3.172(6); K1–C21, 3.184(5); Cs3–C19, 3.282(4); Cs3–C20, 3.171(4); Cs3–C21, 3.197(4); Cs3–C10, 3.184(4); Cs3–C11, 3.158(4); Cs3–C12, 3.349(4); C1–C2–C3, 130.5(4); C19–C20–C21, 129.7(4); C10–C11–C12, 131.2(4).

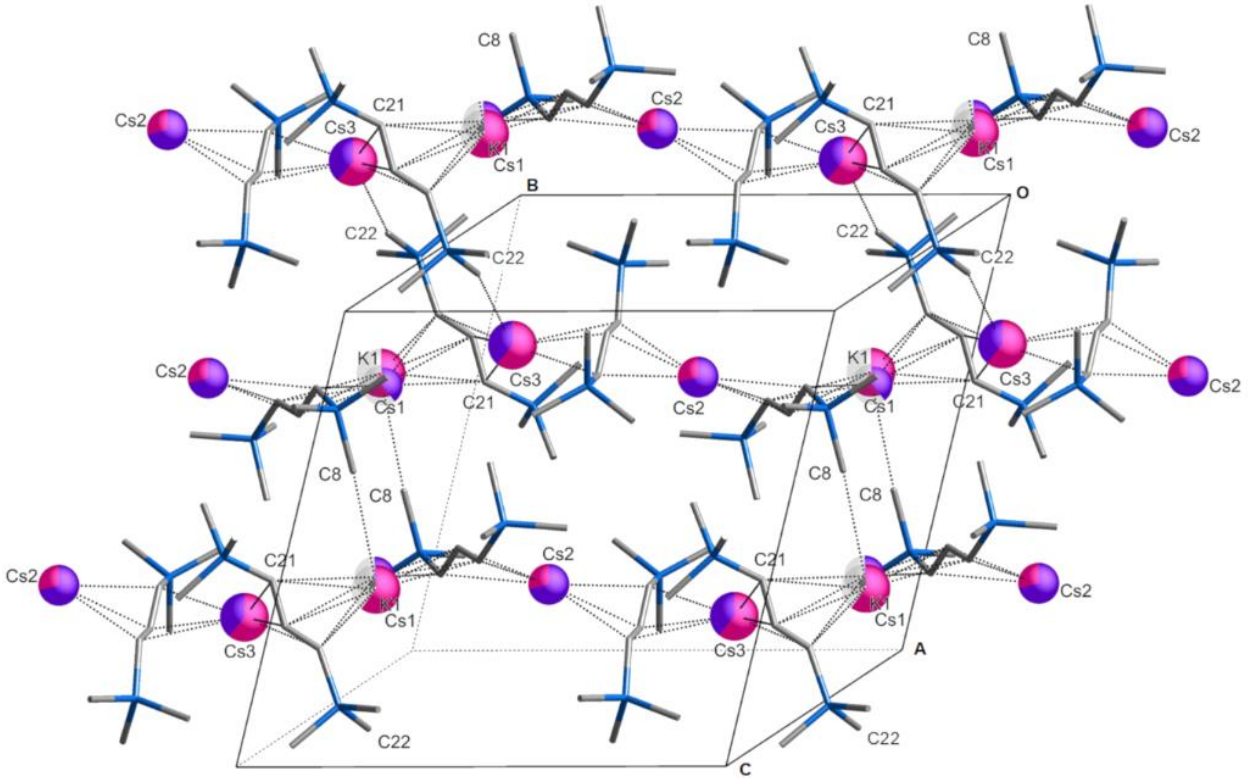

Figure 40. Partial packing diagram of $[CsKA'_2]$, illustrating some of the interchain contacts, predominantly K1···C8 at 3.20 Å, and Cs3···C22 at 3.44 Å, that promote sheet formation. The metal centers are colored in a pie chart fashion according to the proportion of K^+ (purple) or Cs^+ (pink) of each; translucent wedges (visible on K1 and Cs1) indicate the percentage of partial vacancy at the site. The C–C and C–Si bonds are rendered as sticks.

Although the metal–C(allyl) distances span a large range, they do so in a way that reflects the proportion of Cs and K in the metal to which they are bonded. For example, the average distance of Cs2 (0.29 Cs:0.71 K) to the allyl carbons C10–C12 is 3.04 Å. The same allyl is also bonded to Cs3, with a higher percentage of Cs (0.61 Cs:0.39 K), and the average M–C distance is correspondingly longer, at 3.22 Å. It is possible to extract consistent values from the M–C distances that can be assigned to the proportion of K and Cs, namely 2.95 Å and 3.40 Å, respectively (i.e., a hypothetical site that is 0.50 (K):0.50 (Cs) would be expected to exhibit an average M–C(allyl) bond distance of roughly 3.17 Å). These values do not recreate distances in the homometallic complexes exactly (i.e., the average K–C distance in $[KA']_\infty$ is 3.01 Å),[17] but they reflect the relative sizes of the K^+ and Cs^+ cations.

The structure is polymeric in two dimensions in the crystallographic *bc* plane; interchain K···CH_3 and Cs···CH_3 contacts are responsible for generating the 2D arrangement (Figure 41); this is discussed in more detail below.

4.2.4 Structure of $[(C_6H_6)KA']_\infty$

From all the grinds of [KA'] with the alkali metal iodides (excepting CsI), the potassium allyl was the only recoverable material; extracted with toluene, it crystallized from solution as the solvate. A single crystal X-ray study analysis reveals bent polymeric chains of alternating K^+ cations and $[A']^-$ anions. Each potassium is capped with a toluene molecule, bonded through cation–π interactions. The structure suffers from twinning, disorder in the toluene, and weak diffraction, and therefore its structural details are degraded (a depiction of the coordination polymer is available in the appendix). Fortunately, when [KA'] is dissolved in benzene and the solution evaporated, an analogous solvate is obtained, and the resulting crystals are of higher quality than those from toluene. Single crystal X-ray analysis reveals that it has a structure that is qualitatively the same as the toluene solvate, and only the benzene solvate is discussed here.

Like the unsolvated complex $[KA']_\infty$[17] and the related DME and THF solvates $[K(dme)A']_\infty$[22] and $[K(THF)_{3/2}A']_\infty$[18], respectively, $[(C_6H_6)KA']_\infty$ is a coordination polymer with potassium ions linked by bridging π-allyl ligands. The polymer takes the form of bent chains running parallel to the *b* axis (Figure 42). There is only one crystallographically distinct potassium ion in the chains, and a single K···K'···K bending angle of 134.0°. This is different from the pattern found in $[K(THF)_{3/2}A']_\infty$, for example, (i.e., roughly linear K(1)···K(2)···K(1)' sections (170.2°) alternating with strongly bent K(2)···K(1)···K(2)' angles (103.3°)). The K–C_6H_6 ring centroid distance is 2.99 Å, which is typical for K^+···(arene) cation–π interactions.[23,24] The enthalpy of binding ($\Delta H°$) of an isolated K···(benzene or toluene) unit is almost 80 kJ mol^{-1} (see calculated value in Table 7, entry 5); the energy is reduced by about 40% when the ring is bound to the neutral [KA'] fragment (entry 6).

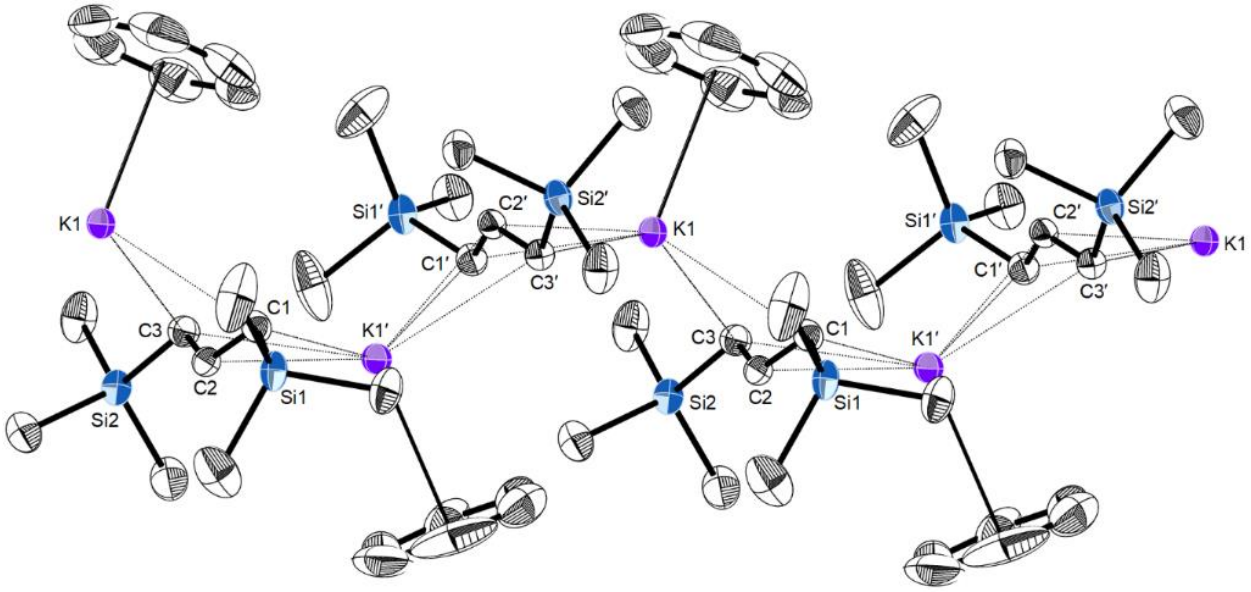

Figure 41. Portion of the polymeric chain of $[(C_6H_6)KA']_\infty$, with thermal ellipsoids drawn at the 50% level. Hydrogen atoms have been removed for clarity. Selected distances (Å) and angles (deg): K1–C1, 3.005(3); K1–C2, 2.963(3); K3–C3, 3.128(3); K1–C1', 2.959(3); K1–C2', 2.983(2); K3–C3', 3.140(3); K1···(C_6H_6 centroid), 2.99(1); K1···K1', 5.39; C1–C2–C3, 130.8(3); K1···K1'···K1, 134.0.

Table 7: Energies of reaction (B3PW91-D3BJ, kJ mol^{-1})

No.	**Reaction**[a]	**Energy ($\Delta H°$, $\Delta G°$)**
1	$K^+ + [C_3H_5]^- \rightarrow [K(C_3H_5)]$	-514.6, -481.5
2	$Cs^+ + [C_3H_5]^- \rightarrow [Cs(C_3H_5)]$	-484.9, -452.2
3	$K^+ + [A']^- \rightarrow [KA']$	-458.4, -426.5
4	$Cs^+ + [A']^- \rightarrow [CsA']$	-430.4, -398.1
5	$K^+ +$ toluene $\rightarrow [(\text{toluene})K]^+$	-78.9, -48.6
6	$[KA'] +$ toluene $\rightarrow [(\text{toluene})KA']$	-48.1, -13.1

[a]For entries 1–4, the def2-TZVPD basis set was used on all atoms. For entries 5 and 6, the def2-TZVP basis set was used on all atoms.

In structurally characterized polymeric $[L_nKA']_\infty$ complexes, the average K–C(allyl) distances span a comparatively narrow range, regardless of coordinated ligands and the change in formal coordination number of the K^+ cation: i.e., 3.01 Å in $[KA']_\infty$, 3.03 Å in $[KA'(THF)_{3/2}]_\infty$ and $[(C_6H_6)KA']_\infty$ (3.04 Å in the poorer quality $[(\text{toluene})KA']_\infty$ structure), and 3.06 Å in $[KA'(\text{dme})]_\infty$.[25] This suggests that the K^+···[A'] interaction is a robust one, and its structure potentially capable of serving as a kind of template for inclusion (see below).

4.2.5 Formation of the heterometallic allyl complex

The net reaction that produced the clearest evidence for mechanochemically promoted alkali metal exchange is given by Equation 5 with $n = 2$ (i.e., Equation 6). Several features of it are noteworthy.

$$2\,[KA'] + CsI \xrightarrow{\bigcirc\!\!\bigcirc} [CsKA'_2] + KI \qquad (6)$$

The ratio of [KA'] to CsI that yielded [CsKA'$_2$] was produced both from a 1:1 and a 3:1 ratio of [KA'] to CsI, and the predicted result from Equation 5, assuming complete reaction, would have been either pure [CsA'] or the heterometallic [CsK$_2$A'$_3$]. That neither of these outcomes was observed, and a non-stoichiometric product was obtained is actually not uncommon in mechanochemical synthesis, and can reflect the fact that products often do not have time to equilibrate or go from metastable to more stable products.[9,11] There can be multiple reasons for this, starting with the high energy environment of grinding that may be far from equilibrium,[26] allowing the kinetic products to be the ones most likely to be isolated. The high concentration of reagents in a solid-state reaction may influence product formation as well. The possibility of partial exchange also needs to be considered. If the cesium iodide were insufficiently reactive, a starting ratio of 3:1 for [KA']:CsI could give rise to products with higher ratios of K to Cs than even [CsK$_2$A'$_3$], such as [CsK$_3$A'$_4$] or [CsK$_4$A'$_5$]. In this light, it is notable that CsI is the limiting reagent in the reaction, and the resulting 1:1 ratio of the metals in the allyl complex suggests that it is a favored composition.

Secondly, the relative free energies of formation of CsI and KI (–341 and –325 kJ mol^{-1}, respectively; $\Delta\Delta G$ = +16 kJ mol^{-1})[27] means that the formation of the metal halide byproduct (KI) is non-spontaneous, and does not contribute to the driving force for the reaction. The relative free energies of the allyl complexes then must provide the difference. There are no experimental values available for the thermodynamic quantities involving potassium and cesium allyls, however, although it would be expected that the smaller K^+ ion would interact more strongly with the allyl anion than would the larger, softer Cs^+ ion.

To explore this and several related points more quantitatively, various features of the K/Cs/[allyl]$^-$ system were modeled with DFT calculations, using the B3PW91 hybrid functional[28,29] with Grimme's -D3 dispersion corrections (GD3-BJ)[30]. A calculation on the simple model systems [K(C$_3$H$_5$)] and [Cs(C$_3$H$_5$)] indicates that, consistent with the above rationale, $\Delta G°_f$ for the potassium complex is more negative than for the cesium complex (by 29.3 kJ mol^{-1}; Table 7, entries 1 and 2). The slightly greater realism provided by comparing the [KA'] and [CsA'] complexes does not meaningfully affect the difference (28.4 kJ mol^{-1}; Table 7, entries 3 and 4). Of course, these are calculations on isolated monomers, and the energetics of formation of the solid-state polymeric forms would be expected to

change these values, but not necessarily in a way that would clearly favor the formation of [CsA'] over [KA']. If so, there would consequently be no thermodynamic driving force for the metathesis reaction. Note that the structure of unsolvated [CsA′] is unknown, but it is presumed to be a coordination polymer, in the manner of its THF-solvate, $[(THF)CsA']_\infty$.[18]

There are several ways that this simple analysis underestimates the energetics involved in the system. For example, full metal exchange does not occur, and the resulting heterometallic allyl complex has additional entropy provided by the two metal ions and the site disorder in the solid. Using a standard formula for the entropy of mixing two species (configurational entropy, $\Delta S_{mix} = -nR(X_A \ln X_A + X_B \ln X_B)$,[31] and with 3 atoms distributed randomly over the three crystallographically identified metal sites, the value of ΔS = +17 J mol^{-1} K^{-1} is obtained. At 298 K, the $-T\Delta S$ value is –5.1 kJ mol^{-1}. As imperfect as this approximation is (e.g., the distribution of metal ions is not completely random, and the coordination environments are not exactly the same), it does suggest one source of driving force not present in the homometallic allyls.

A potentially much more important source of stability in $[CsKA'_2]$ is the existence of multiple intermolecular M···CH_3 interactions, including Cs···CH_3 contacts, obviously energetically significant enough that they support the formation of two-dimensional sheets in the solid state. To appreciate the magnitude of this effect, the relative conformation of the known $[L_nKA']$ complexes are summarized by their (non-bonded) K···K'···K angles (Table 8).

Table 8: Non-bonded intrachain K···K′···K angles in $[L_nKA']$ complexes

Complex	**K···K′···K (deg)**	**Ref.**
$[KA']_\infty$	135.1; 135.7; 118.2	17
$[K(dme)A']_\infty$	153.3, 141.9	22
$[K(dme)A']_\infty$	170.0, 103.3	18
$[(C_6H_6)KA']_\infty$	134.0	this work
$[KCsA'_2]_\infty$	140.3 (K1–Cs2–Cs3); 141.0 (K1–Cs3–Cs2); 107.3 (Cs2–K1–Cs3)	this work

Although the K···K'···K angles are only markers (there are no direct K···K' interactions in any of the complexes), it is notable that both $[KA']_\infty$ and $[CsKA'_2]$ display three such angles, two of which are relatively similar at ca. 135–140°, and a third that is substantially more bent (<120°) (see Appendix, Figure 44, for a visualization of the similarity). The significance of this is that [KA'] can be viewed as a template into which Cs^+ are infused during the grinding. There are adjustments in M–C(allyl) bond distances (see above), but another consequence is the generation of multiple intermolecular M···CH_3 interactions.

Both [KA'] and [CsKA'$_2$] possess K···CH_3 contacts at typical distances ;[32] in [KA'], the two closest are both at 3.23 Å; the third is at 3.35 Å. In [CsKA'$_2$], the closest is at 3.20 Å, with the second at 3.38 Å.

The Cs···CH_3 interactions in [CsKA'$_2$], however, are especially noteworthy. The closest is at 3.44 Å (Cs3···C22), followed by four more at 3.56 Å, and farther ones at 3.67 and 3.74 Å. All these distances are substantially shorter than the sum of the van der Waal's radii of Cs (3.43 Å) and CH_3 (2.00 Å). Intermolecular Cs···CH_3 distances of ca. 3.6 Å and longer are not especially rare, and are strong enough to influence solid state structures. In the dme adduct of cesium [2,4,6-tri(*tert*-butyl)phenolate], for example, a Cs···CH_3 contact of 3.596(5) Å contributes to its form as a 1D coordination polymer.[33] In the cesium salt of the gallium metallate [Cs(toluene)$_2${CN($GaMe_3$)$_2$}], multiple Cs···CH_3 interactions in the range from 3.54–3.64 Å help generate its three-dimensional network structure.[34] Intermolecular Cs···CH_3 distances below 3.5 Å, however, do not appear to have been previously reported.[35] The shortest distance in [CsKA'$_2$], at 3.44 Å, is 2.0 Å less than the sum of the appropriate van der Waal's radii (although less precisely located, the corresponding Cs···H distance (Cs3···H22B) is 3.05 Å, a third less than the sum of the van der Waal's radii (4.63 Å).

Calculations on the model systems [(CH_4)(K,Cs)A'] and [(HMe_2SiMe)(K,Cs)A'] were used to place the energy of the M···methyl interactions in context (views of the optimized pairs are available in Appendix, Figure 45). Despite the gas-phase environment of the calculations, the distance between K^+ and CH_4 is 3.22 Å, a typical value for potassium–methyl interactions in the solid state, as is the $\Delta H°$ of almost 12 kJ mol^{-1}, in the range of hydrogen bonds (Table 9, entries 1 and 2).[32] The distance of K^+ to Me_3SiH, chosen to represent somewhat more accurately the type of interactions occurring in [KCsA'$_2$], is slightly shorter (3.14 Å) and stronger (30 kJ mol^{-1}), probably a result of the lower electronegativity of silicon compared to carbon and the correspondingly more negative methyl groups. The analogous calculations with Cs^+ (Table 9, entries 3 and 4) place the contact distance at 3.62 Å and 3.53 Å for CH_4 and Me_3SiH, respectively, with corresponding enthalpies of –3.9 and –23.6 kJ mol^{-1}. These distances are similar to those found in the solid state, and together with the potassium interactions, evidently help to drive the heterometallic complex formation.

Table 9: Energies of reaction (B3PW91-D3BJ, kJ mol^{-1})

No.	Reaction[a]	Energy
1	[KA′] + CH_4 → [(CH_4)KA′]	-11.9 (Δ*H*°)
2	[KA′] + $SiMe_4$ → [($HSiMe_3$)KA′]	-30.0 (Δ*H*°)
3	[CsA′] + CH_4 → [(CH_4)CsA′]	-3.9 (Δ*H*°)
4	[CsA′] + $SiMe_4$ → [($HSiMe_3$)CsA′]	-23.6 (Δ*H*°)

4.3 Conclusion

Formally, halide metathesis as a synthetic technique depends strongly on the relative thermodynamic stabilities of the starting and final metal halide salts, M'X and MX. Practically, however, the reaction solvent is also a critical assistant in the process, as the insolubility of the MX product can strongly shift the position of equilibrium and drive the reaction. Mechanochemical techniques can be used to provide a driving force for a reaction that would be energetically unfavorable and has no solvent assistance. The formation of the heterometallic [CsKA'$_2$] from the mixture of [KA'] and CsI, even though in low yield, owes its realization to the entropic benefit of a mixed metal system, but even more importantly to the formation of intermolecular M···CH_3 contacts, permitting the formation and stabilization of a sheet structure that ties the coordination polymer chains of M···A' units together. Recognition of this additional source of reaction energy has the potential to extend the usefulness of halide metathesis to systems previously considered too unpromising to explore.

4.4 Appendix

Synthetic Procedures

General Considerations

All syntheses were conducted under rigorous exclusion of air and moisture using Schlenk line and glovebox techniques. Proton (^{1}H) and carbon (^{13}C) spectra were obtained on an Advance AV-400 MHz spectrometer at 400 and 100 MHz, respectively. Proton and carbon were referenced to residual resonances of C_6D_6.

Materials

All anhydrous metal salts and were purchased from Strem or Sigma-Aldrich, stored under an N_2 atmosphere, and used as received. The potassium allyl [KA′] = [K(1,3-$SiMe_3$)C_3H_3] was synthesized by transmetallation of [LiA′][36] with potassium *tert*-butoxide in hexanes solution. Toluene was degassed with argon and dried over activated alumina using a solvent purification system, then stored over 4 Å molecular sieves in a glovebox. Hexanes were distilled under nitrogen over NaK/benzophenone radical[37], then stored over 4 Å molecular sieves in a glovebox. Benzene-d_6 was obtained from Cambridge Isotopes and stored over 4 Å molecular sieves.

Mechanochemical protocol. Planetary milling was performed with a Retsch PM100 mill, 50 mL stainless steel grinding jar type C, and a safety clamp for air-sensitive grinding. Mixer milling was performed with a Retsch model MM200 mill. Ball milling reactions used 50 stainless steel (440 grade) ball bearings ($^3/_{16}$ in (5 mm), 0.44 g) or 3 stainless steel (440 grade) ball bearings ($^1/_2$ in (12.7 mm), 8.4 g) that were thoroughly cleaned with detergent and water, then washed with acetone, and dried in a 125 °C oven prior to use. A typical reaction was sealed under an inert atmosphere prior to grinding. The ground mixture was extracted with minimal hexanes (<100 mL) and filtered through a medium porosity ground glass frit. The extraction is designed to dissolve the complex, and the filtration removes residual KI. The filtrate was then dried under vacuum prior to NMR analysis.

Synthesis of [CsKA′$_2$]. Solid CsI (0.157 g, 0.604 mmol) and K[A′] (0.445 g, 1.98 mmol) were added to a 50 mL stainless steel grinding jar (type C). The jar was charged with stainless steel ball bearings (½ in dia, 3 count) and closed tightly with the appropriate safety closer device under an N_2 atmosphere. The reagents were milled for 15 min at 600 rpm, resulting in a pale yellow-orange solid. The solid was extracted with hexanes and filtered through a medium porosity ground glass frit, providing a yellow-tinted filtrate. Removal of hexanes under vacuum resulted in a turbid yellow solution that deposited a precipitate as the product was concentrated. Removal of hexanes under vacuum yielded a yellow solid in low yield (12 mg, 4% yield). The solid was dissolved in hexanes, and the solution slowly evaporated over the course of a week to promote crystal growth. As the concentration of the solution increased, it became more orange. X-ray analysis of the crystals revealed them to be the bimetallic [CsKA′$_2$] complex. The crystals were highly soluble in C_6D_6, giving a bright red solution. ^{1}H NMR (400 MHz, C_6D_6, 298 K): δ 0.27 (s, 18H, $SiMe_3$); 2.71 (d, 2H, J = 16.0 Hz, $H_{(\alpha,\gamma)}$); 6.58 (t, 1H, J = 16.0 Hz, $H_{(\beta)}$). ^{13}C NMR (100 MHz, C_6D_6, 298K): δ 2.32 ($SiMe_3$); 73.08 ($C_{(\alpha,\gamma)}$); 153.51 ($C_{(\beta)}$).

Procedures for X-Ray Crystallography

[$K_{1.5}Cs_{1.5}$(1,3-($SiMe_3$)$_2$$C_3H_3$)$_3$]

A crystal was placed onto the tip of a thin glass optical fiber and mounted on a Bruker SMART APEX II CCD platform diffractometer at the X-ray Crystallographic Facility, Department of Chemistry, University of Rochester (Rochester, NY). Data collection was conducted at 100 K using MoKα radiation (graphite monochromator, *APEX3*, version 2015.5-2; Bruker AXS: Madison, WI, 2015). The structure was solved using SHELXT-2014/5[38] and refined using SHELXL-2014/7[39]. The space group *P*1 was determined based on intensity statistics. A direct-methods solution was calculated which provided most non-hydrogen atoms from the E-map. Full-matrix least squares / difference Fourier cycles were performed which located the remaining non-hydrogen atoms. All non-hydrogen atoms were refined with anisotropic displacement parameters. Hydrogen atoms on the allylic portions of the anions were found from the difference Fourier map and their positions were refined independently from those of their respective bonded carbon atoms. However, their isotropic displacement parameters were refined relative to the (equivalent) anisotropic displacement parameters of their respective bonded carbon atoms. All other hydrogen

atoms were placed in ideal positions and refined as riding atoms with relative isotropic displacement parameters.

[(benzene)K(1,3-(SiMe$_3$)$_2$C$_3$H$_3$)], [(toluene)K(1,3-(SiMe$_3$)$_2$C$_3$H$_3$)]
X-ray crystallographic data were collected on a Rigaku Oxford Diffraction Supernova diffractometer. Crystal samples were handled under immersion oil and quickly transferred to a cold nitrogen stream. The crystals were kept at 100 K during data collection. Under Olex2,[40] the structure was solved with the SHELXT[38] structure solution program using direct methods and refined with the SHELXL[39] refinement package using least squares minimization. All non-hydrogen atoms were refined with anisotropic displacement parameters.

General Procedures for Calculations
All calculations were performed with the Gaussian 09W[41] or Gaussian 16 (Linux) suite of programs.[42] The B3PW91 functional, which incorporates Becke's three-parameter exchange functional[28] with the 1991 gradient-corrected correlation functional of Perdew and Wang,[29] was used. For dispersion-corrected calculations, Grimme's D3 correction[30] with additional Becke-Johnson damping was used[43] (Gaussian keyword: empiricaldispersion=GD3BJ). For the energy of metal allyl complex formation ($M^+ + [A']^- \rightarrow [MA']$), the def2-TZVPD basis set was used on all atoms, with the accompanying ECP used for Cs.[44] For all other calculations, the def2-TZVP basis set was used on all atoms, with an ECP on Cs. An ultrafine grid was used for all calculations (Gaussian keyword: int=ultrafine).

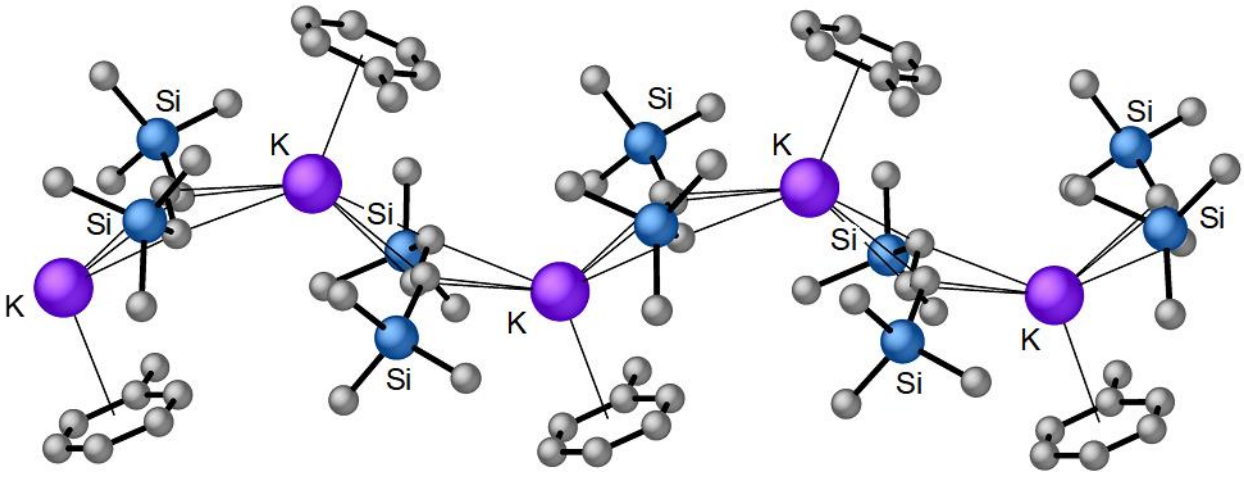

Figure 42. Connectivity of a portion of the coordination polymer chain in [(toluene)KA′]∞. Only one orientation of the toluene ligand is shown. Approximate bond distances (Å) and angles (deg): K···K′ = 5.52; K–C(allyl) (ave) = 3.04; K–ring centroid = 3.01; K···K′···K = 130.

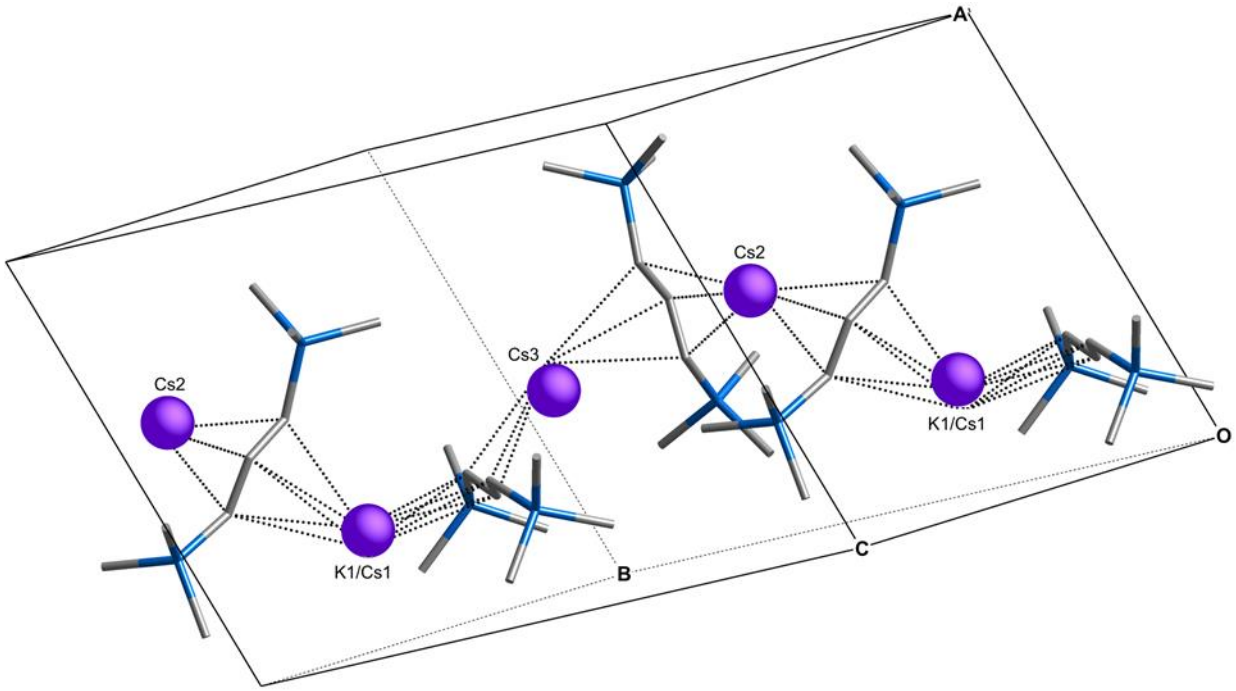

Figure 43. Superposition of a portion of the structures of $[KA']_\infty$ and $[KCsA'_2]_\infty$ (the unit cell is from $[KCsA'_2]$). From $[KA']_\infty$, only the potassium atoms are shown; from $[KCsA'_2]_\infty$, only the allyl ligands (as sticks) are shown, and the dotted lines are drawn to where the disordered potassium/cesium sites would be located. The overlap of the metal sites is not exact, and this view is meant to convey only a general sense of the alignment. For exact M···M′···M′′ angles, see the main text.

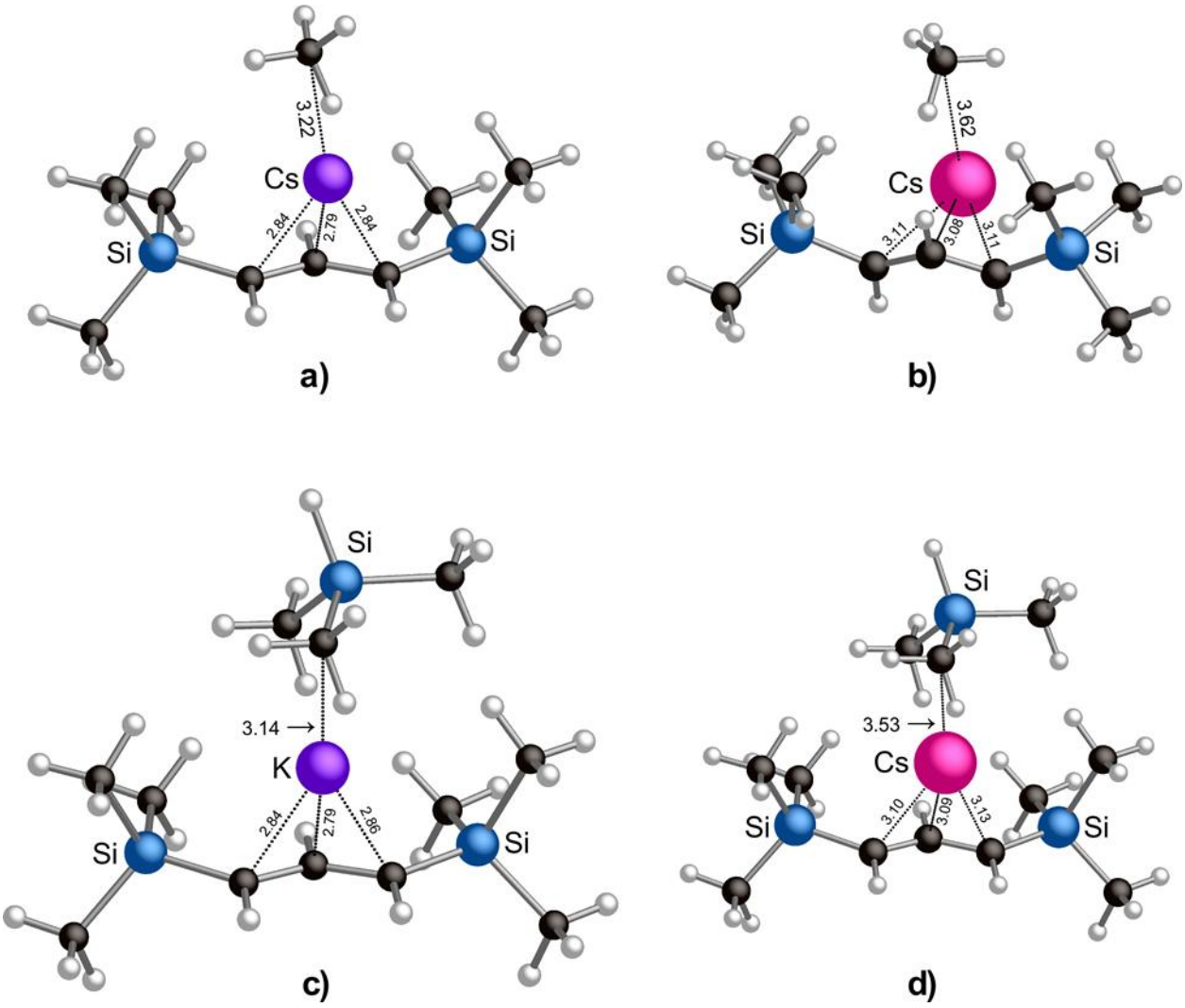

Figure 44. Calculated geometries of [MA′]···Me interactions in: a) [KA′]···CH_4; b) [CsA′]···CH_4; c) [KA′]···$MeSiMe_2H$; d) [CsA′]···$MeSiMe_2H$. For energies associated with the interactions, see the main text.

Table 10: Crystal Data and Summary of X–ray Data Collection

Compound	**$[K_{1.5}Cs_{1.5}(1,3\text{-}(SiMe_3)_2C_3H_3)_3]$**	**$[(benzene)K(1,3\text{-}(SiMe_3)_2C_3H_3)]$**	**$[(toluene)K(1,3\text{-}(SiMe_3)_2C_3H_3)]$**
Empirical formula	$C_{27}H_{63}Cs_{1.5}K_{1.5}Si_6$	$C_{15}H_{27}KSi_2$	$C_{16}H_{29}KSi_2$
Formula weight	814.33	302.64	316.67
Color of compound	yellow	colorless	colorless
Temperature/K	100.0(5)	100	100.01(10)
Crystal system	triclinic	monoclinic	monoclinic
Space group	$P\bar{1}$	$P2_1$	$P2_1/n$
a/Å	11.1741(8)	10.1620(3)	10.2297(11)
b/Å	14.6733(11)	9.93170(18)	10.1301(10)
c/Å	14.7968(11)	10.7700(3)	19.127(2)
α/°	73.9101(15)	90	90
β/°	85.2391(16)	118.137(3)	91.119(10)
γ/°	71.6969(15)	90	90
Volume/Å^3	2213.1(3) Å	958.52(5)	1981.7(4)
Z	2	2	4
ρ_{calc} g/cm^3	1.222	1.049	1.061
μ/mm^{-1}	1.559	3.486	3.391
F(000)	840	328	688
Crystal size/mm^3	0.25 × 0.16 × 0.14	0.316 × 0.185 × 0.073	0.1 × 0.05 × 0.03
Radiation	MoKα (λ = 0.71073)	CuKα (λ = 1.54184)	CuKα (λ = 1.54184)
2Θ range for data collect/°	1.788 to 27.500	4.452 to 73.258	4.625 to 65.078
Index ranges	-14≤ *h* ≤ 14, -19 ≤ *k* ≤ 19, -19 ≤ *l* ≤ 19	-12 ≤ *h* ≤ 12, -12 ≤ *k* ≤ 12, -12 ≤ *l* ≤ 12	-12 ≤ *h* ≤ 12, -11 ≤ *k* ≤ 11, 0 ≤ *l* ≤ 22
Reflections collected	29 788	13 244	3365
Independent reflections	10133 [R_{int} = 0.0374]	3762 [R_{int} = 0.0269]	3365
Data/restraints/parameters	10133/43/404	3762/4/181	3365/180
Goodness-of-fit on F^2	1.046	1.031	1.069
Final *R* indexes [$I > 2\sigma(I)$]	R_1 = 0.0445, wR_2 = 0.1080	R_1 = 0.0209, wR_2 = 0.0539	R_1 = 0.1055, wR_2 = 0.3272
Final *R* indexes [all data]	R1 = 0.0746, wR2 = 0.1234	R_1 = 0.0210, wR_2 = 0.0541	R1 = 0.1271, wR2 = 0.3441
Largest diff. peak/hole/e Å^{-3}	0.938/-0.622	1.42/-0.80	1.51/-0.77

Optimized coordinates of all structures in XYZ format

1
$[K]^+$, K_h; B3PW91-D3BJ/def2TZVPD; ΔG° = -599.721828 au
K 0.000000 0.000000 0.000000
1
$[Cs]^+$, K_h; B3PW91-D3BJ/def2TZVPD; ΔG° = -20.047814 au
Cs 0.000000 0.000000 0.000000
8
$[C_3H_5]^-$, C_1; B3PW91-D3BJ/def2TZVPD; ΔG° = -117.240692 au
C -1.271336 -0.895814 -0.000183
C -0.000001 -0.338094 -0.000054
C 1.271334 -0.895816 -0.000104
H -1.429334 -1.972534 -0.000345
H -0.000001 0.759445 0.000123
H 1.429330 -1.972535 -0.000292
H 2.155335 -0.266292 -0.000014
H -2.155327 -0.266297 -0.000073
9
$[K(C_3H_5)]$, C_s; B3PW91-D3BJ/def2TZVPD; ΔG° = -717.145928 au
C 0.091547 -1.083971 1.259976
H 1.174541 -1.015763 1.374551
H -0.455959 -1.377727 2.146908
C -0.459311 -1.296126 0.000000
H -0.455959 -1.377727 -2.146908
H 1.174541 -1.015763 -1.374551
C 0.091547 -1.083971 -1.259976
H -1.519250 -1.565233 0.000000
K 0.091547 1.428244 0.000000
9
$[Cs(C_3H_5)]$, C_s; B3PW91-D3BJ/def2TZVPD; ΔG° = -137.460753 au
C 1.838331 -0.649397 1.256769
H 2.157136 0.386689 1.373797
H 1.898302 -1.263499 2.147183
C 1.838331 -1.241209 0.000000
H 1.898302 -1.263499 -2.147183
H 2.157136 0.386689 -1.373797
C 1.838331 -0.649397 -1.256769
H 1.697613 -2.325684 0.000000
Cs -0.779972 0.351260 0.000000
32
$[A']^-$, C_1; B3PW91-D3BJ/def2TZVPD; ΔG° = -934.470190 au
C -1.263870 -0.970208 -0.000198
C 0.000000 -0.386600 -0.000065
C 1.263870 -0.970208 -0.000111

C	-3.932017	-0.421855	1.494831
C	-2.521631	1.818193	0.000071
C	-3.932217	-0.421721	-1.494746
C	3.932345	-0.422495	1.494435
C	2.521631	1.818193	0.000868
C	3.931889	-0.421080	-1.495142
H	-1.300798	-2.062731	-0.000385
H	0.000000	0.707706	0.000117
H	1.300799	-2.062731	-0.000280
H	-4.891926	0.104536	1.441175
H	-3.430850	-0.134408	2.423452
H	-4.140611	-1.494968	1.554826
H	-1.955386	2.126946	-0.882594
H	-1.955277	2.126847	0.882701
H	-3.472841	2.359783	0.000163
H	-3.431208	-0.134129	-2.423406
H	-4.892147	0.104609	-1.440875
H	-4.140762	-1.494839	-1.554843
H	3.431441	-0.135332	2.423284
H	4.892293	0.103817	1.440724
H	4.140848	-1.495651	1.553990
H	1.955238	2.127298	-0.881579
H	3.472841	2.359783	0.001005
H	1.955425	2.126495	0.883716
H	4.140516	-1.494157	-1.555685
H	4.891784	0.105320	-1.441322
H	3.430620	-0.133196	-2.423572
Si	-2.813136	-0.051582	-0.000018
Si	2.813136	-0.051582	-0.000002

33

[KA′], C_1; B3PW91-D3BJ/def2TZVPD; ΔG° = -1534.354455 au

C	1.258373	0.014273	-0.838125
C	-0.002479	0.358132	-0.352839
C	-1.262402	-0.000073	-0.830763
C	3.992988	1.432643	-1.153027
C	2.548050	1.399227	1.548070
C	3.801565	-1.134852	0.421080
C	-3.958074	1.507115	-1.116710
C	-2.551114	1.314206	1.593754
C	-3.850235	-1.137132	0.334845
H	1.284152	-0.460152	-1.826731
H	-1.287816	-0.474735	-1.819377
H	4.957361	1.626336	-0.674343
H	3.539355	2.392890	-1.410756
H	4.185445	0.899062	-2.088292
H	1.933762	0.836153	2.256112
H	2.040720	2.346254	1.348921
H	3.497478	1.625371	2.040816

H	3.270221	-1.709994	1.188011
H	4.797194	-0.912775	0.816653
H	3.933352	-1.781077	-0.452831
H	-3.473652	2.463857	-1.327329
H	-4.921297	1.708330	-0.638670
H	-4.156130	1.021413	-2.076537
H	-1.957228	0.706795	2.282393
H	-3.501154	1.539337	2.085764
H	-2.021718	2.258185	1.443291
H	-3.979333	-1.740911	-0.569132
H	-4.847863	-0.908480	0.721355
H	-3.346472	-1.758163	1.084110
Si	2.841870	0.437199	-0.043127
Si	-2.847387	0.429689	-0.041902
H	-0.002893	0.910418	0.590843
K	0.014407	-2.381357	0.030443

33

[CsA′], C_1; B3PW91-D3BJ/def2TZVPD; ΔG° = -954.669641 au

C	1.258288	0.667660	-0.838923
C	-0.000160	0.997515	-0.341741
C	-1.258552	0.667329	-0.838866
C	3.897814	2.292263	-1.031367
C	2.548218	1.813158	1.669196
C	3.906709	-0.472380	0.177628
C	-3.897064	2.294200	-1.029644
C	-2.548548	1.809975	1.670440
C	-3.908088	-0.472388	0.174735
H	1.283486	0.239535	-1.847737
H	-1.283689	0.239196	-1.847675
H	4.860319	2.487321	-0.549154
H	3.375409	3.244759	-1.151009
H	4.098283	1.900174	-2.032566
H	1.985048	1.129355	2.310431
H	1.986826	2.748711	1.609275
H	3.498795	2.026584	2.165396
H	3.449370	-1.172029	0.885859
H	4.906173	-0.237758	0.555293
H	4.031042	-0.994768	-0.776196
H	-3.374037	3.246549	-1.147720
H	-4.859517	2.489124	-0.547264
H	-4.097648	1.903799	-2.031479
H	-1.986369	1.124637	2.310910
H	-3.499107	2.023688	2.166546
H	-1.986150	2.745030	1.612166
H	-4.032692	-0.992875	-0.780090
H	-4.907416	-0.237730	0.552729
H	-3.451323	-1.173729	0.881653
Si	2.843675	1.083706	-0.041880

Si -2.843971 1.083325 -0.041853
H -0.000197 1.498402 0.630195
Cs 0.000288 -2.039280 0.009708
1
[K]$^{+}$, K_h; B3PW91-D3BJ/def2TZVP; ΔG° = -599.721784 au
K 0.000000 0.000000 0.000000
16
[K(toluene)]$^{+}$, C_1; B3PW91-D3BJ/def2TZVP; ΔG° = -871.226474 au
C 0.962286 2.141497 -0.044274
C 0.976974 1.413069 -1.230175
C 1.075622 1.505730 1.196376
H 0.896422 3.223609 -0.081870
C 1.096112 0.026305 -1.199065
H 0.921108 1.931710 -2.180344
C 1.184268 0.111403 1.211461
C 1.199451 -0.622035 0.028636
H 1.138283 -0.539868 -2.121816
H 1.292881 -0.402105 2.160794
H 1.317990 -1.698852 0.065357
C 1.140517 2.298382 2.466249
H 0.590626 3.236995 2.387218
H 0.753919 1.735023 3.316423
H 2.179415 2.552516 2.694488
K -1.765858 0.503718 0.078465
15
(toluene), C_1; B3PW91-D3BJ/def2TZVP; ΔG° = -271.486190 au
C -4.507310 0.809301 -0.002385
C -3.119940 0.812166 0.012204
C -2.404665 2.007381 0.016028
C -3.119713 3.202885 0.010637
C -4.506951 3.206048 -0.003960
C -5.207028 2.007701 -0.011519
H -5.043705 -0.132565 -0.002819
H -2.581006 -0.129403 0.023089
H -2.580542 4.144349 0.020300
H -5.043180 4.148008 -0.005638
H -6.290489 2.007863 -0.019847
C -0.904817 2.007548 -0.000992
H -0.526868 2.020439 -1.028048
H -0.501280 2.885653 0.506205
H -0.501342 1.117247 0.484368
33
[KA′], C_1; B3PW91-D3BJ/def2TZVP; ΔG° = -1534.351892 au
C 1.260365 0.000208 -0.828207
H 1.285787 0.467071 -1.820397
C -0.000100 -0.348409 -0.344975
C -1.260525 0.000699 -0.827975
H -1.285929 0.467549 -1.820174

Si	2.845315	-0.434934	-0.042236
Si	-2.845522	-0.434687	-0.042203
C	-2.550964	-1.318239	1.594336
H	-1.961218	-0.709477	2.285195
H	-3.501867	-1.546482	2.083117
H	-2.018345	-2.260504	1.445026
C	-3.948257	-1.516876	-1.120278
H	-4.911874	-1.721958	-0.644855
H	-4.145759	-1.032401	-2.080741
H	-3.459197	-2.471504	-1.329225
C	-3.856996	1.127272	0.332248
H	-3.984787	1.731894	-0.571294
H	-4.855300	0.893478	0.713621
H	-3.359719	1.749246	1.084950
C	3.856173	1.127232	0.333172
H	3.358484	1.748736	1.085998
H	4.854432	0.893614	0.714772
H	3.984068	1.732270	-0.570079
C	3.948715	-1.516185	-1.120556
H	4.912288	-1.721134	-0.644987
H	3.460064	-2.470894	-1.330084
H	4.146282	-1.031175	-2.080736
C	2.550732	-1.319242	1.593882
H	2.018389	-2.261584	1.444077
H	3.501615	-1.547426	2.082729
H	1.960702	-0.710937	2.284900
H	-0.000120	-0.896589	0.601116
K	0.000529	2.392323	0.030492

48

[(toluene)KA′], C_1; B3PW91-D3BJ/def2TZVP; ΔG° = -1805.843067 au

C	-0.321381	2.143367	-0.781290
H	-0.228298	2.454087	-1.828320
C	0.812211	1.574437	-0.203465
C	1.995442	1.152452	-0.805424
H	2.135221	1.440318	-1.853939
Si	-1.866788	2.526474	0.096769
Si	3.369698	0.318585	0.047043
C	2.989260	0.112936	1.880971
H	2.052331	-0.424176	2.042793
H	3.785381	-0.444734	2.381377
H	2.901262	1.084888	2.372196
C	5.012025	1.227967	-0.118160
H	5.832889	0.682522	0.356663
H	5.270743	1.369449	-1.171448
H	4.948305	2.218222	0.339520
C	3.672658	-1.412161	-0.672627
H	3.875416	-1.348481	-1.746533
H	4.527342	-1.912726	-0.207727

H	2.798250	-2.056417	-0.537193
C	-3.311274	1.499579	-0.588659
H	-3.121687	0.430540	-0.451123
H	-4.262655	1.732909	-0.101156
H	-3.438019	1.680521	-1.660769
C	-2.399838	4.325592	-0.072584
H	-3.361829	4.516094	0.412186
H	-1.654149	4.988591	0.372908
H	-2.496666	4.602085	-1.126400
C	-1.714229	2.117977	1.929469
H	-0.953788	2.740812	2.406341
H	-2.662293	2.291201	2.445615
H	-1.432890	1.074742	2.087947
H	0.726094	1.347124	0.862479
C	-2.351143	-2.676846	0.143492
C	-1.922122	-1.773944	1.120344
C	-1.421505	-3.584451	-0.368714
C	-0.610080	-1.783066	1.576059
H	-2.623814	-1.053485	1.524993
C	-0.106241	-3.598789	0.087757
H	-1.736420	-4.298055	-1.123293
C	0.304095	-2.697808	1.063873
H	-0.297330	-1.068712	2.327774
H	0.597458	-4.317756	-0.316191
H	1.327124	-2.701609	1.417880
C	-3.779326	-2.686767	-0.314868
H	-4.413481	-3.196999	0.415696
H	-4.169551	-1.673608	-0.428320
H	-3.890161	-3.208264	-1.266601
K	-0.114043	-0.548566	-1.748303

5

CH_4, C_1; B3PW91-D3BJ/def2TZVP; ΔG° = -40.497662au

C	-1.278088	-0.691598	-0.579000
H	-0.433917	-0.106479	-0.215856
H	-1.193445	-1.715231	-0.215856
H	-1.278088	-0.691598	-1.668432
H	-2.206902	-0.253085	-0.215856

14

$HSiMe_3$, C_1; B3PW91-D3BJ/def2TZVP; ΔG° = -409.780622

Si	2.767274	0.873835	0.027763
C	0.892787	0.860375	0.006378
H	0.490562	1.398994	0.868683
H	0.504330	1.337327	-0.896658
H	0.504456	-0.160405	0.038937
C	3.403899	0.026597	1.574104
H	3.053722	-1.006833	1.631177
H	4.496220	0.011219	1.595264
H	3.059166	0.546707	2.471938

C	3.403835	2.635115	-0.055294
H	4.496162	2.660882	-0.059200
H	3.054159	3.139603	-0.959211
H	3.058592	3.213856	0.805707
H	3.264487	0.128827	-1.164921

38

[(CH_4)KA′], C_1; B3PW91-D3BJ/def2TZVP; ΔG° = -1574.844841

C	-0.002377	0.757466	2.909640
H	-0.426098	0.071136	2.176212
H	-0.577046	1.685067	2.943894
H	1.042194	0.960921	2.670950
C	-1.263936	-0.727767	-0.957235
C	1.258398	-0.732355	-0.962530
C	-0.002337	-1.077575	-0.479788
H	-0.000711	-1.634603	0.460897
H	-1.295465	-0.250597	-1.944272
H	1.288125	-0.259163	-1.951479
Si	2.836009	-1.143348	-0.151432
Si	-2.844141	-1.134753	-0.148161
C	-4.072096	-1.947643	-1.321933
H	-3.683244	-2.903890	-1.680235
H	-5.038248	-2.128262	-0.842094
H	-4.247684	-1.315769	-2.197341
C	-3.705451	0.429129	0.501814
H	-4.692312	0.217083	0.923918
H	-3.111209	0.905223	1.289357
H	-3.845026	1.157785	-0.303606
C	-2.573292	-2.268500	1.330224
H	-1.935325	-1.811839	2.090928
H	-3.527991	-2.509407	1.805547
H	-2.104528	-3.206287	1.023007
C	3.765858	0.432142	0.360931
H	4.754756	0.214939	0.775407
H	3.910571	1.093278	-0.499733
H	3.210871	0.989903	1.123381
C	4.019579	-2.093702	-1.266867
H	3.586507	-3.055829	-1.551208
H	4.215007	-1.536875	-2.187800
H	4.980843	-2.280783	-0.779561
C	2.538379	-2.147393	1.412824
H	3.485761	-2.370898	1.910605
H	1.907332	-1.612558	2.126854
H	2.049031	-3.096830	1.182882
H	-0.047836	0.288747	3.890858
K	0.008945	1.690708	-0.168958

47

[($HSiMe_3$)KA′], C_1; B3PW91-D3BJ/def2TZVP; ΔG° = -1944.129553

Si	1.548786	-3.197492	-0.875439

C	0.565952	-1.634453	-1.242266
H	0.719849	-0.914053	-0.434050
H	0.912366	-1.204039	-2.187450
H	-0.501514	-1.857295	-1.316621
C	0.959517	-3.972011	0.719879
H	-0.098017	-4.238664	0.665826
H	1.524935	-4.881540	0.936631
H	1.089093	-3.288589	1.562057
C	3.371593	-2.785635	-0.803781
H	3.964978	-3.683869	-0.617457
H	3.716273	-2.345231	-1.742276
H	3.577272	-2.072923	-0.002690
H	1.308688	-4.150143	-1.998688
C	0.591833	1.785454	1.111602
C	-1.837706	1.098802	1.117063
C	-0.473655	0.913902	1.329376
H	-0.189369	-0.096998	1.633093
H	0.333742	2.827575	0.889620
H	-2.166573	2.123197	0.906169
Si	-3.091512	-0.213588	1.252533
Si	2.347894	1.356778	1.334313
C	3.281953	2.645520	2.339972
H	2.868309	2.718285	3.348670
H	4.346202	2.406953	2.421695
H	3.197169	3.633242	1.877690
C	3.262574	1.237611	-0.325995
H	4.329224	1.029070	-0.199952
H	2.847131	0.442351	-0.952275
H	3.177771	2.179638	-0.877790
C	2.516740	-0.315146	2.184746
H	2.001432	-1.106561	1.636819
H	3.567323	-0.604148	2.273629
H	2.089226	-0.280967	3.189480
C	-3.888876	-0.562979	-0.437315
H	-4.704268	-1.289394	-0.371138
H	-4.303763	0.353824	-0.868948
H	-3.155062	-0.966752	-1.144218
C	-4.512106	0.221630	2.409369
H	-4.144067	0.365866	3.428094
H	-4.992420	1.153989	2.098980
H	-5.278631	-0.558406	2.428621
C	-2.301595	-1.822966	1.825427
H	-3.044991	-2.623185	1.871190
H	-1.509559	-2.144786	1.145593
H	-1.861369	-1.716507	2.819626
K	-0.614461	1.273587	-1.437122

33

[CsA′], C_1; B3PW91-D3BJ/def2TZVP; ΔG° = -954.667180 au

Cs	0.000088	-2.027380	-0.124445
C	1.258151	0.716884	-0.854675
C	-1.258451	0.716676	-0.854666
C	-0.000173	1.020308	-0.340920
H	-0.000206	1.468957	0.656228
H	1.284018	0.345858	-1.885612
H	-1.284263	0.345644	-1.885602
Si	-2.843159	1.092355	-0.036992
Si	2.842800	1.092751	-0.036979
C	3.888238	2.366265	-0.951178
H	3.359777	3.320919	-1.011501
H	4.850130	2.537275	-0.458876
H	4.089589	2.037856	-1.974769
C	3.915122	-0.467645	0.084885
H	4.914270	-0.249912	0.473050
H	3.464562	-1.211812	0.750691
H	4.039374	-0.930397	-0.899187
C	2.547804	1.714287	1.716531
H	1.990654	0.989250	2.316384
H	3.498519	1.902843	2.222303
H	1.980883	2.648357	1.715540
C	-3.915283	-0.468173	0.084886
H	-4.914457	-0.250564	0.473056
H	-4.039483	-0.930946	-0.899184
H	-3.464623	-1.212279	0.750690
C	-3.888741	2.365725	-0.951227
H	-3.360396	3.320441	-1.011562
H	-4.090043	2.037271	-1.974814
H	-4.850660	2.536626	-0.458937
C	-2.548258	1.713960	1.716510
H	-3.499001	1.902400	2.222271
H	-1.991017	0.989006	2.316379
H	-1.981460	2.648104	1.715507

38

[(CH_4)CsA′], C_1; B3PW91-D3BJ/def2TZVP; ΔG° = -995.160046 au

C	-0.019240	0.640329	3.020465
H	-0.215038	0.007261	2.155324
H	-0.780328	1.417730	3.099897
H	0.971887	1.087922	2.939393
Cs	0.016536	2.001289	-0.333872
C	-1.260467	-0.758800	-0.987196
C	1.258471	-0.768876	-0.992663
C	-0.001105	-1.079523	-0.487652
H	-0.000176	-1.573141	0.487890
H	-1.292037	-0.350932	-2.003888
H	1.288847	-0.362917	-2.010212
Si	2.838209	-1.146397	-0.167083
Si	-2.841692	-1.122964	-0.157703

C	-4.078003	-1.953528	-1.310048
H	-3.699448	-2.923166	-1.642460
H	-5.046172	-2.110802	-0.826117
H	-4.246547	-1.343300	-2.202117
C	-3.689409	0.463863	0.454136
H	-4.674746	0.266083	0.886421
H	-3.089339	0.954949	1.227795
H	-3.831371	1.173846	-0.367473
C	-2.580182	-2.215303	1.352331
H	-1.939245	-1.738456	2.097722
H	-3.536345	-2.435868	1.834606
H	-2.116835	-3.164219	1.072401
C	3.758482	0.443652	0.317406
H	4.747320	0.236679	0.737084
H	3.903387	1.091988	-0.553028
H	3.199647	1.009072	1.071122
C	4.025569	-2.108124	-1.268383
H	3.600220	-3.079683	-1.531500
H	4.212262	-1.568075	-2.201110
H	4.990461	-2.276533	-0.781471
C	2.551602	-2.118970	1.418253
H	3.502771	-2.334153	1.912562
H	1.928415	-1.567738	2.126441
H	2.057985	-3.071284	1.210688
H	-0.052533	0.024989	3.917935

47

[(HSiMe$_3$)CsA′], C_1; B3PW91-D3BJ/def2TZVP; ΔG° = -1364.442217

Si	1.576822	-3.239908	-0.823831
C	0.583980	-1.703397	-1.259577
H	0.704277	-0.948930	-0.477724
H	0.942948	-1.297719	-2.210325
H	-0.479145	-1.937813	-1.353694
C	0.982625	-3.970128	0.791313
H	-0.071293	-4.250533	0.736424
H	1.556714	-4.865487	1.041835
H	1.095847	-3.258984	1.612569
C	3.396336	-2.810250	-0.749835
H	3.996098	-3.695492	-0.525558
H	3.745006	-2.401440	-1.701151
H	3.588795	-2.066771	0.026087
H	1.361002	-4.236767	-1.913896
Cs	-0.665046	1.563638	-1.699661
C	0.580855	1.799290	1.156781
C	-1.843279	1.105725	1.135634
C	-0.477508	0.907890	1.314048
H	-0.186880	-0.124083	1.526977
H	0.318011	2.855441	1.032742
H	-2.177086	2.142593	1.017233

Si	-3.099498	-0.209650	1.236122
Si	2.340558	1.361342	1.337737
C	3.287033	2.654475	2.325450
H	2.891584	2.726659	3.341444
H	4.353317	2.419673	2.388158
H	3.190759	3.641492	1.863726
C	3.230733	1.238432	-0.336129
H	4.296475	1.018749	-0.222200
H	2.801004	0.446977	-0.957532
H	3.150933	2.181900	-0.886478
C	2.525663	-0.311873	2.180521
H	1.998263	-1.098987	1.638127
H	3.576650	-0.604672	2.250103
H	2.114063	-0.279197	3.191869
C	-3.953146	-0.473901	-0.440600
H	-4.772664	-1.195740	-0.376989
H	-4.374236	0.463789	-0.817915
H	-3.247408	-0.852875	-1.188074
C	-4.479067	0.177242	2.458304
H	-4.077578	0.268784	3.470482
H	-4.961709	1.126800	2.209609
H	-5.250794	-0.597899	2.464009
C	-2.303585	-1.848971	1.705331
H	-3.050783	-2.646434	1.735150
H	-1.535141	-2.141037	0.986393
H	-1.832192	-1.792996	2.689281

4.5 References

(1) Elschenbroich, C. *Organometallics*; 3, Ed.; 2006.

(2) Pearson, R. G. Hard and Soft Acids and Bases. *J. Am. Chem. Soc.* **1963**, *85* (22), 3533–3539.

(3) Borisov, A. P.; Makhaev, V. D.; Usyatinskii, A. Y.; Bregadze, V. I. Solid-State Mechanochemical Synthesis of Bis(Dicarbollyl) Complexes of Cobalt(III), Iron(III) and Chromium(III). *Izv. Akad. Nauk. Ser. Khim.* **1993**, No. 10, 1715–1717.

(4) Gomes, C. S. B.; Gomes, P. T.; Duarte, M. T. α-Diimine Transition-Metal Complexes: Mechanochemistry - A New Synthetic Approach. *J. Organomet. Chem.* **2014**, *760*, 101–107.

(5) Makhaev, V. D.; Borisov, A. P.; Petrova, L. A. Solid-State Mechanochemical Synthesis of Ferrocene. *J. Organomet. Chem.* **1999**, *590* (2), 222–226.

(6) Boyde, N. C.; Rightmire, N. R.; Bierschenk, E. J.; Steelman, G. W.; Hanusa, T. P.; Brennessel, W. W. Reaction Environment and Ligand Lability in Group 4 Cp_2MXY (X, Y = Cl, OtBu) Complexes. *Dalton Trans.* **2016**, *45* (46), 18635–18642.

(7) Boyde, N. C.; Steelman, G. W.; Hanusa, T. P. Multicomponent Mechanochemical Synthesis of Cyclopentadienyl Titanium Tert-Butoxy Halides, $Cp_xTiX_y(O^tBu)_{4-(x+y)}$ (x, y = 1, 2; x = Cl, Br). *ACS Omega* **2018**, *3* (7), 8149–8159.

(8) Peters, D. W.; Blair, R. G. Mechanochemical Synthesis of an Organometallic Compound: A High Volume Manufacturing Method. *Faraday Discuss.* **2014**, *170* (0), 83–91.

(9) Boyde, C. N.; Rightmire, R. N.; Hanusa, P. T.; Brennessel, W. W. Symmetric Assembly of a Sterically Encumbered Allyl Complex: Mechanochemical and Solution Synthesis of the Tris(Allyl)Beryllate, $K[BeA'_3]$ (A′ = 1,3-$(SiMe_3)_2C_3H_3$). *Inorganics* **2017**, *5* (2), 36.

(10) Rightmire, N. R.; Hanusa, T. P.; Rheingold, A. L. Mechanochemical Synthesis of $[1,3\text{-}(SiMe_3)_2C_3H_3]_3$(Al,Sc), a Base-Free Tris(Allyl)Aluminum Complex and Its Scandium Analogue. *Organometallics* **2014**, *33* (21), 5952–5955.

(11) Koby, R. F.; Hanusa, T. P.; Schley, N. D. Mechanochemically Driven Transformations in Organotin Chemistry: Stereochemical Rearrangement, Redox Behavior, and Dispersion-Stabilized Complexes. *J. Am. Chem. Soc.* **2018**, *140* (46), 15934–15942.

(12) Allred, A. L.; Rochow, E. G. A Scale of Electronegativity Based on Electrostatic Force. *J. Inorg. Nucl. Chem.* **1958**, *5*, 264–268.

(13) Chmely, S. C.; Hanusa, T. P. Complexes with Sterically Bulky Allyl Ligands: Insights into Structure and Bonding. *Eur. J. Inorg. Chem*. 2010, pp 1321–1337.

(14) Solomon, S. A; Layfield, R. A. The Coordination Chemistry of Silyl-Substituted Allyl Ligands. *Dalton Trans.* **2010**, *39*, 2469–2483.

(15) Boche, G.; Fraenkel, G.; Cabral, J.; Harms, K.; Van Eikema Hommes, N. J. R.; Lohrenz, J.; Marsch, M.; Schleyer, P. v. R. *Exo*,*Exo*-[1,3-Bis(Trimethylsilyl)Allyl]Lithium-*N*,*N*,*N*',*N*'-Tetramethylethylenediamine Complex: Crystal Structure and Dynamics in Solution. *J. Am. Chem. Soc.* **1992**, *114* (5), 1562–1565.

(16) McMillen, C. H.; Gren, C. K.; Hanusa, T. P.; Rheingold, A. L. A Tetrameric Allyl Complex of Sodium, and Computational Modeling of the ^{23}Na-Allyl Chemical Shift. *Inorganica Chim. Acta* **2010**, *364* (1), 61–68.

(17) Gren, C. K.; Hanusa, T. P.; Rheingold, A. L. Solvent-Resistant Structures of Base-Free Lithium and Potassium Allyl Complexes, $M[(SiMe_3)_nC_3H_{5-n}]$ (M = Li, n = 3; M = K, n = 2). *Main Gr. Chem.* **2009**, *8* (4), 225–235.

(18) Quisenberry, K. T.; Gren, C. K.; White, R. E.; Hanusa, T. P.; Brennessel, W. W. Trimethylsilylated Allyl Complexes of the Heavy Alkali Metals, $M[1,3\text{-}(SiMe_3)_2C_3H_3](THF)_n$ (M = K, Cs). *Organometallics* **2007**, *26* (17), 4354–4356.

(19) Harvey, M. J.; Hanusa, T. P.; Young Victor G., J. Synthesis and Crystal Structure of the

Bis(Allyl)Calcium Complex [Ca{$C_3(SiMe_3)_2H_3$}$_2$·$(THF)_2$]. *Angew. Chem. Int. Ed.* **1999**, *38* (1-2), 217–219.
(20) Speight, I. R.; Chmely, S. C.; Hanusa, T. P.; Rheingold, A. L. Mechanochemically Directed Metathesis in Group 2 Chemistry: Calcium Amide Formation without Solvent. *Chem. Commun.* **2019**, *55*, 2202–2205.
(21) Ojeda-Amador, A. I.; Martínez-Martínez, A. J.; Kennedy, A. R.; O'Hara, C. T. Structural Studies of Cesium, Lithium/Cesium, and Sodium/Cesium Bis(Trimethylsilyl)Amide (HMDS) Complexes. *Inorg. Chem.* **2016**, *55* (11), 5719–5728.
(22) Simpson, C. K.; White, R. E.; Carlson, C. N.; Wrobleski, D. A.; Kuehl, C. J.; Croce, T. A.; Steele, I. M.; Scott, B. L.; Young Victor G.; Hanusa, T. P.; Sattelberger, A. P.; John, K. D. The Role of Alkali Metal Cations in MMA Polymerization Initiated by Neutral and Anionic Allyl Lanthanide Complexes. *Organometallics* **2005**, *24* (15), 3685–3691.
(23) Ma, J. C.; Dougherty, D. A. The Cation-π Interaction. *Chem. Rev.* **1997**, *97* (5), 1303–1324.
(24) Ojeda-Amador, A. I.; Martínez-Martínez, A. J.; Robertson, G. M.; Robertson, S. D.; Kennedy, A. R.; O'Hara, C. T. Exploring the Solid State and Solution Structural Chemistry of the Utility Amide Potassium Hexamethyldisilazide (KHMDS). *Dalton Trans.* **2017**, *46* (19), 6392–6403.
(25) Solomon, S. A; Muryn, C. A; Layfield, R. A. S-Block Metal Complexes of a Bulky, Donor-Functionalized Allyl Ligand. *Chem. Commun.* **2008**, 3142–3144.
(26) Shi, Y. X.; Xu, K.; Clegg, J. K.; Ganguly, R.; Hirao, H.; Friščić, T.; García, F. The First Synthesis of the Sterically Encumbered Adamantoid Phosphazane $P_4(N^tBu)_6$: Enabled by Mechanochemistry. *Angew. Chem. Int. Ed.* **2016**, *55* (41), 12736–12740.
(27) Wagman, D. D.; Evans, W. H.; Parker, V. B.; Schumm, R. H.; Halow, I. *The NBS Tables of Chemical Thermodynamic Properties*; American Chemical Society and the American Institute of Physics for the National Bureau of Standards, 1982.
(28) Becke, A. D. Density-Functional Exchange-Energy Approximation with Correct Asymptotic Behavior. *Phys. Rev. A At. Mol. Opt. Phys.* **1988**, *38* (6), 3098–3100.
(29) Perdew, J. P.; Wang, Y. Accurate and Simple Analytic Representation of the Electron-Gas Correlation Energy. *Phys. Rev. B* **1992**, *45* (23), 13244–13249.
(30) Grimme, S.; Antony, J.; Ehrlich, S.; Krieg, H. A Consistent and Accurate Ab Initio Parametrization of Density Functional Dispersion Correction (DFT-D) for the 94 Elements H-Pu. *J. Chem. Phys.* **2010**, *132* (15), 154104.
(31) Garces, J. The Configurational Entropy of Mixing of Interstitials Solid Solutions. *Appl. Phys. Lett.* **2010**, *96* (16), 161904/1-161904/3.
(32) Kleeberg, C.; Grunenberg, J.; Xie, X. K–H_3C and K–Sn Interactions in Potassium Trimethylstannyl Complexes: A Structural, Mechanochemical, and NMR Study. *Inorg. Chem.* **2014**, *53* (9), 4400–4410.
(33) Westerhausen, M.; Ossberger, M. W.; Alexander, J. S.; Ruhlandt-Senge, K. Influence of the Steric Demand of the 2,4,6-Trialkylphenyl Substituents on the Structures and Reactivity of Diarylzinc. *Z. Anorg. Allg. Chem.* **2005**, *631* (13–14), 2836–2841.
(34) Kopp, M. R.; Neumüller, B. Die Reaktion von Cyanid-Ionen Mit Trimethylgallium. Die Kristallstrukturen von [Cs{$CN(GaMe_3)_2$}]$_n$ Und [$Cs(Toluol)_2${$CN(GaMe_3)_2$}]N. *Z. Anorg. Allg. Chem.* **1998**, *624* (10), 1642–1646.
(35) Groom, C. R.; Bruno, I. J.; Lightfoot, M. P.; Ward, S. C. The Cambridge Structural Database. *Acta Crystallogr. Sect. B* **2016**, *72* (2), 171–179.
(36) Fraenkel, G.; Chow, A.; Winchester, W. R. Dynamics of Solvated Li_+ within *Exo*,*Exo*-[1,3-Bis(Trimethylsilyl)Ally]Lithium *N*,*N*,*N*',*N*'-Tetramethylethylenediamine Complex. *J. Am. Chem. Soc.* **1990**, *112*, 1382–1386.
(37) Armarego, W. L. F.; Chai, C. L. L. Chapter 1 - Common Physical Techniques Used in

Purification; Armarego, W. L. F., Chai, (Sixth E., Eds.; Butterworth-Heinemann: Oxford, 2009; pp 1–60.
(38) Sheldrick, G. SHELXT - Integrated Space-Group and Crystal-Structure Determination. *Acta Crystallogr. Sect. A* **2015**, *71* (1), 3–8.
(39) Sheldrick, G. Crystal Structure Refinement with SHELXL. *Acta Crystallogr. Sect. C* **2015**, *71* (1), 3–8.
(40) Dolomanov, O. V; Bourhis, L. J.; Gildea, R. J.; Howard, J. A. K.; Puschmann, H. OLEX2: A Complete Structure Solution, Refinement and Analysis Program. *J. Appl. Crystallogr.* **2009**, *42* (2), 339–341.
(41) M. J. Frisch, G. W. Trucks, H. B. Schlegel, G. E. Scuseria, M. A. Robb, J. R. Cheeseman, G. Scalmani, V. Barone, G. A. Petersson, H. Nakatsuji, X. Li, M. Caricato, A. Marenich, J. Bloino, B. G. Janesko, R. Gomperts, B. Mennucci, H. P. Hratchian, J. V. Ort, and D. J. F. Gaussian09. *http://www. gaussian. com/*. Gaussian, Inc.: Wallingford CT 2009.
(42) M. J. Frisch, G. W. Trucks, H. B. Schlegel, G. E. Scuseria, M.; A. Robb, J. R. Cheeseman, G. Scalmani, V. Barone, B. Mennucci, G. A. Petersson, H.; Nakatsuji, M. Caricato, X. Li, H. P. Hratchian, A. F. Izmaylov, J. Bloino, G. Zheng, J. L.; Sonnenberg, M. Hada, M. Ehara, K. Toyota, R. Fukuda, J. Hasegawa, M. Ishida, T.; Nakajima, Y. Honda, O. Kitao, H. Nakai, T. Vreven, J. A. Montgomery, Jr., J. E. Peralta, F.; Ogliaro, M. Bearpark, J. J. Heyd, E. Brothers, K. N. Kudin, V. N. Staroverov, R.; Kobayashi, J. Normand, K. Raghavachari, A. Rendell, J. C. Burant, S. S. Iyengar, J.; Tomasi, M. Cossi, N. Rega, J. M. Millam, M. Klene, J. E. Knox, J. B. Cross, V. Bakken, C.; Adamo, J. Jaramillo, R. Gomperts, R. E. Stratmann, O. Yazyev, A. J. Austin, R. Cammi, C.; Pomelli, J. W. Ochterski, R. L. Martin, K. Morokuma, V. G. Zakrzewski, G. A. Voth, P.; Salvador, J. J. Dannenberg, S. Dapprich, A. D. Daniels, Ö. Farkas, J. B. Foresman, J. V.; Ortiz, J. Cioslowski, and D. J. Fox, Gaussian, Inc., Wallingford CT, 2009. Gaussian16 Revision D.01. *http//www. gaussian. com/* **2009**.
(43) Grimme, S.; Ehrlich, S.; Goerigk, L. Effect of the Damping Function in Dispersion Corrected Density Functional Theory. *J. Comput. Chem.* **2011**, *32* (7), 1456–1465.
(44) Rappoport, D.; Furche, F. Property-Optimized Gaussian Basis Sets for Molecular Response Calculations. *J. Chem. Phys.* **2010**, *133* (13), 134105.

Chapter 5

An η^3-Bound Allyl Ligand on Magnesium in a Mechanochemically Generated Mg/K Allyl Complex

Reprinted with permission from Ross F. Koby, Alicia M. Doerr, Nicholas R. Rightmire, Nathan D. Schley, Prof. Brian K. Long, Timothy P. Hanusa

Angew. Chem. Int. Ed. **2020**, *59*, 9542.

5.1 Introduction

Modern synthetic organic chemistry is inconceivable without organometallic compounds of the s-block metals, anchored by the development of the Grignard reagents (around 1900)[1–4] and alkyllithiums (1917).[5,6] Even though there have been spectacular advances that have addressed the limited covalency and metal-centered redox chemistry in Group 2 compounds,[7–9] ligand developments will probably remain the most direct way to work within the constraints of s-block electronic configurations, and these have led, for example, to dramatic developments in polymerization, hydrogenation, hydrosilylation, and hydroamination catalysts.[10–14] A particularly flexible basis for such ligand design is the allyl anion, $[C_3H_5]^-$, and its substituted derivatives. In combination with mechanochemical synthesis, we describe both a new coordination mode for the Mg-allyl bond and the catalytic reactivity of a heterometallic Mg/K-allyl complex, which demonstrate the still unexhausted variety and utility of the s-block-carbon bond.

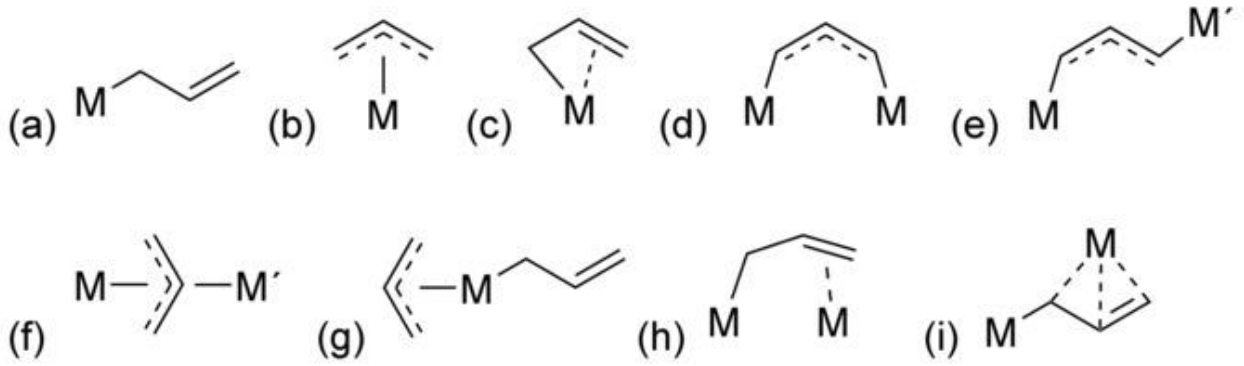

Figure 45. Some of the known bonding modes of the allyl: (a) η^1, (b) η^3, (c) η^1: η^2 (d) cis μ_2- η^1: η^1, (e) trans μ_2- η^1: η^1, (f) μ_2- η^3: η^3, (g) (η^1+ η^3), (h) μ_2- η^1: η^2, (i) μ_2- η^1: η^3.

The parent allyl ligand $[C_3H_5]^-$ is a sterically compact anion that is readily substituted to increase its size, and for associated complexes, their solubility and thermal stability.[15,16] The range of bonding modes documented for the allyl anion and its variants is remarkably large for such a small molecule: the commonly encountered terminal η^1- and η^3-conformations (along with various degrees of slippage) are accompanied with changes in π-electron delocalization (Figure 46a–c). The bridging conformations of the allyl group are even more extensive, and at least six additional allyl-metal bonding modes have been structurally authenticated (Figure 46d–i), although not all with a given metal.[17] However, for the Group 2 metals, only a limited range of bonding patterns has been documented. To date, beryllium compounds have been found with sigma-bound (η^1) (Figure 46a[18] and μ_2-η^1,η^2 allyls (Figure 46h).[19] In contrast, with very rare exceptions, η^3-conformations are uniformly the norm with complexes of the heavier alkaline-earth metals (Ca–Ba).[20–22] Magnesium represents a borderline case; explicit attempts to prepare magnesium species with η^3-bound allyls (Figure 46b) have not been successful,[23] and at one time, based on the absence of any structural evidence to the contrary, sigma bonding was thought to be the preferred bonding mode for allyl ligands in magnesium compounds.[24] Later, a bridged μ_2-η^1,η^2 bonding mode was identified in a dimeric complex (Figure 47), and heterometallic potassium/magnesium species have been found that display additional complex bonding arrangements.[25] Absent single crystal X-ray data, structural confirmation of the Mg–allyl bond ligation mode is difficult, as allylmagnesium species are typically fluxional in solution, with NMR spectra that suggest the presence of *trihapto*-bound ligands. An example is provided by $[MgA'_2(THF)_2]$ (A′ = [1,3-$(SiMe_3)_2C_3H_3$]) (Figure 47a), which displays η^1-bound allyls in its crystal structure, but its solution NMR spectra give the appearance of more symmetrical, η^3-coordinated ligands; $\Delta G^{\ddagger}$ for the rearrangement process is 12.3 kcal mol^{-1}.[26] Despite the lack of evidence in the solid state for η^3-bonded allyls on Mg, calculations have indicated that an unsolvated $[Mg(C_3H_5)_2]$ complex would have η^3-ligands,[26,27] and the occurrence of sigma bonding in known Mg–allyl compounds has been ascribed to the presence of coordinated solvents that cause a shift from η^3 to η^1 bonding.[26]

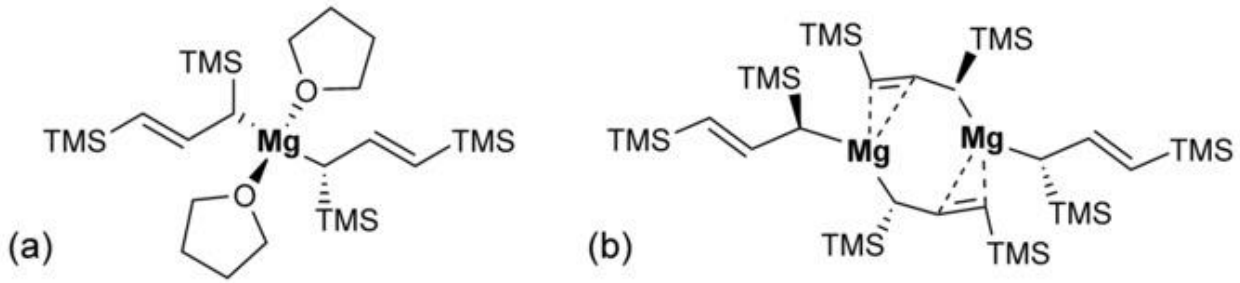

Figure 46. (a) Connectivity of the solvated monomeric magnesium allyl $[MgA'_2(THF)_2]$ (A′ = [1,3-$(SiMe_3)_2C_3H_3$]); (b) connectivity of the unsolvated dimeric magnesium allyl $[\{MgA'_2\}_2]$.

In addition to changing the bonding mode of allyl ligands, coordinated solvent can also affect reactions of the resultant complexes. The potentially depressant effect of such bases in Group 2 compounds was demonstrated by the ability of $[\{BDI^{Dipp}\}CaH]_2$ to insert non-activated α-olefins, generating $[\{BDI^{Dipp}\}CaR]_2$ calcium alkyl species, whereas the related $[\{BDI^{Dipp}\}CaH(THF)]_2$ is essentially inert.[28,29] Similarly, the solvated species $[MgA'_2(THF)_2]$ is inactive as an initiator for methyl methacrylate (MMA) polymerization, which is plausibly the result of the THF ligands hindering access to the metal center.[30] In contrast, preliminary tests (confirmed below) indicated that the unsolvated $[\{MgA'_2\}_2]$ dimer displays modest activity for methyl methacrylate (MMA) polymerization, a result that prompted us to explore the properties of the compound more completely.

The strength of the Mg–THF interaction is such that $[MgA'_2(THF)_2]$ cannot be directly desolvated, and to obtain the solvent-free material the diethyl ether adduct $[MgA'_2(Et_2O)_2]$ must first be prepared and the ether subsequently removed under high vacuum.[26] In an attempt to simplify the process and avoid the use of coordinating solvents, we turned to mechanochemistry, the use of mechanical force or energy to drive reactions.

Mechanochemical synthesis can yield unique products that cannot be prepared from solution-based approaches. In recent years, mechanochemically induced reactions have become more widely employed, although compared to the progress in organic[31–35] and materials chemistry, that in organometallic synthesis is more limited.[32,36–40] In particular, the consequences of removing the solvent from the reaction environment are not yet readily predictable. Some syntheses are 'solvent indifferent' (e.g., that for ferrocene[41]), or at least generate the product expected from the stoichiometry of the reagents (e.g., the formation of $[AlA'_3]$ from the mixture of AlI_3 + 3 K[A′][42]). However, non-stoichiometric outcomes are also common (e.g., the formation of the stannate $K[SnA'_3]$ from a 1:2 reaction of $SnCl_2$ and K[A′][43], or the formation of $K[Ca\{N(TMS)_2\}_3]$ from 1:2 reaction of CaI_2 and $K[N(TMS)_2]$.[44] In these cases, the unexpected complexes appear to be non-equilibrium products, formed too rapidly from the high concentration of reactants in the solid state for the equilibrium stoichiometry to be established.

5.2 Results and Discussion

Even though the possibility certainly existed that something other than the desired $[\{MgA'_2\}_2]$ would be produced on grinding, MgX_2 (X = Cl or Br) was milled with two equivalents of K[A′] for 10–15 min at 600 rpm in a planetary mill. Extraction of the resulting pale orange solid with hexanes (neither of the starting materials is hexanes soluble), filtration of the extract, and removal of solvent from the filtrate left an orange oil. The oil produced highly air- and moisture-sensitive microcrystals (**1**) on standing overnight. ^{1}H NMR spectra display a splitting pattern of 2 triplets, 2 doublets, and 2 singlets, corresponding to a set of two distinct A′ ligands that are in a 2:1 ratio by integration of peak area. Superficially, the splitting pattern and ratio of intensities would suggest a compound with 3*n* (η^3-A′) ligands. In fact, as is typical for allylmagnesium complexes, the compound is fluxional in solution. Cooling a sample even slightly (253 K) reveals new resonances in

the ^{1}H NMR spectrum in tol-d_8, the most obvious of which are an apparent triplet at δ 6.72 (J = 16 Hz), accompanied by a new doublet at δ 2.89. Despite the complexity of the spectrum, there is no evidence for dissociation into [{MgA′ $_2$}$_2$] and K[A′], i.e., the aggregate appears to remain intact. See Appendix for additional details. These resonances are clearly different from those in the more complex spectrum of [{MgA′$_2$}$_2$], which reflect monomer ⇄ dimer rearrangement in solution.[26]

Crystals of **1** suitable for X-ray crystal diffraction were originally grown from a slowly evaporated toluene solution, and although they ultimately yielded a structure of connectivity only quality (Figure 47), several features are worth noting. The complex is a trimetallic monomer with a fundamental composition of 2:1:4 K:Mg:A′, which does not reflect the reagent stoichiometry. One allyl ligand is found η^1-bonded to the Mg center. The other three are bridging, either between the potassium atoms, each of which is capped with a π-bound toluene ligand, or between the magnesium and the potassiums. Unfortunately, owing to disorder in almost all of the trimethylsilyl groups and in one of the toluenes, the quality of structure prevents further discussion of the bonding.

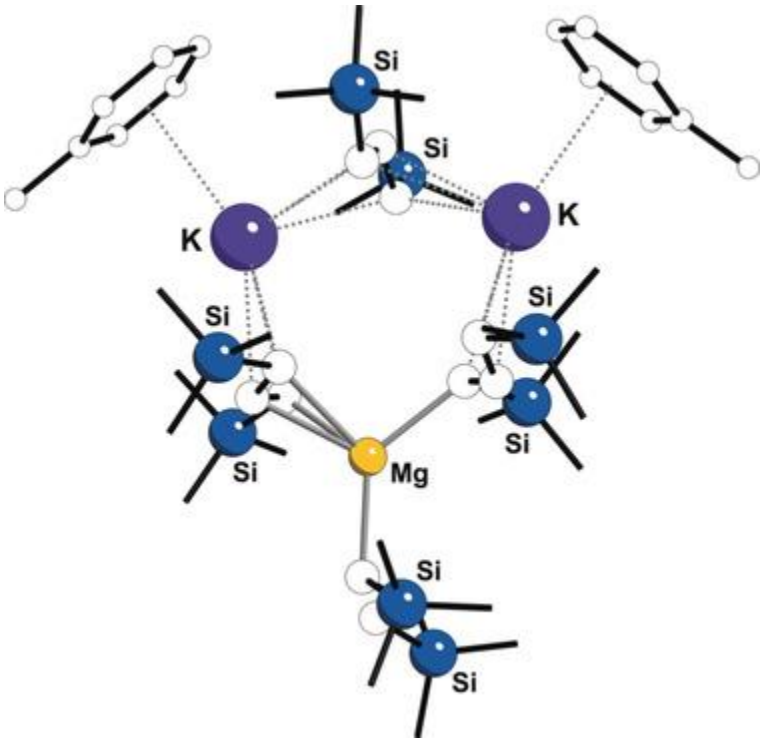

Figure 47. Connectivity-only structure of [((η^6-tol)K)$_2$MgA′$_4$] ([**1**•2(tol)]). For clarity, disorder in a toluene and in the SiMe$_3$ groups is not shown, and all hydrogens have been removed, as have the carbons in the SiMe$_3$ groups.

Higher quality crystals of [**1**•2(tol)] could not be obtained with slow evaporation, but recrystallization from hexanes was successful, leading to a structure free from disorder. Single crystal X-ray diffraction revealed that the 2:1:4 K:Mg:A′ composition of the toluene solvate is maintained, but the unsolvated **1** now forms a 2D coordination polymer (Figures 49, 50), which is isostructural with the Mn(II) analogue.[45] Two of the allyl ligands on the Mg cation are η^1-bonded and the third (C1–C3) is η^3-bonded. Both of the allyls that are η^1-coordinated to Mg are π-bonded to potassium cations, extending the polymer in a sheet in the *ab* plane; the η^3-allyl ligand is terminal. Each of the potassium atoms is coordinated to an additional K[A′] before the chain continues with a Mg core. There are two independent polymer systems in the asymmetric unit. Potassium coordination spheres are completed with methyl groups from symmetry-equivalent polymers, (K···CH_3 = 3.34 Å), and every other layer repeats along the *c*-axis (Figure 50).

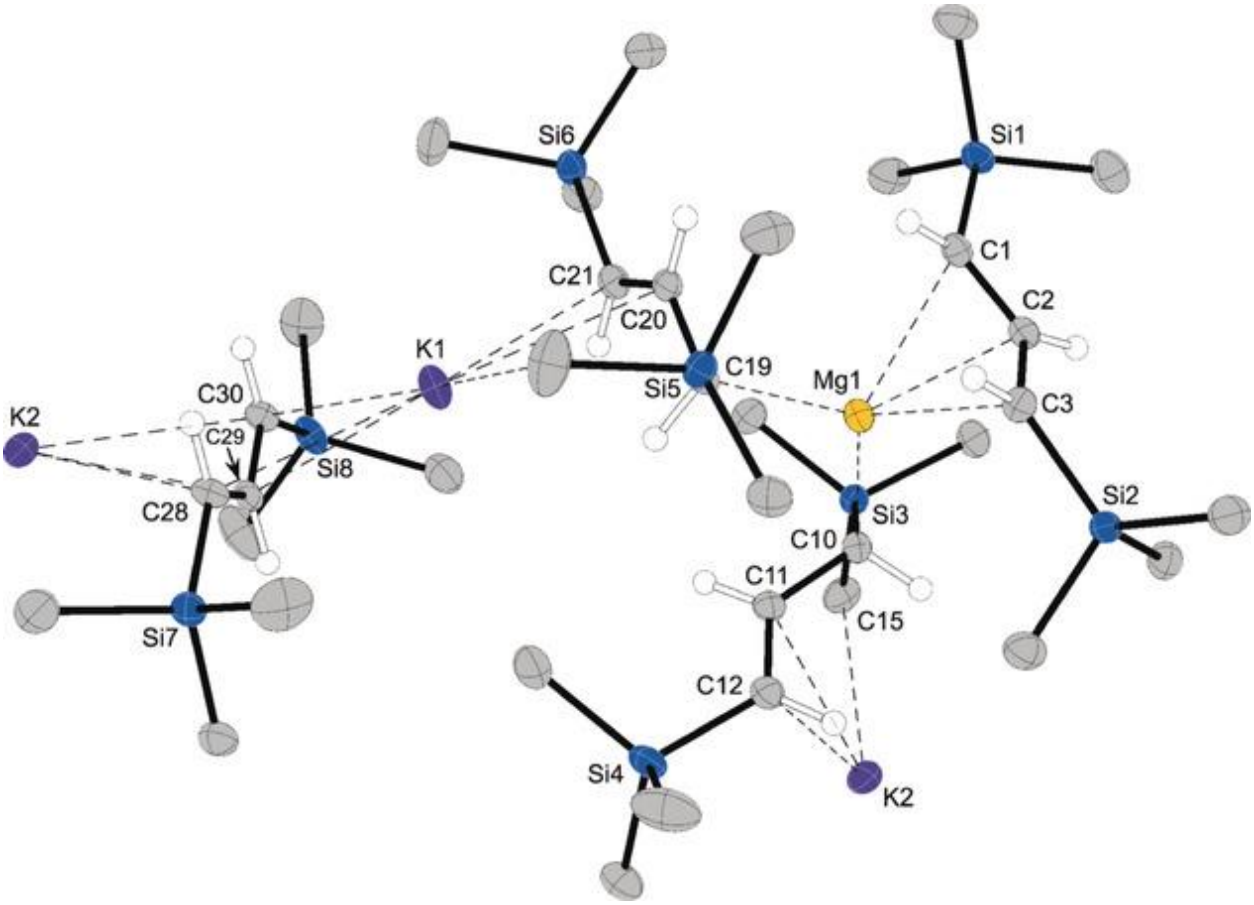

Figure 48. Thermal ellipsoid plot (50% level) of a portion of the coordination polymer of $\{[K_2MgA'_4]\}_n$ (**1**). For clarity, hydrogens have been removed from trimethylsilyl groups. Selected bond distances and angles: Mg1–C19, 2.206(3) Å; Mg1–C10, 2.235(4) Å; Mg1–C1, 2.446(4) Å; Mg1–C2, 2.338(4) Å; Mg1–C3, 2.375(4) Å; C1–C2, 1.389(5) Å; C2–C3, 1.417(4) Å; K1–C21, 2.997(3) Å; K1–C20, 3.206(3) Å; K1···C19, 3.407(3) Å; K1–C28, 3.104 Å; K1–C29, 2.929 Å; K1–C30, 3.002 Å; K2–C11, 3.133(4) Å; K2–C12, 3.057(4) Å; K1···C10, 3.319(4) Å. C1–C2–C3, 128.9(3)°.

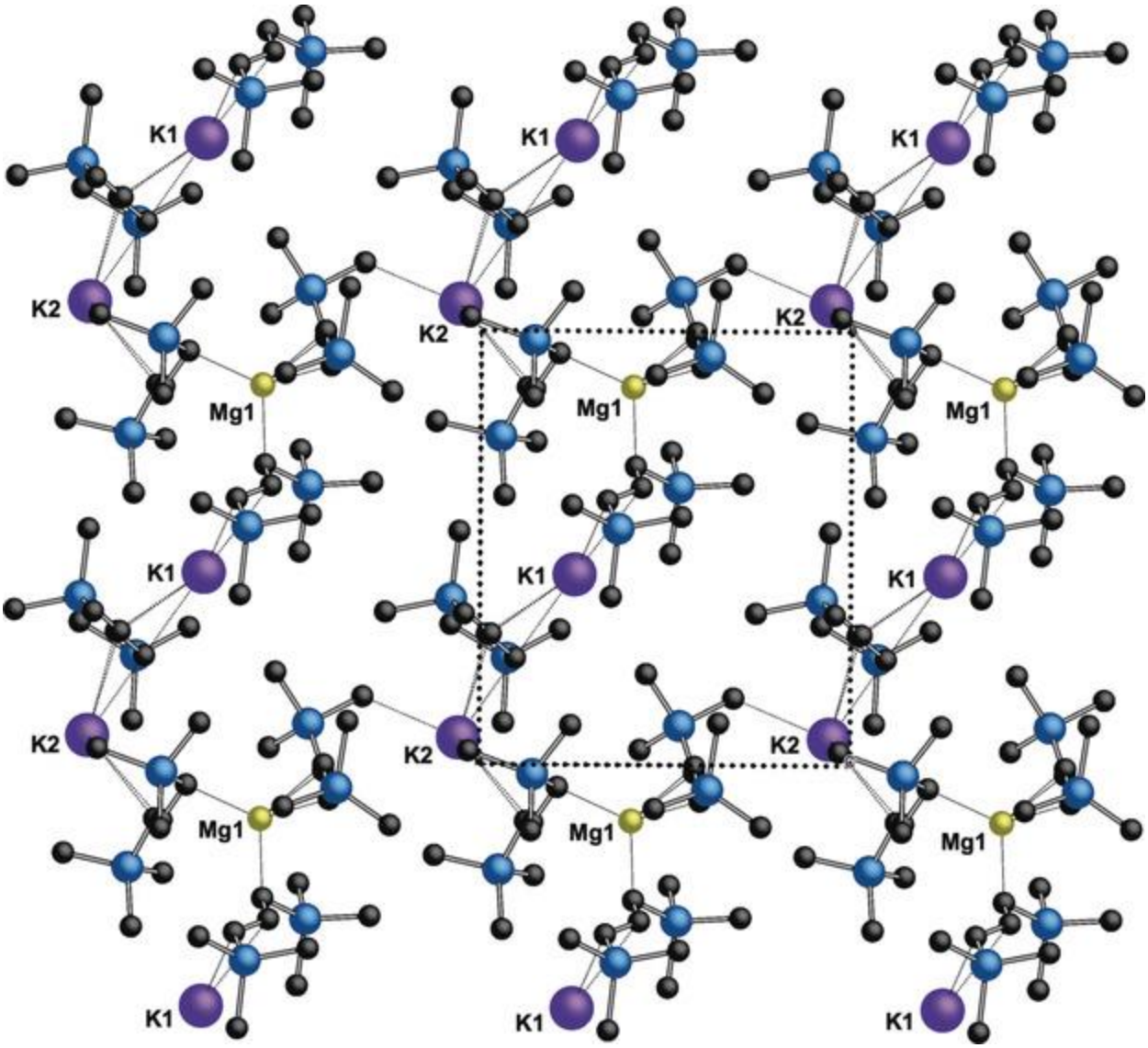

Figure 49. Partial packing diagram of $\{K_2[MgA'_4]\}_n$ (the *c* axis is vertical). Hydrogen atoms are omitted for clarity.

There are two crystallographically independent, but similar, magnesium centers, and only the coordination environment around Mg1 will be discussed here. The two Mg–C bonds to the η^1-bonded allyls are 2.206(3) and 2.235(4) Å, similar to that in [MgA′$_2$(THF)$_2$] (2.197(3) Å). The η^3-bonded allyl is the first structurally authenticated example of such a fragment, as it is both terminal (not bridging as in [{MgA′$_2$}$_2$]) and the C–C bonds in the allyl unit differ by only 0.028 Å, indicating virtually complete electron delocalization in the anion. It is somewhat slipped from symmetrical coordination, with terminal Mg–C bond lengths of 2.375(4) and 2.446(4) Å. Such slippage is common in systems with highly polar metal-allyl bonding.[46]

The bonding of the allyl ligands to the potassiums is irregular; K2 is η^2-bonded to the [C10-C12] allyl at an average distance of 3.10 Å (to C11/C12; the K1···C10 contact is at 3.32 Å). K2 also displays a contact at 3.09 Å to the methyl group C15 on Si3 (the K···H(C) distance is 2.60 Å, which is probably energetically significant). The allyl bridging between K1 and K2 (C28-C30) is fully delocalized ($\Delta_{C\text{-}C}$ = 0.004 Å), and displays μ_2-η^3:η^3 bonding to the potassium atoms, with average K-C distances of 3.050 Å (to K2) and 3.012 Å (to K1). The range of distances is similar to that observed in the coordination polymers [{K[A′]}$_\infty$] and [{K-[A′](THF)$_{3/2}$}$_\infty$].[47]

5.2.1 Polymerization Results

Metal (trimethylsilyl)allyl complexes have been previously evaluated as initiators for the polymerization of MMA.[30,48–50] Consequently, the MMA polymerization activity of **1** was evaluated and compared to the activities of the [{MgA′$_2$}$_2$] complex and the previously reported K[A′].[49] All polymerizations were conducted under an inert atmosphere in which the initiator, MMA (0.5 g), and toluene (2M) were combined and allowed to react at the designated temperature and time, as detailed in Table 1. Room-temperature polymerizations using initiators K[A′], **1**, and [{MgA′$_2$}$_2$] and a high monomer/ initiator loading (100:1) were found to reach 94%, 72%, and 19% yield, respectively, in 24 h (Table 11, entries 1–3). These results are consistent with the hypothesis that the polymerization inactivity of previously reported [MgA′$_2$(THF)$_2$] species is due in part to solvent coordination, thereby hindering monomer coordination to the metal center.[30]

When comparing the polymers produced using K[A′], **1**, and [{MgA′$_2$}$_2$], we found that initiators K[A′] and **1** both produce atactic poly(methylmethacrylate) (PMMA) with similar molecular weights (M_n) and dispersities ($Đ$). In contrast, [{MgA′$_2$}$_2$] produced isotactically enriched PMMA having a significantly higher M_n and a broader dispersity ($Đ$ = 3.83) (Table 11, entry 3). To further investigate the activity of catalyst **1**, MMA polymerizations were conducted at lower initiator loading (250:1) and shorter polymerization time (1 h). Again, initiators K[A′] and **1** exhibited similar activities reaching 90% and 72% yield, respectively (Table 11, entries 4-5), indicating that polymerizations using these initiators are rapid and reach their maximum possible conversion in ≤ 1 h.

However, [{MgA′$_2$}$_2$] exhibited dramatically decreased activity, only producing trace amounts of polymer under identical conditions (Table 11, entry 6).

Table 11: Polymerization of MMA with Initiator K[A]', [$K_2MgA'_4$] (1), and [{MgA'_2}$_2$].[a]

Entry	Initiator	Mono: init	Temp (°C)	Time (h)	Yield [b] (%)	M_n[c] (g/mol)	M_w/M_n	Tacticity[d]
1	K[A']	100:1	RT	24	94	19,100	2.68	26/50/24 (atactic)
2	[$K_2MgA'_4$] (1)	100:1	RT	24	72	17,800	2.76	25/52/23 (atactic)
3	[{MgA'_2}$_2$]	100:1	RT	24	19	113,400	3.83	71/16/12 (isotactic enriched)
4	K[A']	250:1	RT	1	90	25,500	2.37	----------
5	[$K_2MgA'_4$] (1)	250:1	RT	1	72	20,500	2.18	----------
6	[{MgA'_2}$_2$]	250:1	RT	1	Trace	--------	--------	----------
7	K[A']	1000:1	0	1	92	46,900	2.62	----------
8	[$K_2MgA'_4$] (1)	1000:1	0	1	89	27,800	2.89	----------
9	[{MgA'_2}$_2$]	1000:1	0	1	0	--------	--------	----------

[a] General conditions: 0.5 g monomer, 2 M in toluene, quenched with MeOH. [b] Yield was determined based upon isolated polymer mass and initial mass of MMA. [c] Determined using gel permeation chromatography at 40 °C in THF and are reported relative to a PMMA standard. [d] Determined with ^{1}H NMR in $CDCl_3$ by integrating the methyl region.

Lastly, the catalytic activity of **1** was examined for MMA polymerizations at 0 °C and a further decreased initiator loading of 1000:1 (MMA:**1**). K[A′] again exhibited similar activity reaching 92% in 1 h (Table 11, entry 7), whereas initiator **1** exhibited an increase in activity at this lower polymerization temperature, ultimately reaching 89% conversion in 1 h (Table 11, entry 8). Though the source of this increase in activity is not yet fully understood, we hypothesize that this may indicate that initiator **1** undergoes decomposition and/or deactivation at room temperature, which is slowed or suppressed at temperatures at or below 0 °C.[51–54] Finally, and as expected at this point, [{MgA′$_2$}$_2$] exhibited no polymerization activity under these conditions (Table 11, entry 9).

5.2.2 Computational Results

Isolated complexes involving the A′ ligand and a monovalent/ divalent metal combination have to date been of the form [$M^IM^{II}A'_3$], where 3 allyls are bound to the M^{II} metal in a C_3 symmetric *tris*-(η^1) fashion and sequester an [M^I]$^+$ cation in the *ansa*-tris(η^2-olefin) pocket through a cation-π interaction (e.g., Figure 51); such interaction is calculated to contribute as much as 24 kcal mol^{-1} to the stability of the compound when M^I = K.[55,56] The range of M^{II} ions that have been incorporated into structurally characterized compounds includes Zn (for which combinations with M^I = Li, Na, and K are known), Be,[19] and Sn.[43,57] It seemed unusual that this was not the form of the metallate adopted by the Mg derivative, especially as the ionic radii of Mg^{2+} and Zn^{2+}, for example, are similar (0.57 Å and 0.60 Å, respectively, for CN = 4).[58] The electronegativity of Mg (1.31, Pauling scale[59]) is less than any of other divalent metals used to date (1.57, 1.65, and 1.80 for Be, Zn, and Sn, respectively), however, and the Mg–C bond is somewhat more polar than the other M–C cases. The effect that this might have on the relative stability of η^3- over η^1- bonding was

examined with a DFT computational investigation (B3PW91-D3BJ/def2TZVP) of a selected set of $[M^{II}A'_2]$ and $[KM^{II}A']_3$ (M^{II} = Be, Mg, Zn, Sn) complexes (details in the SI). In the optimized $[MA'_2]$ complexes, Zn and Sn have η^1-bound allyls, indicating a preference that is corroborated by the lack of any structurally authenticated η^3-bound allyls on Zn,[60] though some have recently been identified for Sn.[61] For the more electropositive elements (Be, Mg), $[M(\eta^3\text{-}A')_2]$ geometries are lower in energy than the $[M(\eta^1\text{-}A')_2]$ counterparts; the preference for η^3- over η^1- in the case of Be is small (4.4 kcal mol^{-1}), but it doubles to 9.0 kcal mol^{-1} for Mg. Note that in order to maintain η^1-bound ligands, both $[BeA'_2]$ and $[MgA'_2]$ had to be optimized under C_i symmetry. The sigma-bound forms possessed imaginary frequencies, with the largest for $[MgA'_2]$ at -31 cm^{-1}.

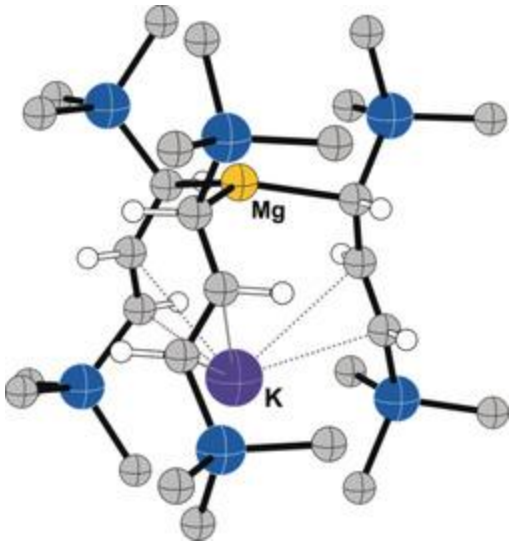

Figure 50. Calculated structure (B3PW91-D3BJ/def2TZVP) of $[Mg(\mu_2\text{-}\eta^1,\eta^2\text{-}A')_3K]$ (C_3 symmetry, H atoms omitted from the TMS groups). Mg–C 2.178 Å; C_α–C_β 1.441 Å; C_β–C_γ 1.364 Å; K···C=2.93, 3.23 Å; sum of C-Mg-C′ 354.4°.

Calculations on the monomeric $[KM^{II}A'_3]$ complexes indicated that all of them were at least local minima on their respective potential energy surfaces. The reason that a monomeric $[KMg(\eta^1\text{-}A')_3]$ complex is not isolated may be largely a result of the preference of magnesium for η^3- over η^1-allyl bonding. In addition, the polymeric structure of **1** provides for an η^3- interaction of the allyls with K^+, which should provide greater stabilization than that from the η^2 cation-π interactions with the C=C double bonds in a $[KMg(\eta^1\text{-}A')_3]$ complex.[62] Finally, issues of coordinative (un)saturation at the metal center may be in play. With the program Solid-G,[63] the net percentage of coordination sphere covered by the ligands in a complex may be estimated as the $G_{complex}$ value (Figure 51). The value for the hypothetical $[MgA'_2]$ is 79.0% (51a), but in the solvated $[MgA'_2(THF)_2]$ complex, it increases to 89.8% (see Appendix). A similar number (93.0%) is calculated for the $[\{MgA'_2\}_2]$ dimer (51b), and also for the Mg supporting the η^3-A′ ligand in **1** (i.e., in the $[K_2MgA'_3]^+$ fragment, at 90.1%, 51c). Note that the coordination environment in **1** was defined as a sphere of 7.6 Å radius around Mg1. This incorporates three complete allyl ligands directly bonded to the Mg and two potassium cations. The $G_{complex}$ value for the 3 allyl ligands around Mg in monomeric $[KMg(\eta^1\text{-}A')_3]$ is 84.9% (51d), roughly halfway

between the values for the exposed [MgA′$_2$] and the enclosure in **1**. This suggests that an undersaturated Mg center may boost its coverage by whatever means are at hand: if THF or Et_2O molecules are available, it will coordinate to them, but if not, the complex will dimerize. Alternatively, the presence of extra K[A′] in the same phase provides an opportunity for metal coordination through the formation of a coordination polymer, which provides better metal saturation than the monomeric [KMg(η^1-A′)$_3$].

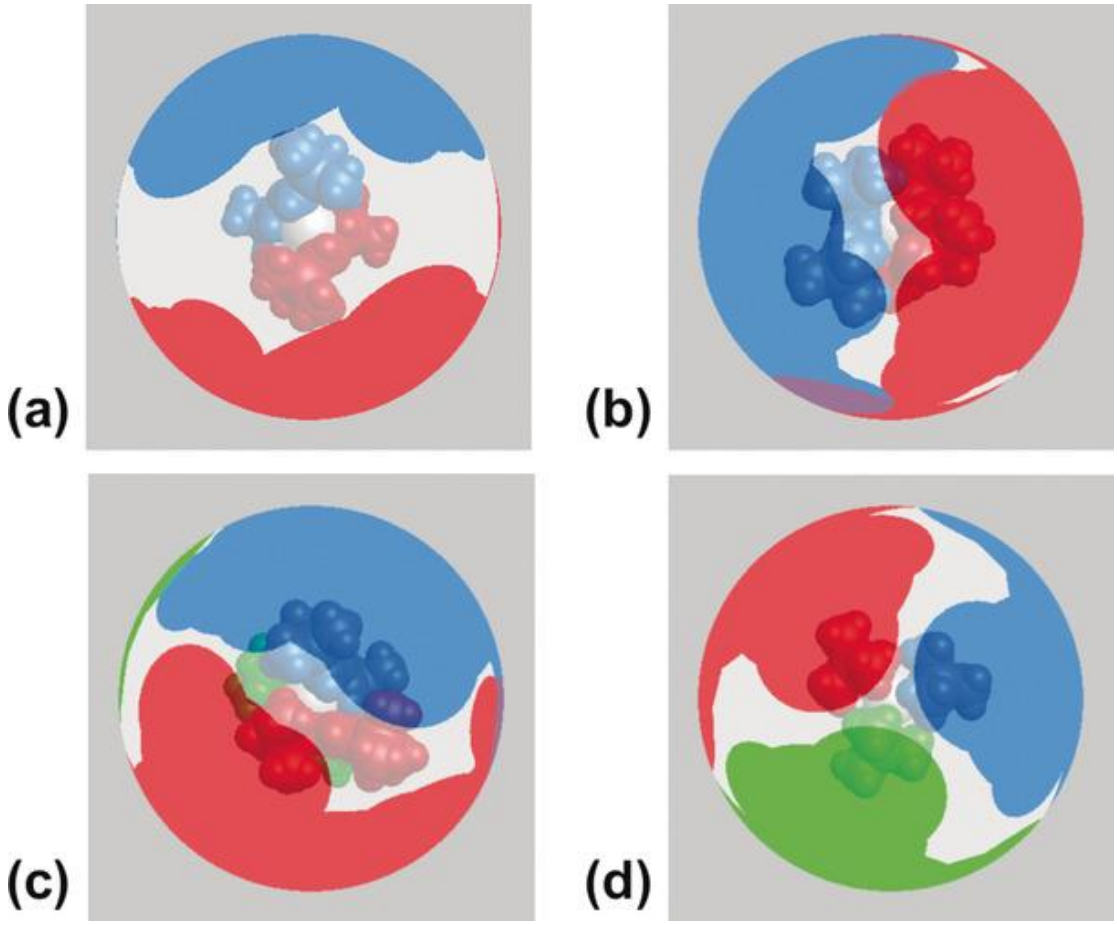

Figure 51. Visualization of the extent of coordination sphere coverage ($G_{complex}$) of: a) [MgA′$_2$], 79.0 %; b) [{MgA′$_2$}$_2$], (C_2 symmetry), 93.0 %; c) [K_2MgA′$_3$]$^+$ (fragment derived from **1**), 90.1 %; d) [MgA′$_3$] fragment, from the hypothetical [KMg(η^1-A′)$_3$] (C_3 symmetry, Mg at the center, K removed), 84.9 %. Optimized coordinates (B3PW91-D3BJ/def2-TZVP) and the program Solid-G were used. The $G_{complex}$ value represents the net coverage, so that regions of the coordination sphere where the projections of the ligands overlap are counted only once.

5.2.3 Requirements for trihapto allyl bonding to Mg

The long-standing difficulty of isolating a compound with an η^3-allyl ligand on Mg seems to conflict with computational evidence suggesting that such a bonding mode should be preferred over an η^1-bonded arrangement. An earlier DFT investigation indicated that the addition of THF to $[Mg(\eta^3\text{-}C_3H_5)_2]$ caused successive slippage of the allyl ligands to $[Mg(\eta^3\text{-}C_3H_5)(\eta^1\text{-}C_3H_5)(THF)]$ and then to $[Mg(\eta^1\text{-}C_3H_5)_2(THF)_2]$.[26] The exact reason for the slippage, whether primarily steric, electronic, or a combination of the two, was left unresolved. That a relatively crowded coordination sphere coverage of 90 % (Figure 52c) is still compatible with an η^3-A′ ligand, however, indicates that slippage of the ligand should not be uncritically ascribed to simple steric effects.

In the allyl anion, the negative charge is concentrated on the terminal carbons.[64] This fact, combined with the calculated $[Mg(\eta^3\text{-}C_3H_5)_2]\rightarrow[Mg(\eta^3\text{-}C_3H_5)(\eta^1\text{-}C_3H_5)(THF)]\rightarrow[Mg(\eta^1\text{-}C_3H_5)_2(THF)_2]$ progression noted above, suggests that the change in allyl hapticity occurs to maintain a roughly tetrahedral distribution of charge around the Mg. The relevance of these results to the structurally authenticated **1** can be appreciated by viewing the η^3-bound allyl from a point almost perpendicular to the C_3 plane (Figure 53). The most negatively charged carbons surrounding the Mg are C1/C3 of the π-bound allyl, and C10 and C19 of the neighboring σ-bonded allyls, which are at similar distances to Mg (2.23 and 2.21 Å, respectively). The angle between the planes defined by C1/Mg/C3 and C10/Mg/C19 is 77.0°.

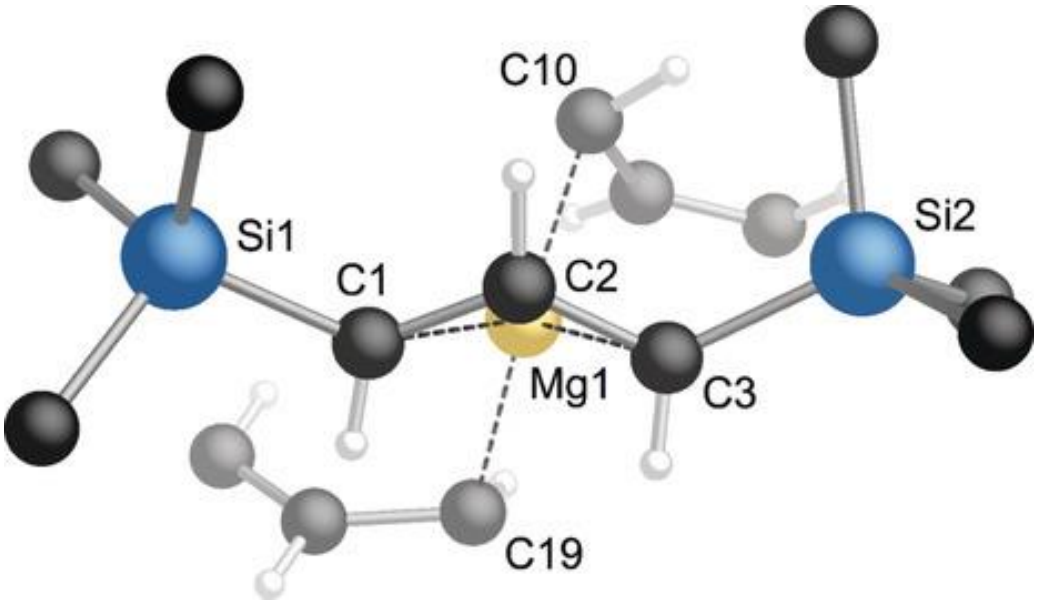

Figure 52. A fragment of the structure of **1**, viewed almost perpendicularly to the η^3-allyl C_3 plane; hydrogens have been removed from the TMS groups. The angle between the planes defined by C1/Mg/C3 and C10/Mg/C19 is 77.0°. The analogous angle calculated for the unsubstituted $[MgK_2(C_3H_5)_3]^+$ cation is 87.0°.

These tetrahedral or pseudo-tetrahedral geometries are related to the unique set of properties magnesium brings to an organometallic complex. The polarity of the Mg–C bond is moderately high, but the electropositivity of Mg is not enough to support the η^3-bonding expected from an essentially ionic interaction, that is, as a $[Mg]^{2+}[C_3H_5]^-$ ion pair, as observed with the alkali metals or heavier Group 2 metals. An orbitally supported η^3-allyl configuration, relying on a formally sp^3-hybridized Mg center, will engage two of the four available orbitals, leaving only two to bind to additional ligands. The tetrahedral arrangement of bonding associated with an η^3-allyl ligand is apparent in a Bader analysis (atoms in molecules, AIM) of $[Mg(C_3H_5)_2]$ and the $[K_2Mg(C_3H_5)_3]^+$ cation (Figure 54). The bond critical paths (BCP) connect the most negative centers in the allyl anions to the Mg centers, whereas in the cation, a single BCP is observed between K^+ and the closest carbon atom of the adjacent allyl, a bonding pattern found before with highly ionic interactions.[65] A more detailed contour mapping of the Mg–allyl interaction in the $[K_2Mg(C_3H_5)_3]^+$ cation is available in the Appendix.

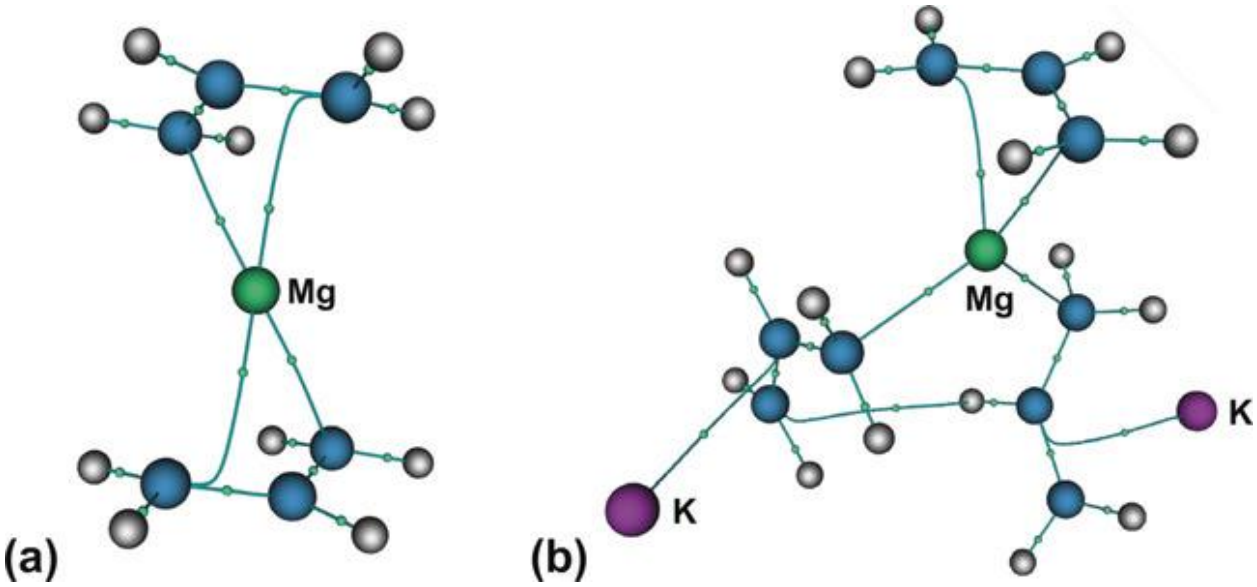

Figure 53. Bond critical points (dots) and bond paths (lines) obtained from AIM calculations for: a) the neutral $[Mg(C_3H_5)_2]$ complex; b) the $[K_2Mg(C_3H_5)_3]^+$ cation. The average electron density of the bond critical points from Mg to the terminal carbons of the allyls in $[Mg(C_3H_5)_2]$ is 0.037 $e^- Å^{-3}$; that to the terminal carbons of the η^3-bound allyl in $[K_2Mg(C_3H_5)_3]^+$ is 0.034 $e^- Å^{-3}$, and to the terminal carbons of the η^1-bound allyls is 0.040 $e^- Å^{-3}$.

A survey of the Cambridge Structural Database (May 2019 release) reveals that all structurally authenticated magnesium compounds with one or more terminal allyl ligands (all σ-bonded) are at least 4-coordinate (see Appendix), which means that if an allyl ligand were to shift to a permanent η^3-configuration, the effective coordination number would rise to at least 5 or greater. Without the electropositive character of the metal or sufficient orbitals to support η^3-allyl bonding under such conditions, the allyl will remain σ-bonded. An illustration of this situation is provided by the PMDTA adducts of lithium and

magnesium allyl complexes, established crystallographically as $[Li(\eta^3\text{-}C_3H_5)(PMDTA)]$[46] and $[Mg(\eta^1\text{-}C_3H_5)(PMDTA)(THF)]^+[B(C_6F_5)_4]^-$.[25] To make the coordination environments equivalent and to remove any effects of crystal packing, the geometries of the neutral $[Li(C_3H_5)(PMDTA)]$ and cationic $[Mg(C_3H_5)(PMDTA)]^+$ cation complexes were optimized at the B3PW91-D3BJ/def2TZVP level. The allyl ligand remains η^3-allyl bound to Li, and η^1-bound to Mg (Figure 55), consistent with the analysis above.

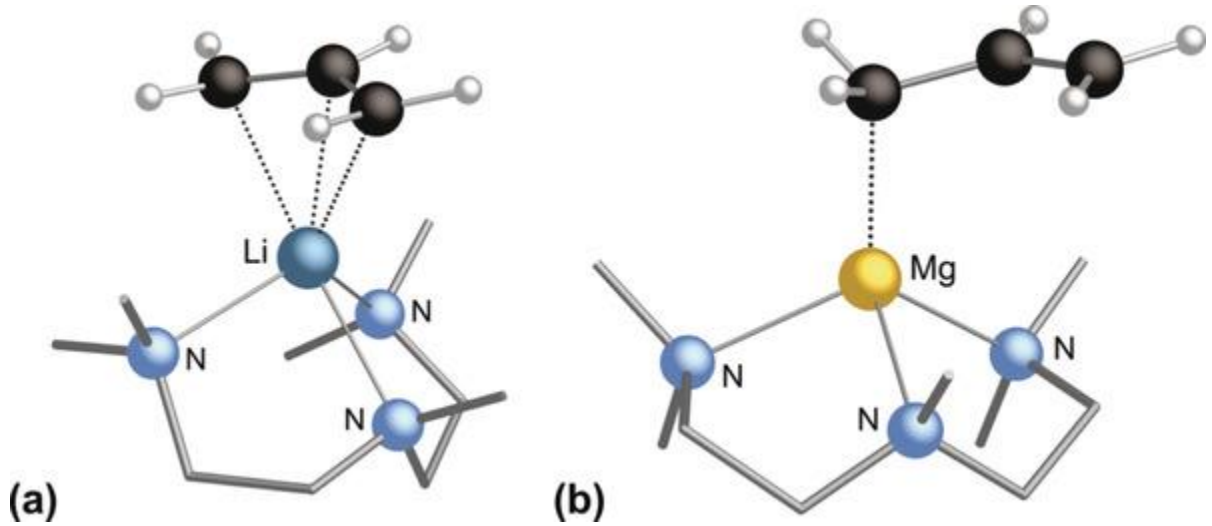

Figure 54. Geometry-optimized structures of a) $[Li(\eta^3\text{-}C_3H_5)(PMDTA)]$ and b) $[Mg(\eta^1\text{-}C_3H_5)(PMDTA)]^+$. The Li–C bonds average to 2.24 Å, and the allyl C–C bonds differ by 0.002 Å. The Mg-C_α distance is 2.112 Å, whereas the other carbons are >2.8 Å away. The allyl C–C bond lengths differ by 0.147 Å.

5.3 Conclusion

We have prepared through mechanochemical synthesis the first compound containing a structurally authenticated η^3-bound allyl ligand on a magnesium center. The rarity of this particular bonding mode appears to stem from a combination of properties particular to magnesium, specifically its intermediate electropositivity and limited set of valence orbitals. To realize the trihapto bonding, a relatively low coordination number for the metal is required, which can be summarized for a monometallic complex with the formula $[(\eta^3\text{-allyl})_xMgX_yL_z]^{2-(x+y)}$ (X is a monoanion; L is a neutral donor) by the relationship $2x+y+z\leq4$. Consequently, if x = 2 (two η^3-allyls), y and z can only be zero, as predicted for the structure of $[Mg(\eta^3\text{-allyl})_2]$. Similarly, if one adds a neutral donor to $[Mg(\eta^3\text{-allyl})_2]$, only one of the allyls can remain η^3-bound, as calculated for $[Mg(\eta^3\text{-}C_3H_5)(\eta^1\text{-}C_3H_5)(THF)]$. The presence of the η^3-A′ ligand in **1** follows from the values x=1, y=2, corresponding to the $[(\eta^3\text{-A}')Mg(\eta^1\text{-A}')_2]^-$ anionic fragment. The isolation of **1** was aided by the bulk of the A′ ligand, which discourages additional coordination, and by the solvent-free mechanochemical synthesis, but there is no reason why this unusual bonding mode could not be recreated in other organomagnesium compounds.

The polymerization of MMA by K[A′], **1**, and [{MgA′$_2$}$_2$] demonstrates the influence of the metal identity on polymerization activity. [{MgA′$_2$}$_2$] is certainly the least active of the three, but does provide some measure of stereocontrol, as evidenced by the enhanced isotacticity of the PMMA produced. K[A′] is by far the most active, and is effective at 1000:1 loading, but produces atatic polymer. The polymerization behavior of **1** appears to be influenced by its preponderance of potassium, in that its activity is far higher than that of [{MgA′$_2$}$_2$], and approaches that of K[A′], and it has also lost any stereocontrol over polymerization, generating only atactic polymer. There has been growing interest in studying the properties of heterometallic main-group systems in both stoichiometric and catalytic contexts,[25,66,67] and the ability to generate new classes of such compounds mechanochemically suggests that expanded investigations of heterometallic reactivity will be possible.

5.4 Appendix

Experimental Section

General Considerations.
All manipulations were performed with the rigorous exclusion of air and moisture using Schlenk or glovebox techniques. Elemental analysis was performed at the University of Rochester CENTC Elemental Analysis Facility by Dr. William Brennessel. Proton and carbon ($^{13}C\{^1H\}$) NMR spectra of the organometallic compounds were obtained on a DRX-500 spectrometer at 500 (^1H) and 125 (^{13}C) MHz or an AV-400 spectrometer at 400 (^1H) and 100 (^{13}C) MHz and were referenced to the residual proton and ^{13}C resonances of C_6D_6. Molecular weights (M_n) of the polymers were determined using a Tosoh EcoSec GPC at 40 °C in THF and referenced to polymethylmethacrylate standards. ^1H NMR of polymers were recorded on a Varian 300 spectrometer and chemical shifts are reported with respect to solvent residual peaks, i.e., δ 7.26 ppm ($CDCl_3$, purchased from Cambridge Isotope Laboratories).

Materials.
$MgCl_2$ and $MgBr_2$ were purchased from commercial suppliers and used as received. The potassium allyl K[A′] = K[(1,3-$SiMe_3$)C_3H_3] was synthesized by transmetallation of Li[A′][68] with potassium *tert*-butoxide in hexanes solution. Toluene was degassed with argon and dried over activated alumina using a solvent purification system, then stored over 4 Å molecular sieves in a glovebox. Hexanes were distilled under nitrogen over NaK/benzophenone radical,[69] then stored over 4 Å molecular sieves. Benzene-d_6 was obtained from Cambridge Isotopes and stored over 4 Å molecular sieves. Methyl methacrylate was purchased from Acros, run through a basic alumina column, dried over 4 Å sieves, vacuum transferred, and then degassed via three freeze-pump-thaw cycles.

Synthesis of [$K_2MgA'_4$].
In a typical reaction, $MgCl_2$ (0.060 g, 0.63 mmol) and K[A′] (0.281 g, 1.25 mmol) were added to a 50 mL stainless steel Retsch milling jar with 25 g (ca. 57 count) of stainless steel (440 grade) ball bearings (3/16 in (5 mm), 0.44 g) under a nitrogen atmosphere in a glovebox. The jar was sealed with a clamp in the glovebox and milled for 15 minutes at 600 rpm in a Retsch PM100 planetary mill. The jar was opened in an ether-free glovebox, and the reaction mixture was extracted with hexanes through a medium-porosity glass fritted funnel. The resulting pale green filtrate was dried under vacuum, and partway through evaporation a dense orange oil collected in the bottom of the flask. The orange oil remained after removal of solvent, out of which grew white crystals (0.174 g, 64% yield). Upon sealing in a glass ampule under nitrogen, the crystals immediately turned red, indicating an extreme sensitivity to trace oxygen and/or heat.

Synthesis of [$K_2MgA'_4$•2(toluene)].
The same procedure was followed as for the unsolvated compound, except that extraction was made using toluene. The toluene filtrate was pale green, and yielded a faintly green oil upon removal of solvent, with sheets of pale green crystals precipitating out. Toluene was partially lost on standing, which was reflected in the elemental analysis. Anal. Calcd for $C_{38}H_{84}K_2MgSi_8$•$(C_7H_8)_{1.5}$: C, 57.88; H, 9.61. Found: C, 57.70; H, 9.30. ^{1}H NMR (400 MHz, C_6D_6): δ 0.179 (s, 8.6H, TMS_A), 0.252 (s, 17.43H, TMS_B), 2.67 (d, $^1J_{H\text{-}H}$ = 16 Hz, 0.96H, $(H_{1,3})_A$), 3.19 (d, $^1J_{H\text{-}H}$ = 15.7 Hz, 1.9H, $(H_{1,3})_B$), 6.61 (t, $^1J_{H\text{-}H}$ = 16 Hz, 0.48H, H_{2A}), 6.94 (t, $^1J_{H\text{-}H}$ = 15.7 Hz, 1H, H_{2B}). $^{13}C\{^1H\}$ NMR (100 MHz, C_6D_6) δ 1.65, 2.47, 70.63, 71.71, 153.81, 157.25.

General MMA Polymerization Conditions.
Under an inert atmosphere, MMA (0.5 g, 5 mmol) was added to a solution of catalyst (50, 20, or 5 μmol) in toluene (2.5 mL). The polymerization was held at the designated temperature and stirred continuously for the time prescribed. The polymerization was quenched via exposure to air and the polymer precipitated via dropwise addition to MeOH. The resultant polymer was isolated via filtration then re-dissolved in CH_2Cl_2, re-precipitated into MeOH, filtered, and dried. Polymer tacticity was determined with ^{1}H NMR in $CDCl_3$.

X-ray Crystallography.
X-ray crystallographic data were collected on a Rigaku Oxford Diffraction Supernova diffractometer. Crystal samples were handled under immersion oil and quickly transferred to a cold nitrogen stream. The crystals were kept at 100 K during data collection. Under Olex2,[70] the structure was solved with the SHELXT[71] structure solution program using direct methods and refined with the SHELXL[72] refinement package using least squares minimization. All non-hydrogen atoms were refined with anisotropic displacement parameters. Crystallographic data for the structure have been deposited with the Cambridge Crystallographic Data Centre as CCDC 1972897, which can be obtained free of charge on application to CCDC, 12 Union Road, Cambridge CB2 1EZ, UK (fax: (+44)1223-336-033; e-mail: deposit@ccdc.cam.ac.uk).

General Procedures for Calculations.
All calculations were performed with the Gaussian 09W[73] or Gaussian 16 (Linux) suite of programs.[74] The B3PW91 functional, which incorporates Becke's three parameter exchange functional with the 1991 gradient-corrected correlation functional of Perdew and Wang, was used.[75,76] To supply dispersion corrections, Grimme's D3 correction[77] with additional Becke-Johnson damping was used.[78] Unless otherwise noted, the basis sets def2TZVP (for neutral and cationic complexes) or def2TZVPD (for anionic complexes) were used on all atoms.[79] Frequency calculations were also done at the triple-zeta level. Calculation of AIM parameters (bond critical paths/points) were performed with the Multiwfn program (3.7 Dev).[80]

Table 12: Comparison of organomagnesium complexes with η^1-bonded allyl ligands (Cambridge Structural Database, May 2019 release)

Entry	Complex	C.N.	Mg–C (Å)	CSD[a] Code	Ref.
1	[{Mg(^{i}Pr$_2$TACN)(η^1-C$_3$H$_5$)$_2$}]	5	2.2568(12)	BARBOO	81
2	[Mg(η^1-C$_3$H$_5$)(tbpamd)]	4	2.133(4)	CIRROL	82
3	[Mg(η^1-C$_3$H$_5$)Cl(tmeda)]$_2$	5	2.179(3)	FOGPAS	83
4	Mg{HC(MeCNC$_6$H$_3$^{i}Pr$_2$-2,6)$_2$}(η^1-C$_3$H$_5$)(THF)	4	2.139(3)	GECRUC	84
5	[Mg(η^1-C$_3$H$_5$)$_2$(THF)(μ_2-1,4-dioxane)]$_n$	5	2.2021(15)	IFOMUN	25
6	[Mg(η^1-C$_3$H$_5$)(PMDTA)(THF)][B(C$_6$F$_5$)$_4$]	5	2.181(3)	IFONAU	25
7	[KMg(η^1-C$_3$H$_5$)$_3$(THF)]	4	2.221(8)[b]	IFONEY	25
8	[K$_2$Mg(η^1-C$_3$H$_5$)$_4$(THF)$_2$]	4	2.24(3)[b]	IFONIC	25
9	*cis*-[(η^1-C$_3$H$_5$)MgBr(dme)$_2$]	6	2.210(8)	OKUSES	85
10	[La(η^3-C$_3$H$_5$)$_3$(μ-1,4-dioxane)·Mg(η^1-C$_3$H$_5$)$_2$(μ-1,4-dioxane)$_{1.5}$]$_\infty$	5	2.196(8)[b]	XAWYEA	[7]
11	[Y(η^3-C$_3$H$_5$)$_3$(μ-1,4-dioxane)·Mg(η^1-C$_3$H$_5$)$_2$(μ-1,4-dioxane)$_{1.5}$]$_\infty$	5	2.189(11)[b]	XAWYIE	[7]
12	[Mg(η^1-(1,3-SiMe$_3$)$_2$C$_3$H$_3$)$_2$(THF)$_2$]	4	2.196(4)[b]	XUBGIL	[8]
13	[{Mg((1,3-SiMe$_3$)$_2$C$_3$H$_3$)$_2$}$_2$] (η^1- ligands)	4	2.139(3)[b]	XUBGOR	[8]
14	[{MgCl(THF)$_2$}$_3$(μ_3-C$_3$H$_5$)$_2$]$_2$[Mg(η^1-C$_3$H$_5$)$_4$]	4	1.996(8)	YEHDEV	[9]

[a]Cambridge Structural Database, May 2019 release; [b]average value

Table 13: Crystal Data and Summary of X-ray Data Collection for $[K_2Mg\{1,3(SiMe_3)_2C_3H_5\}_4]$

Empirical formula	$C_{36}H_{84}K_2MgSi_8$	
Formula weight	844.26	
Temperature	100 K	
Wavelength	0.71073 Å	
Crystal dimensions (mm)	0.165 × 0.12 × 0.079	
Crystal system	Monoclinic	
Space group	$P2_1$	
Unit cell dimensions	a = 11.99006(12) Å	α= 90°
	b = 10.17389(11) Å	β= 96.7825(9)°
	c = 44.7549(4) Å	γ= 90°
	Volume	5421.24(9) Å^3
Z	4	
Density (calculated)	1.034 Mg/m^3	
Absorption coefficient	0.385 mm^{-1}	
F(000)	1848	
Theta range for data collection	3.02 to 27.48°	
Index ranges	-15≤h≤15, -13 ≤k≤13, -58 ≤l≤58	
Reflections collected	24 817	
Observed reflections	22 665	
Absorption correction	Gaussian	
Refinement method	Full-matrix least-squares on F^2	
Data / restraints / parameters	24817 / 913 / 7	
Goodness-of-fit on F^2	1.125	
Final R indices [I>2□(I)]	R_1 = 0.0419, wR_2 = 0.0832	
R indices (all data)	R_1 = 0.0484, wR_2 = 0.0854	
Largest diff. peak and hole	0.357 and -0.241 e$^-$ Å^{-3}	

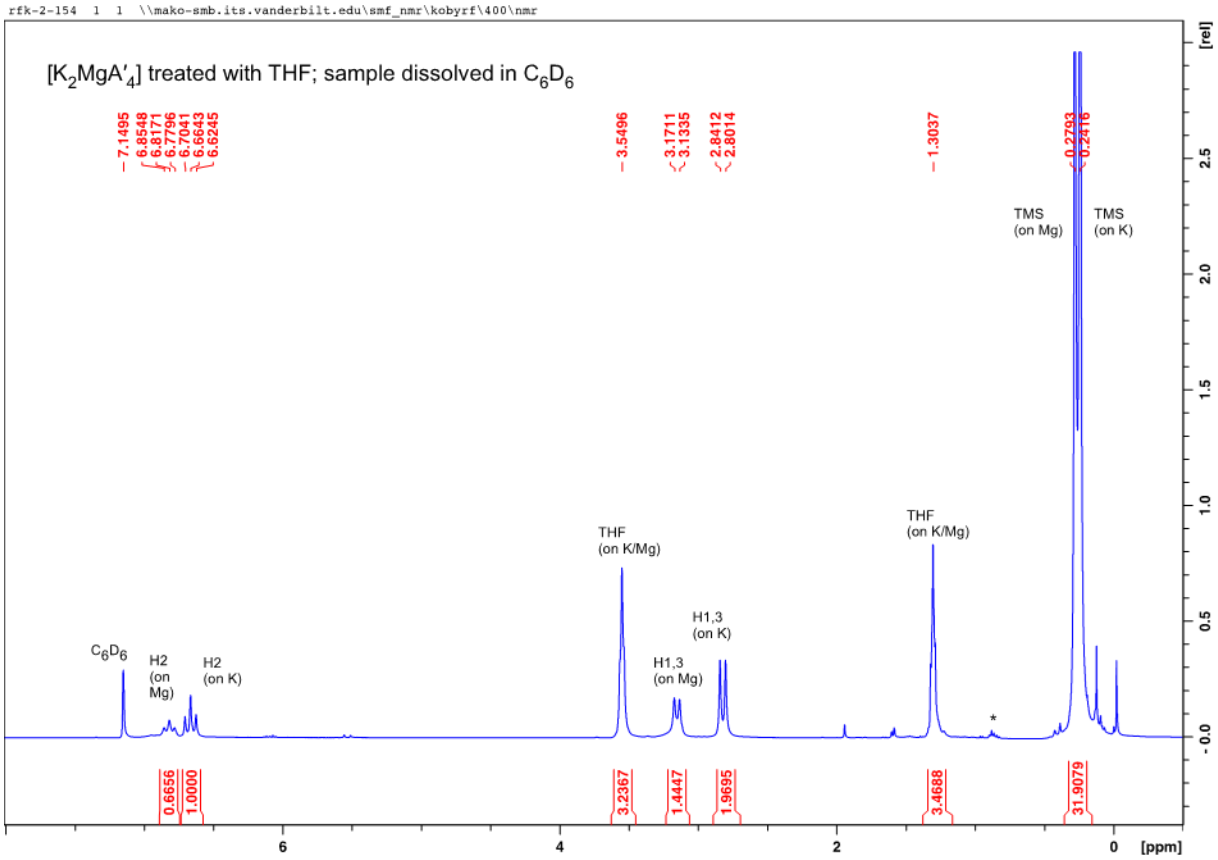

Figure 55. A sample of [$K_2MgA'_4$], prepared from $MgCl_2$ and K[A′], was extracted with hexanes and THF added to the extract. The ^1H NMR spectrum (400 MHz) reveals the presence of both [$MgA'_2(THF)_x$] and K[A′]$(THF)_x$.

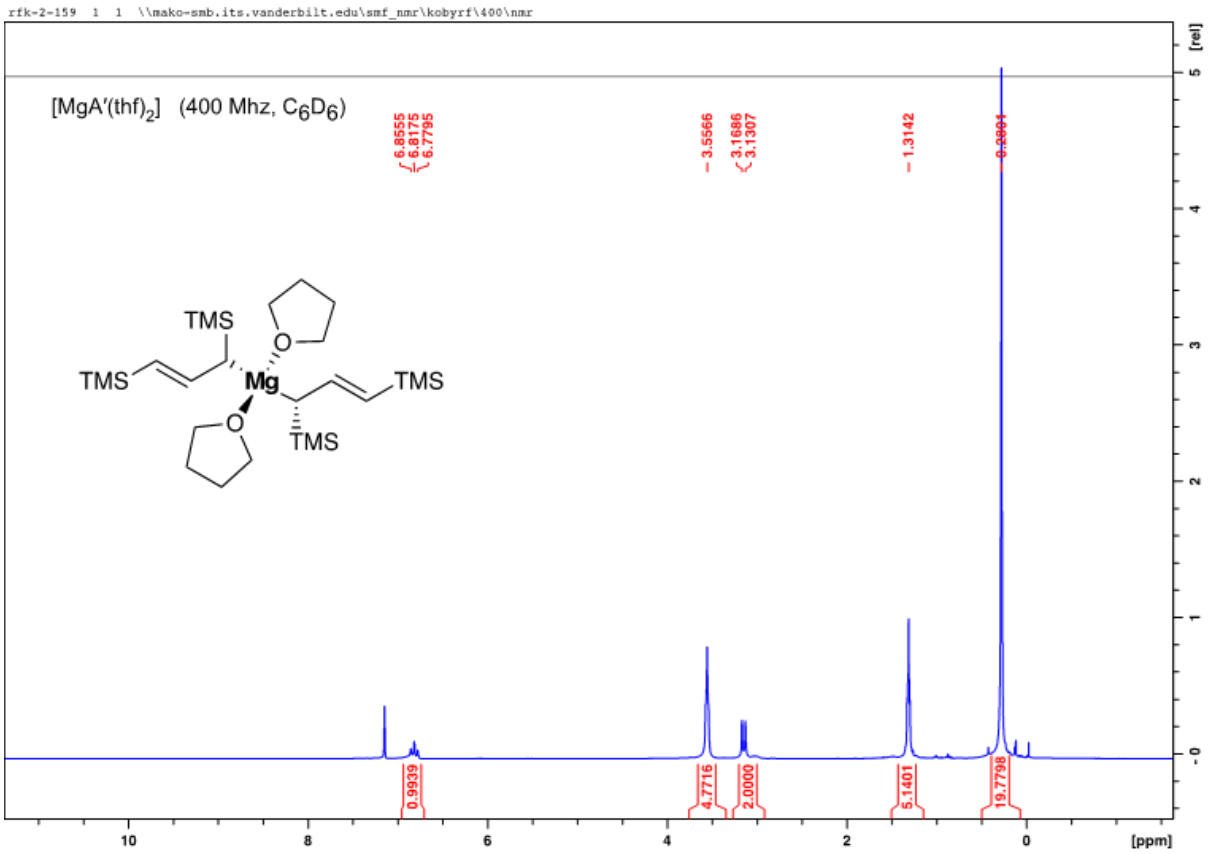

Figure 56. ^{1}H NMR spectrum of [MgA′$_2$(THF)$_2$] alone is shown at right. Note that the value for the resonance of the hydrogens on the β carbons of THF is at δ1.31; it was previously given erroneously as δ1.58 (J. Am. Chem. Soc. **2009**, 131, 6344-6345).

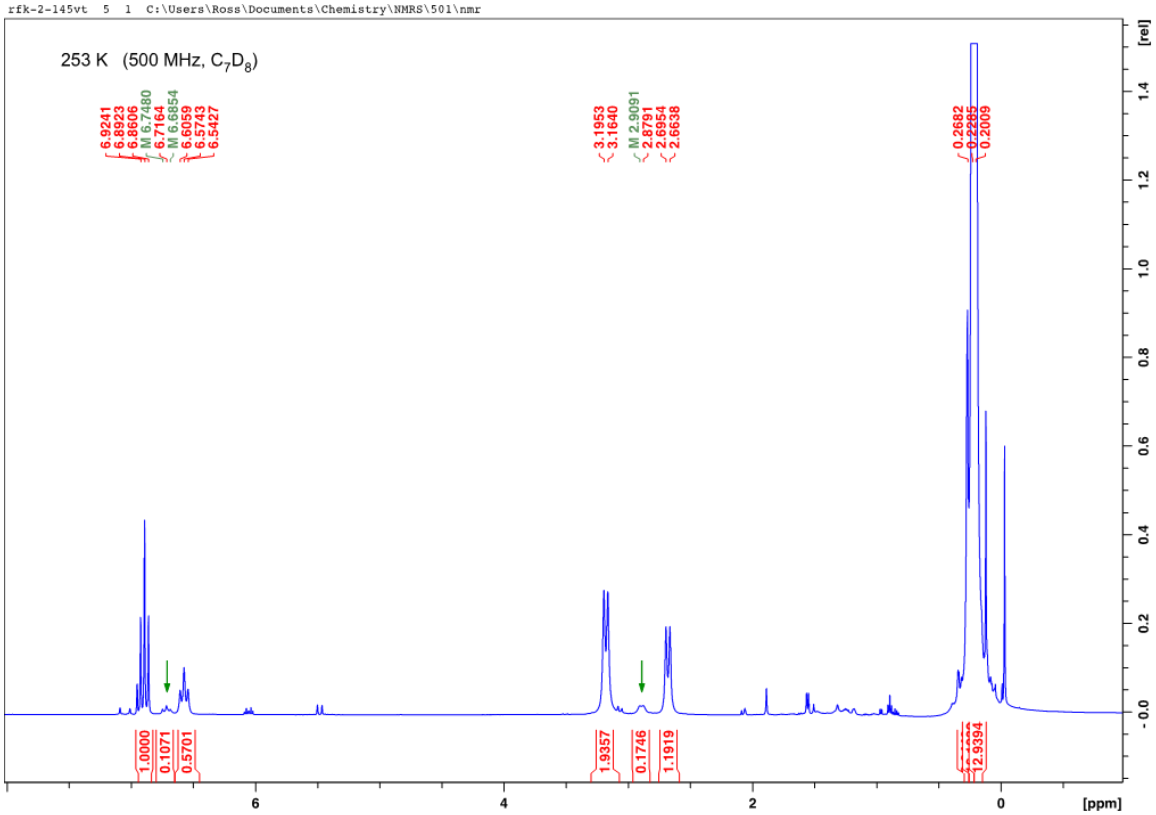

Figure 57. A sample of [$K_2MgA'_4$] cooled to 253 K. The arrows mark the appearance of new resonances from the slowing rearrangements of the allyl ligands.

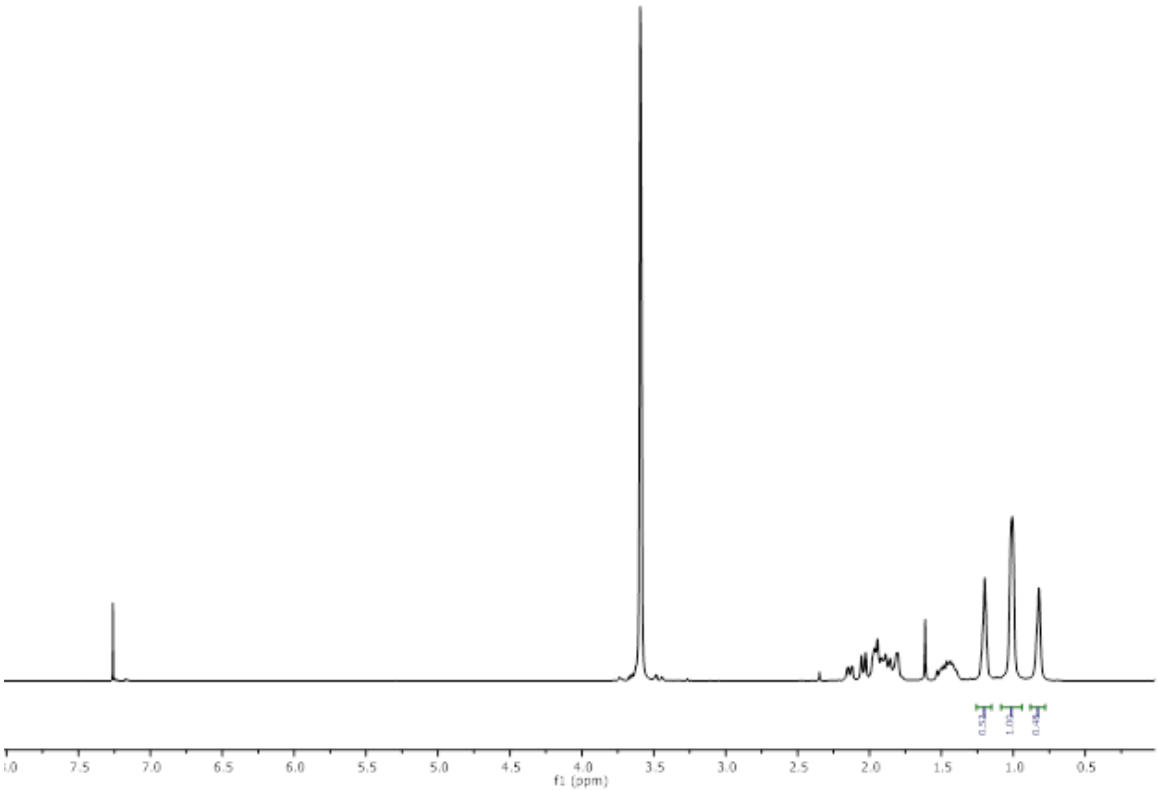

Figure 58. ^{1}H NMR spectrum (300 MHz, 25 °C, $CDCl_3$) of PMMA obtained using K[A'].

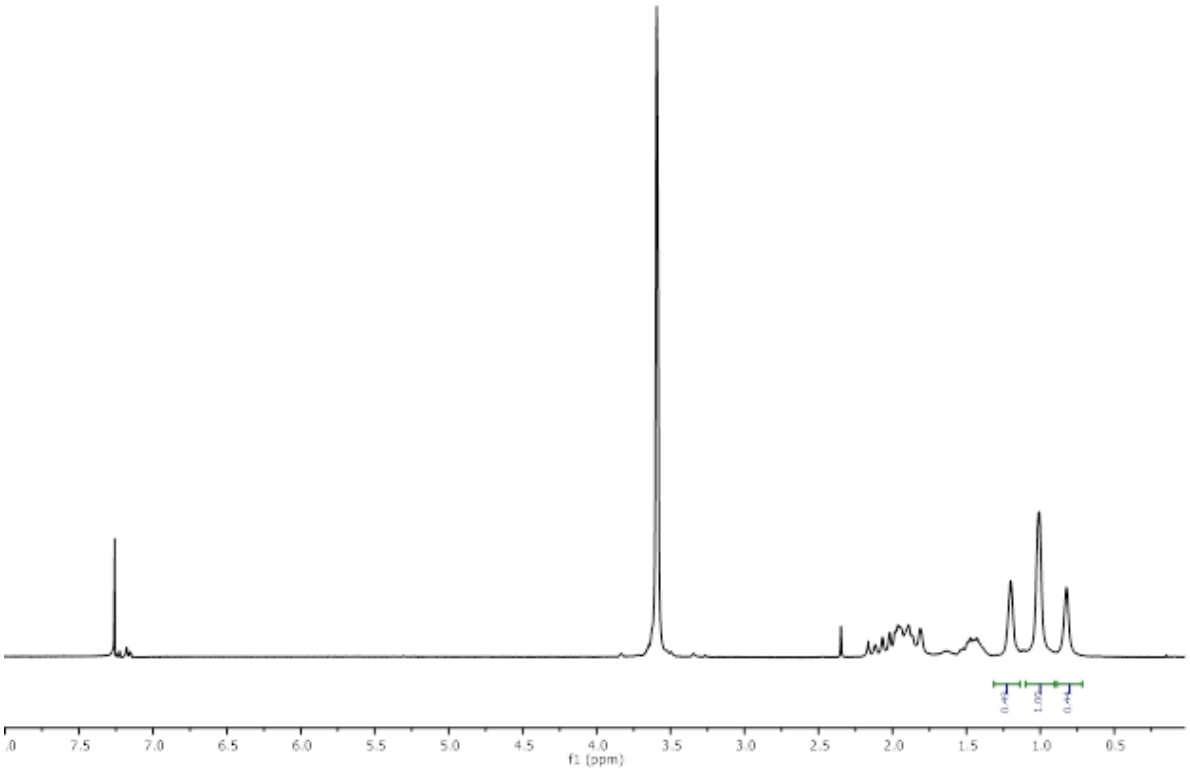

Figure 59. ^{1}H NMR spectrum (300 MHz, 25 °C, $CDCl_3$) of PMMA obtained using [$K_2MgA'_4$].

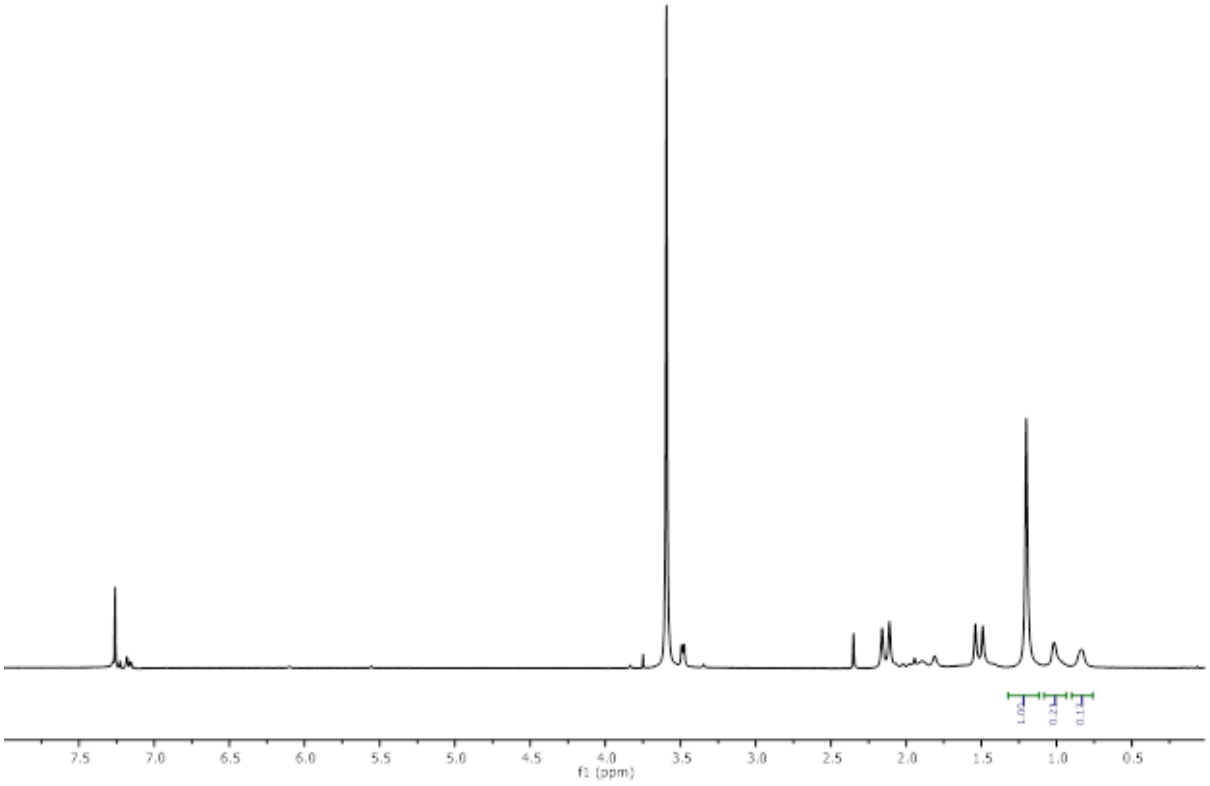

Figure 60. ^{1}H NMR spectrum (300 MHz, 25 °C, $CDCl_3$) of PMMA obtained using [{MgA′$_2$}$_2$].

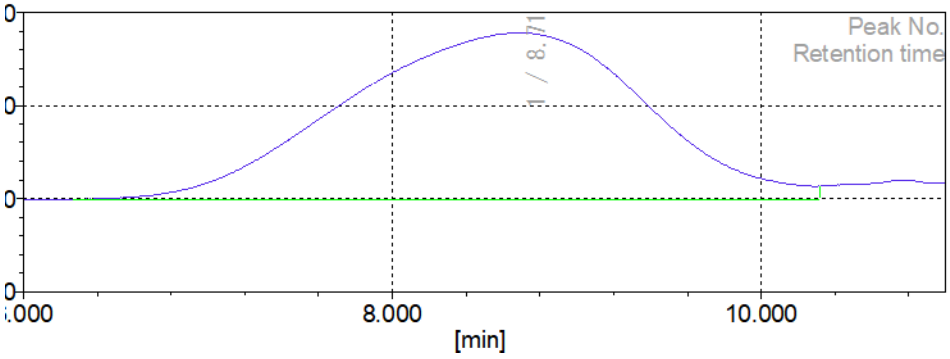

Figure 61. Representative GPC trace of PMMA obtained using K[A′]. Samples measured in THF at 40 °C and referenced using a polymethylmethacrylate standards (Table 11, Entry 1 in main manuscript).

Table 14: Result of molecular weight calculation (RI)

Peak 1 Valley Peak

	[min]	[mV]	[mol]	M_n	19,189
Peak start	6.272	-0.056	1,103,076	M_w	51,505
Peak top	8.710	8.909	25,612	M_z	126,515
Peak end	10.318	0.653	2,156	M_{z+1}	254,913
				M_v	51,505
Height [mV]			8.949	M_p	31,305
Area [mV*sec]			1001.982	M_z/M_w	2.456
Area% [%]			100.000	M_w/M_n	2.684
[eta]			51504.84915	M_{z+1}/M_w	4.949

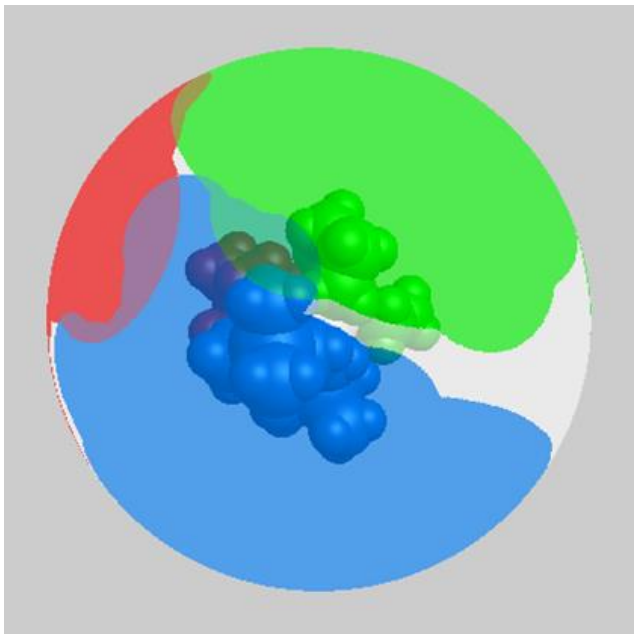

Figure 62. Visualization of the extent of coordination sphere coverage ($G_{complex}$) of [MgA′$_2$(THF)$_2$], 89.8%. The allyl ligands are in red and blue; the THF is in green. Optimized coordinates (B3PW91-D3BJ/def2-TZVP and the program Solid-G were used to generate the figure. The $G_{complex}$ value represents the net coverage, so that regions of the coordination sphere where the projections of the ligands overlap are counted only once.

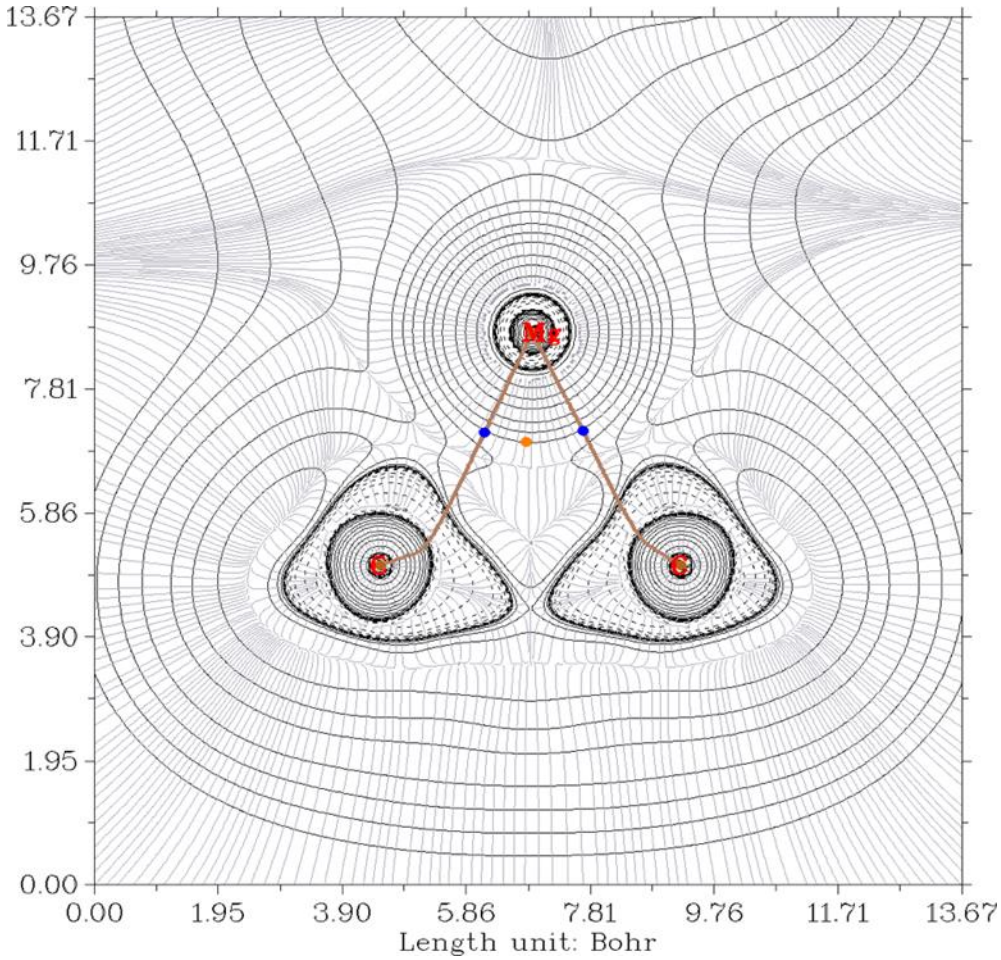

Figure 63. Contour plot of the Laplacian of the electron density in the $[K_2Mg(C_3H_5)_3]^+$ cation, taken through the plane defined by the Mg and the two terminal atoms of the η^3-bound allyl. Bond critical points and paths are also drawn. Calculated at the B3PW91-D3BJ/def2-TZVP level, visualized with the Multiwfn program (3.7 Dev).

Energies of Calculated Geometries (prepared with ESIgen)[86]

[MgA′$_2$(THF)$_2$]

Datum	Value
Charge	0
Multiplicity	1
Stoichiometry	C26H58MgO2Si4
Number of Basis Functions	1396
Electronic Energy (Eh)	-2534.47185882
Sum of electronic and zero-point Energies (Eh)	-2533.689796
Sum of electronic and thermal Energies (Eh)	-2533.637286
Sum of electronic and enthalpy Energies (Eh)	-2533.636342
Sum of electronic and thermal Free Energies (Eh)	-2533.777341
Number of Imaginary Frequencies	0
Mean of alpha and beta Electrons	149

[MgA′$_2$]

Datum	Value
Charge	0
Multiplicity	1
Stoichiometry	C18H42MgSi4
Number of Basis Functions	990
Electronic Energy (Eh)	-2069.45561345
Sum of electronic and zero-point Energies (Eh)	-2068.912926
Sum of electronic and thermal Energies (Eh)	-2068.872363
Sum of electronic and enthalpy Energies (Eh)	-2068.871419
Sum of electronic and thermal Free Energies (Eh)	-2068.986732
Number of Imaginary Frequencies	0
Mean of alpha and beta Electrons	109

[Mg(C$_3$H$_5$)$_2$]

Datum	Value
Charge	0
Multiplicity	1
Stoichiometry	C6H10Mg
Number of Basis Functions	278
Electronic Energy (Eh)	-434.677680255
Sum of electronic and zero-point Energies (Eh)	-434.540976
Sum of electronic and thermal Energies (Eh)	-434.531285
Sum of electronic and enthalpy Energies (Eh)	-434.530341
Sum of electronic and thermal Free Energies (Eh)	-434.575951
Number of Imaginary Frequencies	0
Mean of alpha and beta Electrons	29

[Mg(C$_3$H$_5$)$_2$(THF)]

Datum	Value
Charge	0
Multiplicity	1
Stoichiometry	C10H18MgO
Number of Basis Functions	481
Electronic Energy (Eh)	-667.184907243
Sum of electronic and zero-point Energies (Eh)	-666.928968
Sum of electronic and thermal Energies (Eh)	-666.912965
Sum of electronic and enthalpy Energies (Eh)	-666.91202
Sum of electronic and thermal Free Energies (Eh)	-666.974294
Number of Imaginary Frequencies	0
Mean of alpha and beta Electrons	49

[Mg(C$_3$H$_5$)$_2$(THF)$_2$]

Datum	Value
Charge	0
Multiplicity	1
Stoichiometry	C14H26MgO2
Number of Basis Functions	684
Electronic Energy (Eh)	-899.6822907540001
Sum of electronic and zero-point Energies (Eh)	-899.307825
Sum of electronic and thermal Energies (Eh)	-899.285222
Sum of electronic and enthalpy Energies (Eh)	-899.284278
Sum of electronic and thermal Free Energies (Eh)	-899.36364
Number of Imaginary Frequencies	0
Mean of alpha and beta Electrons	69

[Li(C$_3$H$_5$)(PMDTA)]

Datum	Value
Charge	0
Multiplicity	1
Stoichiometry	C12H28LiN3
Number of Basis Functions	359
Electronic Energy (Eh)	-645.2821034849999
Sum of electronic and zero-point Energies (Eh)	-644.885624
Sum of electronic and thermal Energies (Eh)	-644.865018
Sum of electronic and enthalpy Energies (Eh)	-644.864073
Sum of electronic and thermal Free Energies (Eh)	-644.931924
Number of Imaginary Frequencies	0
Mean of alpha and beta Electrons	62

[Mg(C$_3$H$_5$)(PMDTA)]$^+$

Datum	Value
Charge	1
Multiplicity	1
Stoichiometry	C12H28MgN3(+1)
Number of Basis Functions	368
Electronic Energy (Eh)	-837.605142356
Sum of electronic and zero-point Energies (Eh)	-837.205698
Sum of electronic and thermal Energies (Eh)	-837.185303
Sum of electronic and enthalpy Energies (Eh)	-837.184359
Sum of electronic and thermal Free Energies (Eh)	-837.252843
Number of Imaginary Frequencies	0
Mean of alpha and beta Electrons	66

[Be(η^1-A′)$_2$] (C_i)

Datum	Value
Charge	0
Multiplicity	1
Stoichiometry	C18H42BeSi4
Number of Basis Functions	977
Electronic Energy (Eh)	-1884.14210058
Sum of electronic and zero-point Energies (Eh)	-1883.596922
Sum of electronic and thermal Energies (Eh)	-1883.557384
Sum of electronic and enthalpy Energies (Eh)	-1883.55644
Sum of electronic and thermal Free Energies (Eh)	-1883.671513
Number of Imaginary Frequencies	1
Mean of alpha and beta Electrons	105

[Be(η^3-A′)$_2$]

Datum	Value
Charge	0
Multiplicity	1
Stoichiometry	C18H42BeSi4
Number of Basis Functions	977
Electronic Energy (Eh)	-1884.15519303
Sum of electronic and zero-point Energies (Eh)	-1883.608213
Sum of electronic and thermal Energies (Eh)	-1883.568825
Sum of electronic and enthalpy Energies (Eh)	-1883.567881
Sum of electronic and thermal Free Energies (Eh)	-1883.679293
Number of Imaginary Frequencies	0
Mean of alpha and beta Electrons	105

[Zn(η^1-A′)$_2$] (C_i)

Datum	Value
Charge	0
Multiplicity	1
Stoichiometry	C18H42Si4Zn
Number of Basis Functions	1006
Electronic Energy (Eh)	-3648.79877182
Sum of electronic and zero-point Energies (Eh)	-3648.255772
Sum of electronic and thermal Energies (Eh)	-3648.214546
Sum of electronic and enthalpy Energies (Eh)	-3648.213602
Sum of electronic and thermal Free Energies (Eh)	-3648.332919
Number of Imaginary Frequencies	0
Mean of alpha and beta Electrons	118

[Zn(η^3-A′)$_2$] (C_2)

Datum	Value
Charge	0
Multiplicity	1
Stoichiometry	C18H42Si4Zn
Number of Basis Functions	1006
Electronic Energy (Eh)	-3648.76613033
Sum of electronic and zero-point Energies (Eh)	-3648.224448
Sum of electronic and thermal Energies (Eh)	-3648.184962
Sum of electronic and enthalpy Energies (Eh)	-3648.184018
Sum of electronic and thermal Free Energies (Eh)	-3648.296315
Number of Imaginary Frequencies	2
Mean of alpha and beta Electrons	118

[Sn(η^3-A′)$_2$] (C_2)

Datum	Value
Charge	0
Multiplicity	1
Stoichiometry	C18H42Si4Sn
Number of Basis Functions	1008
Electronic Energy (Eh)	-2083.81181726
Sum of electronic and zero-point Energies (Eh)	-2083.268154
Sum of electronic and thermal Energies (Eh)	-2083.22733
Sum of electronic and enthalpy Energies (Eh)	-2083.226386
Sum of electronic and thermal Free Energies (Eh)	-2083.342815
Number of Imaginary Frequencies	0
Mean of alpha and beta Electrons	114

[KZn(η^3-A′)$_3$](C_3 symm)

Datum	Value
Charge	0
Multiplicity	1
Stoichiometry	C27H63KSi6Zn
Number of Basis Functions	1518
Electronic Energy (Eh)	-5183.45758034
Sum of electronic and zero-point Energies (Eh)	-5182.641389
Sum of electronic and thermal Energies (Eh)	-5182.578373
Sum of electronic and enthalpy Energies (Eh)	-5182.577429
Sum of electronic and thermal Free Energies (Eh)	-5182.742941
Number of Imaginary Frequencies	0
Mean of alpha and beta Electrons	179

[KMg(η^3-A′)$_3$](C_3 symm)

Datum	Value
Charge	0
Multiplicity	1
Stoichiometry	C27H63KMgSi6
Number of Basis Functions	1502
Electronic Energy (Eh)	-3604.11207381
Sum of electronic and zero-point Energies (Eh)	-3603.296538
Sum of electronic and thermal Energies (Eh)	-3603.233616
Sum of electronic and enthalpy Energies (Eh)	-3603.232671
Sum of electronic and thermal Free Energies (Eh)	-3603.397804
Number of Imaginary Frequencies	0
Mean of alpha and beta Electrons	170

[KSn(η^3-A′)$_3$](C_3 symm)

Datum	Value
Charge	0
Multiplicity	1
Stoichiometry	C27H63KSi6Sn
Number of Basis Functions	1520
Electronic Energy (Eh)	-3618.47562802
Sum of electronic and zero-point Energies (Eh)	-3617.659428
Sum of electronic and thermal Energies (Eh)	-3617.596576
Sum of electronic and enthalpy Energies (Eh)	-3617.595632
Sum of electronic and thermal Free Energies (Eh)	-3617.758354
Number of Imaginary Frequencies	0
Mean of alpha and beta Electrons	175

[KBe(η^3-A′)$_3$](C_3 symm)

Datum	Value
Charge	0
Multiplicity	1
Stoichiometry	C27H63BeKSi6
Number of Basis Functions	1489
Electronic Energy (Eh)	-3418.81372823
Sum of electronic and zero-point Energies (Eh)	-3417.993388
Sum of electronic and thermal Energies (Eh)	-3417.932067
Sum of electronic and enthalpy Energies (Eh)	-3417.931123
Sum of electronic and thermal Free Energies (Eh)	-3418.091708
Number of Imaginary Frequencies	0
Mean of alpha and beta Electrons	166

[$K_2Mg(C_3H_5)_3$]$^+$

Datum	Value
Charge	1
Multiplicity	1
Stoichiometry	C9H15K2Mg(+1)
Number of Basis Functions	575
Electronic Energy (Eh)	-1751.67801881
Sum of electronic and zero-point Energies (Eh)	-1751.471651
Sum of electronic and thermal Energies (Eh)	-1751.452736
Sum of electronic and enthalpy Energies (Eh)	-1751.451791
Sum of electronic and thermal Free Energies (Eh)	-1751.52422
Number of Imaginary Frequencies	0
Mean of alpha and beta Electrons	59

[K_2MgA′$_3$]$^+$

Datum	Value
Charge	1
Multiplicity	1
Stoichiometry	C27H63K2MgSi6(1+)
Number of Basis Functions	1535
Electronic Energy (Eh)	-4203.87614377
Sum of electronic and zero-point Energies (Eh)	-4203.058553
Sum of electronic and thermal Energies (Eh)	-4202.994287
Sum of electronic and enthalpy Energies (Eh)	-4202.993343
Sum of electronic and thermal Free Energies (Eh)	-4203.159511
Number of Imaginary Frequencies	0
Mean of alpha and beta Electrons	179

5.5 References

(1) Grignard, V. Mixed Organomagnesium Combinations and Their Application in Acid, Alcohol, and Hydrocarbon Synthesis. *Ann. Chim. Phys.* **1901**, *24*, 433–490.

(2) Grignard, V. Some New Organometallic Combinations of Magnesium and Their Application to the Synthesis of Alcohols and Hydrocarbons. *C. R. Hebd. Seances Acad. Sci.* **1900**, *130*, 1322–1324.

(3) Grignard, V. Mixed Organomagnesium Compounds. *C. R. Hebd. Seances Acad. Sci.* **1901**, *132*, 558–561.

(4) Ziegler, D. S.; Wei, B.; Knochel, P. Improving the Halogen–Magnesium Exchange by Using New Turbo-Grignard Reagents. *Chem.—Eur. J.* **2019**, *25* (11), 2695–2703.

(5) Schlenk, W.; Holtz, J. Über Die Einfachsten Metallorganischen Alkaliverbindungen. *Ber. Dtsch. Chem. Gesell.* **1917**, *50* (1), 262–274.

(6) Wietelmann, U.; Klett, J. 200 Years of Lithium and 100 Years of Organolithium Chemistry. *Z. Anorg. Chem.* **2018**, *644* (4), 194–204.

(7) Krieck, S.; Gorls, H.; Yu, L.; Reiher, M.; Westerhausen, M. Stable "Inverse" Sandwich Complex with Unprecedented Organocalcium(I): Crystal Structures of $[(THF)_2Mg(Br)\text{-}C_6H_2\text{-}2,4,6\text{-}Ph_3]$ and $[(THF)_3Ca\{\mu\text{-}C_6H_3\text{-}1,3,5\text{-}Ph_3\}Ca(THF)_3]$. *J. Am. Chem. Soc.* **2009**, *131* (8), 2977–2985.

(8) Green, S. P.; Jones, C.; Stasch, A. Stable Adducts of a Dimeric Magnesium(I) Compound. *Angew. Chem., Int. Ed.* **2008**, *47* (47), 9079–9083.

(9) Bonyhady, S. J.; Jones, C.; Nembenna, S.; Stasch, A.; Edwards, A. J.; McIntyre, G. J. β-Diketiminate-Stabilized Magnesium(I) Dimers and Magnesium(II) Hydride Complexes: Synthesis, Characterization, Adduct Formation, and Reactivity Studies. *Chem.—Eur. J.* **2010**, *16* (3), 938–955.

(10) Spielmann, J.; Buch, F.; Harder, S. Early Main-Group Metal Catalysts for the Hydrogenation of Alkenes with H2. *Angew. Chem., Int. Ed.* **2008**, *47* (49), 9434–9438.

(11) Spielmann, J.; Harder, S. Reduction of Ketones with Hydrocarbon-Soluble Calcium Hydride: Stoichiometric Reactions and Catalytic Hydrosilylation. *Eur. J. Inorg. Chem.* **2008**, No. 9, 1480–1486.

(12) Harder, S. From Limestone to Catalysis: Application of Calcium Compounds as Homogeneous Catalysts. *Chem. Rev.* **2010**, *110* (7), 3852–3876.

(13) Bauer, H.; Alonso, M.; Färber, C.; Elsen, H.; Pahl, J.; Causero, A.; Ballmann, G.; De Proft, F.; Harder, S. Imine Hydrogenation with Simple Alkaline Earth Metal Catalysts. *Nat. Catal.* **2018**, *1* (1), 40–47.

(14) Bauer, H.; Alonso, M.; Fischer, C.; Rösch, B.; Elsen, H.; Harder, S. Simple Alkaline-Earth Metal Catalysts for Effective Alkene Hydrogenation. *Angew. Chem. Int. Ed.* **2018**, *57* (46), 15177–15182.

(15) Chmely, S. C.; Hanusa, T. P. Complexes with Sterically Bulky Allyl Ligands: Insights into Structure and Bonding. *Eur. J. Inorg. Chem.*. 2010, pp 1321–1337.

(16) Solomon, S. A; Layfield, R. A. The Coordination Chemistry of Silyl-Substituted Allyl Ligands. *Dalton Trans.* **2010**, *39*, 2469–2483.

(17) Lichtenberg, C.; Okuda, J. Structurally Defined Allyl Compounds of Main Group Metals: Coordination and Reactivity. *Angew. Chem. Int. Ed.* **2013**, *52* (20), 5228–5246.

(18) Chmely, S. C.; Hanusa, T. P.; Brennessel, W. W. Bis(1,3-Trimethylsilylallyl)Beryllium. *Angew. Chem. Int. Ed.* **2010**, *49* (34), 5870–5874.

(19) Boyde, C. N.; Rightmire, R. N.; Hanusa, P. T.; Brennessel, W. W. Symmetric Assembly of a Sterically Encumbered Allyl Complex: Mechanochemical and Solution Synthesis of the Tris(Allyl)Beryllate, $K[BeA'_3]$ ($A' = 1,3\text{-}(SiMe_3)_2C_3H_3$). *Inorganics* **2017**, *5* (2), 36.

(20) Jochmann, P.; Maslek, S.; Spaniol, T. P.; Okuda, J. Allyl Calcium Compounds: Synthesis and Structure of Bis(η^3-1-Alkenyl)Calcium. *Organometallics* **2011**, *30* (7), 1991–1997.
(21) Lichtenberg, C.; Jochmann, P.; Spaniol, T. P.; Okuda, J. The Allylcalcium Monocation: A Bridging Allyl Ligand with a Non-Bent Coordination Geometry. *Angew. Chem. Int. Ed.* **2011**, *50* (25), 5753–5756.
(22) Jochmann, P.; Davin, J. P.; Maslek, S.; Spaniol, T. P.; Sarazin, Y.; Carpentier, J.-F.; Okuda, J. Allyl Strontium Compounds: Synthesis, Molecular Structure and Properties. *Dalton Trans.* **2012**, *41* (30), 9176–9181.
(23) Bailey, P. J.; Liddle, S. T.; Morrison, C. A.; Parsons, S. The First Alkaline Earth Metal Complex Containing a μ-η^1:η^1 Allyl Ligand: Structure of $[\{HC[C(tBu)NC_6H_3(CHMe_2)_2]_2Mg(C_3H_5)\}_6]$. *Angew. Chem. Int. Ed.* **2001**, *40* (23), 4463–4466.
(24) Solomon, S. A; Muryn, C. A; Layfield, R. A. S-Block Metal Complexes of a Bulky, Donor-Functionalized Allyl Ligand. *Chem. Commun.* **2008**, 3142–3144.
(25) Lichtenberg, C.; Spaniol, T. P.; Peckermann, I.; Hanusa, T. P.; Okuda, J. Cationic, Neutral, and Anionic Allyl Magnesium Compounds: Unprecedented Ligand Conformations and Reactivity toward Unsaturated Hydrocarbons. *J. Am. Chem. Soc.* **2013**, *135* (2), 811–821.
(26) Chmely, S. C.; Carlson, C. N.; Hanusa, T. P.; Rheingold, A. L. Classical versus Bridged Allyl Ligands in Magnesium Complexes: The Role of Solvent. *J. Am. Chem. Soc.* **2009**, *131* (18), 6344–6345.
(27) Walczak, K.; Friedrich, J.; Dolg, M. Fully Automated Incremental Evaluation of MP2 and CCSD(T) Core, Core-Valence and Valence Correlation Energies. *Chem. Phys.* **2010**, *376* (1), 36–45.
(28) Wilson, A. S. S.; Hill, M. S.; Mahon, M. F.; Dinoi, C.; Maron, L. Organocalcium-Mediated Nucleophilic Alkylation of Benzene. *Science (80-.).* **2017**, *358* (6367).
(29) Wilson, A. S. S.; Dinoi, C.; Hill, M. S.; Mahon, M. F.; Maron, L. Heterolysis of Dihydrogen by Nucleophilic Calcium Alkyls. *Angew. Chem., Int. Ed.* **2018**, *57* (47), 15500–15504.
(30) Quisenberry, K. T.; White, R. E.; Hanusa, T. P.; Brennessel, W. W. Allyl Complexes of the Heavy Alkaline-Earth Metals: Molecular Structure and Catalytic Behavior. *New J. Chem.* **2010**, *34* (8), 1579–1584.
(31) Tan, D.; Loots, L.; Friščić, T. Towards Medicinal Mechanochemistry: Evolution of Milling from Pharmaceutical Solid Form Screening to the Synthesis of Active Pharmaceutical Ingredients (APIs). *Chem. Commun.* **2016**, *52* (50), 7760–7781.
(32) Hernández, J. G.; Bolm, C. Altering Product Selectivity by Mechanochemistry. *J. Org. Chem.* **2017**, *82* (8), 4007–4019.
(33) Andersen, J.; Mack, J. Mechanochemistry and Organic Synthesis: From Mystical to Practical. *Green Chem.* **2018**, *20*, 1435-1443.
(34) Howard, J. L.; Cao, Q.; Browne, D. L. Mechanochemistry as an Emerging Tool for Molecular Synthesis: What Can It Offer? *Chem. Sci.* **2018**, *9* (12), 3080–3094.
(35) Friščić, T.; Mottillo, C.; Titi, H. M. Mechanochemistry for Synthesis. *Angew. Chem. Int. Ed.* **2020**, *59* (3), 1018–1029.
(36) Rightmire, N. R.; Hanusa, T. P. Advances in Organometallic Synthesis with Mechanochemical Methods. *Dalton Trans.* **2016**, *45* (6), 2352–2362.
(37) Gečiauskaitė, A. A.; García, F. Main Group Mechanochemistry. *Beilstein Journal of Organic Chemistry*. 2017, pp 2068–2077.
(38) Tan, D.; García, F. Main Group Mechanochemistry: From Curiosity to Established Protocols. *Chemical Society Reviews*. 2019.
(39) Hernandez, J. G.; Bolm, C. $[Cp^*RhCl_2]_2$: Mechanosynthesis and Applications in C-H Bond Functionalisations under Ball-Milling Conditions. *Chem. Commun.* **2015**, *51* (63), 12582–

12584.
(40) Budny-Godlewski, K.; Justyniak, I.; Leszczyński, M. K.; Lewiński, J. Mechanochemical and Slow-Chemistry Radical Transformations: A Case of Diorganozinc Compounds and TEMPO. *Chem. Sci.* **2019**, *10* (30), 7149–7155.
(41) Makhaev, V. D.; Borisov, A. P.; Petrova, L. A. Solid-State Mechanochemical Synthesis of Ferrocene. *J. Organomet. Chem.* **1999**, *590* (2), 222–226.
(42) Rightmire, N. R.; Hanusa, T. P.; Rheingold, A. L. Mechanochemical Synthesis of [1,3-$(SiMe_3)_2C_3H_3]_3$(Al,Sc), a Base-Free Tris(Allyl)Aluminum Complex and Its Scandium Analogue. *Organometallics* **2014**, *33* (21), 5952–5955.
(43) Koby, R. F.; Hanusa, T. P.; Schley, N. D. Mechanochemically Driven Transformations in Organotin Chemistry: Stereochemical Rearrangement, Redox Behavior, and Dispersion-Stabilized Complexes. *J. Am. Chem. Soc.* **2018**, *140* (46).
(44) Speight, I. R.; Chmely, S. C.; Hanusa, T. P.; Rheingold, A. L. Mechanochemically Directed Metathesis in Group 2 Chemistry: Calcium Amide Formation without Solvent. *Chem. Commun.* **2019**, *55*, 2202–2205.
(45) Engerer, L. K.; Carlson, C. N.; Hanusa, T. P.; Brennessel, W. W.; Young, V. G. σ-vs π-Bonding in Manganese(II) Allyl Complexes. *Organometallics* **2012**, *31* (17), 6131–6138.
(46) Schümann, U.; Weiss, E.; Dietrich, H.; Mahdi, W. Über Metallalkyl- Und Aryl-Verbindungen: XXXV. Zur Struktur von Allyllithium. Darstellung Und Kristallstruktur Einer Monomeren Allyllithium-Verbindung, Allyl(Pentamethyldiethylentriamin)Lithium, $LiC_3H_5(Me_2NC_2H_4N(Me)C_2H_4NMe_2)$. *J. Organomet. Chem.* **1987**, *322* (3), 299–307.
(47) Gren, C. K.; Hanusa, T. P.; Rheingold, A. L. Solvent-Resistant Structures of Base-Free Lithium and Potassium Allyl Complexes, $M[(SiMe_3)_nC_3H_{5-n}]$ (M = Li, n = 3; M = K, n = 2). *Main Gr. Chem.* **2009**, *8* (4), 225–235.
(48) Quisenberry, K. T.; Gren, C. K.; White, R. E.; Hanusa, T. P.; Brennessel, W. W. Trimethylsilylated Allyl Complexes of the Heavy Alkali Metals, $M[1,3-(SiMe_3)_2C_3H_3](THF)_n$ (M = K, Cs). *Organometallics* **2007**, *26* (17), 4354–4356.
(49) Simpson, C. K.; White, R. E.; Carlson, C. N.; Wrobleski, D. A.; Kuehl, C. J.; Croce, T. A.; Steele, I. M.; Scott, B. L.; Young Victor G.; Hanusa, T. P.; Sattelberger, A. P.; John, K. D. The Role of Alkali Metal Cations in MMA Polymerization Initiated by Neutral and Anionic Allyl Lanthanide Complexes. *Organometallics* **2005**, *24* (15), 3685–3691.
(50) Woodman, T. J.; Schormann, M.; Hughes, D. L.; Bochmann, M. Sterically Hindered Lanthanide Allyl Complexes and Their Use as Single-Component Catalysts for the Polymerization of Methyl Methacrylate and ε-Caprolactone. *Organometallics* **2004**, *23* (12), 2972–2979.
(51) Parry, A. Anionic Polymerization. In *React., Mech. Struct. Polym. Chem.*; Wiley, 1974; pp 350–382.
(52) Li, Y.; Deng, H.; Brittain, W.; Chisholm, M. S. Polymerization of Methyl Methacrylate Using Organocalcium Compounds. *Polym. Bull.* **1999**, *42* (6), 635–639.
(53) Zhou, S.-L.; Wang, S.-W.; Yang, G.-S.; Liu, X.-Y.; Sheng, E.-H.; Zhang, K.-H.; Cheng, L.; Huang, Z.-X. Synthesis, Structure, and Catalytic Activity of Tetracoordinate Lanthanide Amides $[(Me_3Si)_2N]_3Ln(\mu\text{-}Cl)Li(THF)_3$ (Ln = Nd, Sm, Eu). *Polyhedron* **2003**, *22* (7), 1019–1024.
(54) Boffa, L. S.; Novak, B. M. *Transition Metal Catalysis in Macromolecular Design*; American Chemical Society, 2000.
(55) Gren, C. K.; Hanusa, T. P.; Rheingold, A. L. Threefold Cation-π Bonding in Trimethylsilylated Allyl Complexes. *Organometallics* **2007**, *26* (7), 1643–1649.
(56) Reddy, A. S.; Zipse, H.; Sastry, G. N. Cation-π Interactions of Bare and Coordinatively

Saturated Metal Ions: Contrasting Structural and Energetic Characteristics. *J. Phys. Chem. B* **2007**, *111* (39), 11546–11553.
(57) Layfield, R. A.; García, F.; Hannauer, J.; Humphrey, S. M. Ansa-Tris(Allyl) Complexes of Alkali Metals: Tripodal Analogues of Cyclopentadienyl and Ansa-Metallocene Ligands. *Chem. Commun.* **2007**, *499* (47), 5081–5083.
(58) Shannon, R. Revised Effective Ionic Radii and Systematic Studies of Interatomic Distances in Halides and Chalcogenides. *Acta Crystallogr. Sect. A* **1976**, *32* (5), 751–767.
(59) Allred, A. L. Electronegativity Values from Thermochemical Data. *J. Inorg. Nucl. Chem.* **1961**, *17*, 215–221.
(60) Lichtenberg, C.; Engel, J.; Spaniol, T. P.; Englert, U.; Raabe, G.; Okuda, J. Bis(Allyl)Zinc Revisited: Sigma versus Pi Bonding of Allyl Coordination. *J. Am. Chem. Soc.* **2012**, *134* (23), 9805–9811.
(61) Krebs, K. M.; Wiederkehr, J.; Schneider, J.; Schubert, H.; Eichele, K.; Wesemann, L. η^3-Allyl Coordination at Tin(II)—Reactivity towards Alkynes and Benzonitrile. *Angew. Chem. Int. Ed.* **2015**, *54* (18), 5502–5506.
(62) Koby, R. F.; Rightmire, N. R.; Schley, N. D.; Hanusa, T. P.; Brennessel, W. W. Halide Metathesis in Overdrive: Mechanochemical Synthesis of a Heterometallic Group 1 Allyl Complex. *Beilstein J. Org. Chem.* **2019**, *15*, 1856–1863.
(63) Guzei, I. A.; Wendt, M. An Improved Method for the Computation of Ligand Steric Effects Based on Solid Angles. *Dalton Trans.* **2006**, No. 33, 3991–3999.
(64) Elschenbroich, C. *Organometallics*; 3, Ed.; 2006.
(65) Takagi, N.; Schmidt, M. W.; Nagase, S. Ga-Ga Multiple Bond in Na_2[Ar*GaGaAr*] (Ar* = C_6H_3-2,6-(C_6H_2-2,4,6-*i*-Pr_3)$_2$). *Organometallics* **2001**, *20* (8), 1646–1651.
(66) Martinez-Martinez, A. J.; O'Hara, C. T. Lithium, Sodium, and Potassium Magnesiate Chemistry: A Structural Overview. *Adv. Organomet. Chem.* **2016**, *65*, 1–46.
(67) Robertson, S. D.; Uzelac, M.; Mulvey, R. E. Alkali-Metal-Mediated Synergistic Effects in Polar Main Group Organometallic Chemistry. *Chem. Rev.* **2019**.
(68) Fraenkel, G.; Chow, A.; Winchester, W. R. Dynamics of Solvated Li+ within *Exo*,*Exo*-[1,3-Bis(Trimethylsilyl)Ally]Lithium *N*,*N*,*N*',*N*'-Tetramethylethylenediamine Complex. *J. Am. Chem. Soc.* **1990**, *112*, 1382–1386.
(69) Armarego, W. L. F.; Chai, C. L. L. Chapter 1 - Common Physical Techniques Used in Purification; Armarego, W. L. F., Chai, C. L. L. (Sixth E., Eds.; Butterworth-Heinemann: Oxford, 2009; pp 1–60.
(70) Dolomanov, O. V; Bourhis, L. J.; Gildea, R. J.; Howard, J. A. K.; Puschmann, H. OLEX2: A Complete Structure Solution, Refinement and Analysis Program. *J. Appl. Crystallogr.* **2009**, *42* (2), 339–341.
(71) Sheldrick, G. SHELXT - Integrated Space-Group and Crystal-Structure Determination. *Acta Crystallogr. Sect. A* **2015**, *71* (1), 3–8.
(72) Sheldrick, G. Crystal Structure Refinement with SHELXL. *Acta Crystallogr. Sect. C* **2015**, *71* (1), 3–8.
(73) M. J. Frisch, G. W. Trucks, H. B. Schlegel, G. E. Scuseria, M. A. Robb, J. R. Cheeseman, G. Scalmani, V. Barone, G. A. Petersson, H. Nakatsuji, X. Li, M. Caricato, A. Marenich, J. Bloino, B. G. Janesko, R. Gomperts, B. Mennucci, H. P. Hratchian, J. V. Ort, and D. J. F. Gaussian09. *http://www. gaussian. com/*. Gaussian, Inc.: Wallingford CT 2009.
(74) M. J. Frisch, G. W. Trucks, H. B. Schlegel, G. E. Scuseria, M.; A. Robb, J. R. Cheeseman, G. Scalmani, V. Barone, B. Mennucci, G. A. Petersson, H.; Nakatsuji, M. Caricato, X. Li, H. P. Hratchian, A. F. Izmaylov, J. Bloino, G. Zheng, J. L.; Sonnenberg, M. Hada, M. Ehara, K. Toyota, R. Fukuda, J. Hasegawa, M. Ishida, T.; Nakajima, Y. Honda, O. Kitao, H. Nakai, T.

Vreven, J. A. Montgomery, Jr., J. E. Peralta, F.; Ogliaro, M. Bearpark, J. J. Heyd, E. Brothers, K. N. Kudin, V. N. Staroverov, R.; Kobayashi, J. Normand, K. Raghavachari, A. Rendell, J. C. Burant, S. S. Iyengar, J.; Tomasi, M. Cossi, N. Rega, J. M. Millam, M. Klene, J. E. Knox, J. B. Cross, V. Bakken, C.; Adamo, J. Jaramillo, R. Gomperts, R. E. Stratmann, O. Yazyev, A. J. Austin, R. Cammi, C.; Pomelli, J. W. Ochterski, R. L. Martin, K. Morokuma, V. G. Zakrzewski, G. A. Voth, P.; Salvador, J. J. Dannenberg, S. Dapprich, A. D. Daniels, Ö. Farkas, J. B. Foresman, J. V.; Ortiz, J. Cioslowski, and D. J. Fox, Gaussian, Inc., Wallingford CT, 2009. Gaussian16 Revision D.01. *http//www. gaussian. com/* **2016**.

(75) Becke, A. D. Density-Functional Exchange-Energy Approximation with Correct Asymptotic Behavior. *Phys. Rev. A At. Mol. Opt. Phys.* **1988**, *38* (6), 3098–3100.

(76) Perdew, J. P.; Wang, Y. Accurate and Simple Analytic Representation of the Electron-Gas Correlation Energy. *Phys. Rev. B* **1992**, *45* (23), 13244–13249.

(77) Grimme, S.; Antony, J.; Ehrlich, S.; Krieg, H. A Consistent and Accurate Ab Initio Parametrization of Density Functional Dispersion Correction (DFT-D) for the 94 Elements H-Pu. *J. Chem. Phys.* **2010**, *132* (15), 154104.

(78) Grimme, S.; Ehrlich, S.; Goerigk, L. Effect of the Damping Function in Dispersion Corrected Density Functional Theory. *J. Comput. Chem.* **2011**, *32* (7), 1456–1465.

(79) Rappoport, D.; Furche, F. Property-Optimized Gaussian Basis Sets for Molecular Response Calculations. *J. Chem. Phys.* **2010**, *133* (13), 134105.

(80) Lu, T.; Chen, F. Multiwfn: A Multifunctional Wavefunction Analyzer. *J. Comput. Chem.* **2012**, *33* (5), 580–592.

(81) Schnitzler, S.; Cui, P.; Spaniol, T. P.; Okuda, J. Molecular Magnesium Hydrides Supported by an Anionic Triazacyclononane-Type Ligand. *Dalton Trans.* **2017**, *46* (6), 1761–1765.

(82) Sánchez-Barba, L. F.; Garcés, A.; Fajardo, M.; Alonso-Moreno, C.; Fernández-Baeza, J.; Otero, A.; Antiñolo, A.; Tejeda, J.; Lara-Sánchez, A.; López-Solera, M. I. Well-Defined Alkyl Heteroscorpionate Magnesium Complexes as Excellent Initiators for the ROP of Cyclic Esters. *Organometallics* **2007**, *26* (25), 6403–6411.

(83) Marsch, M.; Harms, K.; Massa, W.; Boche, G. Crystal Structure of the H1-Allyl-Grignard Compound Bis(Allylmagnesium Chloride-TMEDA). *Angew. Chem. Int. Ed. English* **1987**, *26* (7), 696–697.

(84) Sánchez-Barba, L. F.; Hughes, D. L.; Humphrey, S. M.; Bochmann, M. Ligand Transfer Reactions of Mixed-Metal Lanthanide/Magnesium Allyl Complexes with β-Diketimines: Synthesis, Structures, and Ring-Opening Polymerization Catalysis. *Organometallics* **2006**, *25* (4), 1012–1020.

(85) Vestergren, M.; Eriksson, J.; Håkansson, M. Chiral Cis-Octahedral Grignard Reagents. *J. Organomet. Chem.* **2003**, *681* (1), 215–224.

(86) Rodríguez-Guerra Pedregal, J.; Gómez-Orellana, P.; Maréchal, J.-D. ESIgen: Electronic Supporting Information Generator for Computational Chemistry Publications. *J. Chem. Inf. Model.* **2018**, *58* (3), 561–564.

Chapter 6

Mechanochemical Formation, Solution Rearrangements, and Catalytic Behavior of a Polymorphic Ca/K Allyl Complex

Reprinted with permission from Ross F. Koby, Alicia M. Doerr, Nicholas R. Rightmire, Nathan D. Schley, Prof. Brian K. Long, Timothy P. Hanusa

Chem. Eur. J. 2021, 27, 1– 9 © 2021 Wiley-VCH GmbH

6.1 Introduction

The fundamental organizing principles of the periodic table suggest that compounds containing metals of the same group and with similar ligands should display related properties. Hence Grignard-like reactivity was anticipated from organocalcium compounds when research on the latter started over a century ago.[1,2] Until the importance of metal coordination sphere saturation and kinetic stabilization were recognized, however, the multi-decadal efforts to extrapolate the chemistry of magnesium to its heavier congeners were largely unproductive. This was noted in *Advanced Inorganic Chemistry*, where the organometallic compounds of calcium, strontium, and barium are described as "relatively obscure and of little utility. "[3] It is now well documented that the coordination and organometallic chemistry of calcium, strontium, and barium differs significantly from that of magnesium analogues.[4,5] Calcium compounds in particular have been the subject of intense interest as initiators of polymerization,[6–8] hydrogenation,[9–11] and hydroelementation reactions,[12–19] and as promoters of nucleophilic alkylation.[20]

Central to the modern development of organo-Ca, -Sr, and -Ba chemistry has been the increasingly sophisticated use of large, sterically bulky ligands that provide hydrocarbon solubility and suppress undesirable behavior, such as ether cleavage or Schlenk-type ligand redistribution. Whole classes of organoalkaline-earth species, such as those possessing π-delocalized anions as ligands (e.g., cyclopentadienyl and allyl groups)[21–25] are now known that are relatively resistant to solvent attack, and are in fact frequently isolated as solvates. Such coordinated solvents can still affect subsequent reactivity, however. We have recently shown, for example, that the unsolvated $\{[MgA'_2]_2\}$ (A′ = 1,3-$(SiMe_3)_2C_3H_3$) allyl complex is a modestly active initiator of methyl methacrylate polymerization, yielding isotactically enriched poly(methyl methacrylate) (PMMA).[26] The solvated $[MgA'_2(THF)_2]$ complex, in contrast, is completely inactive for this purpose,[27] a likely consequence of the congestion of the coordination sphere by the bound THF ligands. Other examples of solvent-suppressed reactivity in Group 2 complexes are known.[20,28]

The potential inhibitory effect of coordinated solvents raises the countervailing possibility that complexes known to be active reagents or catalytic initiators *despite* the

presence of coordinated solvents (e.g., [CaA′$_2$(THF)$_2$] or [SrA′$_2$(THF)$_2$] for MMA polymerization)[27] might be more reactive in an unsolvated form. Of course, an unsolvated (and potentially coordinatively undersaturated) complex may dimerize or oligomerize, altering its reactivity, but in solution an active monomeric form could exist in equilibrium with a more highly coordinated and sterically crowded arrangement. This happens in the case of {[MgA′$_2$]}$_2$ ⇄ 2 [MgA′$_2$],[29] and even with caveats about extrapolating from the behavior of magnesium to the heavier alkaline-earths, could occur in calcium or strontium systems as well (Figure 64).[26]

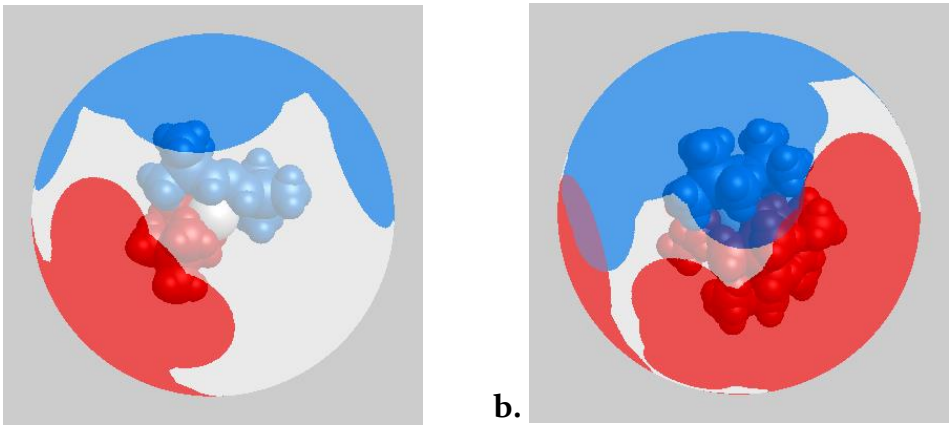

Figure 64. Visualization of the extent of coordination sphere coverage ($G_{complex}$) calculated for: (a) [CaA′$_2$], 71.2%; (b) {[CaA′$_2$]}$_2$, 90.4%. Optimized coordinates (B3PW91-D3BJ/def2TZVP) and the program Solid-G were used to predict the $G_{complex}$ value; the latter represents the net coverage, so that regions of the coordination sphere where the projections of the ligands overlap are counted only once. For comparison, the values for [MgA′$_2$] and {[MgA′$_2$]}$_2$ are 79.0% and 93.0%, respectively. The high $G_{complex}$ values of the Ca and Mg dimers are suggestive of enough steric crowding to make partial dissociation in solution likely; this is known to occur for the Mg system.

Ethers are widely used in the synthesis of organoalkaline-earth compounds, and form the most common solvates. Their removal from oxophilic metal centers can be challenging if not impossible, and the preparation of unsolvated species may require alternate synthetic procedures. Attempts to remove diethyl ether from the solvated [BeA′$_2$(Et$_2$O)] resulted in the compound's decomposition,[30] and unlike [MgA′$_2$(Et$_2$O)$_2$], the [MgA′$_2$(THF)$_2$] analog could not be desolvated under prolonged vacuum.[29]

A direct way to circumvent strongly coordinating solvents is simply to avoid their use during synthesis This can be done through solvent-free mechanochemical methods. Although long known, mechanochemistry in the form of grinding and ball milling has emerged in the past decade as a powerful synthetic tool, with solvent use minimized during synthesis.[31–36] Through these means, mechanochemistry has provided access to a range of compounds that could not be isolated because they are attacked by, or are unstable in, conventional reaction solvents.[37–39]

The synthesis of group 2 compounds frequently employs halide metathesis as a synthetic method, and under mechanochemical conditions reagent stoichiometry is not a reliable guide to the composition of products. During grinding, reagents are placed in conditions far from equilibrium, and the reaction speed may not allow for equilibration or redistribution to occur. In addition, the high reagent concentration and the potential coordinative undersaturation of the expected products can lead to the isolation of unanticipated products. For instance, '-ate'-type species can form instead of the intended neutral complexes, as when milling two equivalents of K[A′] with $MgCl_2$ produces $K_2[MgA'_4]$ rather than the expected $[MgA'_2]$.[26]

It should be noted that the mechanochemical generation of -ate species, should it occur, may be an advantage for the production of catalytically useful compounds, as initiator activity in anionic polymerizations has been correlated with net negative charges on the complex.[40] Neither the neutral $[Mg(C_3H_5)_2]$ complex nor the cationic species $[Mg(C_3H_5)(THF)_5]^+$ will initiate butadiene polymerization, for example.[40] The heavier species $[Ca(C_3H_5)_2]$ will, however, and the heterometallic complex $Ca[Mg(C_3H_5)_4]$ species is even more active, a difference associated with the dianionic charge on the magnesiate. If this is the case, calciate- or strontiate-based initiators ($[Ca(allyl)_3]^-$, $[Sr(allyl)_3]^-$) may possess higher levels of activity than their neutral counterparts. Described here are the results of the search for an unsolvated calcium allyl, the solvent-free mechanochemical synthesis of a bulky allyl calciate that in its initially isolated form requires arene solvation for stability, and that in its more thermodynamically stable form displays reactivity as a polymerization initiator under mild conditions.

6.2 Results and Discussion

The known neutral complex $[CaA'_2(THF)_2]$ is a product of solution-based chemistry,[18] and attempting to avoid the use of ethers to generate an unsolvated $[CaA'_2]$ complex by using toluene as a solvent is unsuccessful. Stirring 2:1 mixture of K[A′] and CaI_2 in toluene overnight leaves only the starting materials (^{1}H NMR evidence). This is unsurprising, given the low solubility of K[A′] in toluene, and the complete insolubility of CaI_2 in the same. The lack of reaction is also evidence that the formation of $K[CaA'_3]$ from the milled reaction mixture is not simply a result of the workup in toluene (*vide infra*). Furthermore, an effort to prepare a bulky allyl calciate in THF solution with the use of a 3:1 ratio of the potassium allyl to calcium iodide (eq 1) yielded only the neutral complex.[27]

$$3\ K[A'] + CaI_2 \xrightarrow{THF\ /\!/} K[CaA'_3(thf)_x]\ (+\ 2\ KI) \qquad 3\ K[A'] + CaI_2 \xrightarrow{THF} [CaA'_2(thf)_2]\ (+\ K[A']\ +\ 2\ KI) \tag{1}$$

Allyl substitution on the calcium center may stop at the bis(allyl) stage as a consequence of a third allyl's inability to dislodge the strongly coordinating THF.

A mechanochemical approach to generating the neutral allyl complex was then attempted. Grinding a mixture of K[A'] and CaI_2 (2:1 equivalents) for 15 minutes at 600 rpm in a planetary ball mill leaves a highly air-sensitive pale-yellow powder that is somewhat soluble in toluene. Filtering a toluene extract through a fine porosity glass frit yields a transparent yellowish-orange solution. Drying under vacuum leaves an orange oil that eventually solidifies. An ^{1}H NMR study of the oil indicated the presence of apparently π-bound A′ ligands, and the pattern of 2 singlets (from TMS), 1 doublet (from H1 and H3), and 2 triplets (from H2) was originally attributed to an allyl calcium species with multiple allyl environments but accidentally overlapping doublets.

Systematic variation of reaction conditions revealed that there were two products generated whose formation could be changed by varying the grinding time. One of the products (**1**) is preferentially formed at short milling times (5-10 min) and the other (**2**) is produced after extended milling (15-20 min). Outside the mill, **1** spontaneously transforms into **2** either in the solid state (over 3 days) or in hydrocarbon solution (from minutes to days). The transformation is accompanied by a shift and intensification of color from yellow to red-orange, but with no other obvious signs of decomposition (e.g., formation of a precipitate, change in solubility), and it seems that **1** is a metastable form of **2** (Figure 66). Elemental analysis of **2** is consistent with the formula K[CaA′$_3$], which is not the stoichiometrically expected product from the reaction. In an attempt to optimize its yield, a 3:1 combination of K[A′] and CaI_2 was ground together, but the additional K[A′] did not appear to participate in the reaction, and it could be identified with ^{1}H NMR spectroscopy separately from K[CaA′$_3$]. K[CaA′$_3$] was also the only identifiable product (^{1}H NMR) from a 1:1 grind of K[A′] and CaI_2. Clearly K[CaA′$_3$] is the preferred product from these reactions, much as K[BeA′$_3$] is found to be the only product regardless of whether 1:1, 2:1, or 3:1 ratios of K[A′] and $BeCl_2$ are ground.[41]

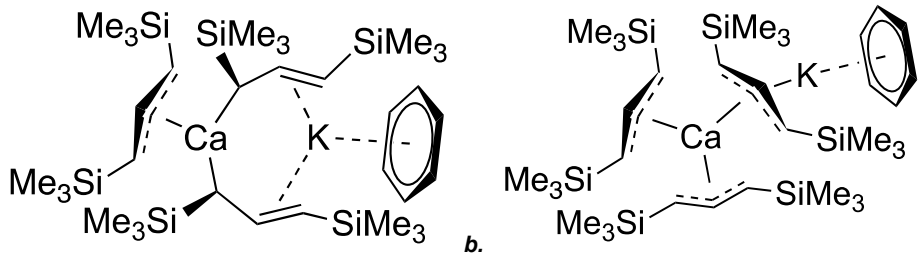

Figure 65. Proposed structures of arene-solvated versions of K[CaA′$_3$]: (a) **1** ([C_6H_6•K[Ca(η^3-A′)(η^1-A′)$_2$]), the initially isolated product; (b) **2** ([C_6H_6•K[Ca(η^3-A′)$_3$]), the form obtained after rearrangement. See the computational results section for rationalizations of these structures.

Compounds **1** and **2** have distinctive ^{1}H NMR spectra (see Table 15), and although the ligands appear η^3-bound, A′ anions on electropositive metals are known to be fluxional, and even those found to be η^1-bound in the solid state (e.g., on Be,[41] Zn,[42] Al,[37] Ga[43]) appear π-bound in solution. The most obvious difference between **1** and **2** is the chemical shift of

the central hydrogen on the A′ ligand, which appears as a triplet, owing to coupling with the two terminal hydrogens. The shift in **1** (δ 7.25, $^{1}J_{H\text{-}H}$ = 16 Hz) moves upfield in **2** (δ 6.99, $^{1}J_{H\text{-}H}$ = 16 Hz). In allyl complexes containing the A′ ligand, a shift for the central hydrogen more downfield than δ 7.0 is unusual; for example, it appears at δ 6.69 for K[A′] (η^3-bound) and at δ 6.83 for [MgA′$_2$(THF)$_2$] (η^1-bound).[29] Although not completely diagnostic, shifts near or greater than δ 7.0 have been observed before in A′-ate complexes that have σ-bound ligands in the solid state (Table 15). It is possible, in fact likely, that a complex featuring one or more σ-bonded ligands is present here, a point discussed in the computational section.

Compound **1** has a complex interaction with solvents. In anything other than neat arenes, the rate of conversion of **1** into **2** is rapid. Even in a 90:10 (C_6D_6):(hexanes) mixture, conversion to **2** occurs quickly (<10 min). Not surprisingly, attempts to crystallize **1** by layering mixtures of hexane, toluene, and/or $(SiMe_3)_2O$, or by evaporation from hexanes or $(SiMe_3)_2O$ inevitably yields crystals of **2**. Even from a neat arene solvent, crystallization that is slow enough to form well-defined crystals always produces only **2**.

An ^{1}H NMR study was conducted over four days at 6-hr intervals to study the rate of transformation as a function of time and solvent composition. The results in neat C_6D_6 are detailed in the Appendix (Figure 83), but in summary, there is a long induction period for the transformation of **1** to **2**, but once it begins, it is fairly rapid. Specifically, a sample of **1** appears unchanged for slightly less than two days (42 hr), but by 48 hr, the distinctive resonances of **2** are clearly evident (ca. 15% of the total). Over the next 30 hr (a total of 78 h since the start), virtually complete conversion to **2** occurs. Such behavior has some of the hallmarks of an autocatalytic reaction,[44] but the difficulty in characterizing the form(s) of **1** in solution (see below) means that detailed analysis of this point would not be justified. Autocatalysis is possible if the induction period reflects rapid interconversion between various polymorphs of solvated **1** (see ref. 23 for the underlying theory). Several speculative intermediates are possible (see the Computational Results section for examples), but constructing a catalytic cycle would require more conjecture, the validity of which would be extremely difficult, if not impossible, to judge.

In toluene, the UV-vis spectrum of **2** displays a broad absorbance at 316 nm, tailing into the visible region (see Appendix). The absorbance is probably associated with transitions involving the allyl anion. [45]

Table 15: ^{1}H NMR Shifts in C_6D_6 for Selected Electropositive [A′] Complexes

Complex	TMS (s)	$H_{1,3}$ ($^1J_{H-H}$, Hz)	H_2 ($^1J_{H-H}$, Hz)	Ref.
1	0.34	3.33 (16)	7.25 (16)	a
2	0.21	3.32 (16)	6.99 (16)	a
K[BeA′$_3$]^b	0.22	3.21 (br)	6.97 (16)	[20
Na[ZnA′$_3$] ^{b}	0.16	4.00 (br)	7.59 (16)	[21]
K[ZnA′$_3$] ^{b}	0.23	3.42 (15)	7.05 (15)	[21]
K[A′]^c	0.23	2.78 (16)	6.69 (16)	[26]

a. this work. B. η^1-bound in the solid state. C. η^3-bound in the solid state.

6.2.1 Crystallographic Results

Compound **2** crystallizes from hexanes within two days as pale yellow, nearly colorless blocks with the composition of $\{K[CaA'_3]\}_n$ (Figure 67). The whole comprises a coordination polymer with the three A′ ligands η^3-bound to calcium, one of which is terminal, and two in μ_2-η^3:η^3 modes. The K^+ counterion interacts with two of the A′ ligands, also in a μ_2-η^3:η^3 mode. Around the calcium, the allyl ligands are arranged in an irregular fashion, with Ca–C distances ranging from 2.573–2.752 Å, with an average of 2.67 Å. Despite the bond length variation, partially a result of the mix of terminal and bridging allyls, the average distance is similar to that found in [CaA′$_2$(THF)$_2$] (2.654(5) Å), which reflects the same formal coordination number of calcium (6). The K–C distances span a large range from 2.92–3.33 Å, averaging to 3.12 Å. The coordination polymer chains persist in the solid state even with intercalated solvent molecules. A second crystal form of the calciate (**2b**) was obtained when a C_6D_6 solvate crystallized slowly from a sample in an NMR tube. Its gross structure is the same as **2**, comprising the coordination polymer with a terminal A′ ligand on calcium, and the other two allyls bridging between calcium and potassium (Figure 68). In **2b**, the polymer chains have moved apart, generating cavities as large as 156 Å^3 that are filled with benzene. The closest $C_{benzene}$···Me–Si contact is at 3.78 Å, roughly the sum of appropriate van der Waals radii (1.7 $Å_{arene\ ring}$ + 2.0 $Å_{Me}$).[46]

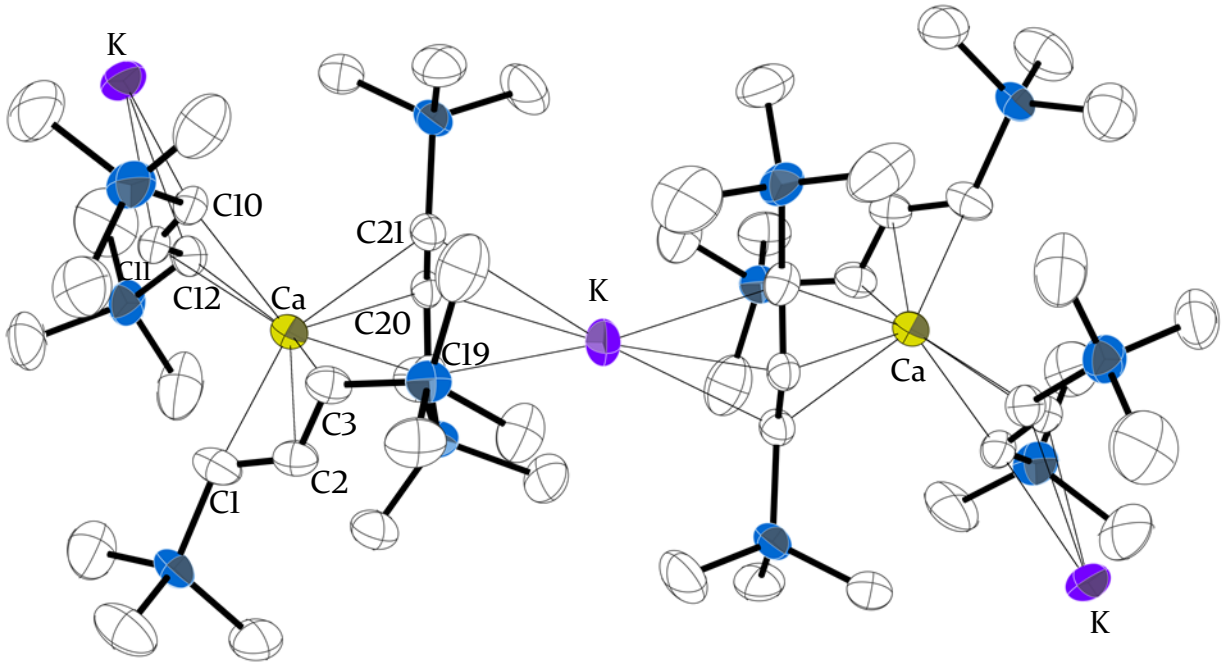

Figure 66. Thermal ellipsoid plot (50% level) of a portion of the coordination polymer of $\{K[CaA'_3]\}_n$ (**2**$_n$). Hydrogen atoms have been removed for clarity. Selected bond distances (Å) and angles (°): Ca–C1, 2.643(3); Ca–C2, 2.672(3); Ca–C3, 2.649(3); Ca–C10, 2.642(3); Ca–C11, 2.573(3); Ca–C12, 2.600(16); Ca–C19, 2.750(15); Ca–C20, 2.715(3); Ca–C21, 2.752(3); K–C19, 3.012(16); K–C20, 3.103(7); K–C21, 3.327(7); Ca···K, 5.055(8); C1–C2–C3, 128.1(5), C10–C11–C12, 128.8(5), C19–C20–C21, 130.6(5), Ca···K···Ca′, 175.2, K···Ca···K′, 122.3.

A further example of the stability of the $\{K[CaA'_3]\}_n$ chains was obtained when **2** was crystallized more slowly from commercial hexanes. The resulting iridescent rhombi (**2c**) were found to have grown in the polar space group $P2_1$, different from that for **2** ($P2_1/m$) or **2b** ($P2_1/n$). The crystals of **2c** incorporate methylcyclopentane into the lattice as $\{K[CaA'_3]\bullet C_5H_9Me\}_n$; the alicycle is a common component of hexanes. Methylcyclopentane comprises about 10% of commercial hexanes mixtures (Oakwood Chemicals). Its boiling point of 72 °C (cf. 69 °C for *n*-hexane) means that it is not routinely separated from other C_6 alkanes. It should be noted that there are 52 methylcylcopentane solvates in the CCSD (Nov. 2019 release). The general connectivity is not in doubt, with the same $\{CaA'_3$-(μ-K)-$CaA'_3\}_n$ motif found in **2** and **2b**, but owing to several crystallographic issues, further discussion of **2c** is not warranted (see Appendix for figures).

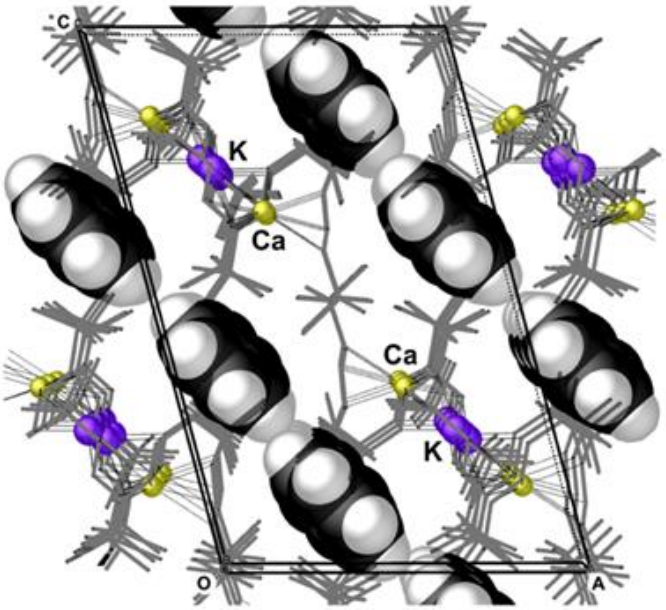

Figure 67. Portion of the coordination polymer of $\{K[CaA'_3]\bullet C_6D_6\}_n$ (**2b**), projected down the crystallographic *b* axis. Carbon-carbon and carbon-silicon bonds are shown as sticks, and interstitial benzene molecules are displayed with space-filling parameters. A thermal ellipsoid plot of **2b** is available in the Appendix (Figure 74).

6.2.2 Computational Results

The formation of **1** provides an unusual glimpse into a mechanochemically generated, relatively long-lived, but fundamentally transient complex.[47] Such species are becoming increasingly recognized features of mechanochemical synthesis, and their appearance and transformations have been followed in reactions that generate organic products,[48] MOFs,[49,50] and coordination polymers,[51] and studied with the use of synchrotron-based spectroscopy,[51,52] time-resolved *in situ* Raman spectra,[53] or combination techniques.[54,55] Although **1** and **2** can be distinguished with NMR spectra, and the **1** → **2** conversion can be suppressed for several days with appropriate solvent choice, we were interested in developing computational models for the two species that might help us understand their nature and conversions more fully.

Several guiding principles were used during the construction of the models: 1) the base formulas of **1** and **2** are the same, i.e., $K[CaA'_3]$, and they are presumed to be monomeric in solution; 2) there is some σ-bonding character to the allyls in **1**, even though fluxionality makes the allyls appear to be π-bound; 3) in solution, interaction with arenes slows, but does not ultimately prevent the conversion of **1** to **2**. This suggests the operation of a cation–π interaction of the arenes with one or both of the metals in both forms of the complex.[56,57] Hence a mechanism that involves the (temporary) displacement of arene(s) from **1**, thus allowing rearrangement to **2** to occur would seem to be likely. Certainly more than one solvent molecule surrounds **1** and **2** when they are in solution, and the application

of a solvation model (e.g., PCM[58]) might be appropriate in this context, but preliminary calculations with this approach suggested that explicit modeling of the metal-arene interaction was critical, and we opted to use a discrete solvent approach.

A model for the solution structure of **2** was the most straightforward, as we assumed it could be represented as a fragment of the solid-state coordination polymer. A calcium center, three surrounding η^3-A′ ligands, and a K^+ ion on the opposite face of one of allyls served as the basis of the model. A single C_6H_6 molecule was placed in a capping position over the potassium (**2**•C_6H_6; Figure 65b). A DFT calculation with the B3PW91-D3BJ/def2SVP combination (the level of calculation used for all molecules in this section) found the structure to be a minimum on the potential energy surface. Any comparisons with the crystal structure of **2** must be made with some caution, as there are two terminal A′ ligands in this model for **2**, and only one that is bridging, the reverse of the case in the coordination environment around Ca^{2+} in the solid-state structure. The K^+ ion is coordinated by only one anionic ligand in the model, as distinct from two in the crystal. Nevertheless, several parameters compare well between the model and the crystal structure. The Ca–C distances average to 2.63 Å, slightly shorter than in the solid state (2.67 Å). The K^+–C(allyl) distance averages to 2.99 Å, notably shorter than in the crystal structure (3.15 Å), but a reasonable consequence of its being bound to only one anionic ligand, rather than two as in the polymer. In the model, there is auxiliary coordination to the K^+ by a neighboring CH_3 group (3.17 Å), and of course by the C_6H_6 ring, with a K^+···centroid distance of 3.22 Å. The latter is comparable to the 3.25 Å K^+···ring centroid distance calculated for the monomeric [(C_6H_6)KA′] complex (see the Appendix, Figure 81).

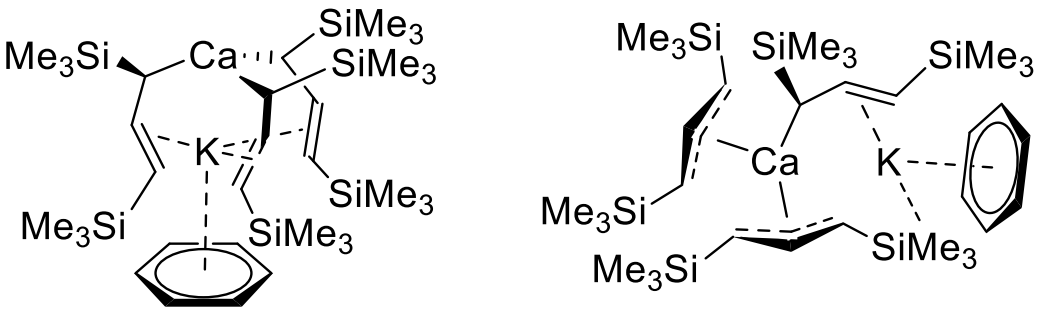

Figure 68: Structures of proposed but rejected models for **1**; (a) a C_3-symmetric version, in which the allyl ligands adopt a μ_2-η^1:η^2 arrangement; (b) a mixed hapticity version with two η^3- and one η^1-allyl on Ca. The preferred model for **1** is found in Figure 65a.

A model for **1** was not as easily constructed as for **2**. To accommodate the presence of η^1-allyls, an initial guess was a structure related to K[MA′$_3$] (M = Be,[41] Zn,[59] Sn[38,60]), in which the allyl ligands adopt a μ_2-η^1:η^2 bonding mode, being σ-bonded to the divalent metal

and with cation-π interactions between the K^+ ion and the double bonds of the allyl ligands. An additional cation-π interaction would exist between K^+ and an arene ring capping one end (Figure 68a). A Ca^{2+} center coordinated by all- η^1-bonded allyls could explain the instability of **1** over time, a consequence of the strong preference for η^3- over η^1-bound allyl ligands on calcium.[61] A calculation for the 68a model of **1** found it to be a local minimum, and the average Ca–C bond length of 2.514 Å is similar to the crystallographically characterized calciate $K[Ca\{CH(SiMe_3)_2\}_3]$ (2.50(1) Å).[62]

Though initially appealing, this structure was ultimately considered not the most likely model for **1**•C_6H_6. The C_3-symmetric $K[MA'_3]$ framework has never been observed when M is a highly electropositive metal; even Mg (χ = 1.31) does not form such a complex.[26] In the present case, the incorporation of Ca (χ = 1.00) would appear to have even less chance of success. Furthermore, the 68a model offers no obvious mechanism for the experimentally observed arene stabilization. Reoptimization of the 68a structure without the benzene increases the separation between the Ca^{2+} and K^+ by 0.47 Å, but the all σ-bonded framework is left otherwise intact (see Appendix for details).

Of course, all the allyls in **1** need not be σ-bonded to Ca^{2+}, and it would be stabilizing if any of the ligands were π-bonded to Ca^{2+}. Two additional models for **1** with mixed hapticity allyl ligands were thus considered; one with two η^3-A′ and one η^1-A′ ligand (Figure 68b) and another with one η^3-A′ and two η^1-A′ ligands (Figure 65a). In both cases, the K^+ is coordinated by the double bond(s) of the η^1-allyl(s) and an associated C_6H_6. Although the interaction of the K^+ with the allyl ligands is not the same, the proposed 65a structure has similarities with the known mixed hapticity $K_2[Mg(\eta^3\text{-A}')(\eta^1\text{-A}')_3]$ magnesiate.[26]

Both calcium structures are minima on their respective energy surfaces and are lower in energy than the all-σ bound version (68a). The 68b version by itself, with its two η^3-A′ ligands on Ca^{2+}, is lower in energy than the preferred Figure 65a alternative ($\Delta G°$ = -6.1 kcal mol^{-1}), but despite the coordination to the K^+ by a neighboring CH_3 group (3.07 Å) and C_6H_6 ring, the potassium remains coordinatively undersaturated. Removal of the C_6H_6 still leaves Ca^{2+} with $(\eta^3)_2(\eta^1)$-coordinated A′ ligands, but the K^+ now has a more complicated bridging interaction with the allyls, and is approached by two CH_3 groups (both at 3.10 Å; the Appendix presents a figure of this configuration (Figure 79)). The undersaturation at potassium is probably the reason that the loss of C_6H_6 is endothermic by +11.8 kcal mol^{-1} ($\Delta H°$), leading to a small but positive free energy change ($\Delta G°$ = +3.2 kcal mol^{-1}); the resistance to arene loss makes it an unlikely candidate for the structure of **1**.

In the optimized structure of **1**•C_6H_6 with$(\eta^3)(\eta^1)_2$-coordinated allyls on Ca (Figure 66a), the average K^+···C distance to the double-bonded carbons of the two η^1-bonded allyls is 3.00 Å, which is slightly shorter than the comparable distances in $K[ZnA'_3]$ (3.08 Å) or $K[BeA'_3]$ (3.05 Å), and consistent with the interaction's energetic importance.

When the C_6H_6 is removed and the structure reoptimized, a process that involves only a small free energy change ($\Delta G°$ = -1.7 kcal mol^{-1}) (Figure 80), one of the σ-bonded allyls becomes π-bonded ; the average Ca–C distances for the two η^3-A′ ligands is 2.62 Å, almost identical to the distance in the calculation for the monomeric **2** (2.63 Å) and the π-electrons in both ligands are delocalized. There are limits to what can be expected from a gas-phase approximation, of course, and the third allyl is still η^1-bound to the Ca (2.60 Å), but the K^+ is now η^3-bonded to the ligand, with an average K–C distance of 2.99 Å. Owing to the substantial rearrangement that occurs on removal of the C_6H_6, we favor this mixed hapticity species (Figure 65a) as the most likely model of those considered for **1**•C_6H_6. The conversion of the preferred solvated models (**1**•C_6H_6 → **2**•C_6H_6 is spontaneous by 7.7 kcal mol^{-1} ($\Delta G°$).

6.2.3 Polymerization Results

Group 1 and 2 metal (trimethylsilyl)allyl complexes are known to be initiators for the polymerization of methyl methacrylate (MMA),[27,42,63,64] and it was expected that **2** would likely follow suit. The MMA polymerization activity of **2** was evaluated in toluene (0.5 M) at several temperatures, as detailed in Table 16. In order to obtain tractable data, polymerizations were conducted at high monomer:initiator ratios (1000:1). Regardless of temperature, polymer yields were low to moderate (22–49%), displayed high dispersities ($Đ$ = 8.2–10.4), and were isotactically enriched (see Appendix). It was noted that previous studies have shown that the related initiator K[A′] produces only atactic PMMA (entry 5),[63,65] whereas [$CaA'_2(THF)_2$] also generates isotactically enriched PMMA in toluene.[27] Although the temperature dependence of anionic polymerizations is known to be small relative to cationic systems,[66] an expected increase in turnover frequency (TOF) was observed for polymerizations conducted at 0 °C (entries 1-2), which may be a result of the suppression of deleterious “backbiting” reactions and initiator degradation.[67,68] However, the TOF of polymerizations conducted at -78 °C are essentially the same as those at 25 °C, as has been observed when other ion pairs are involved in propagation.[69–71]

The broad PMMA dispersities observed when using initiator **2** is similar to those previously observed when using Grignard reagents as initiators in MMA polymerizations.[72] Such compounds are subject to Schlenk equilibria (2 $RMgX \rightleftarrows R_2Mg + MgX_2$), which means there are multiple active sites and the likelihood of side reactions, both of which may complicate initiation and propagation during the polymerization. A directly analogous rearrangement (i.e., $K[CaA'_3] \rightleftarrows K[A'] + [CaA'_2]$) is probably not relevant here, as the low solubility of K[A′] would shift the equilibrium far to the right, removing $K[CaA'_3]$ from solution. Instead, we hypothesize that varying amounts of aggregation may be occurring that could contribute to the broad dispersities observed.

In comparison to MMA polymerizations, the polymerization of dienes with s-block complexes has received much less study.[5] The stereochemistry and regiochemistry of conjugated diene insertion is more complex than with alkenes. For example, butadiene can give rise to *cis*- and *trans*-1,4-isomers, and the stereocenter generated from 1,2-

polymerization of butadiene opens the possibility for isotactic, syndiotactic, and atactic microstructures. Isoprene polymerization is even more complex: 1,4 insertions can lead to *cis*- and *trans*- isomers, and 1,2 and 3,4 insertions generate chiral centers with extra possibilities for microstructural arrangements (Figure 69).

Calcium and barium complexes have been examined as initiators of butadiene polymerization, but studies of isoprene polymerization with the heavy Group 2 elements are rare. The fluorenyl complex {(Me$_3$Si-fluorenyl)[*o*-(dimethylamino)benzyl]Ca}$_2$ ([(DMAT)(9-TMS-Fl)Ca]$_2$) and the benzyl derivative (DMAT)$_2$Ca(THF)$_2$ (DMAT = 2-dimethylamino-α-trimethylsilyl-benzyl) have been used as initiators for isoprene polymerization in cyclohexane, and give mixtures of 1,2-/3,4-/1,4-insertion products (Table 16, entries 14,15).[73]

The potassium allyl complex K[A′] was found to be inactive as an initiator for isoprene polymerization (Table 16, entry 10, and Appendix), as was the solvated [CaA′$_2$(THF)$_2$] (entry 11). However, complex **2** initiates isoprene polymerization in toluene (entry 6) at room temperature and atmospheric pressure, producing polyisoprene in high yield and low dispersity. As a note, these are the mildest conditions yet reported for a heavy Group 2 isoprene polymerization initiator. For polymerizations using initiator **2**, only two insertion products are observed, 1,4- and 3,4-, in a 63:37 ratio (see Appendix for details). Repetition of the reaction at 50 °C and 80 °C (entries 7,8) indicate that the initiator remains active, repeatedly producing yields ≥98%. However, polyisoprene molecular weights (M_n) were observed to decrease by 13% at 50 °C, and by 30% at 80 °C, and $Đ$ values increased modestly, by 0.2–0.3. Such a decrease in M_n is characteristic of increased chain transfer at elevated temperatures, which is also known to broaden dispersity.[74]

Finally, the deleterious effect that THF has on the initiating ability should be noted. Addition of an equivalent of THF to a solution of **2** (Table 16, entry 9) completely suppresses any isoprene polymerization activity. Furthermore, the combination of K[A′] and [CaA′$_2$(THF)$_2$] (entry 12) is also inactive, indicating that they do not associate to generate an '-ate'-type species. This underscores the critical importance of the initial solvent-free mechanochemical synthesis for the subsequent reactivity of the K[CaA′$_3$] system.

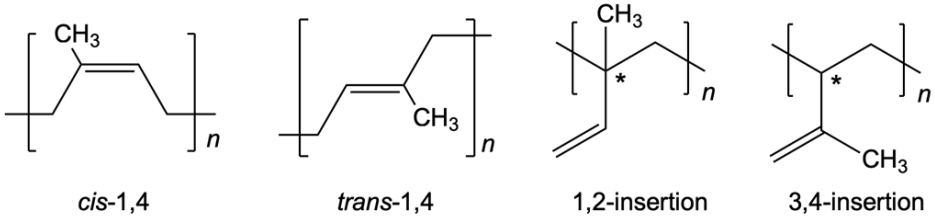

Figure 69. Stereochemical possibilities for polyisoprenes.

Table 16: Polymerization Results with **2**[a]

(A) Polymerization of MMA[a]

Entry	Initiator	Mono/ cat	Temp (°C)	Time	Yield (%)	TOF (min^{-1})	M_n (g/mol)	*Đ*	Tacticity[c]	Ref.
1	K[CaA′$_3$] (2)	1000	RT	8 min	22	27	63,600[b]	8.44[b]	69/22/9 (isotactic enriched)	this work
2	K[CaA′$_3$] (2)	1000	0	8 min	49	61	75,700[b]	8.25[b]	64/25/11 (isotactic enriched)	this work
3	K[CaA′$_3$] (2)	1000	–78	8 min	23	29	76,300[b]	10.41[b]	66/28/6 (isotactic enriched)	this work
4	(n-Bu)MgBr	50	–78	72 hr	14		7,420	11.2	21/15/64 (syndiotactic enriched)	69–71
15	K[A′]	1000	–78	0.5 m	87	1150	—	—	25/53/22 (atactic)	69–71

[a] Conditions for initiation with K[CaA′$_3$]: 0.25 g monomer, 0.5 M with respect to monomer in toluene, cooled to the respective temperature before monomer addition, then quenched with acidic MeOH and precipitated into MeOH.
[b] Number average molecular weights (M_n) and dispersities (*Đ*) were measured via GPC at 40 °C in THF, and are reported relative to PMMA standards.
[c] Tacticities are reported as percent mm/mr/rr triads as determined from ^{1}H NMR spectra

(B) Polymerization of Isoprene

Entry	Initiator	Mono/ cat	Temp (°C)	Time (h)	Yield (%)	M_n (g/mol)	*Đ*[b]	1,2/1,4/3,4[c]	Ref.
6	K[CaA′$_3$] (2)[a]	200	RT	12	98	16,300[b]	1.27[b]	0/63/37	this work
7	K[CaA′$_3$] (2)[a]	200	50	12	99	14,200	1.63	0/64/36	this work
8	K[CaA′$_3$] (2)[a]	200	80	12	98	11,400	1.52	0/64/36	this work
9	K[CaA′$_3$] + 1 eq THF [a]	200	RT	12	0	—	—	—	this work
10	K[A′][a]	200	RT	12	0	—	—	—	this work
11	[CaA′$_2$(THF)$_2$][a]	200	RT	12	0	—	—	—	this work
12	K[A′] + [CaA′$_2$(THF)$_2$] [a]	200	RT	12	0	—	—	—	this work
13	*sec*-BuLi		80	2	—	39,300	1.04		75–77
14	(DMAT)$_2$Ca(THF)$_2$	100	50	1	—	20,600	1.30	22/52/26	75–77
15	[(DMAT)(9-TMS-Fl)Ca]$_2$	100	50	0.25	—	15,400	1.26	11/52/37	75–77

a Conditions: 0.25 g monomer, 4 mL toluene, quenched with acidic MeOH and precipitated into MeOH.
b Number average molecular weights (M_n) and dispersities (*Đ*) were measured via GPC at 30 °C in THF using triple detection.
c Tacticities are reported as percent mm/mr/rr triads as determined from ^{1}H NMR spectra.

6.3 Conclusion

In addition to its benefits as a 'green' approach to synthesis, mechanochemistry offers a valuable way to generate molecules that are unavailable from solution-based methods. When describing the outcome of a reaction, there is a potential difference between the initial product and the results of the first contact of such species with the solvent(s) during the rest of the reaction time and during workup. Compounds that are prepared and isolated from solvent-based conditions have undergone a type of "selection by solution", and potentially useful molecules can be lost by that initial interaction. Mechanochemically based synthesis, in contrast, permits a separation between an initially formed product and the changes that might occur during a solvent-based workup. Note that workup in solution is not an absolute necessity in all cases. The product may be formed with essentially no by-products,[78] or it might be purified by a solvent-free method, e.g., sublimation. Small amounts of solvents are often required, however, for the workup of organometallic compounds prepared with grinding or milling.

The absence of ethers in the attempted synthesis of [CaA′$_2$] leads instead, owing to coordinative unsaturation, to the formation of the "-ate" complex K[CaA′$_3$]. The heterohaptic allyl complex undergoes smooth conversion to a still highly active, all-π-bound polymorph. Such behavior highlights a synergy between the solid state and solution environments that likely exists with other heterometallic main group metal complexes, most probably with strontium and barium, and which presents additional possibilities for generating highly active reagents and catalytic initiators.

6.4 Appendix

Experimental Procedures

General Considerations. All manipulations were performed with the rigorous exclusion of air and moisture using Schlenk or glovebox techniques in a glovebox free of coordinating solvents. Proton and carbon ($^{13}C\{^1H\}$) NMR spectra of the organometallic compounds were obtained on an AV-400 spectrometer at 400 (^1H) and 100 (^{13}C) MHz or an AV-600 spectrometer at 600 (^1H) and 150 (^{13}C) MHz and were referenced to the residual proton and ^{13}C resonances of C_6D_6. Elemental analyses were performed at the University of Rochester CENTC Elemental Analysis Facility by Dr. William Brennessel. Molecular weights (M_n) of the PMMA were determined using a Tosoh EcoSec GPC at 40 °C in THF and referenced to polymethylmethacrylate standards. Molecular weights (M_n) the polyisoprene were determined using a Malvern Omisec system using triple detection and three Viscotek styrene divinylbenzene copolymer columns (in series T3000, T4000, and T5000) at a flow rate of 1 mL min^{-1} and thermostatted to 30 °C with THF as the eluent. ^1H NMR of polymers were recorded on a Varian 300 spectrometer and chemical shifts are reported with respect to solvent residual peaks, i.e., δ 7.26 ppm ($CDCl_3$, purchased from Cambridge Isotope Laboratories).

Materials. CaI_2 was purchased from commercial suppliers and used as received. The potassium allyl K[A′] = K[(1,3-$SiMe_3$)C_3H_3] was synthesized by transmetallation of Li[A′][79] with potassium *tert*-butoxide in hexanes solution. Toluene was degassed with argon and dried over activated alumina using a solvent purification system, then stored over 4Å molecular sieves in a glovebox. Hexanes were distilled under nitrogen over NaK/benzophenone radical,[80] then stored over 4 Å molecular sieves. $(SiMe_3)_2O$ was purchased from commercial suppliers, distilled over sodium under nitrogen atmosphere, and stored over 4 Å molecular sieves in a glovebox. Benzene-d_6 was obtained from Cambridge Isotopes and stored over 4 Å molecular sieves. Methyl methacrylate (MMA) was purchased from Acros, run through a basic alumina column, dried over 4 Å sieves, vacuum transferred, and then degassed via three freeze-pump-thaw cycles. Isoprene was purchased from Acros, distilled from CaH_2, and degassed via three freeze-pump-thaw cycles.

Mechanochemical protocol. Ball milling reactions used 50 stainless steel (440 grade) ball bearings ($^3/_{16}$ in (5 mm), 0.44 g) that were thoroughly cleaned with detergent and water, then washed with acetone, and dried in a 125 °C oven prior to use. Planetary milling was performed with a Retsch PM100 mill, 50 mL stainless steel grinding jar type C, and a safety clamp for air-sensitive grinding. A typical reaction involved 250 mg total sample weight, sealed under an inert atmosphere. The ground mixture was extracted with minimal solvent (<100 mL) and filtered through a fine porosity ground glass frit. The extraction is designed to dissolve the complex, and the filtration removes traces of KI. The filtrate was then dried under vacuum prior to NMR analysis.

Synthesis of K[CaA′$_3$] (1) (initial product). In a typical reaction, CaI_2 (0.098 g, 0.333 mmol) and K[A′] (0.150 g, 0.668 mmol) were added to a 50 mL stainless steel Retsch milling jar with 25 g (~57 count) of stainless steel (440 grade) ball bearings (3/16 in (5 mm), 0.44 g) under a nitrogen atmosphere in a glovebox. The jar was sealed with a clamp in the glovebox and milled for 10 minutes at 600 rpm in a Retsch PM100 planetary mill. The jar was opened in an ether-free glovebox, and the reaction mixture was extracted with toluene (<100 mL) through a fine-porosity glass fritted funnel. The resulting yellow filtrate was dried under vacuum, and a yellow oil was collected in the bottom of the flask. ^{1}H NMR (600 MHz, C_6D_6): δ 0.343 (s, 18 H, TMS), δ 3.33 (d, $^1J_{H\text{-}H}$ = 16.15 Hz, 2 H, $H_{1,3}$), δ 7.25 (t, $^1J_{H\text{-}H}$ = 16.15 Hz, 1 H, H_2). $^{13}C\{^1H\}$ NMR (150 MHz, C_6D_6): δ 2.38, 77.16, 159.83.

Synthesis of K[CaA′$_3$] (2) (rearrangement product). In a typical reaction, CaI_2 (0.098 g, 0.333 mmol) and K[A′] (0.150 g, 0.668 mmol) were added to a 50 mL stainless steel Retsch milling jar with 25 g (~57 count) of stainless steel (440 grade) ball bearings (3/16 in (5 mm), 0.44 g) under a nitrogen atmosphere in a glovebox. The jar was sealed with a clamp in the glovebox and milled for 20 minutes at 600 rpm in a Retsch PM100 planetary mill. The jar was opened in an ether-free glovebox, and the reaction mixture was extracted with toluene (<100 mL) through a fine-porosity glass fritted funnel. The resulting yellow filtrate was dried under vacuum, and an orange oil was collected in the bottom of the flask. When under vacuum for an extended period of time, the orange oil becomes a white solid, signifying loss of toluene (25 mg, 0.034 mmol, 15%). This is reflected in the elemental

analysis, which was consistent with [KCaA′$_3$(toluene)$_{0.5}$], $C_{27}H_{63}CaKSi_6$•$(C_7H_8)_{0.5}$: C, 53.75; H, 9.91. Found: C, 53.34; H, 9.92. ^{1}H NMR (600 MHz, C_6D_6): δ 0.21 (s, 18 H, TMS), δ 3.32 (d, $^1J_{H-H}$ = 16 Hz, 2H, $H_{1,3}$), δ 6.99 (br, 1H, H_2). $^{13}C\{^1H\}$ NMR (150 MHz, C_6D_6): δ 1.79, 79.87, 161.40.

General MMA Polymerization Conditions. Under an inert atmosphere, MMA (0.25 g, 2.5 mmol) was added to a solution of (**2**) (2.5 μmol) in toluene (5 mL) cooled to the designated temperature. The polymerization was held at the designated temperature and stirred continuously for 8 min. The reaction was quenched by addition of acidic methanol (3 mL) and the polymer precipitated via dropwise addition to MeOH. The resultant polymer was isolated via filtration and dried. Polymer tacticity was determined with ^{1}H NMR in $CDCl_3$.[81,82]

General Isoprene Polymerization Conditions. Under an inert atmosphere, isoprene (0.25 g, 3.67 mmol) was added to a solution of (**2**) (11.7 mg, 0.0184 mmol) in toluene (4 mL) at the designated temperature in a vial sealed with a Teflon faced cap. The polymerization was stirred continuously for 12 h at the designated temperature. The polymerization was quenched with acidic methanol (3 mL) and the polymer precipitated via dropwise addition to MeOH. The methanol was decanted off then the polymer was dried. Polymer regiochemistry was determined with ^{1}H NMR in $CDCl_3$.[83–85]

Procedures for X-ray Crystallography

(1) A crystal (0.36 x 0.24 x 0.20 mm^3) was placed onto the tip of a thin glass optical fiber and mounted on a Bruker SMART APEX II CCD platform diffractometer at the X-ray Crystallographic Facility, Department of Chemistry, University of Rochester, Rochester, NY for data collection at 100.0(5) K.[86] A preliminary set of cell constants and an orientation matrix were calculated from reflections harvested from three orthogonal wedges of reciprocal space. The full data collection was carried out using MoKα radiation (graphite monochromator) with a frame time of 60 seconds and a detector distance of 4.03 cm. A randomly oriented region of reciprocal space was surveyed: four major sections of frames were collected with 0.50° steps in ω at four different ϕ settings and a detector position of -38° in 2θ. The intensity data were corrected for absorption.[87] Final cell constants were calculated from the *xyz* centroids of 3884 strong reflections from the actual data collection after integration.[88] The structure was solved using SHELXT-2014/5 [89] and refined using SHELXL-2014/7.[90] The space group $P2_1/m$ was determined based on systematic absences and intensity statistics. A direct-methods solution was calculated which provided most non-hydrogen atoms from the E-map. Full-matrix least squares / difference Fourier cycles were performed which located the remaining non-hydrogen atoms. All non-hydrogen atoms were refined with anisotropic displacement parameters. All hydrogen atoms were placed in ideal positions and refined as riding atoms with relative isotropic displacement parameters. The asymmetric unit contains one calcium cation on a crystallographic mirror plane, one potassium cation near a crystallographic inversion center, and three allyl ligands whose occupancies are restricted to one half because they are disordered as a set over crystallographic symmetry. Because the silicon atoms are approximately evenly spaced

from one another (about 6 Å apart), the connecting allyls are able to connect in two directions, and thus the structure is a disorder of the two motifs, the ratio of which is exactly 0.50:0.50 due to the aforementioned crystallographic symmetry. The $SiMe_3$ group containing Si5 is modeled as disordered over two additional positions (0.82:0.18).

(**2b,2c**) X-ray crystallographic data were collected on a Rigaku Oxford Diffraction Supernova diffractometer at Vanderbilt University. Crystal samples were handled under immersion oil and quickly transferred to a cold nitrogen stream. The crystals were kept at 100 K during data collection. Under Olex2,[91] the structure was solved with the SHELXT[89] structure solution program using direct methods and refined with the SHELXL[90] refinement package using least squares minimization. All non-hydrogen atoms were refined with anisotropic displacement parameters.

Crystallographic data for the structure have been deposited with the Cambridge Crystallographic Data Centre as CCDC 2024008 (**2**), 2024009 (**2b**), and 2024040 (**2c**). Copies of the data can be obtained free of charge on application to CCDC, 12 Union Road, Cambridge CB2 1EZ, UK (fax: (+44)1223-336-033; e-mail: deposit@ccdc.cam.ac.uk).

General Procedures for Calculations

All calculations were performed with the Gaussian 09W[92] or Gaussian 16 (Linux) suite of programs.[93] The B3PW91 functional, which incorporates Becke's three-parameter exchange functional with the 1991 gradient-corrected correlation functional of Perdew and Wang, was used.[94,95] To supply dispersion corrections, Grimme's D3 correction[96] with additional Becke-Johnson damping was used (Gaussian keyword: empiricaldispersion=GD3BJ).[97] Unless otherwise noted, the def2SVP basis set was used on all atoms.[98] Frequency calculations were also done at the double-zeta level. An ultrafine grid was used for all calculations (Gaussian keyword: int=ultrafine).

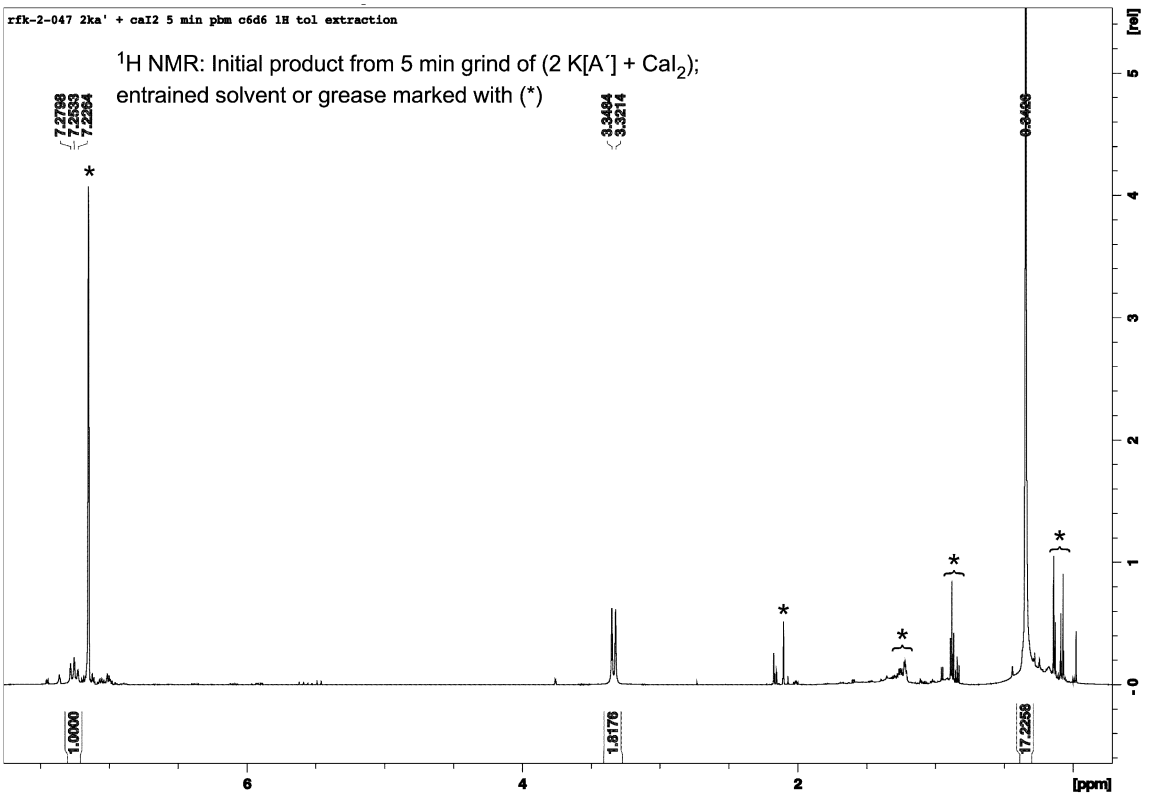

Figure 70. ^{1}H NMR spectrum of initial product (**1**) from K[A´] + CaI_2

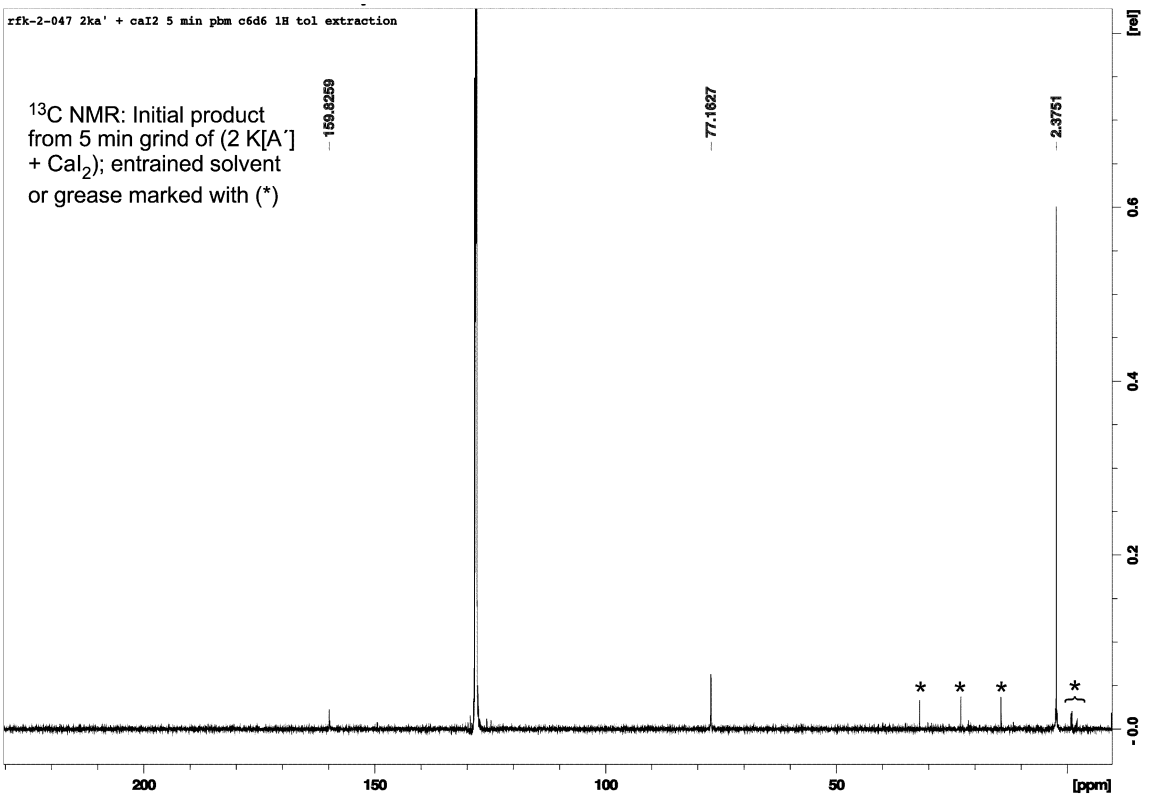

Figure 71. ^{13}C NMR spectrum of initial product (**1**) from K[A´] + CaI_2

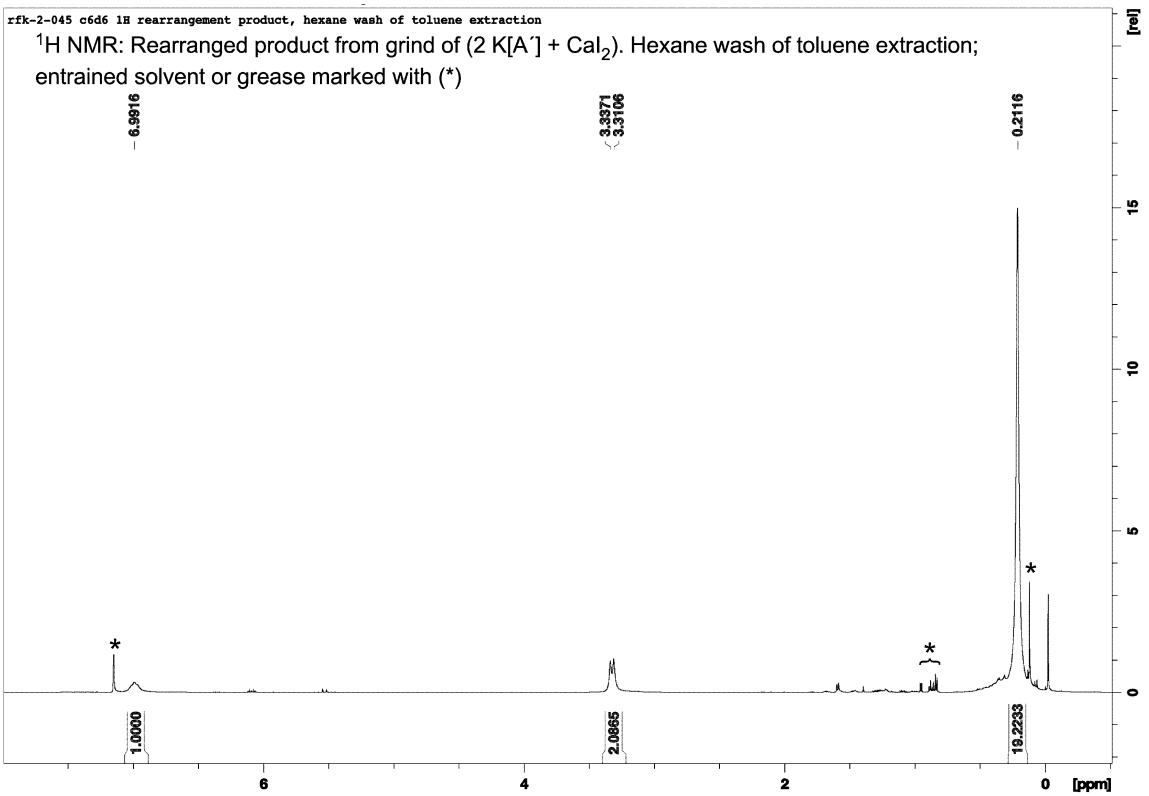

Figure 72. [1]H NMR spectrum of rearrangement product (**2**) from K[A´] + CaI_2

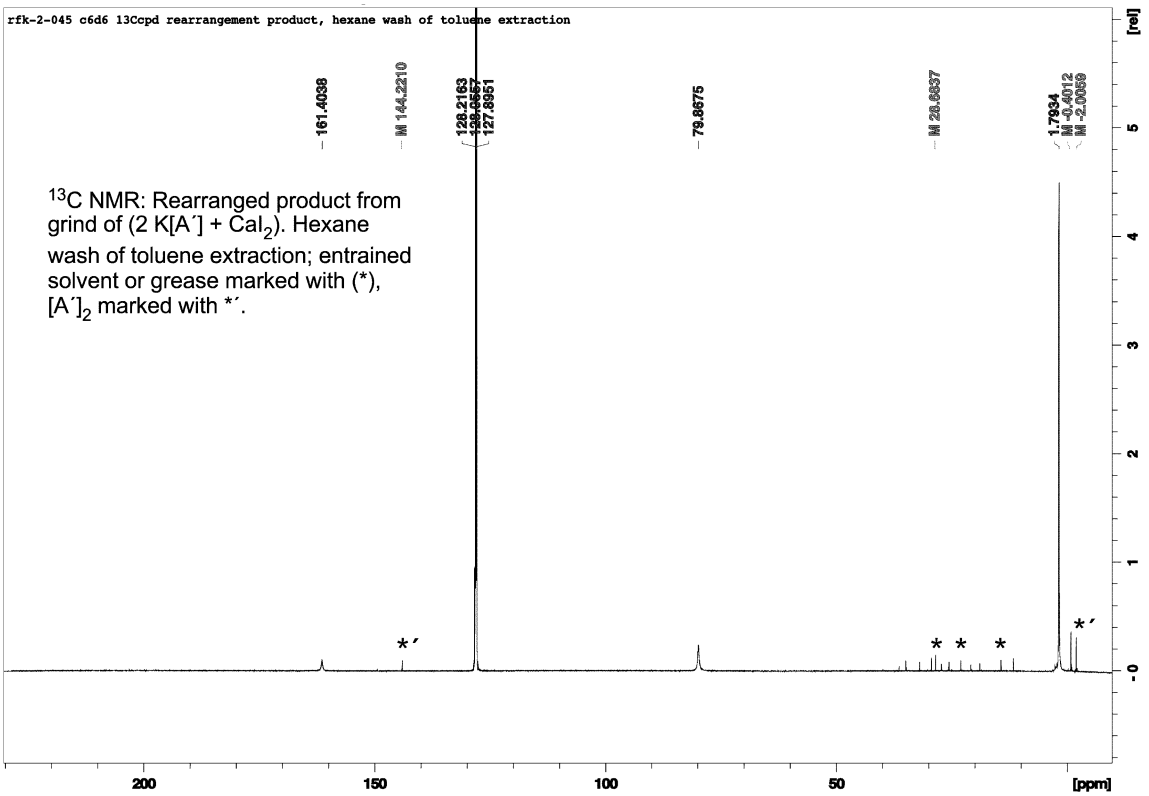

Figure 73. [13]C NMR spectrum of rearrangement product (**2**) from K[A´] + CaI_2

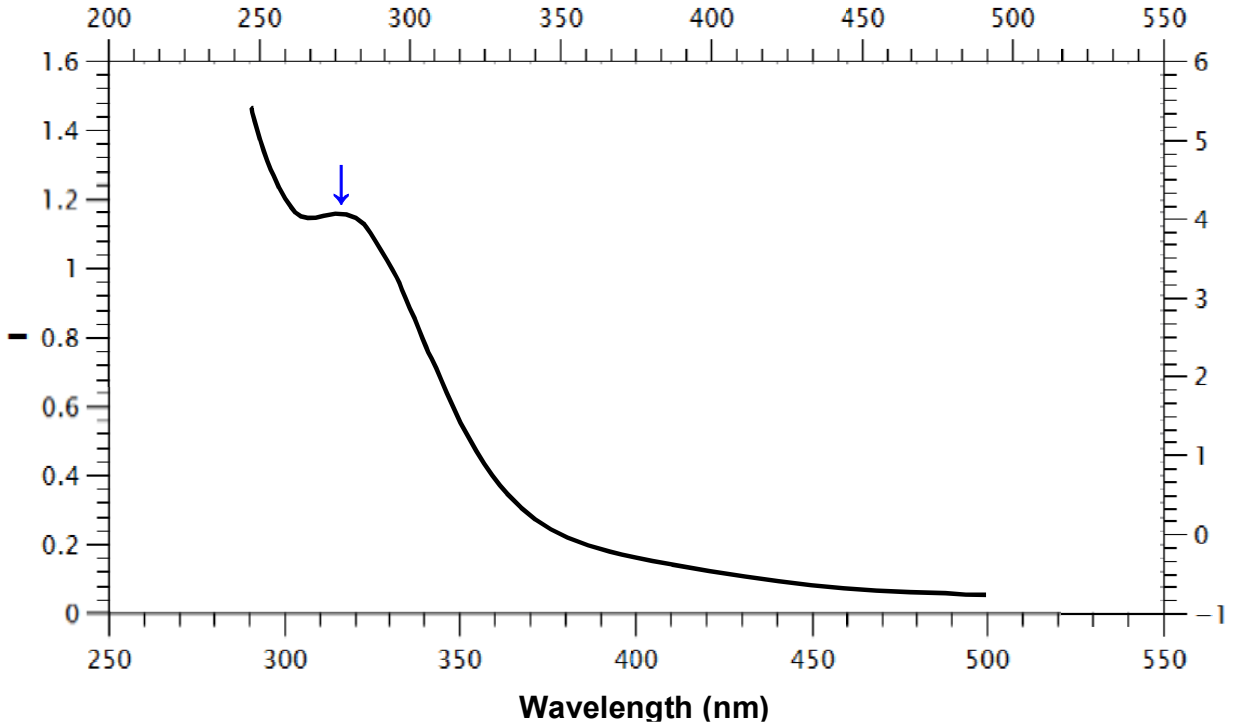

Figure 74. UV-vis spectrum of K[CaA′$_3$] in toluene. The peak underneath the arrow is at 316 nm.

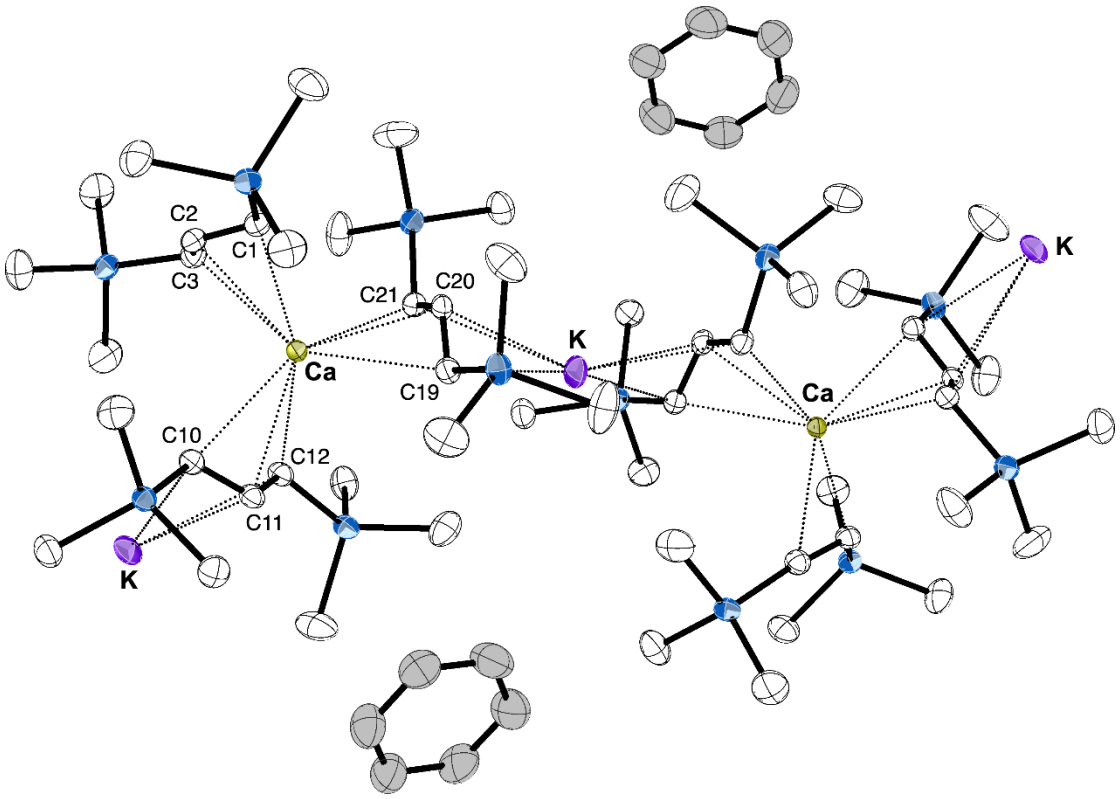

Figure 75. Portion of the coordination polymer of $\{K[CaA'_3]\bullet C_6D_6\}_n$ (**2b**). Thermal ellipsoids have been drawn at 50%, and hydrogen atoms have been removed for clarity. Selected bond distances (Å) and angles (°): Ca–C1, 2.623(2); Ca–C2, 2.635(2); Ca–C3, 2.611(2); Ca–C10, 2.654(2); Ca–C11, 2.670(2); Ca–C12, 2.726(2); Ca–C19, 2.695(2); Ca–C20, 2.640(2); Ca–C21, 2.711(2); K–C19, 3.127(2); K–C20, 2.933(2); K–C21, 3.107(2); Ca1···K, 5.153; Ca2···K, 5.053; Ca···K···Ca′, 170.4, K···Ca···K′, 114.6.

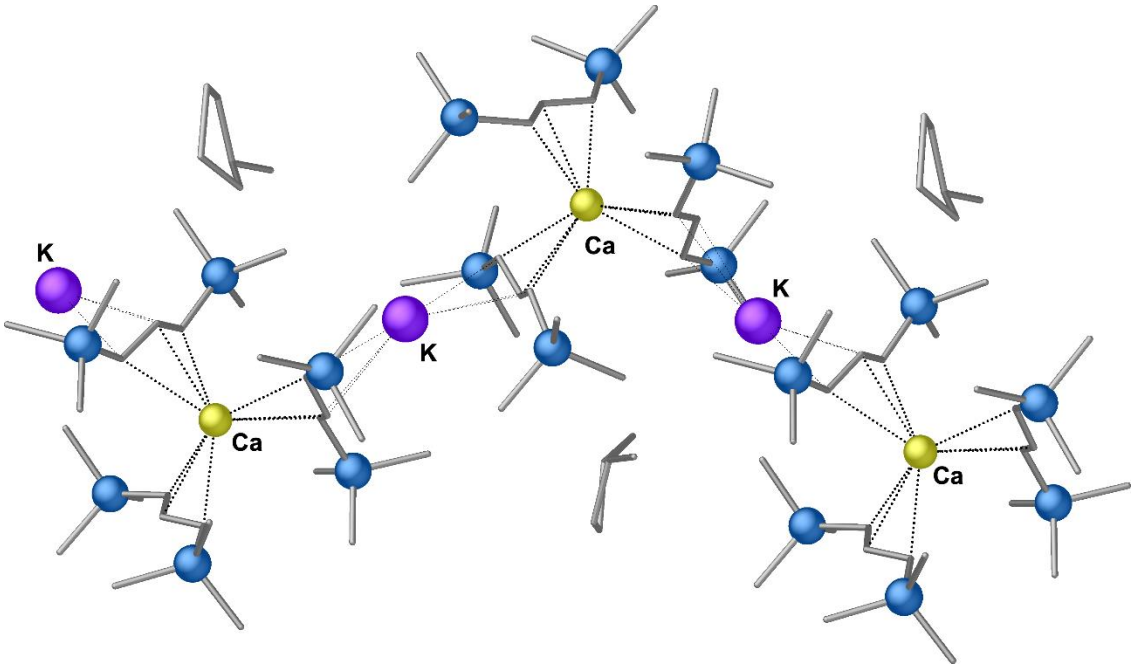

Figure 76. Portion of the coordination polymer of $\{K[CaA'_3]\bullet C_5H_9Me\}_n$ (**2c**), with carbon-carbon and carbon-silicon bonds shown as sticks. Hydrogen atoms have been removed for clarity, and only one conformation of the disordered methylcyclopentane is presented.

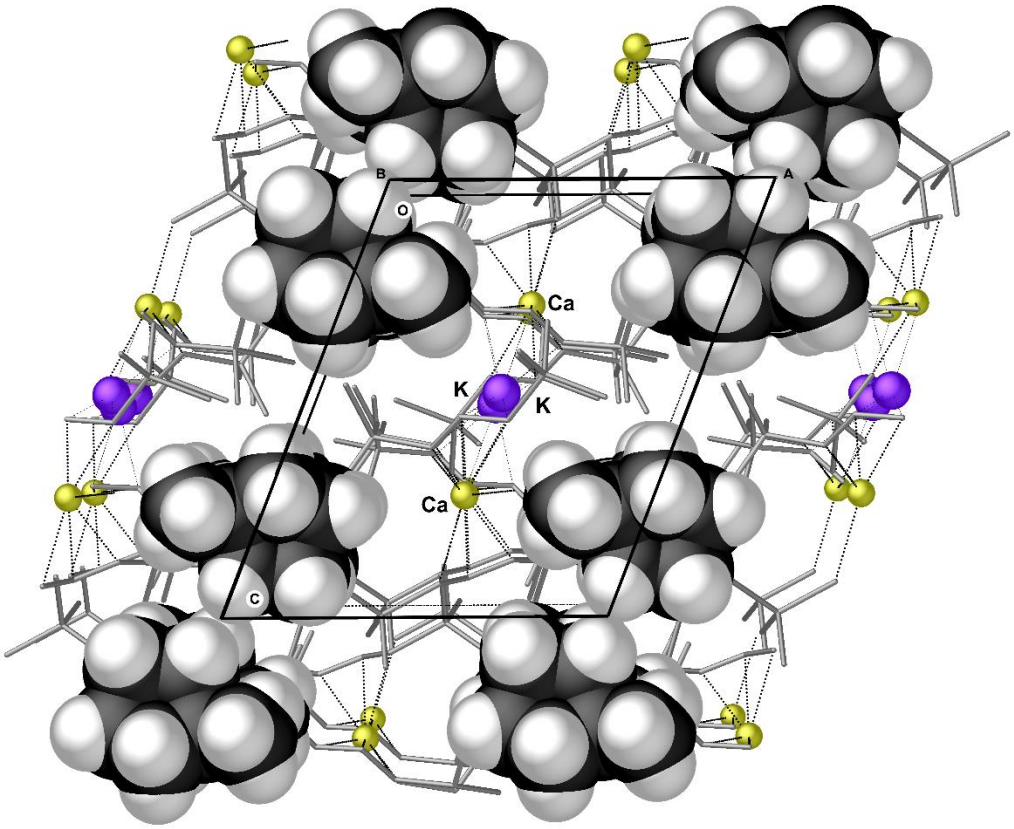

Figure 77. Portion of the coordination polymer of $\{K[CaA'_3]\bullet C_5H_9Me\}_n$ (**2c**), projected down the crystallographic *b* axis. Carbon-carbon and carbon-silicon bonds are shown as sticks, and interstitial methylcyclopentane molecules are displayed with space-filling parameters.

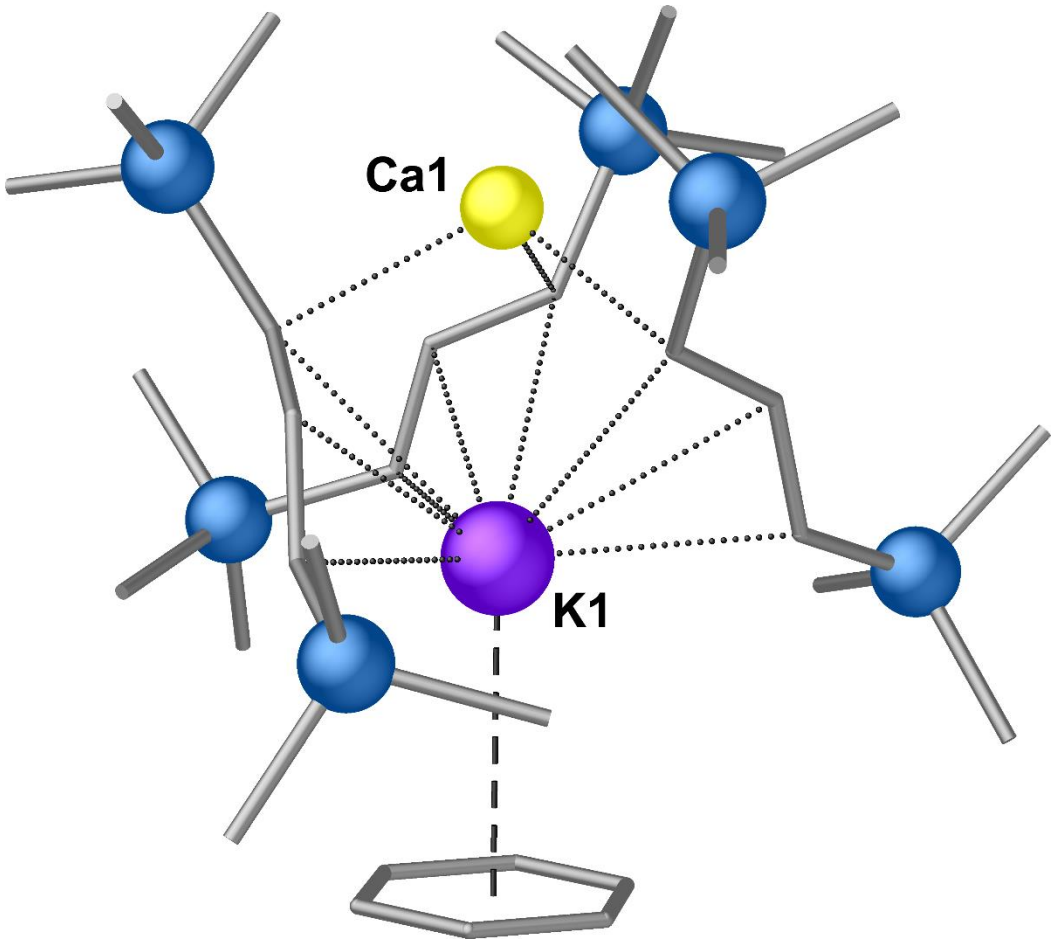

Figure 78. Calculated geometry (B3PW91-D3BJ/def2SVP) of an approximately C_3-symmetric version of **1**•C_6H_6, in which the allyl ligands adopt a μ_2-η^1: η^3 arrangement (Figure 68a in the main text). Carbon-carbon and carbon-silicon bonds are shown as sticks. Selected bond distances (Å): Ca1–C, 2.514; average K1–C (η^3-A′), 3.115; K1···(ring centroid), 3.339; Ca1···K1 separation: 3.401.

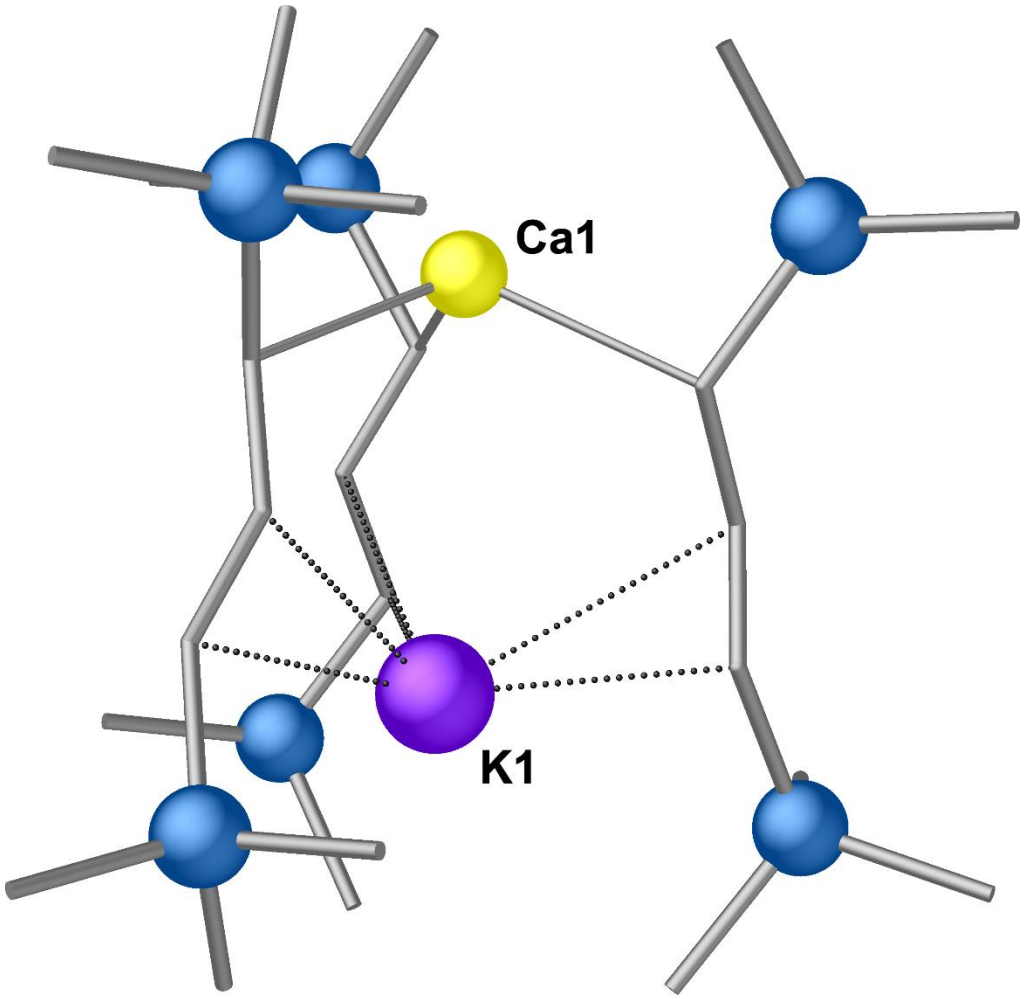

Figure 79. Calculated geometry (B3PW91-D3BJ/def2SVP) of an approximately C_3-symmetric version of **1**, obtained by reoptimizing the **1**•C_6H_6 model (Figure 68a in the main text) with the C_6H_6 removed. Carbon-carbon and carbon-silicon bonds are shown as sticks. Selected bond distances (Å): average Ca1–C, 2.495; average K1–C (η^2-A′), 3.059; Ca1···K1 separation, 3.874.

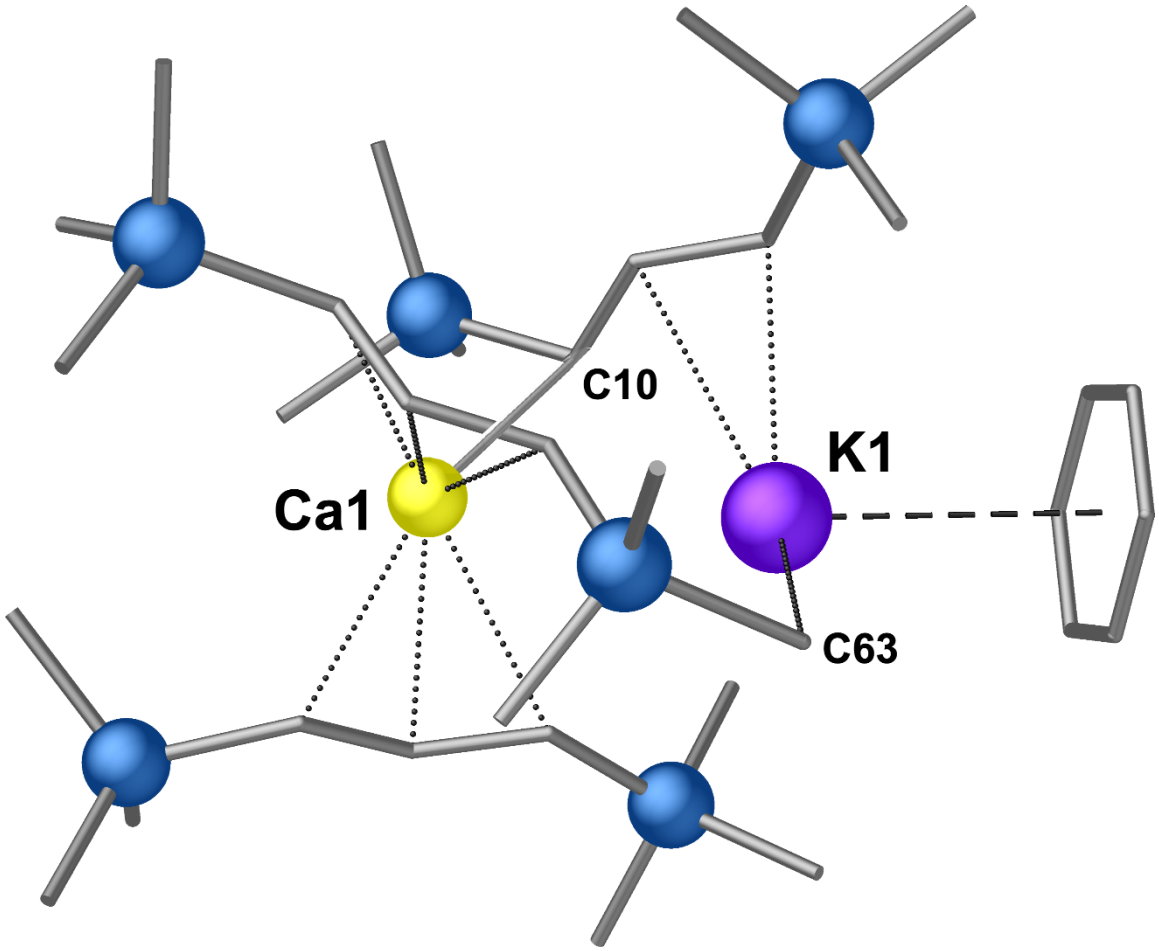

Figure 80. Calculated geometry (B3PW91-D3BJ/def2SVP) of a (C_6H_6)•K[Ca(π-A′)$_2$(σ-A′)] model of **1** (Figure 68b in the main text). Carbon-carbon and carbon-silicon bonds are shown as sticks. Selected bond distances (Å): average Ca1–C(η^3-A′), 2.617; Ca1–C10: 2.602; average K1–C(η^2-A′), 2.970; K1···C63, 3.074; K1···(ring centroid), 3.390.

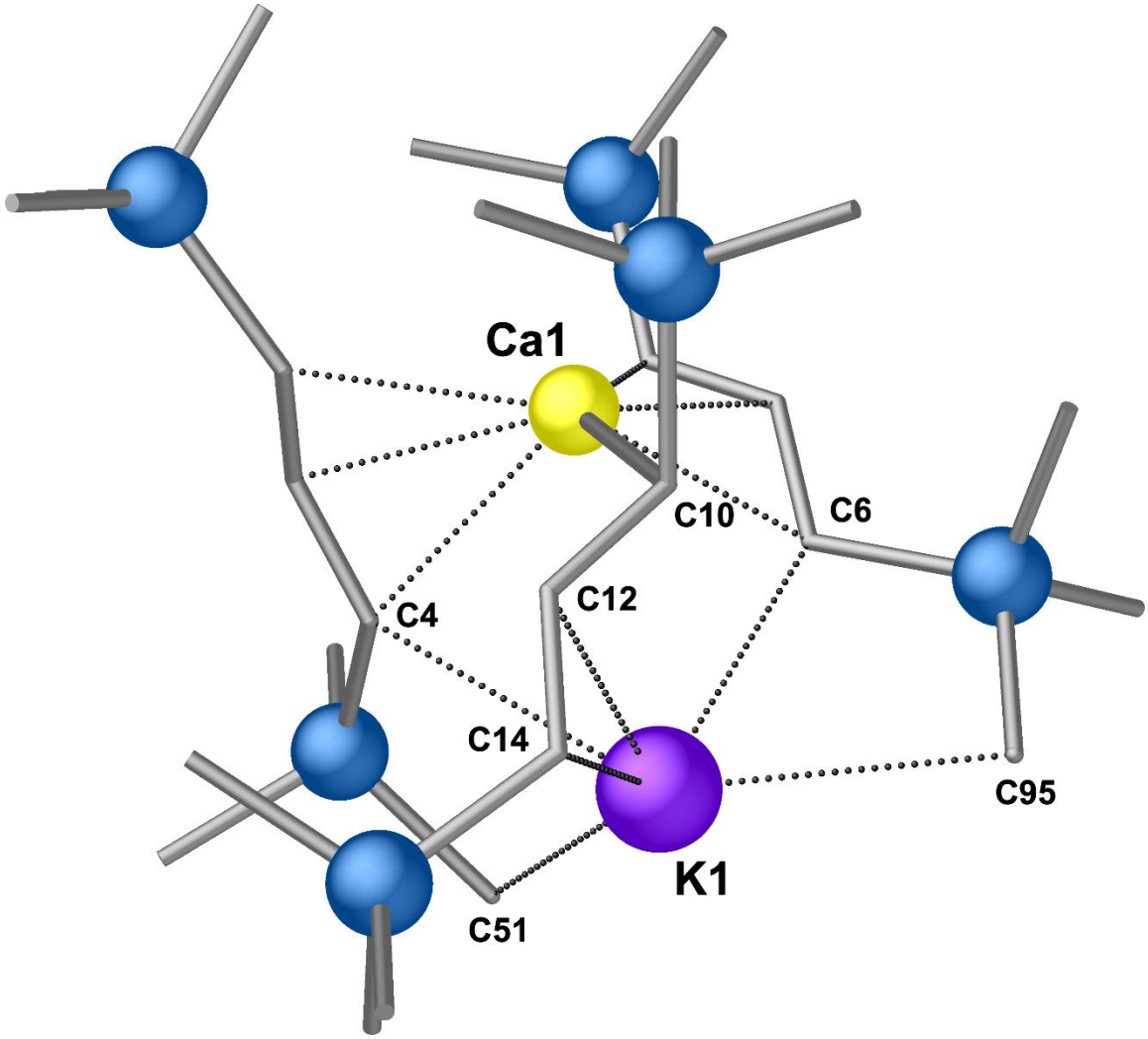

Figure 81. Calculated geometry (B3PW91-D3BJ/def2SVP) of a version of **1**, obtained by reoptimizing the (C_6H_6)•K[Ca(π-A′)$_2$(σ-A′)] model (Figure 68b in the main text) with the C_6H_6 removed. Carbon-carbon and carbon-silicon bonds are shown as sticks. Selected bond distances (Å): average Ca1–C(η^3-A′), 2.622; Ca1–C10: 2.602; K1–C4: 3.090; K1–C6: 3.096; K1–C12: 3.075; K1–C14: 2.846; K1–C51: 3.095; K1–C95: 3.101.

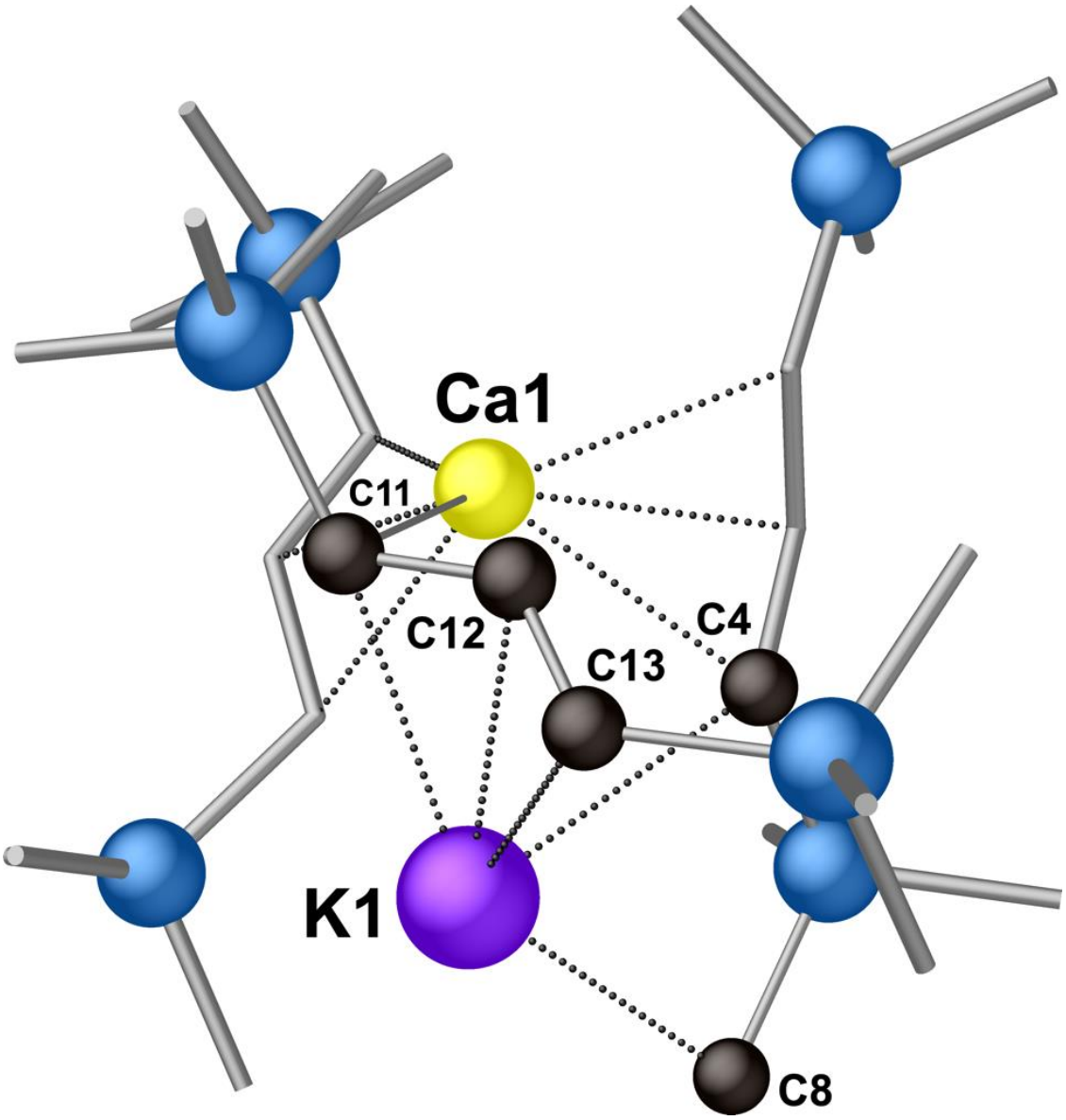

Figure 82. Calculated geometry (B3PW91-D3BJ/def2SVP) of a version of **1**, obtained by reoptimizing the (C_6H_6)•K[Ca(π-A′)(σ-A′)$_2$] model (Figure 65a in the main text) with the C_6H_6 removed. Carbon-carbon and carbon-silicon bonds are shown as sticks. Selected bond distances (Å): average Ca1–C(η^3-A′), 2.621; Ca1–C11: 2.604; average K1–C(η^3-A′), 2.986; K1–C4: 3.056; K1–C8: 3.060.

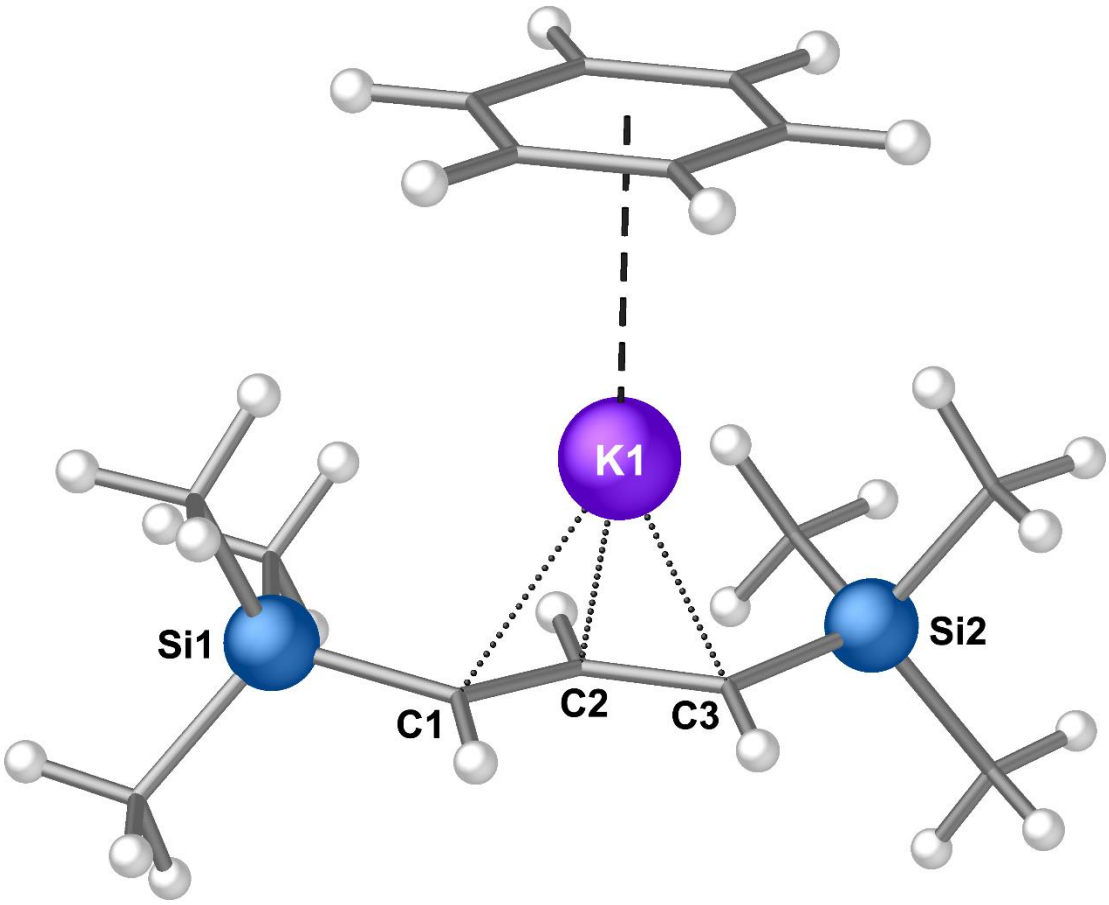

Figure 83. Calculated structure [(C_6H_6)•KA′] (B3PW91-D3BJ/def2SVP), with carbon-carbon and carbon-silicon bonds shown as sticks. Selected bond distances (Å): K1–C1, 2.871; K1–C2, 2.783; K1–C3, 2.877; C1–Si1, 1.830; C3–Si2, 1.831; K1···(ring centroid), 3.250.

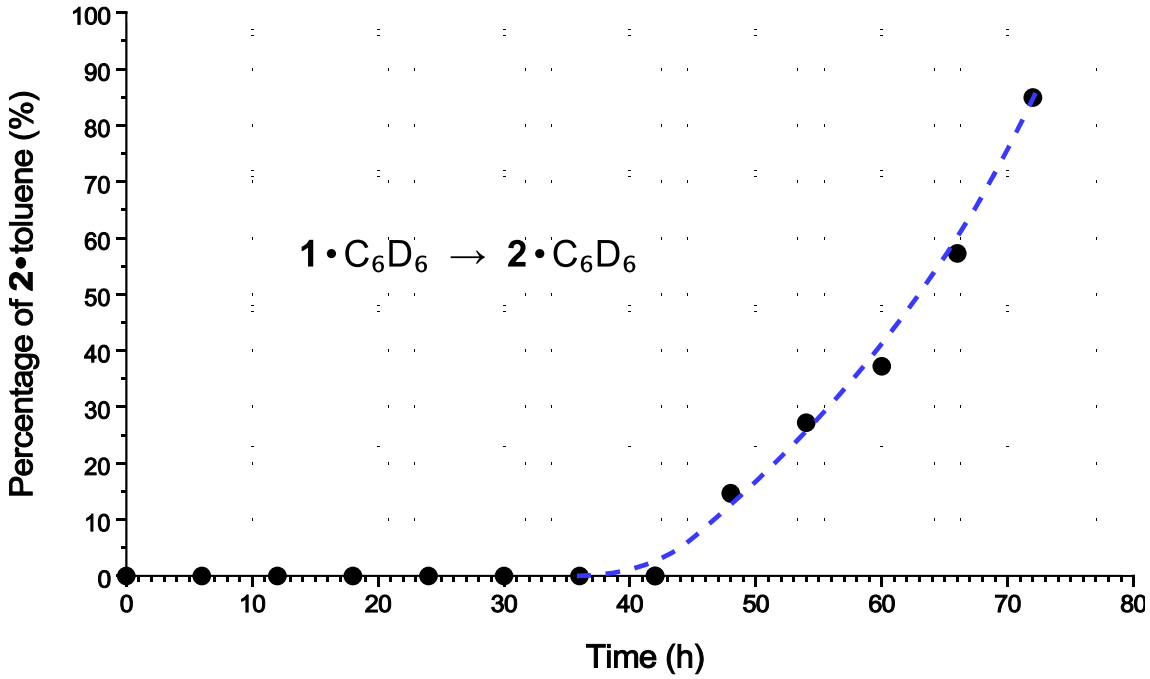

Figure 84. Change in the composition of a solution of **1** in neat C_6D_6, as measured with ^1H NMR spectroscopy. There is no evidence for the presence of the rearrangement product **2** until more than 40 h have passed. The line through the data points is meant as a guide to the eye; it does not represent a calculated fit.

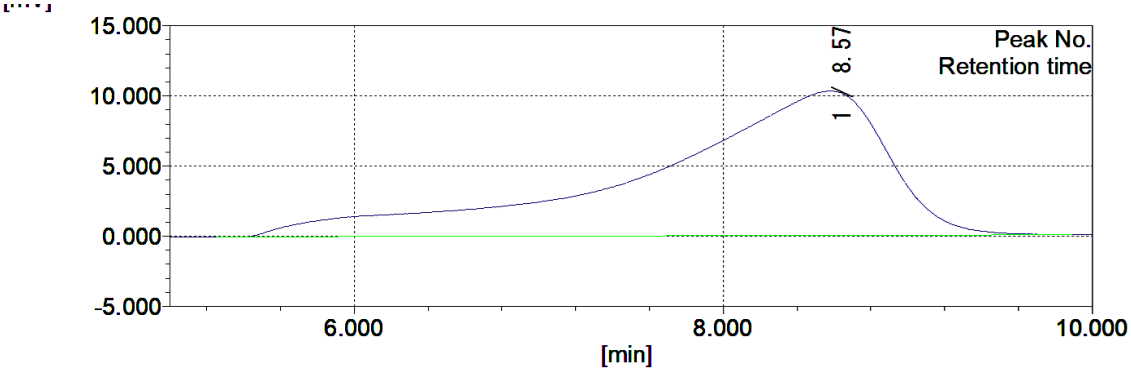

Figure 85. Representative GPC trace of PMMA obtained with K[CaA'$_3$] (**2**) at RT. Samples measured in THF at 40 °C and referenced using PMMA standards (Table 16, entry 1 in main text).

Table 17: GPC trace data and resulting molecular weight calculation (MMA run 1)

	[min]	[mV]	[mol]
Peak start	5.257	-0.067	694,010,710
Peak top	8.575	10.364	43,417
Peak end	9.892	0.105	5,932
Height [mV]			10.305
Area [mV*sec]			919.680
Area% [%]			100.000
[eta]			537010.16727

Mn	63,634
Mw	537,010
Mz	51,774,362
Mz+1	393,725,613
Mv	537,010
Mp	43,417
Mz/Mw	96.412
Mw/Mn	8.439
Mz+1/Mw	733.181

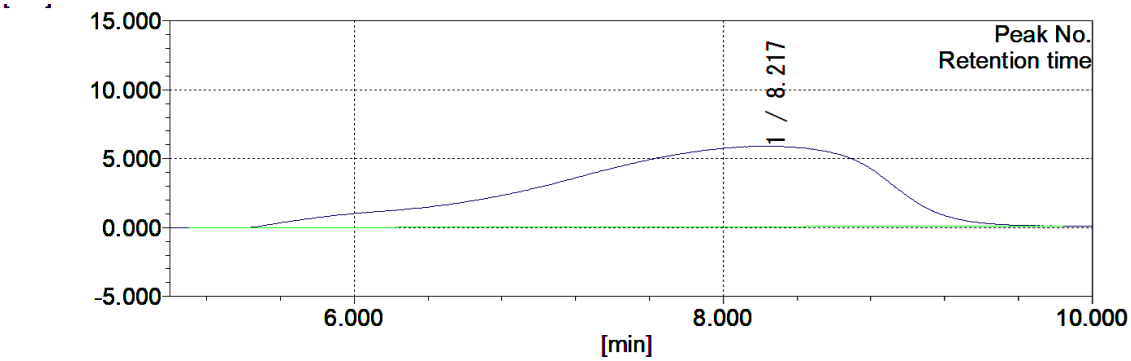

Figure 86. Representative GPC trace of PMMA obtained with K[CaA'$_3$] (**2**) at 0 °C. Samples measured in THF at 40 °C and referenced using PMMA standards (Table 16, entry 2 in main text).

Table 18: GPC trace data and resulting molecular weight calculation (MMA Run 2)

	[min]	[mV]	[mol]
Peak start	5.108	-0.022	999,999,999
Peak top	8.217	5.917	68,788
Peak end	9.847	0.123	6,392
Height [mV]			5.845
Area [mV*sec]			718.291
Area% [%]			100.000
[eta]			624316.73911

Mn	75,698
Mw	624,317
Mz	246,918,228
Mz+1	892,166,904
Mv	624,317
Mp	63,161
Mz/Mw	395.502
Mw/Mn	8.247
Mz+1/Mw	1429.029

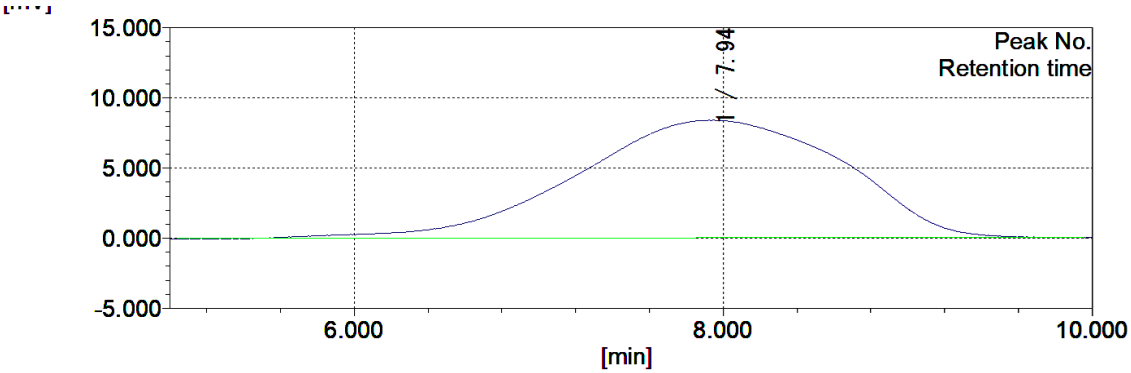

Figure 87. Representative GPC trace of PMMA obtained with K[CaA'$_3$] (**2**) at -78 °C. Samples measured in THF at 40 °C and referenced using PMMA standards (Table 16, entry 3 in main text).

Table 19: GPC trace data and resulting molecular weight calculation (MMA Run 3)

	[min]	[mV]	[mol]		
Peak start	5.038	-0.037	999,999,999	Mn	76,285
Peak top	7.945	8.415	97,982	Mw	794,243
Peak end	9.962	0.036	5,281	Mz	657,597,981
				Mz+1	947,509,873
				Mv	794,243
Height [mV]			8.378	Mp	88,165
Area [mV*sec]			833.426	Mz/Mw	827.956
Area% [%]			100.000	Mw/Mn	10.412
[eta]			794242.89642	Mz+1/Mw	1192.972

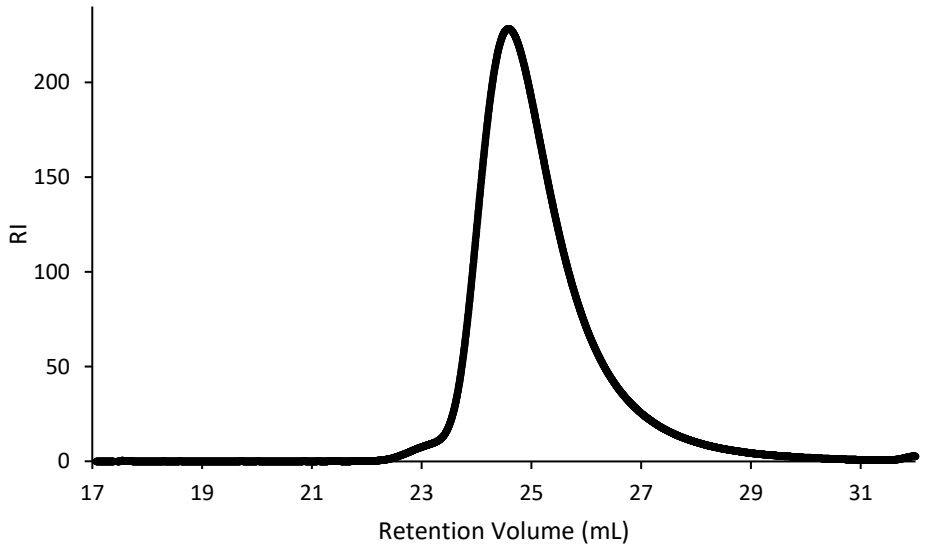

Figure 88. Representative GPC trace of polyisoprene obtained with K[CaA'$_3$] (**2**) at RT. Samples measured in THF at 30 °C and reported as absolute molecular weight (Table 16, entry 6 in main text).

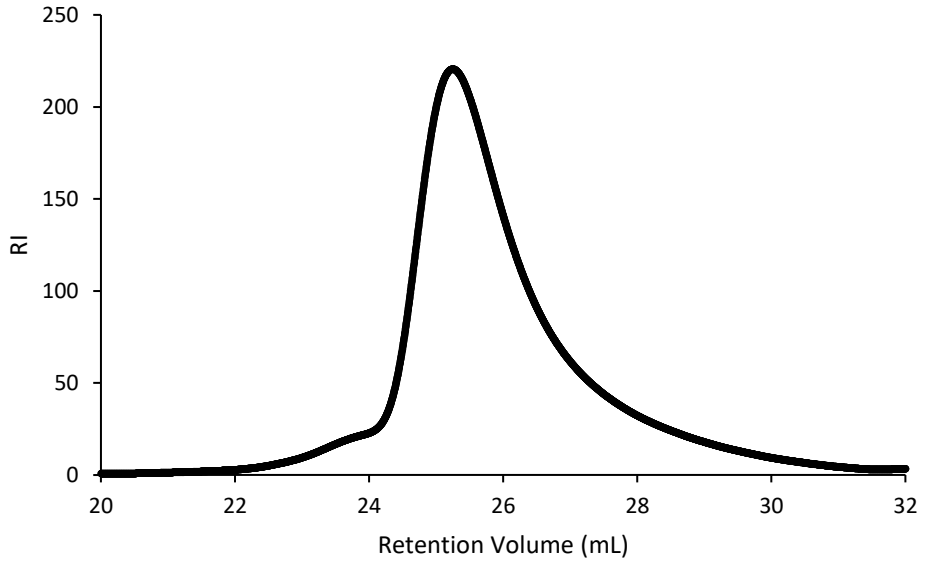

Figure 89. Representative GPC trace of polyisoprene obtained with K[CaA'$_3$] (**2**) at 50 °C. Samples measured in THF at 30 °C and reported as absolute molecular weight (Table 16, entry 7 in main text).

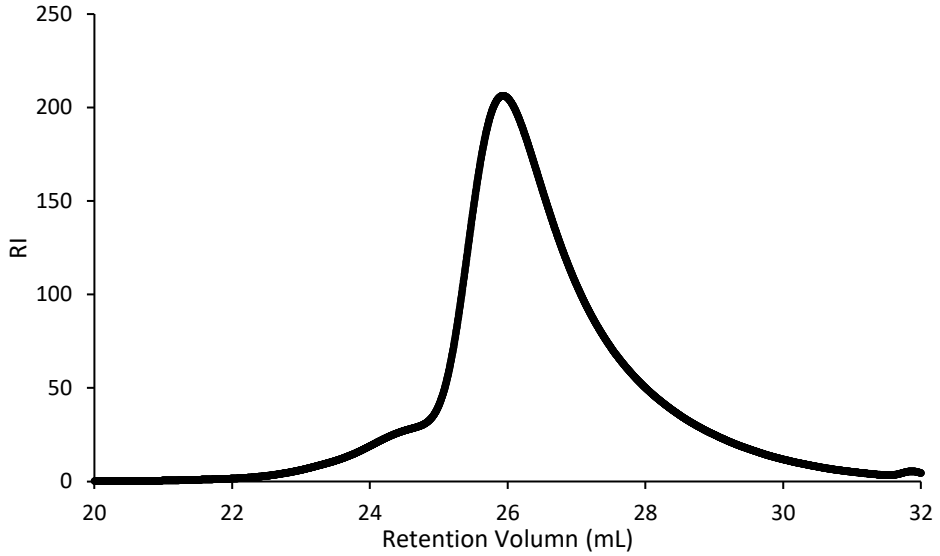

Figure 90. Representative GPC trace of polyisoprene obtained with K[CaA'$_3$] (**2**) at 80 °C. Samples measured in THF at 30 °C and reported as absolute molecular weight (Table 16, entry 8 in main text).

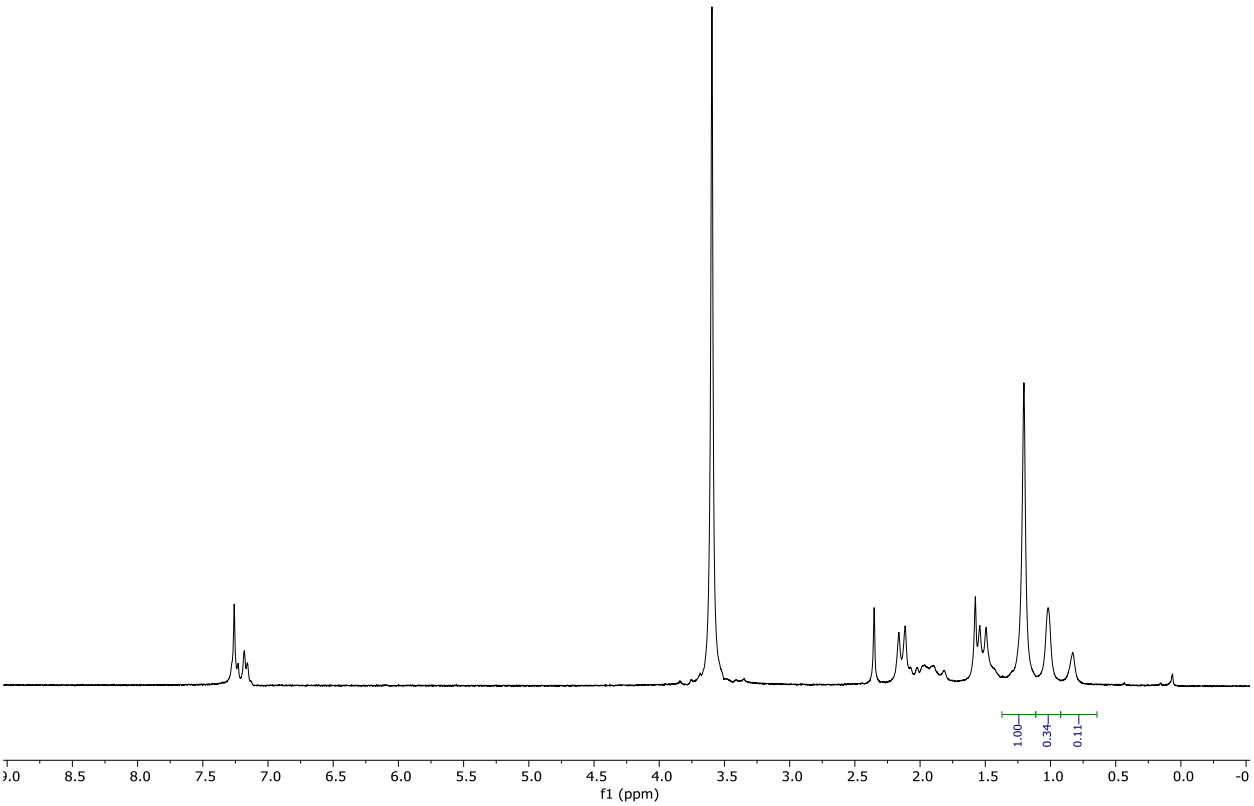

Figure 91. ^{1}H NMR spectrum (300 MHz, 25 °C, $CDCl_3$) of PMMA obtained using K[CaA′$_3$] (**2**) at RT.

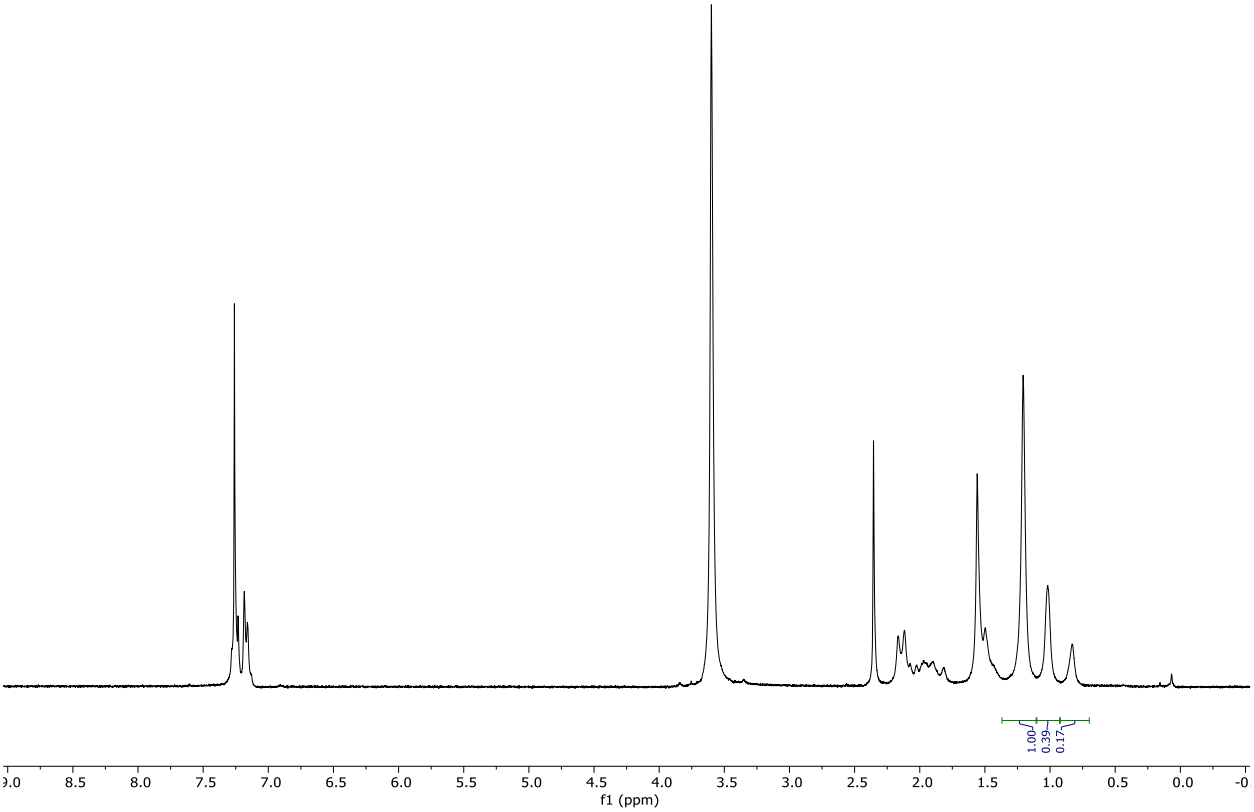

Figure 92. ^{1}H NMR spectrum (300 MHz, 25 °C, $CDCl_3$) of PMMA obtained using K[CaA′$_3$] (**2**) at 0 °C.

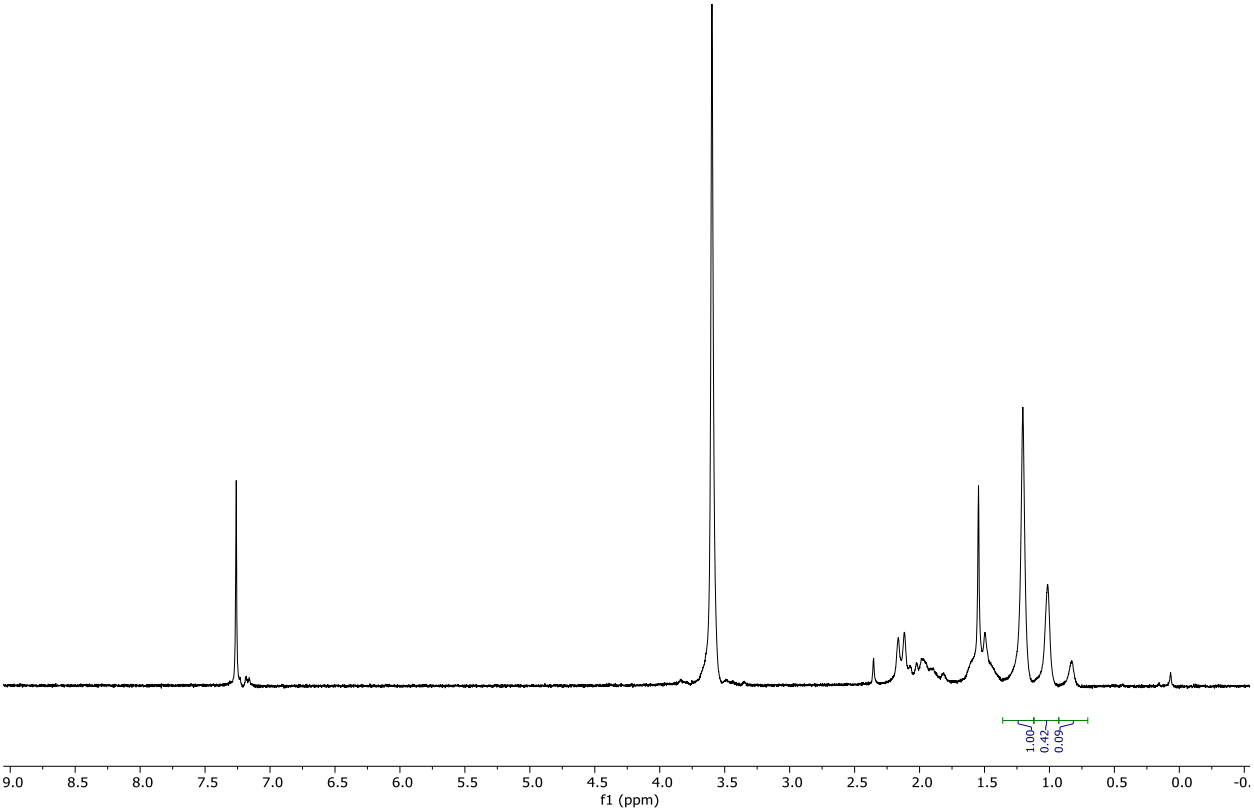

Figure 93. ^{1}H NMR spectrum (300 MHz, 25 °C, $CDCl_3$) of PMMA obtained using K[CaA′$_3$] (**2**) at -78 °C.

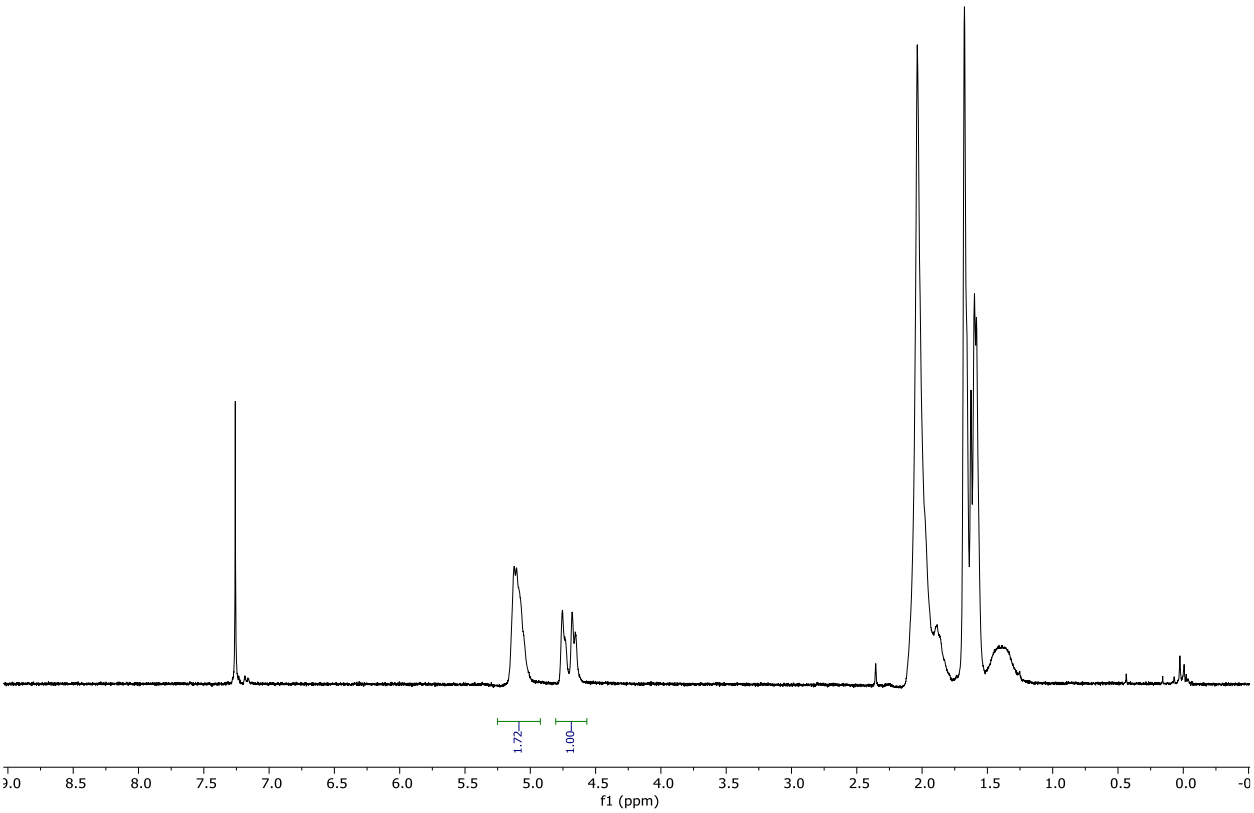

Figure 94. ^{1}H NMR spectrum (300 MHz, 25 °C, $CDCl_3$) of polyisoprene obtained using K[CaA′$_3$] (**2**) at RT.

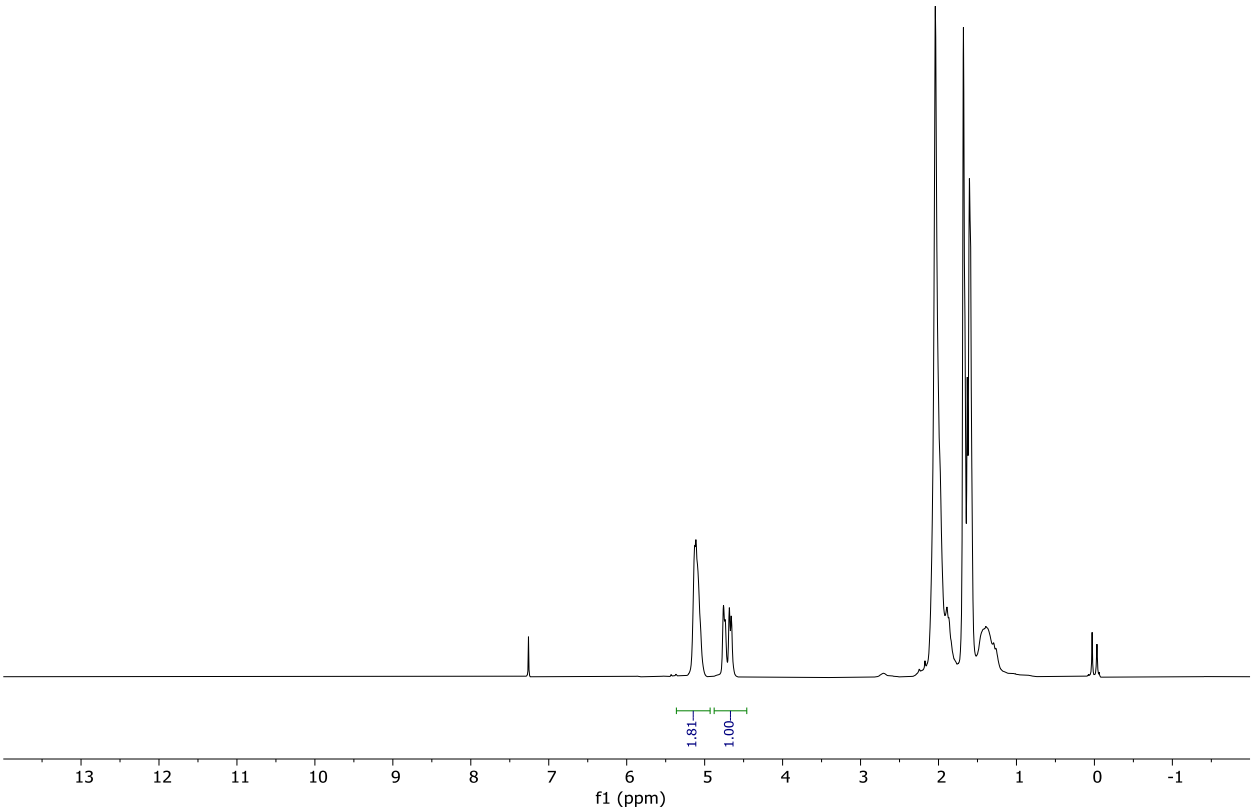

Figure 95. ^{1}H NMR spectrum (300 MHz, 25 °C, $CDCl_3$) of PMMA obtained using K[CaA'$_3$] (**2**) at 50 °C.

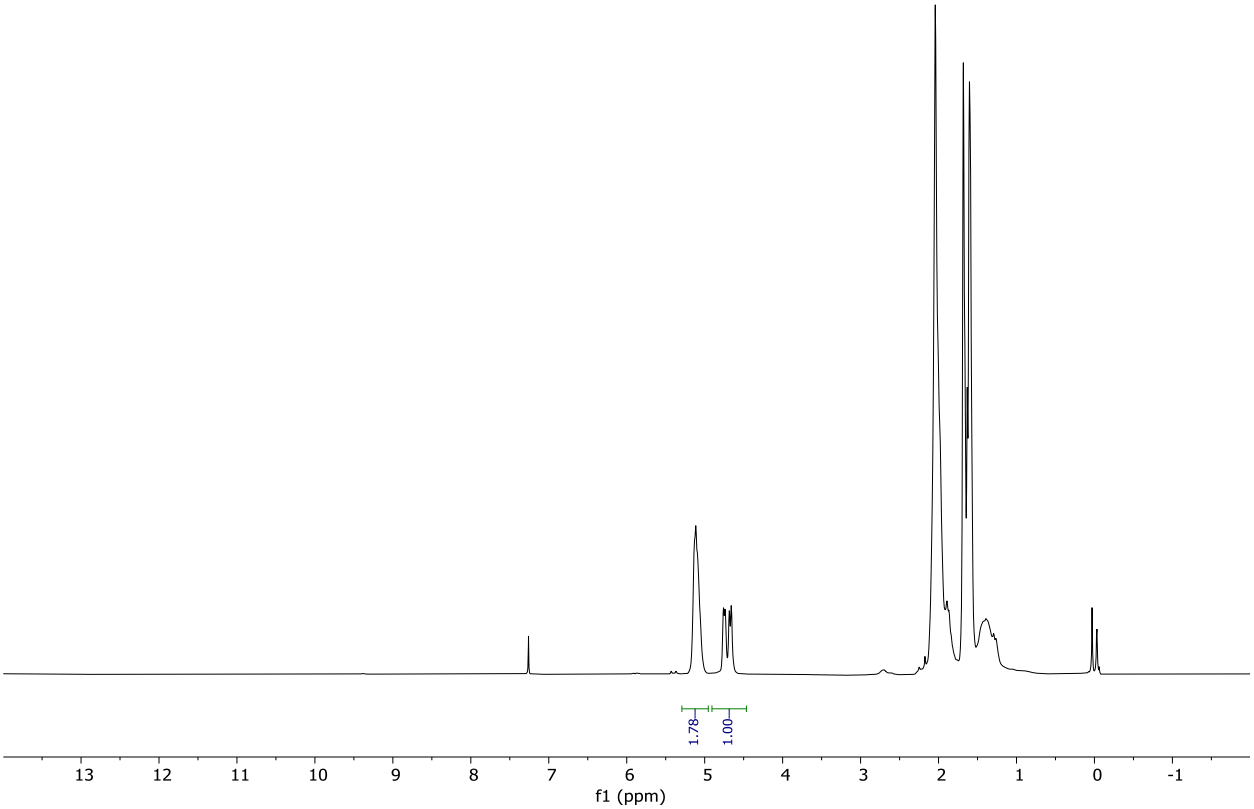

Figure 96. ^{1}H NMR spectrum (300 MHz, 25 °C, $CDCl_3$) of PMMA obtained using K[CaA'$_3$] (**2**) at 80 °C.

Table 20: Crystal Data and Summary of X–ray Data Collection of Calcium Compounds

Compound	**{KCa{1,3-(SiMe$_3$)$_2$C$_3$H$_3$}$_3$}$_n$ (2)**	**{[KCa{1,3-(SiMe$_3$)$_2$C$_3$H$_3$}$_3$•C$_6$D$_6$}$_n$ (2b)**	**{[KCa{1,3-(SiMe$_3$)$_2$C$_3$H$_3$}$_3$•C$_5$H$_9$Me}$_n$ (2c)**
Empirical formula	$C_{27}H_{63}CaKSi_6$	$C_{27}H_{63}CaKSi_6$•C_6D_6	$C_{27}H_{63}CaKSi_6$•C_6H_{12}
Formula weight	635.49	713.60	719.65
Color of compound	pale yellow	pale yellow	orange
Temperature/K	100.0(5)	100	183
Crystal system	monoclinic	monoclinic	monoclinic
Space group	$P2_1/m$	$P2_1/n$	$P2_1$
a/Å	11.235(2)	13.4801(3)	11.1995(10)
b/Å	17.338(3)	17.1263(3)	16.7329(11)
c/Å	11.856(2)	20.6565(3)	13.5654(13)
α/°	90	90	90
β/°	115.571(4)	104.8787(17)	111.347(11)
γ/°	90	90	90
Volume/Å^3	2083.4(7)	4608.96(14)	2367.7(4)
Z	2	4	2
ρ_{calc} g/cm^3	1.013	1.028	1.009
μ/mm^{-1}	0.437	3.604	3.507
F(000)	696	1560	792
Crystal size/mm^3	0.36 × 0.24 × 0.20	0.219 × 0.107 × 0.066	0.123 × 0.049 × 0.021
Radiation	MoKα (λ = 0.71073)	CuKα (λ = 1.5418)	CuKα (λ = 1.54184)
Θ range for data collect/°	1.904 to 29.629	3.40 to 73.43	3.498 to 68.106
Index ranges	-15 ≤ *h* ≤ 15, -24 ≤ *k* ≤ 24, -16 ≤ *l* ≤ 16	-16 ≤ *h* ≤ 15, -20 ≤ *k* ≤ 19, -23 ≤ *l* ≤ 25	-9 ≤ *h* ≤ 12, -19 ≤ *k* ≤ 19, -16 ≤ *l* ≤ 10
Reflections collected	30 710	35 462	8115
Independent reflections	6049 [R_{int} = 0.0445]	2407 [R_{int} = 0.0379, R_{sigma} = 0.0317]	5624 [R_{int} = 0.0524, R_{sigma} = 0.0959]
Data/restraints/parameters	6049/30/356	9099/0/388	5624/194/446
Goodness-of-fit on F^2	1.032	1.027	1.049
Final *R* indexes [$I > 2\sigma(I)$]	R_1 = 0.0457, wR_2 = 0.1162	R_1 = 0.0343, wR_2 = 0.0841	R_1 = 0.0711, wR_2 = 0.1640
Final *R* indexes [all data]	R1 = 0.0796, wR2 = 0.1398	R_1 = 0.0415, wR_2 = 0.0883	R1 = 0.0948, wR2 = 0.1803
Largest diff. peak/hole/e Å^{-3}	0.455/-0.184	0.404/-0.427	0.76/-0.73
Flack parameter	N/A	N/A	0.27(3)

6.5 References

(1) Beckmann, E. Einige Anwendungen von Metallischem Calcium. *Ber. Dtsch. Chem. Gesell.* **1905**, *38* (1), 904–906.

(2) Krieck, S.; Westerhausen, M. Reimagining the Grignard Reaction. *Encyclopedia of Inorganic and Bioinorganic Chemistry*. December 23, 2015, pp 1–17.

(3) Cotton, F. A.; Wilkinson, G. *Advanced Inorganic Chemistry: A Comprehensive Text.* 4th Ed.; Wiley: New York, 1980, p. 271.

(4) Westerhausen, M.; Gärtner, M.; Fischer, R.; Langer, J. Aryl Calcium Compounds: Syntheses, Structures, Physical Properties, and Chemical Behavior. *Angew. Chem. Int. Ed.* **2007**, *46* (12), 1950–1956.

(5) Harder, S., *Early Main Group Metal Catalysis: Concepts and Reactions*; Wiley-VCH: Weinheim, 2020; pp 31–57.

(6) Harder, S. The Chemistry of Ca^{II} and Yb^{II}: Astoundingly Similar But Not Equal! *Angew. Chem. Int. Ed.* **2004**, *43* (20), 2714–2718.

(7) Yildirim, I.; Crotty, S.; Loh, C. H.; Festag, G.; Weber, C.; Caponi, P.-F.; Gottschaldt, M.; Westerhausen, M.; Schubert, U. S. End-Functionalized Polylactides Using a Calcium-Based Precatalyst: Synthesis and Insights by Mass Spectrometry. *J. Polym. Sci. Part A Polym. Chem.* **2016**, *54* (3), 437–448.

(8) Yildirim, I.; Yildirim, T.; Kalden, D.; Festag, G.; Fritz, N.; Weber, C.; Schubert, S.; Westerhausen, M.; Schubert, U. S. Retinol Initiated Poly(Lactide)s: Stability upon Polymerization and Nanoparticle Preparation. *Polym. Chem.* **2017**, *8* (30), 4378–4387.

(9) Schuhknecht, D.; Lhotzky, C.; Spaniol, T. P.; Maron, L.; Okuda, J. Calcium Hydride Cation $[CaH]^+$ Stabilized by an *NNNN*-Type Macrocyclic Ligand: A Selective Catalyst for Olefin Hydrogenation. *Angew. Chem. Int. Ed.* **2017**, *56* (40), 12367–12371.

(10) Bauer, H.; Alonso, M.; Färber, C.; Elsen, H.; Pahl, J.; Causero, A.; Ballmann, G.; De Proft, F.; Harder, S. Imine Hydrogenation with Simple Alkaline Earth Metal Catalysts. *Nat. Catal.* **2018**, *1* (1), 40–47.

(11) Harder, S.; Martin, J.; Knüpfer, C.; Eyselein, J.; Färber, C.; Grams, S.; Langer, J.; Thum, K.; Wiesinger, M. Highly Active Superbulky Alkaline Earth Metal Amide Catalysts for Hydrogenation of Challenging Alkenes and Aromatic Rings. *Angew. Chem. Int. Ed.* **2020**, *n/a* (n/a).

(12) Schuhknecht, D.; Spaniol, T. P.; Maron, L.; Okuda, J. Regioselective Hydrosilylation of Olefins Catalyzed by a Molecular Calcium Hydride Cation. *Angew. Chem. Int. Ed.* **2020**, *59* (1), 310–314.

(13) Mukherjee, D.; Schuhknecht, D.; Okuda, J. Hydrido Complexes of Calcium: A New Family of Molecular Alkaline-Earth-Metal Compounds. *Angew. Chem. Int. Ed.* **2018**, *57* (31), 9590–9602.

(14) Jochmann, P.; Davin, J. P.; Spaniol, T. P.; Maron, L.; Okuda, J. A Cationic Calcium Hydride Cluster Stabilized by Cyclen-Derived Macrocyclic *N*,*N*,*N*,*N* Ligands. *Angew. Chem. Int. Ed.* **2012**, *51* (18), 4452–4455.

(15) Krieck, S.; Kalden, D.; Oberheide, A.; Seyfarth, L.; Arndt, H.-D.; Görls, H.; Westerhausen, M. Synthesis and Catalytic Activity of Tridentate N-(2-Pyridylethyl)-Substituted Bulky Amidinates of Calcium and Strontium. *Dalton Trans.* **2019**, *48* (7), 2479–2490.

(16) Ziemann, S.; Krieck, S.; Görls, H.; Westerhausen, M. 1,2-Bis(Anilido)Ethane Complexes of Calcium and Potassium: Synthesis, Structures, and Catalytic Activity. *Organometallics* **2018**, *37* (6), 924–933.

(17) Al-Shboul, T. M. A.; Görls, H.; Westerhausen, M. Calcium-Mediated Hydrophosphination of

Diphenylethyne and Diphenylbutadiyne as Well as Crystal Structure of 1,4-Diphenyl-1,4-Bis(Diphenylphosphanyl)Buta-1,3-Diene. *Inorg. Chem. Commun.* **2008**, *11* (12), 1419–1421.
(18) Younis, F. M.; Krieck, S.; Al-Shboul, T. M. A.; Görls, H.; Westerhausen, M. Calcium-Mediated Catalytic Synthesis of 1-(Diorganylamino)-1,4-Diphenyl-4-(Diphenylphosphanyl)Buta-1,3-Dienes. *Inorg. Chem.* **2016**, *55* (9), 4676–4682.
(19) Harder, S.; Spielmann, J. Calcium-Mediated Hydroboration of Alkenes: "Trojan Horse" or "True" Catalysis? *J. Organomet. Chem.* **2012**, *698*, 7–14.
(20) Wilson, A. S. S.; Hill, M. S.; Mahon, M. F.; Dinoi, C.; Maron, L. Organocalcium-Mediated Nucleophilic Alkylation of Benzene. *Science (80-.).* **2017**, *358* (6367).
(21) Hanusa, T. P. Ligand Influences on Structure and Reactivity in Organoalkaline Earth Chemistry. *Chem. Rev.* **1993**, *93* (3), 1023–1036.
(22) Hanusa, T. P. New Developments in the Cyclopentadienyl Chemistry of the Alkaline-Earth Metals. *Organometallics* **2002**, *21* (13), 2559–2571.
(23) Chmely, S. C.; Hanusa, T. P. Complexes with Sterically Bulky Allyl Ligands: Insights into Structure and Bonding. *European Journal of Inorganic Chemistry*. 2010, pp 1321–1337.
(24) Solomon, S. a; Layfield, R. a. The Coordination Chemistry of Silyl-Substituted Allyl Ligands. *Dalton Trans.* **2010**, *39*, 2469–2483.
(25) Lichtenberg, C.; Okuda, J. Structurally Defined Allyl Compounds of Main Group Metals: Coordination and Reactivity. *Angew. Chem. Int. Ed.* **2013**, *52* (20), 5228–5246.
(26) Koby, R. F.; Doerr, A. M.; Rightmire, N. R.; Schley, N. D.; Long, B. K.; Hanusa, T. P. An η^3-Bound Allyl Ligand on Magnesium in a Mechanochemically Generated Mg/K Allyl Complex. *Angew. Chem. Int. Ed.* **2020**, *132* (59), 9542–9549.
(27) Quisenberry, K. T.; White, R. E.; Hanusa, T. P.; Brennessel, W. W. Allyl Complexes of the Heavy Alkaline-Earth Metals: Molecular Structure and Catalytic Behavior. *New J. Chem.* **2010**, *34* (8), 1579–1584.
(28) Wilson, A. S. S.; Dinoi, C.; Hill, M. S.; Mahon, M. F.; Maron, L. Heterolysis of Dihydrogen by Nucleophilic Calcium Alkyls. *Angew. Chem., Int. Ed.* **2018**, *57* (47), 15500–15504.
(29) Chmely, S. C.; Carlson, C. N.; Hanusa, T. P.; Rheingold, A. L. Classical versus Bridged Allyl Ligands in Magnesium Complexes: The Role of Solvent. *J. Am. Chem. Soc.* **2009**, *131* (18), 6344–6345.
(30) Chmely, S. C.; Hanusa, T. P.; Brennessel, W. W. Bis(1,3-Trimethylsilylallyl)Beryllium. *Angew. Chem. Int. Ed.* **2010**, *49* (34), 5870–5874.
(31) Hernández, J. G.; Butler, I. S.; Friščić, T. Multi-Step and Multi-Component Organometallic Synthesis in One Pot Using Orthogonal Mechanochemical Reactions. *Chem. Sci.* **2014**, *5* (9), 3576–3582.
(32) Do, J.-L.; Friščić, T. Mechanochemistry: A Force of Synthesis. *ACS Cent. Sci.* **2017**, *3* (1), 13–19.
(33) Friščić, T.; Mottillo, C.; Titi, H. M. Mechanochemistry for Synthesis. *Angew. Chem. Int. Ed.* **2020**, *59* (3), 1018–1029.
(34) Hernández, J. G.; Bolm, C. Altering Product Selectivity by Mechanochemistry. *J. Org. Chem.* **2017**, *82* (8), 4007–4019.
(35) Kubota, K.; Takahashi, R.; Ito, H. Mechanochemistry Allows Carrying out Sensitive Organometallic Reactions in Air: Glove-Box-and-Schlenk-Line-Free Synthesis of Oxidative Addition Complexes from Aryl Halides and Palladium(0). *Chem. Sci.* **2019**, *10* (22), 5837–5842.
(36) Pang, Y.; Ishiyama, T.; Kubota, K.; Ito, H. Iridium(I)-Catalyzed C–H Borylation in Air by Using Mechanochemistry. *Chem.—Eur. J.* **2019**, *25* (18), 4654–4659.
(37) Rightmire, N. R.; Hanusa, T. P.; Rheingold, A. L. Mechanochemical Synthesis of [1,3-

$(SiMe_3)_2C_3H_3]_3$(Al,Sc), a Base-Free Tris(Allyl)Aluminum Complex and Its Scandium Analogue. *Organometallics* **2014**, *33* (21), 5952–5955.
(38) Koby, R. F.; Hanusa, T. P.; Schley, N. D. Mechanochemically Driven Transformations in Organotin Chemistry: Stereochemical Rearrangement, Redox Behavior, and Dispersion-Stabilized Complexes. *J. Am. Chem. Soc.* **2018**, *140* (46), 15934–15942.
(39) Shi, Y. X.; Xu, K.; Clegg, J. K.; Ganguly, R.; Hirao, H.; Friščić, T.; García, F. The First Synthesis of the Sterically Encumbered Adamantoid Phosphazane $P_4(N^tBu)_6$: Enabled by Mechanochemistry. *Angew. Chem. Int. Ed.* **2016**, *55* (41), 12736–12740.
(40) Lichtenberg, C.; Spaniol, T. P.; Peckermann, I.; Hanusa, T. P.; Okuda, J. Cationic, Neutral, and Anionic Allyl Magnesium Compounds: Unprecedented Ligand Conformations and Reactivity toward Unsaturated Hydrocarbons. *J. Am. Chem. Soc.* **2013**, *135* (2), 811–821.
(41) Boyde, C. N.; Rightmire, R. N.; Hanusa, P. T.; Brennessel, W. W. Symmetric Assembly of a Sterically Encumbered Allyl Complex: Mechanochemical and Solution Synthesis of the Tris(Allyl)Beryllate, K[BeA′ 3] (A′ = 1,3-$(SiMe_3)_2C_3H_3$). *Inorganics* **2017**, *5* (2), 36.
(42) Quisenberry, K. T.; Gren, C. K.; White, R. E.; Hanusa, T. P.; Brennessel, W. W. Trimethylsilylated Allyl Complexes of the Heavy Alkali Metals, M[1,3-$(SiMe_3)_2C_3H_3$]$(THF)_n$ (M = K, Cs). *Organometallics* **2007**, *26* (17), 4354–4356.
(43) Gren, C. K.; Hanusa, T. P.; Brennessel, W. W. Allyl Complexes of Heavy Group 13 Elements: Structure and Bonding in $[1,3\text{-}(SiMe_3)_2C_3H_3]_3Ga$. *Polyhedron* **2006**, *25* (2), 286–292.
(44) Bissette, A. J.; Fletcher, S. P. Mechanisms of Autocatalysis. *Angew. Chem. Int. Ed.* **2013**, *52* (49), 12800–12826.
(45) Quisenberry, K. T.; Smith, J. D.; Voehler, M.; Stec, D. F.; Hanusa, T. P.; Brennessel, W. W. Trimethylsilylated Allyl Complexes of Nickel. The Stabilized Bis(π-Allyl)Nickel Complex $[\eta^3\text{-}1,3\text{-}(SiMe_3)_2C_3H_3]_2Ni$ and Its Mono(π-Allyl)NiX (X = Br, I) Derivatives. *J. Am. Chem. Soc.* **2005**, *127* (12), 4376–4387.
(46) Pauling, L. *The Nature of the Chemical Bond*, 3rd ed.; Cornell University Press: Ithaca, 1960.
(47) Howard, J. L.; Brand, M. C.; Browne, D. L. Switching Chemoselectivity: Using Mechanochemistry to Alter Reaction Kinetics. *Angew. Chem. Int. Ed.* **2018**, *57* (49), 16104–16108.
(48) Užarević, K.; Halasz, I.; Friščić, T. Real-Time and In Situ Monitoring of Mechanochemical Reactions: A New Playground for All Chemists. *J. Phys. Chem. Lett.* **2015**, *6* (20), 4129–4140.
(49) Užarević, K.; Ferdelji, N.; Mrla, T.; Julien, P. A.; Halasz, B.; Friščić, T.; Halasz, I. Enthalpy vs. Friction: Heat Flow Modelling of Unexpected Temperature Profiles in Mechanochemistry of Metal–Organic Frameworks. *Chem. Sci.* **2018**, *9* (9), 2525–2532.
(50) Speight, I. R.; Huskić, I.; Arhangelskis, M.; Titi, H. M.; Stein, R. S.; Hanusa, T. P.; Friščić, T. Disappearing Polymorphs in Metal–Organic Framework Chemistry: Unexpected Stabilization of a Layered Polymorph over an Interpenetrated Three-Dimensional Structure in Mercury Imidazolate. *Chem. Eur. J.* **2020**, *26* (8), 1811–1818.
(51) Halasz, I.; Kimber, S. A. J.; Beldon, P. J.; Belenguer, A. M.; Adams, F.; Honkimäki, V.; Nightingale, R. C.; Dinnebier, R. E.; Friščić, T. In Situ and Real-Time Monitoring of Mechanochemical Milling Reactions Using Synchrotron X-Ray Diffraction. *Nat. Protoc.* **2013**, *8*, 1718.
(52) Friščić, T.; Halasz, I.; Beldon, P. J.; Belenguer, A. M.; Adams, F.; Kimber, S. A. J.; Honkimäki, V.; Dinnebier, R. E. Real-Time and in Situ Monitoring of Mechanochemical Milling Reactions. *Nat. Chem.* **2013**, *5*, 66.
(53) Gracin, D.; Štrukil, V.; Friščić, T.; Halasz, I.; Užarević, K. Laboratory Real-Time and In Situ Monitoring of Mechanochemical Milling Reactions by Raman Spectroscopy. *Angew. Chem., Int. Ed.* **2014**, *53*, 6193.

(54) Batzdorf, L.; Fischer, F.; Wilke, M.; Wenzel, K.-J.; Emmerling, F. Direct In Situ Investigation of Milling Reactions Using Combined X-Ray Diffraction and Raman Spectroscopy. *Angew. Chem. Int. Ed.* **2015**, *54* (6), 1799–1802.
(55) Lukin, S.; Stolar, T.; Tireli, M.; Blanco, M. V; Babić, D.; Friščić, T.; Užarević, K.; Halasz, I. Tandem In Situ Monitoring for Quantitative Assessment of Mechanochemical Reactions Involving Structurally Unknown Phases. *Chem. Eur. J.* **2017**, *23*, 13941.
(56) Gallivan, J. P.; Dougherty, D. A. Cation-π Interactions in Structural Biology. *Proc. Natl. Acad. Sci.* **1999**, *96* (17), 9459 LP – 9464.
(57) Cheng, Y.-H.; Liu, L.; Fu, Y.; Chen, R.; Li, X.-S.; Guo, Q.-X. Counterion Effects on the Cation–π Interaction between Alkaline Earth Cations and Benzene. *J. Phys. Chem. A* **2002**, *106* (46), 11215–11220.
(58) Tomasi, J.; Mennucci, B.; Cammi, R. Quantum Mechanical Continuum Solvation Models. *Chem. Rev.* **2005**, *105* (8), 2999–3094.
(59) Gren, C. K.; Hanusa, T. P.; Rheingold, A. L. Threefold Cation-π Bonding in Trimethylsilylated Allyl Complexes. *Organometallics* **2007**, *26* (7), 1643–1649.
(60) Layfield, R. A.; García, F.; Hannauer, J.; Humphrey, S. M. Ansa-Tris(Allyl) Complexes of Alkali Metals: Tripodal Analogues of Cyclopentadienyl and Ansa-Metallocene Ligands. *Chem. Commun.* **2007**, *499* (47), 5081–5083.
(61) Jochmann, P.; Maslek, S.; Spaniol, T. P.; Okuda, J. Allyl Calcium Compounds: Synthesis and Structure of Bis(H3-1-Alkenyl)Calcium. *Organometallics* **2011**, *30* (7), 1991–1997.
(62) Hitchcock, P. B.; Khvostov, A. V; Lappert, M. F. Synthesis and Structures of Crystalline Bis(Trimethylsilyl)Methanido Complexes of Potassium, Calcium and Ytterbium. *J. Organomet. Chem.* **2002**, *663* (1), 263–268.
(63) Simpson, C. K.; White, R. E.; Carlson, C. N.; Wrobleski, D. A.; Kuehl, C. J.; Croce, T. A.; Steele, I. M.; Scott, B. L.; Young Victor G.; Hanusa, T. P.; Sattelberger, A. P.; John, K. D. The Role of Alkali Metal Cations in MMA Polymerization Initiated by Neutral and Anionic Allyl Lanthanide Complexes. *Organometallics* **2005**, *24* (15), 3685–3691.
(64) Woodman, T. J.; Schormann, M.; Hughes, D. L.; Bochmann, M. Sterically Hindered Lanthanide Allyl Complexes and Their Use as Single-Component Catalysts for the Polymerization of Methyl Methacrylate and ε-Caprolactone. *Organometallics* **2004**, *23* (12), 2972–2979.
(65) White, R. E. PhD Thesis, Vanderbilt University, 2006.
(66) Su, W.-F. Ionic Chain Polymerization BT - Principles of Polymer Design and Synthesis; Su, W.-F., Ed.; Springer Berlin Heidelberg: Berlin, Heidelberg, 2013; pp 185–218.
(67) Parry, A. Anionic Polymerization. In *React., Mech. Struct. Polym. Chem.*; Wiley, 1974; pp 350–382.
(68) Boffa, L. S.; Novak, B. M. *Transition Metal Catalysis in Macromolecular Design*; American Chemical Society, 2000.
(69) Szwarc, M. Living Polymers and Mechanisms of Anionic Polymerization. *Living Polym. Mech. Anionic Polym.* **1983**, *49*, 1–177.
(70) Hatada, K.; Shinozaki, T.; Ute, K.; Kitayama, T. Preparation of PMMA Macromers by O-Vinylbenzylmagnesium Chloride and Their Polymerization. *Polym. Bull.* **1988**, *19* (3), 231–237.
(71) Hatada, K.; Nakanishi, H.; Ute, K.; Kitayama, T. Studies on *p*- and *m*-Vinylbenzylmagnesium Chlorides as Initiators and Monomers—Preparations of Macromers and Poly(Grignard Reagent). *Polym. J.* **1986**, *18* (8), 581–591.
(72) Hatada, K.; Ute, K.; Tanaka, K.; Okamoto, Y.; Kitayama, T. Living and Highly Isotactic Polymerization of Methyl Methacrylate by *t*-C_4H_9MgBr in Toluene. *Polym. J.* **1986**, *18* (12),

1037–1047.
(73) Feil, F. PhD Thesis, Universität Konstanz, 2002.
(74) Nuyken, O. *Neodymium Based Ziegler Catalysts-Fundamental Chemistry*; Nuyken, O., Ed.; Springer: Berlin Heidelberg, 2006; Vol. 204.
(75) Jochmann, P.; Dols, T. S.; Spaniol, T. P.; Perrin, L.; Maron, L.; Okuda, J. Bis(Allyl)Calcium. *Angew. Chem. Int. Ed.* **2009**, *48* (31), 5715–5719.
(76) Nakhmanovich, B. I.; Basova, R. V; Arest-yakubovich, A. A. Anionic Polymerization and Copolymerization of Hydrocarbon Monomers Catalyzed by Organobarium Initiators. *J. Macromol. Sci. Part A - Chem.* **1975**, *9* (4), 575–596.
(77) *Michelin et Cie*; Comp. General. Etabl. Michelin; 1971.
(78) Tan, D.; Loots, L.; Friščić, T. Towards Medicinal Mechanochemistry: Evolution of Milling from Pharmaceutical Solid Form Screening to the Synthesis of Active Pharmaceutical Ingredients (APIs). *Chem. Commun.* **2016**, *52* (50), 7760–7781.
(79) Fraenkel, G.; Chow, A.; Winchester, W. R. Dynamics of Solvated Li^+ within *Exo*,*Exo*-[1,3-Bis(Trimethylsilyl)Ally]Lithium *N*,*N*,*N*',*N*'-Tetramethylethylenediamine Complex. *J. Am. Chem. Soc.* **1990**, *112*, 1382–1386.
(80) Armarego, W. L. F.; Chai, C. L. L. Chapter 1 - Common Physical Techniques Used in Purification; Armarego, W. L. F., Chai, C. L. L. (Sixth E., Eds.; Butterworth-Heinemann: Oxford, 2009; pp 1–60.
(81) Ober, C. K. Polymer Tacticity in Simulated NMR Spectra. *J. Chem. Educ.* **1989**, *66* (8), 645.
(82) Strauch, J. W.; Fauré Jean-Luc; Bredeau, S.; Wang, C.; Kehr, G.; Fröhlich, R.; Luftmann, H.; Erker, G. (Butadiene)Metallocene/$B(C_6F_5)_3$ Pathway to Catalyst Systems for Stereoselective Methyl Methacrylate Polymerization: Evidence for an Anion Dependent Metallocene Catalyzed Polymerization Process. *J. Am. Chem. Soc.* **2004**, *126* (7), 2089–2104.
(83) Jia, X.; Zhang, X.; Gong, D. 1,2 Enriched Polymerization of Isoprene by Cobalt Complex Carrying Aminophosphory Fused (PN_3) Ligand. *J. Polym. Sci. Part A Polym. Chem.* **2018**, *56* (20), 2286–2293.
(84) Yu, C.; Zhou, D.; Yan, X.; Gao, F.; Zhang, L.; Zhang, S.; Li, X. Cis-1,4-Polymerization of Isoprene by 1,3-Bis(Oxazolinymethylidene)Isoindoline-Ligated Rare-Earth Metal Dialkyl Complexes. *Polymers* . 2017.
(85) Ricci, G.; Leone, G.; Boglia, A.; Boccia, A. C.; Zetta, L. *Cis*-1,4-*Alt*-3,4 Polyisoprene: Synthesis and Characterization. *Macromolecules* **2009**, *42* (23), 9263–9267.
(86) Bruker. APEX2. Bruker AXXS: Madison, Wisconsin, USA 2013.
(87) Sheldrick, G. SADABS. University of Göttingen: Göttingen, Germany 2012.
(88) Bruker. SAINT. Bruker AXS Inc.: Madison, Wisconsin, USA 2012.
(89) Sheldrick, G. SHELXT - Integrated Space-Group and Crystal-Structure Determination. *Acta Crystallogr. Sect. A* **2015**, *71* (1), 3–8.
(90) Sheldrick, G. Crystal Structure Refinement with SHELXL. *Acta Crystallogr. Sect. C* **2015**, *71* (1), 3–8.
(91) Dolomanov, O. V; Bourhis, L. J.; Gildea, R. J.; Howard, J. A. K.; Puschmann, H. OLEX2: A Complete Structure Solution, Refinement and Analysis Program. *J. Appl. Crystallogr.* **2009**, *42* (2), 339–341.
(92) M. J. Frisch, G. W. Trucks, H. B. Schlegel, G. E. Scuseria, M. A. Robb, J. R. Cheeseman, G. Scalmani, V. Barone, G. A. Petersson, H. Nakatsuji, X. Li, M. Caricato, A. Marenich, J. Bloino, B. G. Janesko, R. Gomperts, B. Mennucci, H. P. Hratchian, J. V. Ort, and D. J. F. Gaussian09. *http://www. gaussian. com/*. Gaussian, Inc.: Wallingford CT 2009.
(93) M. J. Frisch, G. W. Trucks, H. B. Schlegel, G. E. Scuseria, M.; A. Robb, J. R. Cheeseman, G. Scalmani, V. Barone, B. Mennucci, G. A. Petersson, H.; Nakatsuji, M. Caricato, X. Li, H. P.

Hratchian, A. F. Izmaylov, J. Bloino, G. Zheng, J. L.; Sonnenberg, M. Hada, M. Ehara, K. Toyota, R. Fukuda, J. Hasegawa, M. Ishida, T.; Nakajima, Y. Honda, O. Kitao, H. Nakai, T. Vreven, J. A. Montgomery, Jr., J. E. Peralta, F.; Ogliaro, M. Bearpark, J. J. Heyd, E. Brothers, K. N. Kudin, V. N. Staroverov, R.; Kobayashi, J. Normand, K. Raghavachari, A. Rendell, J. C. Burant, S. S. Iyengar, J.; Tomasi, M. Cossi, N. Rega, J. M. Millam, M. Klene, J. E. Knox, J. B. Cross, V. Bakken, C.; Adamo, J. Jaramillo, R. Gomperts, R. E. Stratmann, O. Yazyev, A. J. Austin, R. Cammi, C.; Pomelli, J. W. Ochterski, R. L. Martin, K. Morokuma, V. G. Zakrzewski, G. A. Voth, P.; Salvador, J. J. Dannenberg, S. Dapprich, A. D. Daniels, Ö. Farkas, J. B. Foresman, J. V.; Ortiz, J. Cioslowski, and D. J. Fox, Gaussian, Inc., Wallingford CT, 2009. Gaussian16 Revision D.01. *http//www. gaussian. com/* **2009**.

(94) Becke, A. D. Density-Functional Exchange-Energy Approximation with Correct Asymptotic Behavior. *Phys. Rev. A At. Mol. Opt. Phys.* **1988**, *38* (6), 3098–3100.

(95) Perdew, J. P.; Wang, Y. Accurate and Simple Analytic Representation of the Electron-Gas Correlation Energy. *Phys. Rev. B* **1992**, *45* (23), 13244–13249.

(96) Grimme, S.; Antony, J.; Ehrlich, S.; Krieg, H. A Consistent and Accurate Ab Initio Parametrization of Density Functional Dispersion Correction (DFT-D) for the 94 Elements H-Pu. *J. Chem. Phys.* **2010**, *132* (15), 154104.

(97) Grimme, S.; Ehrlich, S.; Goerigk, L. Effect of the Damping Function in Dispersion Corrected Density Functional Theory. *J. Comput. Chem.* **2011**, *32* (7), 1456–1465.

(98) Rappoport, D.; Furche, F. Property-Optimized Gaussian Basis Sets for Molecular Response Calculations. *J. Chem. Phys.* **2010**, *133* (13), 134105.

Chapter 7

Di(indenyl)beryllium

7.1 Introduction

Among the many accomplishments of E. O. Fischer and his coworkers was the synthesis of beryllocene, $[Be(C_5H_5)_2]$, in 1959.[1] It and its substituted derivatives have been among the most intensively studied main-group metallocenes, an interest that started with the discovery of beryllocene's nonzero dipole moment (2.24 *D* in C_6H_{12} at 25 °C),[1] ruling out a ferrocene-like structure with D_{5h} or D_{5d} symmetry. The results of electron diffraction data,[2,3] Raman spectroscopy,[4] and X-ray diffraction,[5–7] bolstered with molecular dynamics[8,9] and density functional theory calculations,[10] eventually converged on an η^5-η^1 "slip-sandwich" structure in the solution and solid state (Figure 97a). Among the substituted beryllocenes are various methylated versions, including the bulky $[Be(C_5Me_5)_2]$, which uniquely possesses a η^5-η^5 structure and appreciably longer Be–C bonds than other beryllocenes.

Despite potential for use in hydrogen storage, catalysis, and other fields, beryllium chemistry is severely understudied. Much of "classic" organoberyllium chemistry in fact stems from the work of Geoffrey Coates from the 1950s–1970s.[11–14] Beryllium chemistry is often discouraged or prohibited due to its reputation for toxicity and carcinogenicity, which has resulted in starting materials becoming increasingly difficult to obtain or banned. Chronic beryllium disease / berylliosis are well documented in the manufacturing industry from aerosolized beryllium particles, and consequently the danger of beryllium compounds themselves is treated similarly, as it is not well understood.[15–17] These factors, along with a focus on organotransition metal chemistry, have resulted in a drought of beryllium chemistry since Coates' work. Specifically, the homoleptic organoberyllium compounds that have been crystallographically characterized almost exclusively contain alkyl- or cyclopentadienyl substituents. In this work, we report the expansion of this series to include a di-indenylberyllium species with (η^5-η^1) bonding.

The indenyl ligand has long been considered to be an analog of the cyclopentadienyl anion (Fischer prepared $[Fe(C_9H_7)_2]$ in 1953),[18] but because of its benzo moiety, the indenyl anion is able to undergo changes in ligation (e.g., $\eta^5 \rightleftarrows \eta^3$) more easily than $[Cp]^-$. It could alter the delicate balance between Be–C bond strength, favored by σ-bonding, and Cp delocalization energy, favored by π-bonding.[19] Curiously, no organoberyllium complexes containing indenyl ligands have ever been reported, although they are known for all of the rest of the non-radioactive s-block elements.[20–22] We hope that our efforts herein will add

to our fundamental knowledge of Be–C carbon bonding, and close the gap as the last missing class of indenyl complexes of the s-block elements.

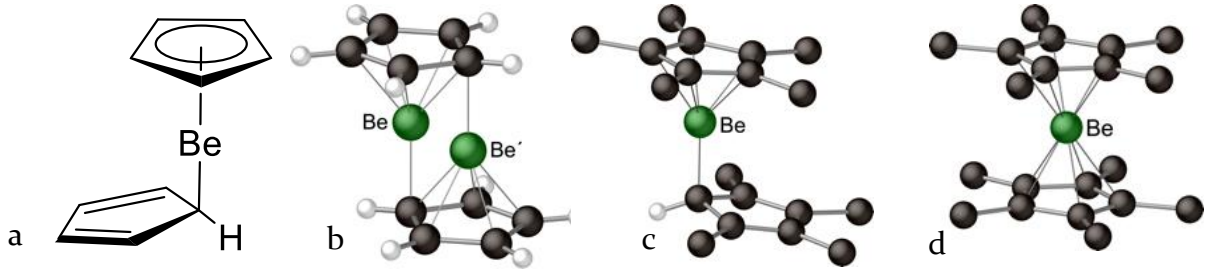

Figure 97. a) Schematic of the bonding in the monomeric [Be(C_5H_5)$_2$]; b) beryllocene as found in the solid state (the Be and Be′ are each at one-half occupancy); c) structure of the mixed ring beryllocene [Be(η^5-C_5Me_5)(η^1-C_5Me_4H)]; structure of the η^5-η^5 structure of [Be(C_5Me_5)$_2$].

7.2 Results and Discussion

In our pursuit of a beryllium indenyl compound, a halide metathesis between 2 equiv. K[1,3-TMS_2Ind] and $BeBr_2$ in THF was attempted. The result was an intractable mixture of indenyl compounds with an extremely broad signal in the ^{9}Be NMR spectrum at 3.6 ppm, which could correspond to solvated starting material or beryllium indenyl products.[23] A halide test on this reaction mixture using $AgNO_3$ lead to a large amount of cream-colored precipitate and reduced silver. Unfortunately, even after surveying the literature and calculating shifts for a variety of possible or related compounds, it is difficult to say more besides definitively stating that there is some halide-containing material present. There may be starting material ($BeBr_2$•THF_x), decomposition products relating to solvent, or partial substitution products (e.g., [Be(1,3-TMS_2Ind)Br•$(THF)_x$])

The difficulty in assembling beryllium sandwich compounds has been observed before (e.g., the synthesis of decamethylberyllocene stops at Cp*BeX if forcing conditions are not used).[24,25] For this reason, multiple attempts under harsher conditions were made to achieve complete indenyl substitution. High temperature reflux in 1:1 toluene:diethyl ether for 3.5 days, as used by the Carmona group for synthesizing Cp^*_2Be, resulted only in the formation of decomposition products with no ^{9}Be NMR signal from a hexane extract of the reaction mixture. However, analyzing the reaction after just 18 hours shows 2 signals, at δ = 3.97 and -17.3 ppm. The signal at -17.3 ppm is close to the shift of -18.5 reported for [Cp_2Be] in toluene,[26] allowing us to tentatively identify the signal as a beryllium indenyl complex, if not the fully substituted [(1,3-TMS_2Ind)$_2$Be]. Unfortunately, due to the mixture of presumed beryllium indenyl product, starting material, and decomposition, the beryllium-containing product was not separable from the oily mixture, and since longer reactions results in more decomposition, these conditions are unlikely to allow isolation of the desired product.

Given our recent successes in mechanochemical synthesis,[27–32] we hoped that ball milling could provide a simpler, faster, safer, and cleaner route to this new compound. Grinding and milling reagents together without solvent has emerged in recent years as a powerful method for synthesizing organometallic molecule that that would otherwise been inaccessible owing to deleterious interactions with solvents.[33] After milling K[1,3-TMS_2Ind] and $BeBr_2$ together for 15 minutes, followed by extraction of the ground mixture with minimal hexanes, an almost colorless oil is obtained from evaporation of the filtrate. The oil solidified into tan-to-colorless needles that in C_6D_6 provided an ^{1}H NMR spectrum corresponding to one set of indenyl signals different from those of K[1,3-TMS_2Ind]. The ^{9}Be NMR spectrum again consisted of a singlet at δ -17.3 ppm.

A single crystal X-ray analysis revealed the sample to be the mono(indenyl) species [Be(1,3-TMS_2Ind)Br] (Figure 98). The compound is monomeric, which unlike related Cp*BeX structures,[34] does not display obvious intermolecular interactions in the solid state. The beryllium atom is bonded in an η^5-manner to the 5-membered ring of the indenyl ligand. Consistent with the asymmetry in the indenyl ligand compared to the C_5-symmetric Cp*, the spread of Be–C distances in **1** (1.86–1.93 Å, Δ = 0.07 Å) is considerably larger than in the Cp* analogue (Δ = 0.008 Å).

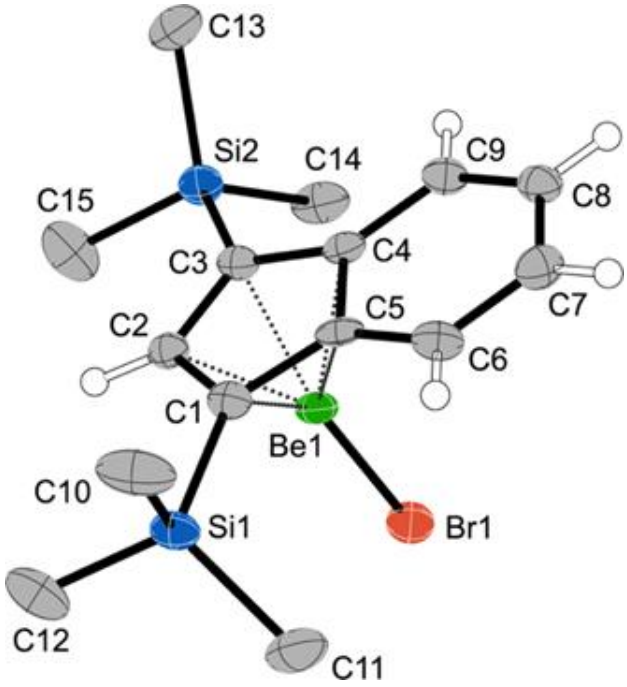

Figure 98. Thermal ellipsoid plot (50% level) of [Be(1,3-$TMS)_2C_9H_5$)] (**1**); for clarity, hydrogen atoms have been removed from the trimethylsilyl groups. Selected bond distances (Å) and angles (°): Be1–Br1, 2.039(8); Be1–C1, 1.883(10); Be1–C2, 1.857(9); Be1–C3, 1.882(10); Be1–C4, 1.926(10); Be1–C5, 1.925(10); C1–C2, 1.436(8); C1–C5, 1.438(9); C2–C3, 1.425(8); C3–C4, 1.444(9); C4–C5, 1.449(8); C1–Si1 1.871(6); C3–Si2 1.888(6); Be1–Ω, 1.447; Br1–Be1–Ω, 172.1.

Longer ball milling reactions or liquid-assisted grinding (LAG) with toluene were attempted to achieve full substitution on the beryllium center, but did not change the reaction outcome, yielding only **1**. Although there is a danger in concluding from the failure of synthetic attempts that a compound is not isolable with standard synthetic approaches (this was at one time thought to be the case for [Cp*$_2$Be]), this may truly be the case for [Be(1,3-TMS$_2$Ind)$_2$]. DFT calculations indicate that although an η^5-η^1 form of [Be(1,3-TMS$_2$Ind)$_2$] is a minimum on the PES, its $G_{complex}$ value, a measure of the occupancy of the coordination sphere,[35] is 91.9%, which may be prohibitively congested for such a small metal (see section 7.2.1 and Appendix,).

After coming to the conclusion that complete indenyl substitution with the 1,3-TMS$_2$Ind ligand was unlikely to be a promising avenue, the parent indenyl anion was used in attempts to isolate a bis(indenyl) complex. As with **1**, the reaction of K[C$_9$H$_7$] and BeBr$_2$ in THF yielded a product with ^{1}H NMR resonances that may correspond to the parent indene, and ^{9}Be NMR reveals a sharp resonance at 3.3 ppm, which given the broad, uninterpretable resonances in the proton NMR spectrum, can likely be attributed to solvated BeBr$_2$ or decomposition products (also observed in reactions with K[1,3-TMS$_2$Ind] in THF), as a small amount of white smoke is released if BeBr$_2$ is added quickly to THF.[23] The reaction mixture was evaporated and re-extracted with hexanes, then filtered through a fine glass fritted funnel. This yielded no residue, which in addition to the previous ^{9}Be NMR resonance, points to solvated BeBr$_2$ or otherwise hexane-insoluble decomposition products. The reaction between K[C$_9$H$_7$] and BeBr$_2$ was repeated in Et$_2$O overnight, and the C$_6$D$_6$ extraction of the dried reaction mixture showed no identifiable beryllium or indenyl signals in ^{1}H or ^{9}Be spectra. Based on these experiments, a solution route to an isolable and characterizable beryllium complex with unsubstituted indenyl ligands(s) seemed unfeasible.

Again, we turned to ball milling as a solution. When a 2:1 mixture of K[C$_9$H$_7$] and BeBr$_2$ is milled for 15 minutes, a hexanes extract of the ground solid can be filtered to leave a colorless solution that upon evaporation leaves a clear, colorless oil (**2**). The oil crystallizes extremely rapidly into small colorless blocks when mechanically disturbed. ^{1}H NMR spectra of **2** contained resonances consistent with a coordinated indenyl ligand, and intriguingly, ^{9}Be NMR displayed a single peak at δ = -19.1 ppm.

Eventually, crystalline blocks of **2** large enough for a single crystal X-ray study were obtained, and they proved to be of the di(indenyl) complex [Be(C$_9$H$_7$)$_2$] (Figure 99). The molecules are monomeric and comprise a mixed hapticity (η^5-η^1) metallocene with marked similarities to that of beryllocene. The two compounds in fact crystallize in the same monoclinic space group ($P2_1/c$, with Z = 4) but **2** does not display the 2-fold disorder found in [Be(C$_5$H$_5$)$_2$], which blends the structural parameters of the rings and makes the locations of the hydrogens more ambiguous than normal. The crystals of **2** in fact provided a very high-quality structure, in which all the hydrogens were located and their positions refined

with isotropic thermal parameters. The molecules are well-separated, with no geometric distortions that could be assigned to crystal packing (the closest intermolecular H···H′ contact is at 2.57 Å, outside the sum of the van der Waals' radii for hydrogen of 2.4 Å).[36]

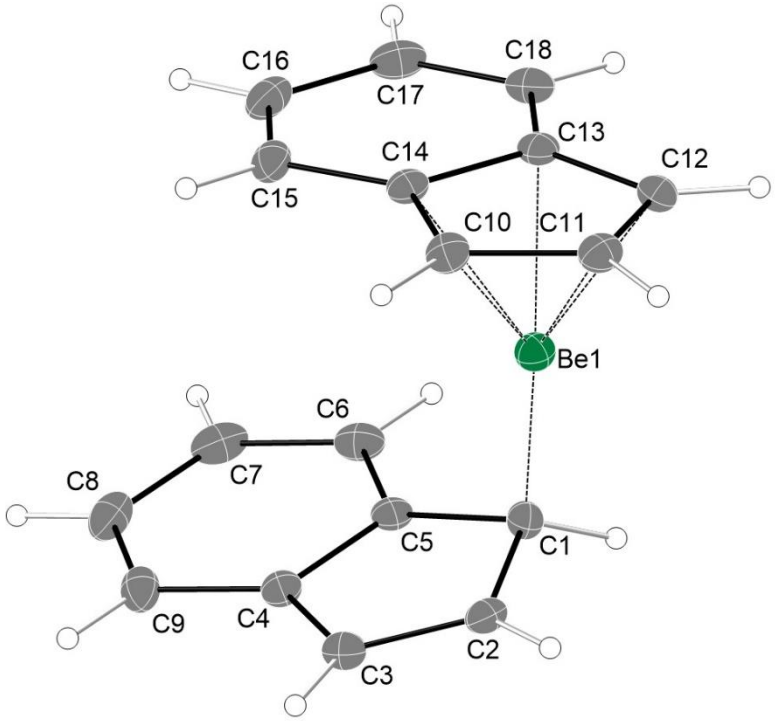

Figure 99. Thermal ellipsoid plot (50% level) of $[Be(C_9H_7)_2]$ (**2**). Selected bond distances (Å) and angles (°): Be1–C1, 1.746(2); C1–C2, 1.479(1); C1–C5, 1.482(1); C2–C3, 1.356(1); C3–C4, 1.449(1); C4–C5, 1.419(1); Be1–C10, 1.893(2); Be1–C11, 1.875(2); Be1–C12, 1.887(2); Be1–C13, 1.950(2); Be1–C14, 1.950(2); C10–C11 1.417(2); C10–C14 1.433(1); C11–C12, 1.418(1); C12–C13 1.433(1); C13–C14, 1.442(1); Be1–Ω, 1.475; C1–Be1–Ω, 174.9; Be1–C1–C2, 102.56(8); Be1–C1–C5, 104.51(8); Be1–C1–H1, 108.4(8).

It is particularly interesting / exculpatory that the two indenyls are unique and coordinated to just one beryllium center, as small changes in light group 2 coordination environments can cause significant structural changes. This is exemplified by the structure of $[Mg(C_9H_7)_2]$ vs magnesocene, and our previous investigation of magnesium allyls. Magnesocene is isostructural to ferrocene, while $[Mg(C_9H_7)_2]$ has a complicated polymeric structure where each magnesium center appears to be η^5, η^1, and η^2 coordinated to a mix of terminal and bridging indenyls.[20,37] However, the di-THF solvated $[Mg(THF)_2(C_9H_7)_2]$ has two η^3-coordinated indenyls.[38] The small size and lack of directional orbitals is one common explanation for this sensitivity, but a more nuanced argument is that Mg and Be sit at the interface of the ionic-covalent divide.

The average Be–C distance to the η^5-bonded ring is 1.911(4) Å, (1.475 Å to the ring centroid), very close to the comparable distances in the octa- and nonamethyl beryllocenes ($[Be(C_5Me_4H)_2]$ and $[Be(C_5Me_4H)(C_5Me_5)]$, respectively, and slightly shorter than in the

parent [Be(C_5H_5)$_2$] (1.505 Å). All of these are noticeably shorter than the analogous 1.655(1) Å distance found in the sterically crowded decamethyl derivative [Be(η^5-C_5Me_5)$_2$]. Just like other known beryllocene analogs, **2** exhibits fluctional ring behavior even at low temperature.[25,39,40] This can be seen in the ^{1}H and ^{9}Be NMR spectrum in C_7D_8 at -70 °C, though the ^{9}Be resonance does become significantly more broad (see Appendix).

The parallels with the octa- and nona-methylberyllocenes extend to the Be–C(H) bond to the η^1-ring in **2**. At 1.746(2) Å, it is similar to the 1.77 Å distance found in the methylated beryllocenes, and again shorter than in beryllocene itself (1.826(6) Å], though that is an averaged value due to the disordered η^1-η^5 rings.

7.2.1 Computational work

Despite the large body of work on beryllocene, the only reference to indenylberyllium compounds in the open literature is work on MNDO calculations where Be is used as a d-electron free surrogate for transition metals.[41] It was calculated that the Be atom would be slightly more stable η^1-bonded to indenyl over the η^5 form, but this was discounted because MNDO is known to underestimate multicenter bonding (e.g., the η^5 form). To determine a reasonable modern computational method, calculations with a variety of functionals were performed on beryllocene and [Be(^{4Me}Cp)$_2$], with B3PW91 matching experimental values closely.

After determining that B3PW91 would be a reliable functional to use with this beryllium chemistry, we set out to answer a few questions that were amenable to computational investigation. These included identification of presumably solvated species from solution-phase reactions, and understanding the structural and thermodynamic differences between beryllium Cp and indenyl complexes, both in substituted and unsubstituted forms. Unfortunately, calculations on a variety of hypothetical compounds with multiple functionals and basis sets were unable to identify any of the unknown ^{9}Be NMR signals. See Appendix for details.

Given the decomposition of the K[(1,3-TMS_2Ind)] reaction in solution and identification of a partial substitution product **1** only at higher temperature, it is unlikely that a di-indenyl complex [Be(1,3-TMS_2Ind)$_2$] is being formed at all; at high (or any) temperature it may be unstable and rapidly decompose once formed. Alternatively, due to the bulk of the trimethylsilyl groups, the [1,3-TMS_2Ind]$^-$ anion may bind more weakly than the parent indenyl. This may allow preferential interaction with ethereal solvents, preventing substitution of the remaining bromide with a second indenyl ligand.

We hypothesized that the increased steric bulk of 1,3-TMS_2Ind actually resulted in a weaker Be-C bond, with the resulting instability explaining our inability to isolate [Be(TMS_2Ind)$_2$]. To investigate this computationally, metal-ligand bond dissociation free energies were calculated from the reaction:

$$[BeL_2] \rightarrow [LBe]^+ + L^-$$

by optimizing and then obtaining the Gibbs free energy of each species, and solving for the energy difference for the left and right side of the reaction. As seen in table 21, while $[Be(Cp)_2]$ and $[Be(Ind)_2]$ have similar BDE values for the loss of one anionic ligand, the trimethylsilylated indenyl results in a lower BDE by almost 25 kcal mol^{-1}. This may be indicative of a significantly weaker M-C bond, which may explain our inability to isolate $[Be(1,3\text{-}TMS_2Ind)_2]$. For more details, see the Appendix.

Table 21: BDE calculations of $[BeL_2] \rightarrow [LBe]^+ + L^-$ (B3PW91-D3BJ/def2TZVPD)

ΔG° (kcal mol^{-1})	L = Cp	L = C_9H_7	L = 1,3-TMS_2Ind
$[BeL_2] \rightarrow [LBe]^+ + L^-$	174.4	179.2	155.7

Combined with experiments, these calculations show that the 1,3-TMS_2Ind ligand was indeed an unsuitable ligand for our purpose, most likely due to its considerable steric bulk. Though there is often a tendency to move to bulkier ligands to stabilize reactive species, especially given our progress in understanding dispersion interactions, for a small metal like beryllium it may in fact be counterproductive.

To quantify this supposition, we applied the Solid-G program to the known and calculated beryllocene analog structures. Solid-G is a program that calculates steric shielding of the central atom of a complex, given as the $G_{complex}$ value, where 100% refers to complete shielding. All structures used for Solid-G calculations have been optimized with B3PW91 at the def2TZVP level.

Table 22: Solid-G values of related beryllium structures

Complex	$G_{complex}$ Value (%)	Ref. for structure
$[Be(1,3\text{-}TMS_2C_3H_3)_2]$	91.9	from calculation
$[BeInd_2]$	81.4	this work
$[BeCp_2]$	81.8	from calculation
$[Be\ ^{(Me4}Cp)_2]$	84.7	[39]
$[BeCp^*_2]$	90.6	[39]
[Be(1,3-TMS_2Ind)Br]	**86.2**	**this work**

While the difference in steric saturation between $[BeCp^*_2]$ and $[Be^{Me4}Cp_2]$ appears to be due to a shift from η^5-η^1 to η^5-η^5 coordination, the saturation for the theoretical $Be[(1,3\text{-}TMS)_2C_3H_3]_2$ must be related to the trimethylsilyl groups, and explains why a

minimum cannot be found for the η^5-η^5 geometry, as it is already extremely sterically crowded.

Our previous work on beryllium chemistry resulted in the synthesis of the bulky allyl complex [Be{1,3-$(SiMe_3)_2C_3H_3$}$_2$], and a crystal structure of the diethyl ether solvate. Calculations on the unsolvated form showed that at the B3PW91/def2TZVP level, an η^3-η^3 coordination mode was 4.9 kcal mol^{-1} more stable than the η^1-η^1 form. As has been shown, this preference for π-coordination does not extend to the beryllium indenyls or cyclopentadienyls, except for $BeCp^*_2$. Calculations on the $Be[C_9H_7]_2$ show that an η^5-η^1 arrangement is 4.65 kcal mol^{-1} more stable than the η^5-η^5 arrangement. A simple explanation for this invokes the octet rule; Cp^- and Ind^- are L_2X type ligands, meaning that an η^5-η^5 [$BeCp^*_2$], for example, is formally a 10-electron complex. Though the 8-electron rule may be thought of as more of a guideline for systems that are at the border of covalent/ionic bonding, [$BeCp^*_2$] has extremely long Be-C bonds that may be rationalized by the metal center's being electronically oversaturated.

The electronic effect of the trimethylsilyl substituents may be another potential explanation for the unsuitability of [1,3-TMS_2Ind]$^-$ anion as a ligand for beryllium. Silyl groups are commonly thought to be electron-donating groups, but they also exhibit the β-silicon effect, where Si-C hyperconjugation contributes to a weakening of metal-ligand bonds in delocalized systems such as allyls.[42–44] Though a paper varying trimethylsilyl substitution patterns for indenyltitanium compounds shows experimental evidence that a trimethylsilyl group at either the 1- or 2- position donates electron density, this and other reports systematically studying metal-indenyl interactions focus almost exclusively on transition metals.[45–49] Because the d-orbital interaction with delocalized ligands is such a significant driver of coordination mode and reactivity for transition metals, it is tenuous to extrapolate some of these findings to main-group elements. As an example, studies focused on the electronic properties of indenyl ligands using electrochemical redox potentials cannot deconvolute the electronic effect of the ligand from the increased propensity for ring slippage's effect on redox potentials, meaning it is challenging to make broad statements about the differences between indenyl and cyclopentadienyl or other π-delocalized ligands even for transition metals.[49]

7.3 Conclusion

We show that mechanochemistry most simply provides access to what may be the closest structural/crystallographic analog to beryllocene, providing more definitive evidence of its connectivity and structure. In addition, this work shows that mechanochemistry provides an alternative route for the synthesis of compounds that can be or use reagents that are sensitive to the often-reactive solvents (THF, etc.) that are conventionally required. This work also provides a counterexample to the prevailing wisdom that large, bulky ligands are necessary for the isolation of unique or reactive species. Instead of needing bulky ligands to protect the metal center, using

mechanochemistry we were able to design a system where protection was not necessary. This resulted in our desired reaction, full substitution at the metal center.

7.4 Appendix

Experimental Section

General Considerations. All manipulations were performed with the rigorous exclusion of air and moisture using Schlenk or glovebox techniques. All glassware was dried by flame or in an oven at 140 °C overnight. Elemental analysis was performed at the University of Rochester CENTC Elemental Analysis Facility by Dr. William Brennessel. Proton and beryllium (^{9}Be) NMR spectra of the organometallic compounds were obtained on a DRX-500 spectrometer at 500 (^{1}H) and 70.4 (^{9}Be) MHz. Proton and carbon (^{13}C{^{1}H}) spectra were obtained on an AV-600 spectrometer at 600 (^{1}H) and 150 (^{13}C) MHz or an AV-400 spectrometer at 400 (^{1}H) and 100 (^{13}C) MHz. Proton and carbon spectra were referenced to the residual proton and ^{13}C resonances of C_6D_6, and beryllium spectra to the ^{9}Be signal at 0.0 ppm of $Be(H_2O)_4^{2+}$ in D_2O.

Materials. $BeCl_2(L)$ (L = Et_2O, THF) was prepared by the action of 4M HCl in dioxane on chunks of Be metal in L = Et_2O or THF. For the potassium indenyl K[C_9H_7], indene was passed through a column of activated alumina, then distilled under vacuum. The purified indene was freeze/pump/thawed three times, brought into a nitrogen atmosphere glovebox, then deprotonated with potassium hexamethyldisilazide in toluene overnight. A tan solid precipitated and was collected by filtering the reaction mixture through a medium glass fritted funnel, followed by washing three times with hexanes. Residual hexanes dried from the tan solid to leave a white solid. Beryllium bromide was synthesized according to previously established procedures from the elements.[50] 1,3-$TMS_2C_9H_6$ was synthesized using a procedure adapted from the literature.[51] This was deprotonated using potassium hexamethyldisilazide and isolated as an off-white solid after collecting in a medium glass fritted funnel and washed three times with hexanes.

Toluene was degassed with argon and dried over activated alumina using a solvent purification system, then stored over 4 Å molecular sieves in a glovebox. Hexanes were distilled under nitrogen over Na/benzophenone radical,[52] then stored over 4 Å molecular sieves in a N_2-atmosphere glovebox. THF was refluxed under nitrogen over Na/K/benzophenone until purple, distilled under nitrogen, and stored over 4 Å molecular sieves in a N_2-atmosphere glovebox. Benzene-d_6 was obtained from Cambridge Isotopes and stored over 4 Å molecular sieves in a N_2-atmosphere glovebox.

Synthesis of [Be(1,3-TMS_2Ind)Br] (1). In a typical reaction, $BeBr_2$ (0.030 g, 0.178 mmol) and K[1,3-TMS_2Ind] (0.106 g, 0.355 mmol) were added to a 50 mL stainless steel Retsch milling jar with 25 g (ca. 57 count) of stainless steel (440 grade) ball bearings (3/16 in (5 mm), 0.44 g) under a nitrogen atmosphere in a glovebox. The jar was sealed with a clamp in the glovebox and milled for 15 minutes at 600 rpm in a Retsch PM100 planetary mill.

The jar was opened in a glovebox, and the reaction mixture was extracted with hexanes through a fine-porosity glass fritted funnel. The resulting clear filtrate was dried under vacuum, leaving an oil that quickly formed large amounts of short and stubby clear, tan/green-tinged needle-like crystals. (0.044 g, 71% yield). Due to extreme air sensitivity, evacuated ampoules of **1** prepared for sealing decomposed immediately (by visual inspection) upon removal from the glovebox. Because of this exceptional sensitivity, despite repeated attempts, satisfactory EA was unobtainable. ^{9}Be NMR (70.4 MHz, C_6D_6): δ = -17.29 (s) ^{1}H NMR (500 MHz, C_6D_6): δ 0.132 (s, 36H, TMS), 6.54 (s, 1.99H, -HC=C), 7.10 (m, $^{1}J_{H-H}$ = 3.03 Hz, 2.24H, arom), 7.56 (m, $^{1}J_{H-H}$ 3.03 Hz, 2.18H, arom). $^{13}C\{^{1}H\}$ NMR is unobtainable due to the extreme oxygen- and moisture-sensitivity. The included ^{13}C spectrum shows decomposition, likely from protonation. Anal Calcd for $C_{15}H_{23}BeBrSi_2$: C, 51.7, H, 6.65. Found: C, 68.19, H, 8.87. Analysis for the indene $C_{15}H_{24}Si_2$, C, 69.15, H, 9.29

Synthesis of [Be(Ind)$_2$] (2). A similar procedure was followed for the synthesis of [Be(Ind)$_2$] as for **1**. $BeBr_2$ (0.030 g, 0.18 mmol) and K[C_9H_7] (0.055 g, 0.36 mmol) were subjected to the same conditions as **1**, and again filtered with hexanes. When the clear filtrate was dried under vacuum, a clear oil was left. This oil crystallizes rapidly upon physical disturbance, leaving transparent/white crystals. The hexane filtrate was lightly dun/tan colored, and yielded a faintly dun/tan colored oil upon removal of solvent, with sheets of pale off-white (pale brown) crystals precipitating out (0.0207 g, 48%). ^{9}Be NMR (70.4 MHz, C_6D_6) δ = -19.14 (s) ^{1}H NMR (600 MHz, C_6D_6): δ 5.14 (d, $^{1}J_{H-H}$ = 3.43 Hz, 1.95H) 6.02 (t, $^{1}J_{H-H}$ = 3.48 Hz, 1H), 7.03 (arom, mult, 2.13H), 7.23 (arom, mult, 1.97H) $^{13}C\{^{1}H\}$ NMR (150 MHz, C_6D_6) δ 121.74, 122.70, 128.34, 132.10. Anal. Calcd for $C_{14}H_{18}Be$: C, 90.34; H, 5.90. Found: C, 89.37; H, 5.86

High temperature reaction of K[1,3TMS$_2$Ind] and BeBr$_2$ in 1:1 toluene:Et$_2$O. Following Carmona's procedure for the synthesis of [BeCp*$_2$], a high temperature reaction was attempted. A 1:1 mixture of dry Et_2O and toluene was added to an oven-dried 250 mL Schlenk flask with a Teflon stir bar. To this, K[1,3-TMS_2Ind] (0.124 g, 0.415 mmol) and $BeBr_2$ (0.035 g, 0.207 mmol) were added. This was brought out of the glovebox, and cycled three times onto a Schlenk line. Under positive N_2 flow, an oven dried reflux condenser was attached to the flask. The reaction was heated in an oil bath that was gradually heated to 95 °C. The reaction slowly turned pink in the first 48 h, and then turned yellow with a white deposit settling on the side of the flask. After 3.5 days, the reaction was removed from the oil bath, allowed to cool, and the solvent was removed. Extraction of the resulting residue with hexanes, filtration of the extract through a glass fine fritted funnel, and evaporation under vacuum left a thick orange oil. A C_6D_6 NMR sample was made of the resulting oil, which showed what appears to be the protonated indene and another decomposition product in the ^{1}H NMR spectrum and no discernible ^{9}Be NMR signal.

However, stopping the reaction at 18 hours and removing the flask from the 90 °C oil bath causes a shift in color from pink to orange. Removing the solvent leaves a deep

orange oil, which was extracted with hexanes and filtered through a fine glass fritted funnel before being evaporated under vacuum. An NMR sample was made of the resulting orange residue, which showed ^{9}Be resonances at δ -17.3 (**1**) and 3.97. The ^{1}H NMR spectrum shows a ~5:1 ratio of **1** to the coupled indenyl.

Reaction of K[1,3-TMS$_2$Ind] and BeBr$_2$ in THF Inside a glovebox, *ca* 7 mL of THF was added to an oven-dried 20 mL glass vial with glass stir bar. To avoid reaction (white smoke), $BeBr_2$ (20 mg, 0.12 mmol) was added slowly while stirring. After stirring for ~5 minutes, all the $BeBr_2$ had dissolved, leaving a clear solution. To this solution, K[1,3-TMS$_2$Ind] (71 mg, 0.24 mmol) was slowly added with stirring. The reaction mixture immediately turned slightly pearlescent and pink. The reaction was allowed to stir overnight. After stirring was stopped, a white precipitate settled, presumably KBr, leaving a translucent pink solution. This mixture was then transferred into an Erlenmeyer flask and the solvent removed under vacuum. The solid residue was extracted with C_6D_6 to prepare a solution for NMR analysis, which was then filtered through oven-dried Celite into an NMR tube. ^{1}H NMR reveals a spectrum similar but not identical to the presumably coupled indenyl from the reaction conducted under Carmona's high temperature forcing conditions. ^{9}Be NMR reveals an extremely broad ($w_{1/2}$ = ~128 Hz) resonance centered at δ 3.7 ppm. Attempts to isolate an organic residue by filtration of the hexane extract through a fine glass fritted funnel resulted in an oil that could not be coaxed to crystallize.

Reaction of K[C$_9$H$_7$] and BeBr$_2$ in THF
Inside a glovebox, ~7 mL of THF was added to an oven dried 20 mL glass vial with glass stir bar. To avoid reaction (white smoke), $BeBr_2$ (20 mg, 0.12 mmol) was added slowly while stirring. After stirring for ~5 minutes, all $BeBr_2$ dissolved, leaving a clear solution. To this solution, KC_9H_7 (37 mg, 0.24 mmol) was slowly added while stirring. The reaction mixture immediately turned slightly pearlescent and became slightly cloudy. The reaction was allowed to stir overnight. The solvent was removed, leaving a yellowish residue. This was extracted with C_6D_6 and filtered through oven-dried Celite into an NMR tube. The resulting ^{1}H NMR spectrum consists of extremely broad solvent and what appears to be indene resonances. ^{9}Be NMR (70.4 MHz, C_6D_6): δ = 3.32 (s).

Reaction of K[C$_9$H$_7$] and BeBr$_2$ in Et$_2$O
Inside a glovebox, ~10 mL of Et_2O was added to an oven dried 20 mL glass vial with glass stir bar. $BeBr_2$ (15 mg, 0.09 mmol) was added slowly while stirring. After stirring for ~10 minutes, all the $BeBr_2$ had dissolved, leaving a clear solution. To this solution, K[C_9H_7] (27 mg, 0.18 mmol) was slowly added while stirring. The reaction mixture turned slightly pearlescent over the course of 20 min. The reaction was allowed to stir overnight, whereupon the solution turned slightly pinkish and a white solid deposited above the solution level. After stirring was stopped, a white precipitate settled, presumably KBr, leaving a translucent pink solution. This mixture was then transferred into an Erlenmeyer flask and the solvent removed under vacuum. There did not appear to be visible residue but the flask was extracted with C_6D_6 to prepare an NMR solution, which was then filtered

through oven-dried Celite into an NMR tube. The recorded ^{1}H NMR spectrum shows only solvent peaks, and the ^{9}Be shows no discernable signal.

X-ray Crystallography. X-ray crystallographic data were collected on a Rigaku Oxford Diffraction Supernova diffractometer. Crystal samples were handled under immersion oil and quickly transferred to a cold nitrogen stream. The crystals were kept at 100 K during data collection. Under Olex2,[53] the structure was solved with the SHELXT[54] structure solution program using direct methods and refined with the SHELXL[55] refinement package using least squares minimization. All non-hydrogen atoms were refined with anisotropic displacement parameters.

General Procedures for Calculations. All calculations were performed with the Gaussian 16 (Linux and Windows) suite of programs.[56] The B3PW91 functional, which incorporates Becke's three-parameter exchange functional with the 1991 gradient-corrected correlation functional of Perdew and Wang, was used.[57] To supply dispersion corrections, Grimme's D3 correction[58] with additional Becke-Johnson damping was used.[59] Unless otherwise noted, the basis sets def2TZVP or def2TZVPD (for BDE calculations) were used on all atoms.[60] Frequency calculations were also done at the triple-zeta level. Coordination sphere saturation values were determined using Solid-G.[61]

NMR Calculations

To aid in the understanding of structural phenomena and identify unknown species, DFT calculations were done on a variety of isolated and theoretical organoberyllium compounds. Initially, the B3LYP/6-311G+g(2d,p) method developed at LANL was used,[62] but because most hybrid functionals and reasonably-sized basis sets give equivalent results for NMR calculations of neutral compounds,[63] B3PW91/def2TZVP was used in later computations. In the table below (Table 23), it is evident that the effect on calculated chemical shifts from a change in functional is negligible in comparison to moving to a true split-valence basis set (def2TZVP vs 6-311+G(2d,p)). In any case, none of the methods were able to exactly match the experimental NMR shifts (for [$BeInd_2$], -23.74 ppm B3PW91/def2TZVP, -24.57 ppm B3LYP/6-311G+g(2d,p) vs experimental value of -19.3 ppm in C_6D_6), which the group at LANL claimed was possible.

For each method, the ^{9}Be NMR standard ($Be(H_2O)_4^{2+}$) was first calculated. Then, structures for each compound were optimized at the desired level (B3LYP/6-311G+g(2d,p) or B3PW91/def2TZVP) in addition to frequency calculations to ensure the optimized geometry represented a minimum energy structure. The values in the table were calculated as: (standard isotropic shielding constant – calculated structure isotropic shielding value)

Table 23: Tabulated ^{9}Be NMR calculations (all values in ppm from Be^{2+} cation)

Complex	B3PW91/ def2TZVP	B3LYP/ 6-311G+g(2d,p)	B3LYP/ def2TZVP	**Exper**.
[$BeInd_2$**]**	-23.74	-24.57	-23.56	-19.3
[$Be(1,3\text{-}TMS_2Ind)_2$**]**	-16.68			
[BeInd•**THF]**	15.11	16.06	15.86	
[$BeInd_2$•**2THF]**	7.02	7.20	7.41	
[IndBe**[**$N(SiMe_3)_2$**]**	-19.46			
[$Be(1,3\text{-}TMS_2Ind)Br$]	-17.96			-17.29
[$Be(Cp^{4Me}{}_2)$]	-20.34	-21.27	-20.08	
[Be**Cp*$_2$**]				–21.7
Cp_2Be				-18.5
[BeIndBr]	-20.44	-19.86	-20.31	
[BeIndBr•2THF]	7.12			
[$Be(1,3\text{-}TMS_2Ind)Br$•THF]	6.33			
[$Be(1,3\text{-}TMS_2Ind)Br$•2THF]	16.27			

BDE calculations

The method used by Frenking and coworkers[64] was employed to investigate the bonding of various ligands with beryllium. The reaction:

$$[BeL_2] \rightarrow [LBe]^+ + L^-$$

was investigated (L = indenyl or cyclopentadienyl). The energy required for this reaction can be used as a measure of ligand strength (i.e., a stronger ligand is harder to displace), especially when compared across multiple ligands. A geometry optimization and frequency calculation must be done for each fragment. In this case, ΔG° was the thermochemical parameter of interest, and because an anionic fragment was involved, the def2TZVPD basis set, which includes diffuse functions, was used, along with B3PW91, the functional found to be appropriate for organoberyllium systems. The net BDEs calculated are of course positive, because the [BeL_2] compounds are stable and energy is required to remove a ligand as an anion.

Table 24: Detailed values for BDE calculations of $[BeL_2] \rightarrow [LBe]^+ + L^-$ using B3PW91-D3BJ, def2TZVPD (ΔG°, kcal mol^{-1})

L	[BeL_2]	$[BeL]^+$	$[L]^-$	Net
$[C_5H_5]^-$	-252087	-130499	-121413	174.3622
$[C_9H_7]^-$	-444836	-217794	-226863	179.1946
$[(1,3\text{-}TMS)_2Ind]^-$	-1470487	-730630	-739701	155.6756

Table 25: Crystal Data and Summary of X-ray Data Collection for [Be(1,3-TMS_2Ind)Br] (**1**).

Empirical formula	$C_{15}H_{23}BeBrSi_2$	
Formula weight	348.43	
Temperature	100.01(10) K	
Wavelength	1.54184 Å	
Crystal size	0.336 x 0.025 x 0.018 mm^3	
Crystal system	Orthorhombic	
Space group	*Pnma*	
Unit cell dimensions	a = 14.5296(4) Å	α = 90°.
	b = 6.65866(13) Å	β = 90°.
	c = 18.6670(4) Å	γ = 90°.
Volume	1805.98(7) $Å^3$	
Z	4	
Density (calculated)	1.281 Mg/m^3	
Absorption coefficient	4.235 mm^{-1}	
F(000)	720	
Theta range for data collection	3.855 to 71.042°	
Index ranges	$-17 \leq h \leq 15$, $-8 \leq k \leq 8$, $-22 \leq l \leq 21$	
Reflections collected	11316	
Independent reflections	1888 [R(int) = 0.0535]	
Completeness to theta = 67.684°	100.0 %	
Absorption correction	Gaussian	
Max. and min. transmission	1.000 and 0.527	
Refinement method	Full-matrix least-squares on F^2	
Data / restraints / parameters	1888 / 0 / 169	
Goodness-of-fit on F^2	1.270	
Final R indices [I>2sigma(I)]	R_1 = 0.0420, wR_2 = 0.0867	
R indices (all data)	R_1 = 0.0489, wR_2 = 0.0888	
Largest diff. peak and hole	0.338 and -0.574 e^- $Å^{-3}$	

Table 26: Crystal Data and Summary of X-ray Data Collection for [Be(Ind)$_2$] (**2**).

Empirical formula	$C_{18}H_{14}Be$	
Formula weight	239.30	
Temperature	99.95(13) K	
Wavelength	1.54184 Å	
Crystal size	0.157 x 0.114 x 0.08 mm^3	
Crystal system	Monoclinic	
Space group	$P2_1/n$	
Unit cell dimensions	a = 11.28662(16) Å	α = 90°.
	b = 10.17191(11) Å	β = 106.3379(13)°
	c = 11.50513(14) Å	γ = 90°.
Volume	1267.53(3) Å^3	
Z	4	
Density (calculated)	1.254 Mg/m^3	
Absorption coefficient	0.519 mm^{-1}	
F(000)	504	
Theta range for data collection	4.849 to 73.377°.	
Index ranges	$-13 \le h \le 13$, $-12 \le k \le 12$, $-14 \le l \le 13$	
Reflections collected	14 937	
Independent reflections	2524 [R(int) = 0.0282]	
Completeness to theta = 67.684°	100.0 %	
Absorption correction	Gaussian	
Max. and min. transmission	1.000 and 0.799	
Refinement method	Full-matrix least-squares on F^2	
Data / restraints / parameters	2524 / 0 / 188	
Goodness-of-fit on F^2	1.073	
Final R indices [I>2sigma(I)]	R_1 = 0.0348, wR_2 = 0.0845	
R indices (all data)	R_1 = 0.0375, wR_2 = 0.0868	
Largest diff. peak and hole	0.207 and -0.256 e$^-$ Å^{-3}	

Figure 100. ^{1}H NMR spectrum of **1** ([Be(1,3-TMS_2Ind)Br]) in C_6D_6

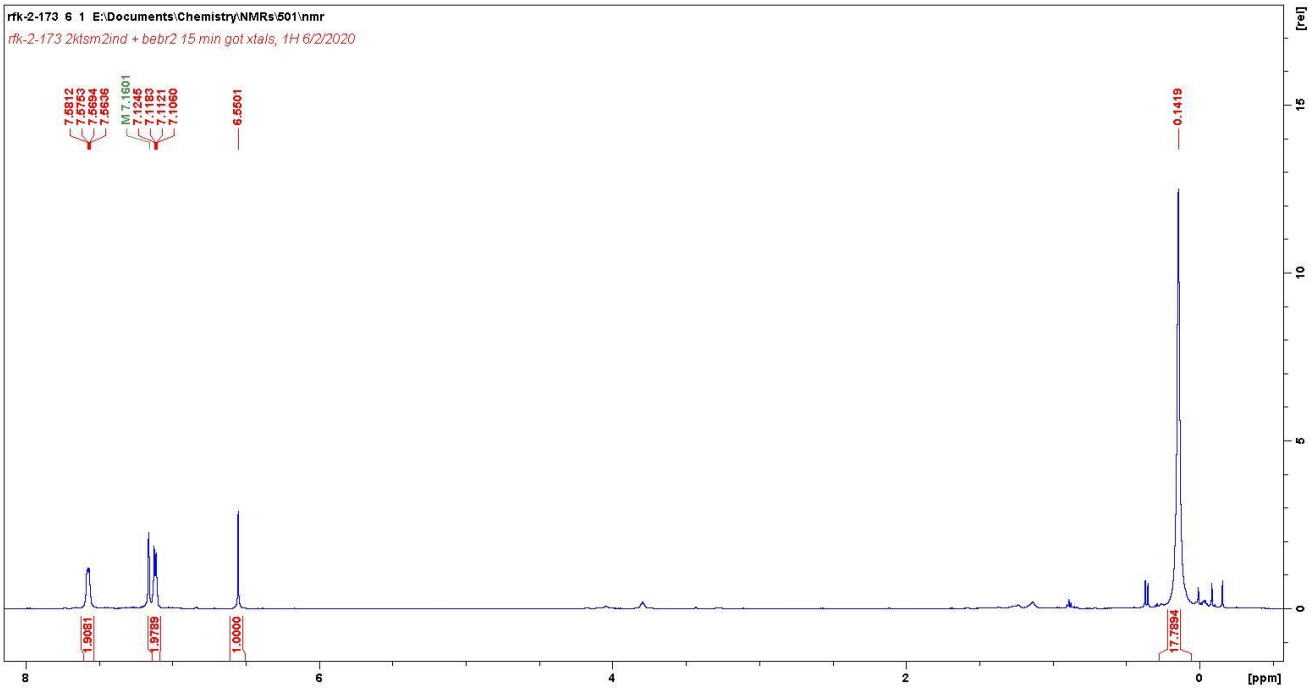

Figure 101. Attempted ^{13}C NMR spectrum of **1** ([Be(1,3-TMS_2Ind)Br]) in C_6D_6 (decomposition and protonation product)

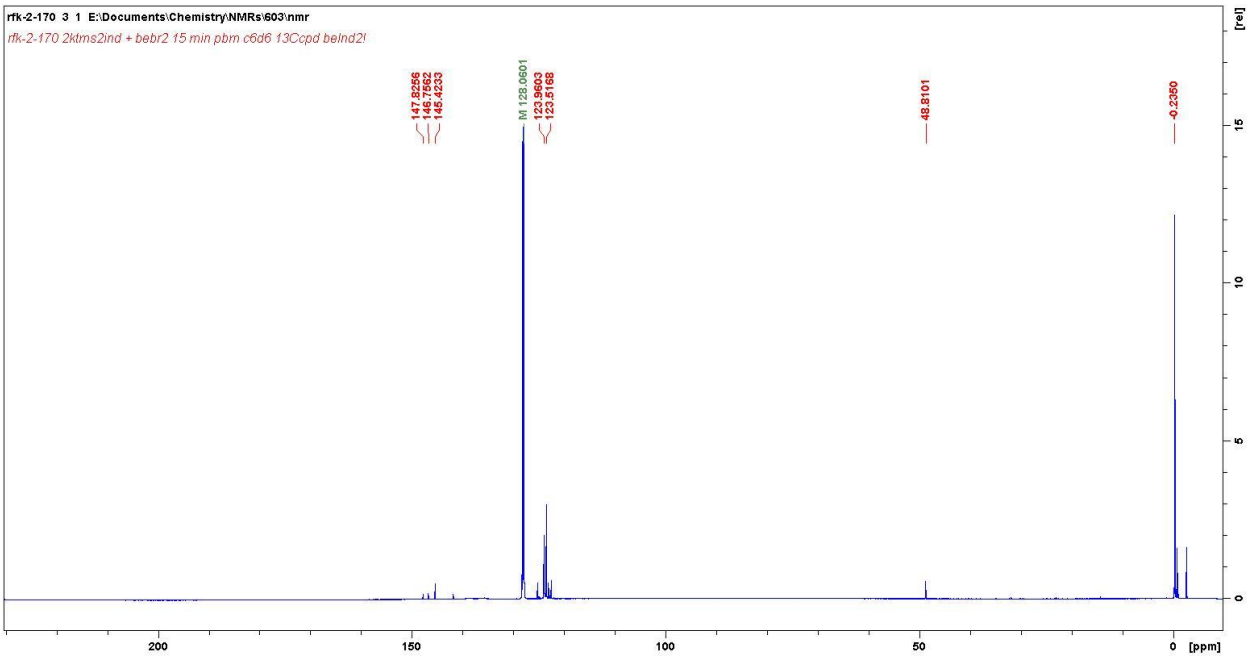

Figure 102. ^{9}Be NMR spectrum of **1** ([Be(1,3-TMS$_2$Ind)Br]) in C_6D_6

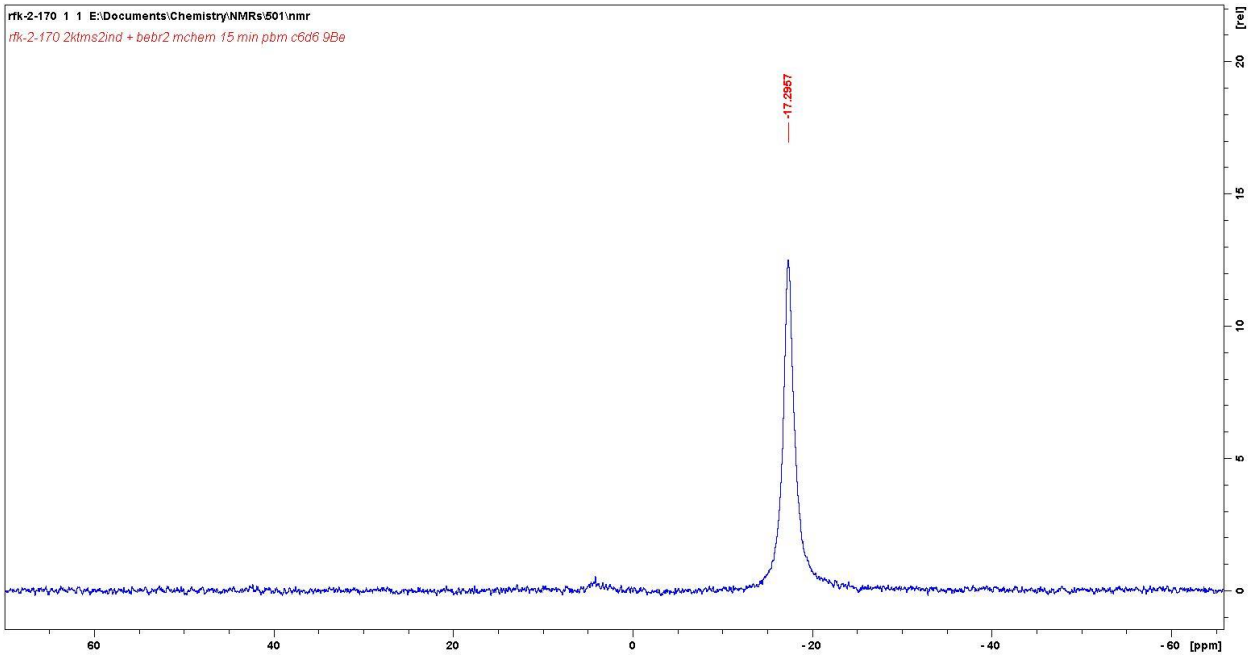

Figure 103. ^{1}H NMR spectrum of **2** ($[Be(C_9H_7)_2]$) in C_6D_6

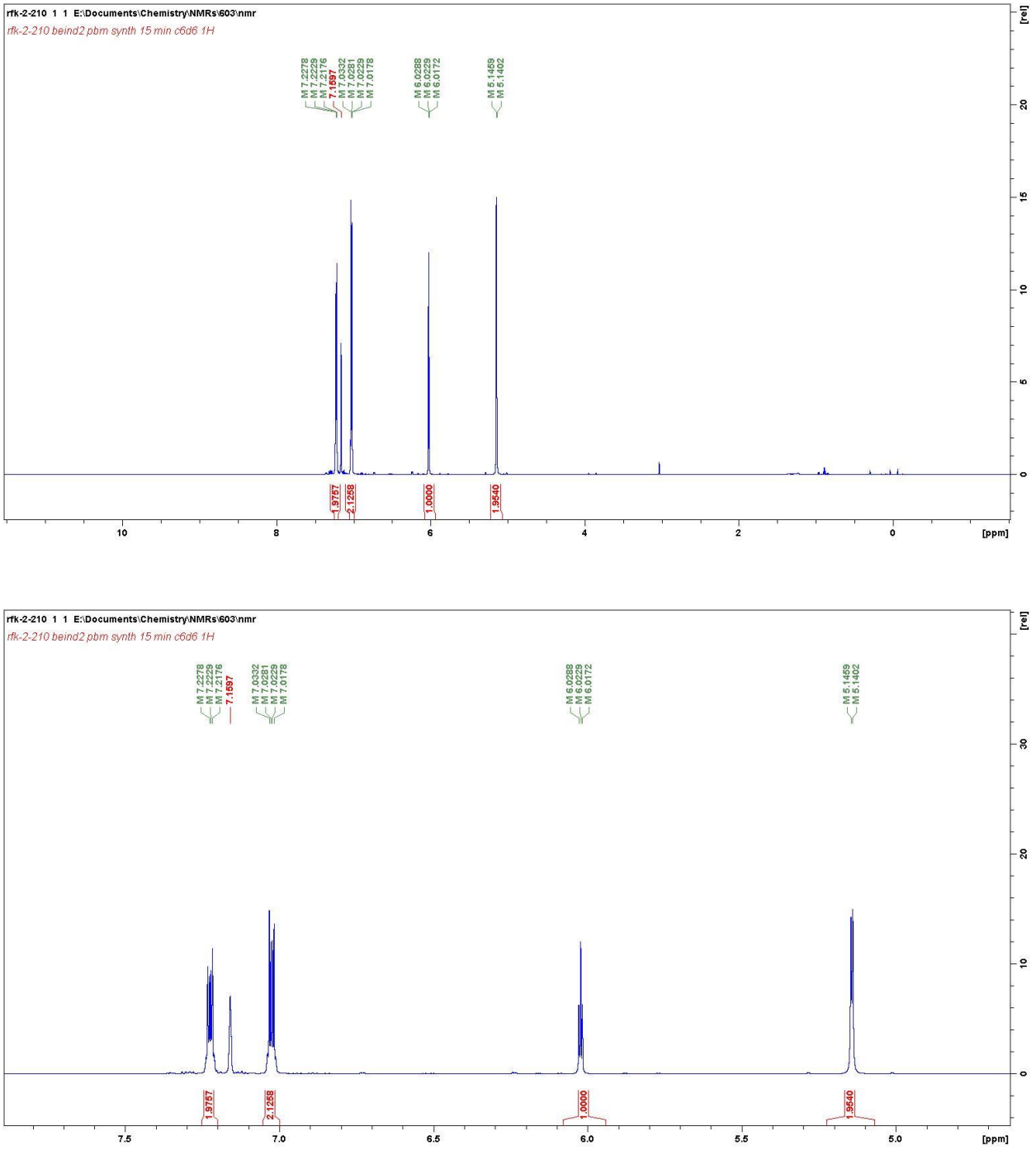

Figure 104. ^{13}C NMR spectrum of **2** ($[Be(C_9H_7)_2]$) in C_6D_6

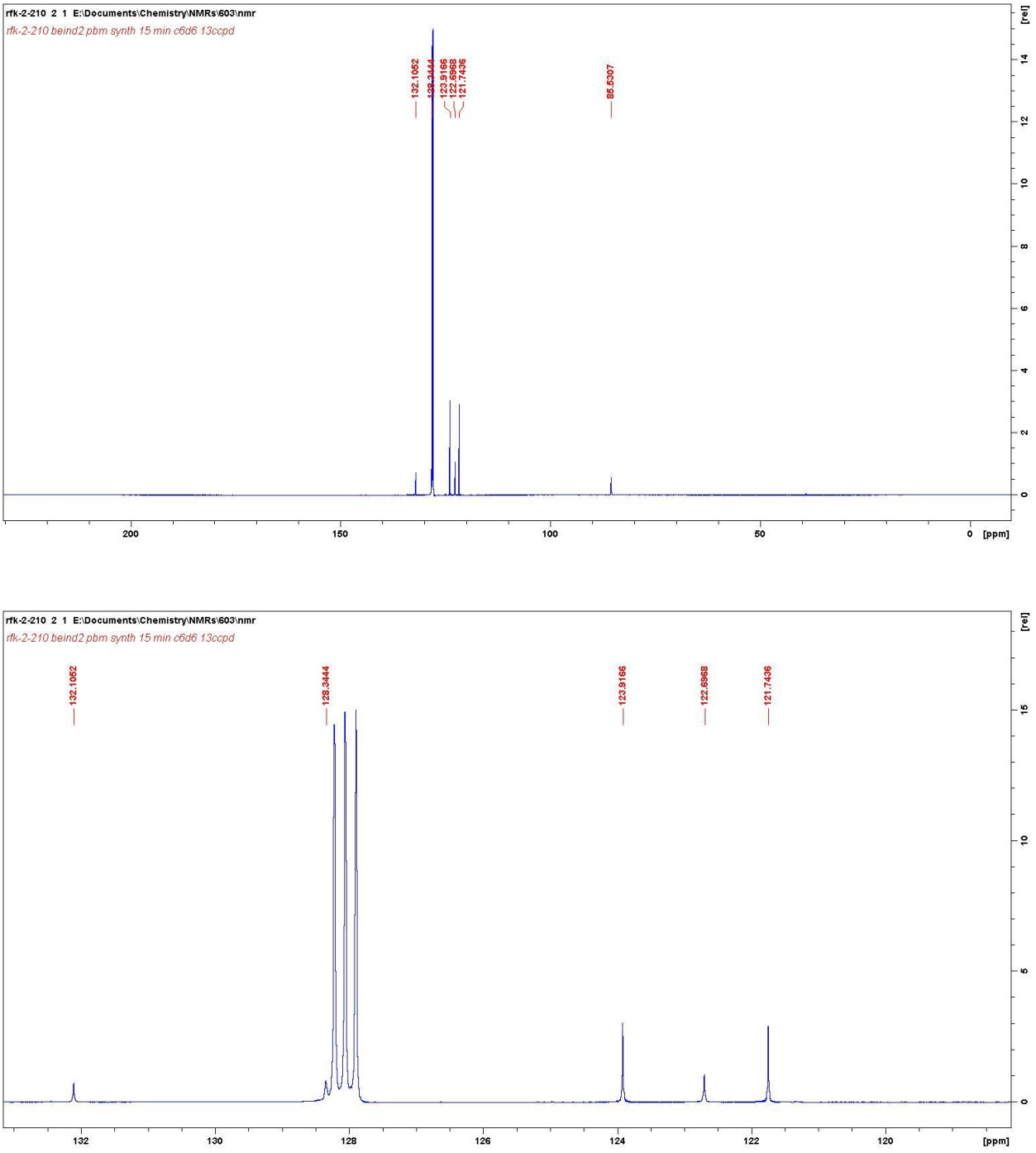

Figure 105. ^{9}Be NMR spectrum of **2** ($[Be(C_9H_7)_2]$) in C_6D_6

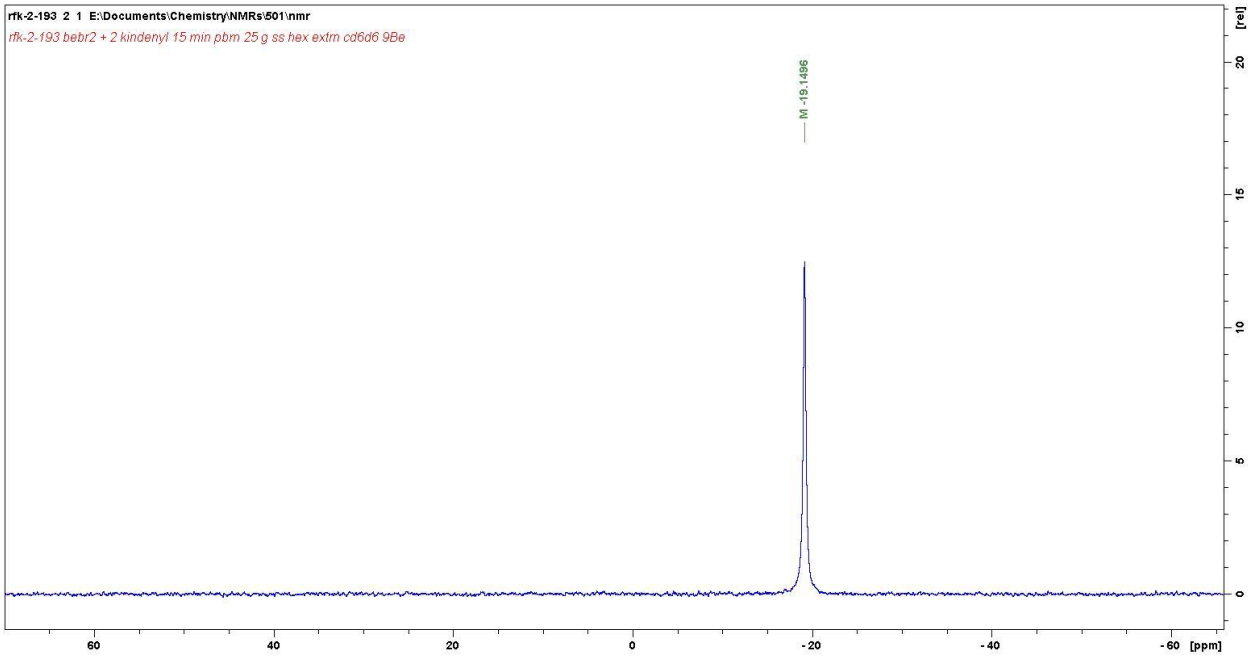

Figure 106. ^{1}H NMR spectrum of **2** ($[Be(C_9H_7)_2]$) in tol-d_8 at 203 K (-70 ° C)

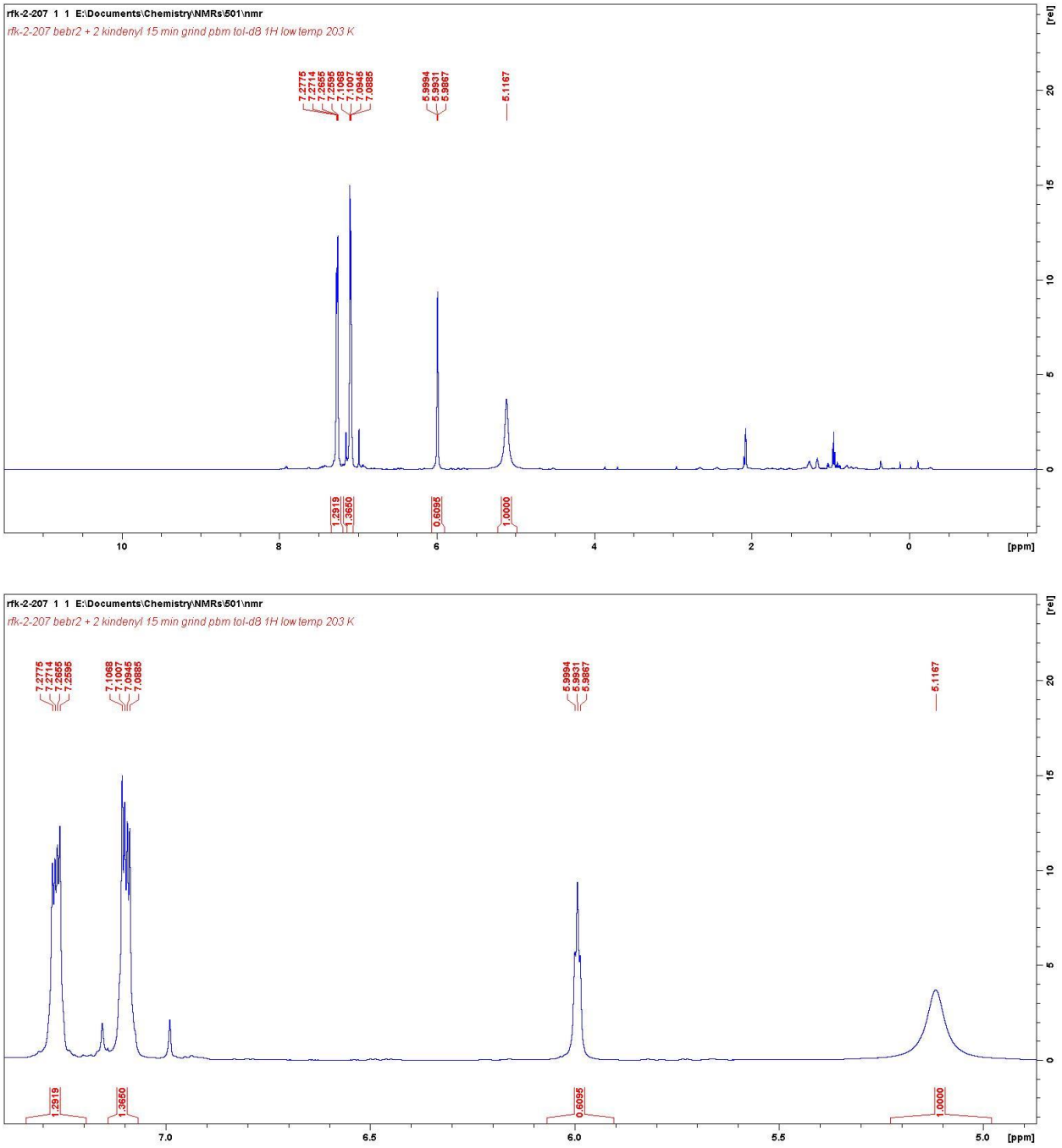

Figure 107. ^{9}Be NMR spectrum of **2** ([Be(C_9H_7)$_2$]) in tol-d_8 at 203 K (-70 ° C)

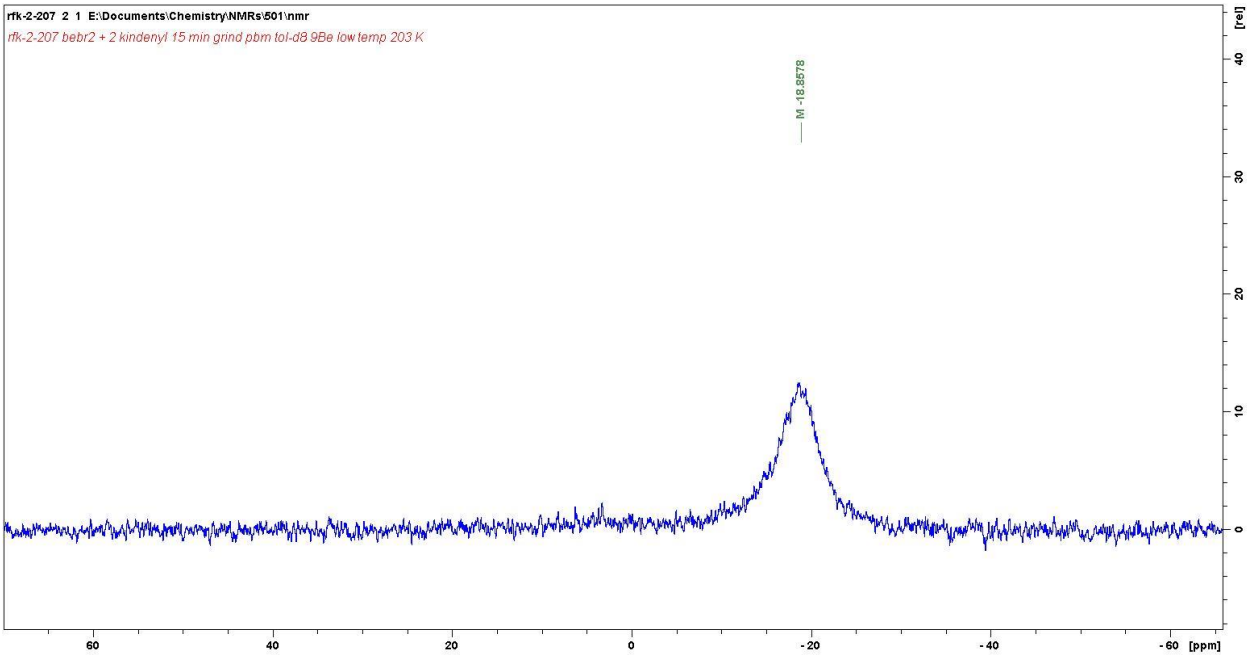

Figure 108. ^{1}H NMR spectrum of reaction of 2 K[1,3-TMS_2Ind] in THF overnight

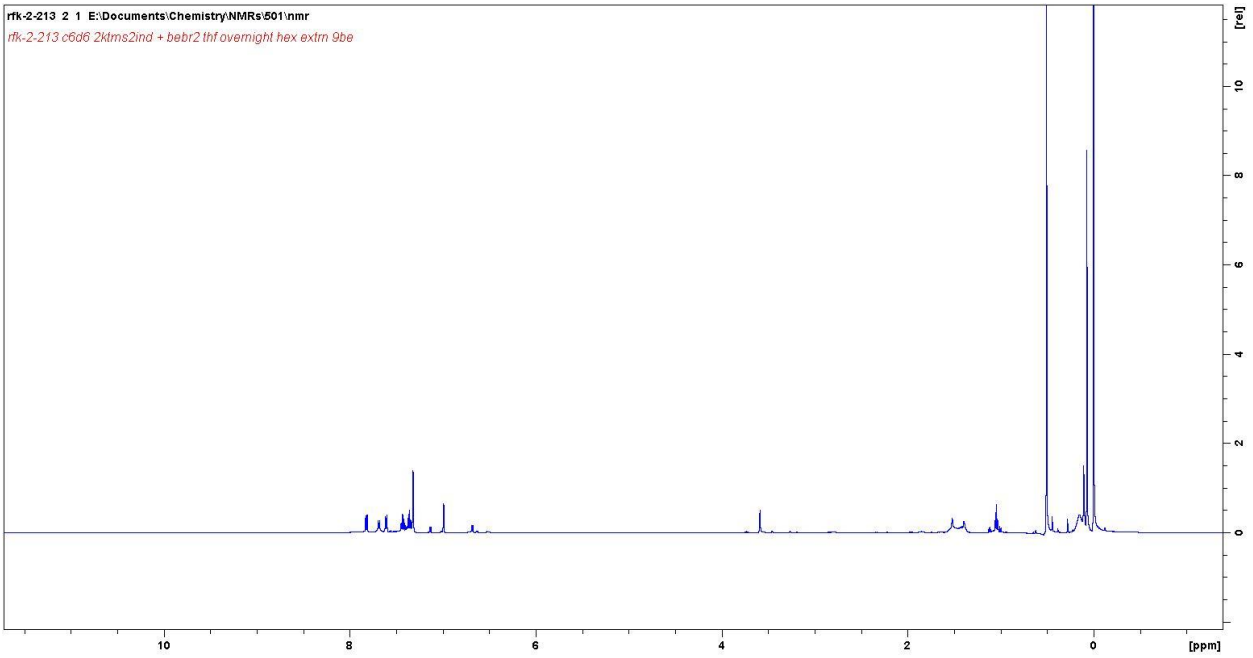

Figure 109. ^{9}Be NMR spectrum of reaction of 2 K[1,3-TMS_2Ind] + $BeBr_2$ in THF overnight

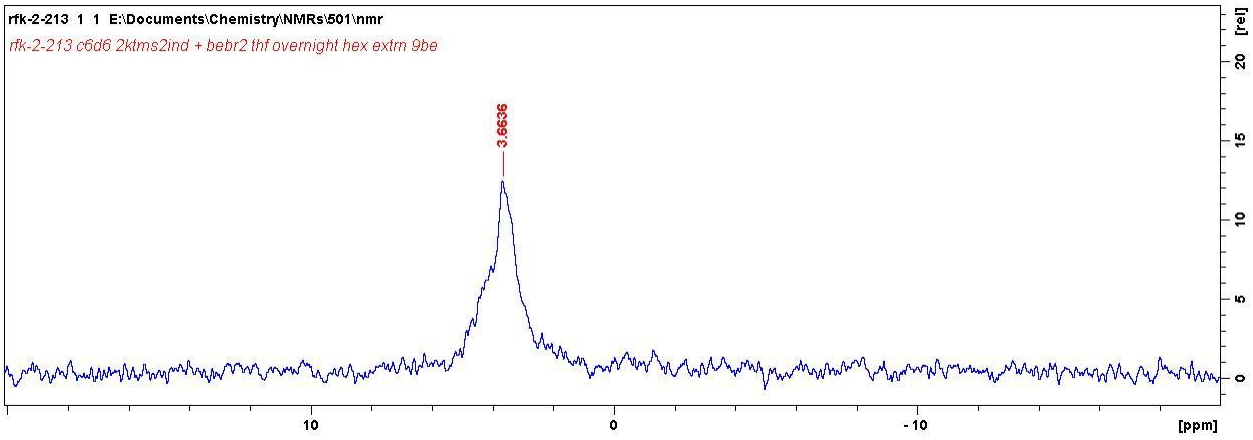

Figure 110. ^{1}H NMR spectrum of high temperature reaction of 2 K[1,3-TMS_2Ind] + $BeBr_2$ for 3.5 days

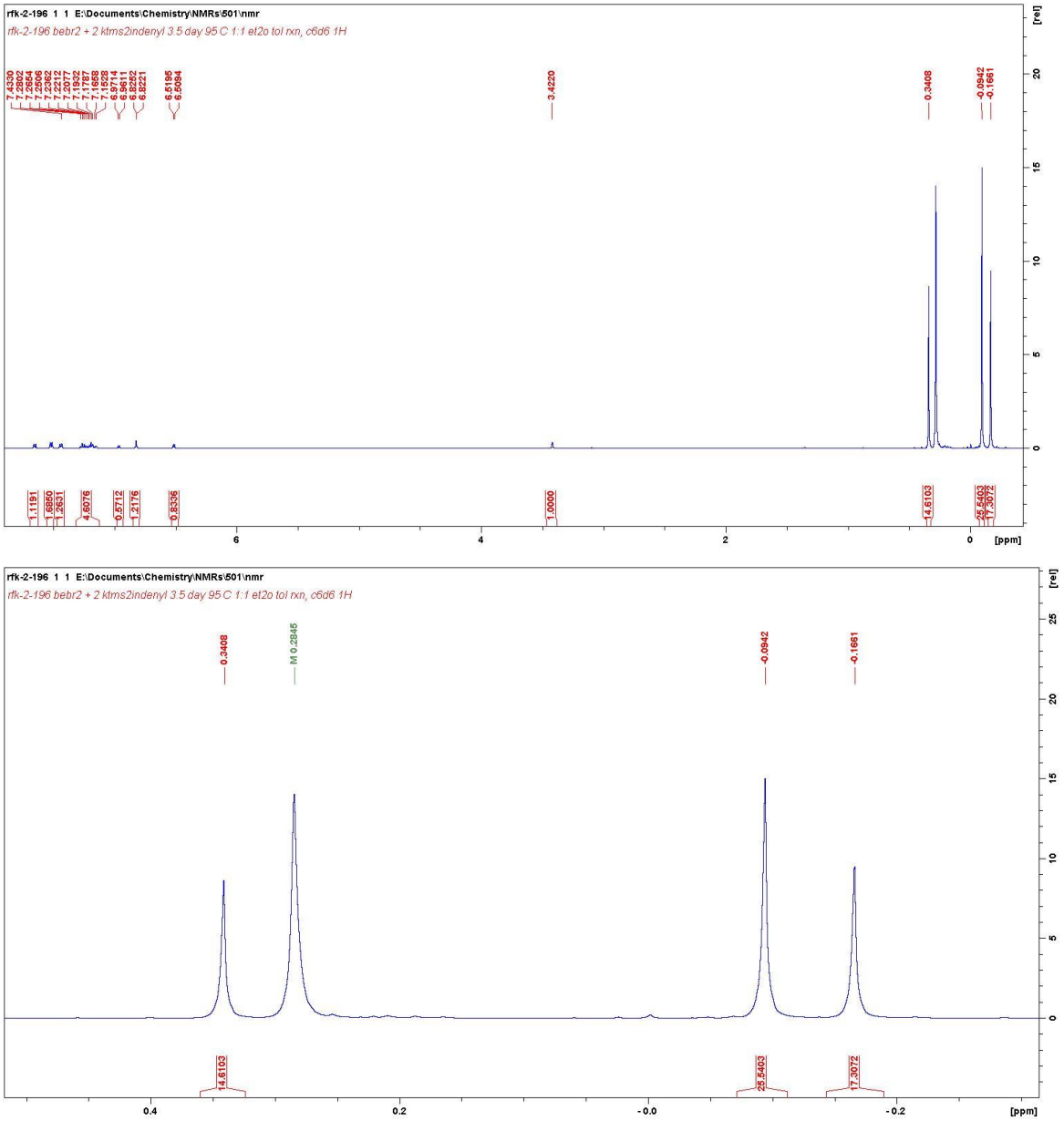

In the spectrum above, note that the peak at 0.286 ppm is likely silicone grease, though the pattern of peaks is misleading and was initially thought to be the result of two coupled TMS_2indenyl ligands

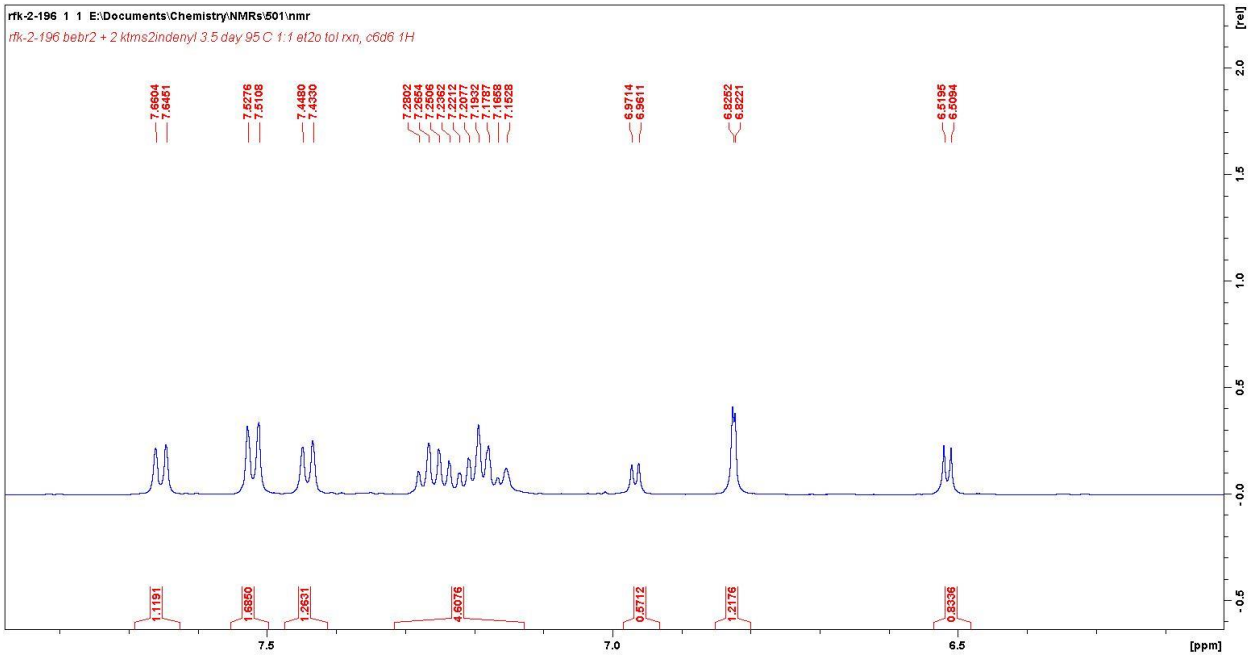

Figure 1l1. Comparison high temperature reaction of 2 K[1,3-TMS_2Ind] + $BeBr_2$ for 3.5 days with room temperature reaction in THF, ^{1}H NMR spectra

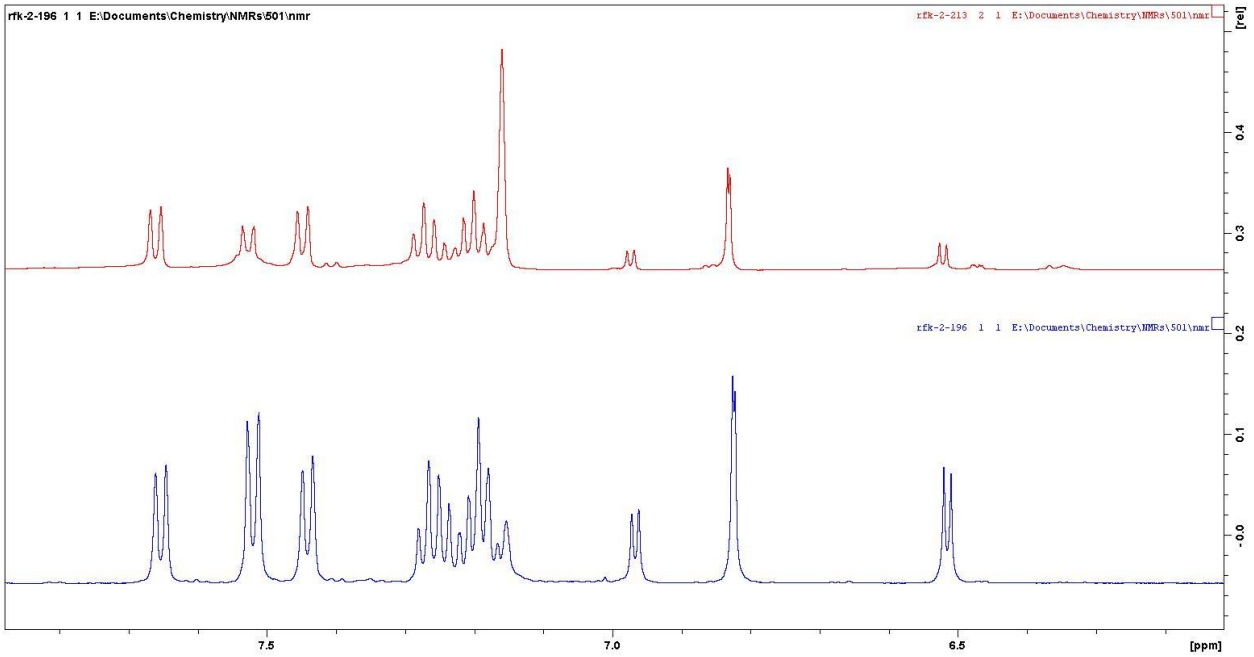

Note that many of the same peaks are present, but with some in different relative intensities. This demonstrates that there are likely at least 2 decomposition products at room temperature in THF and at elevated temperature in 1:1 Et_2O:toluene.

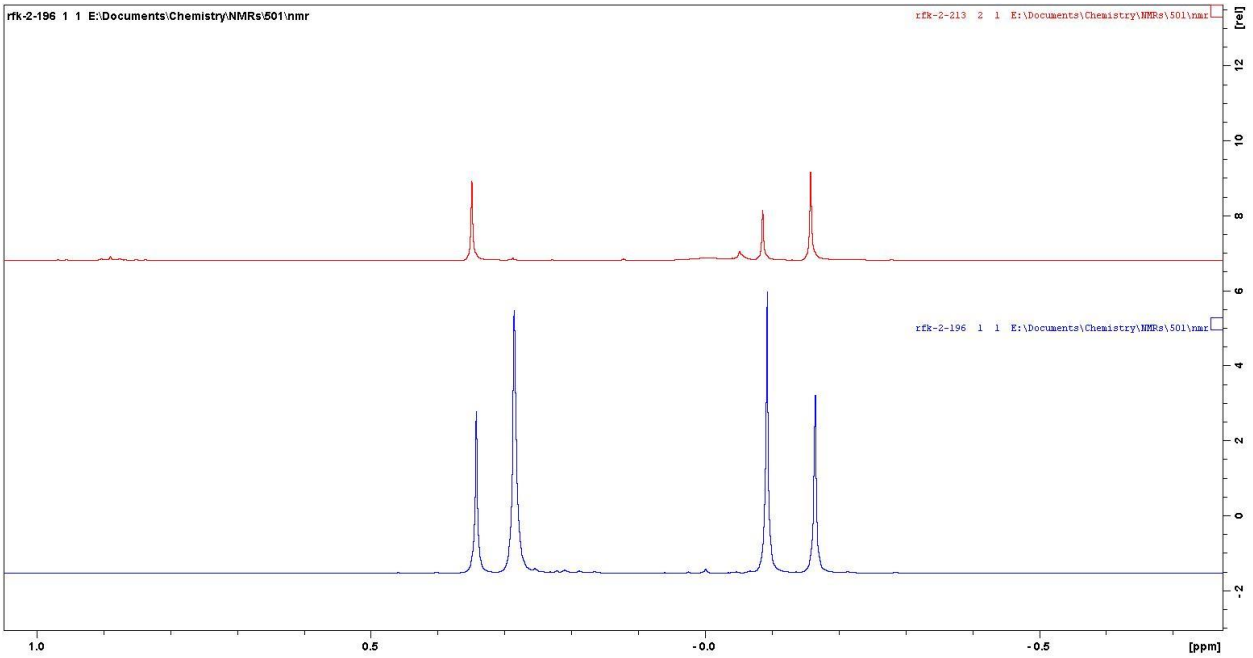

Except for the peak at 0.286 ppm (2nd from left in blue spectrum, silicone grease), the TMS peaks match up. Two peaks may be from the protonation product (indene).

Figure 112. ^{9}Be NMR spectrum of high temperature reaction of 2 K[1,3-TMS_2Ind] + $BeBr_2$ for 3.5 days

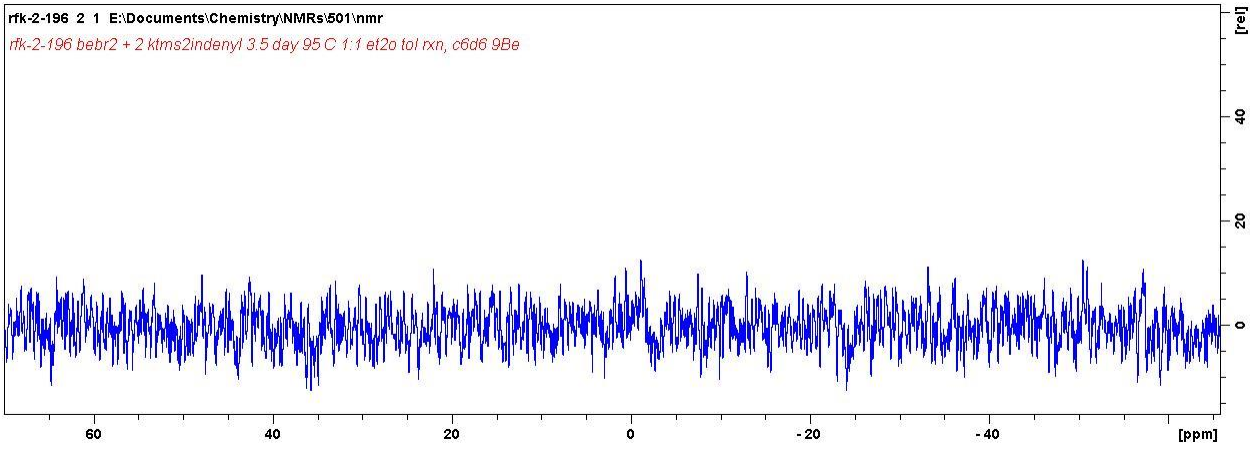

Figure 113. ^{1}H NMR spectrum of high temperature reaction of 2 K[1,3-TMS_2Ind] + $BeBr_2$ for 18 hours

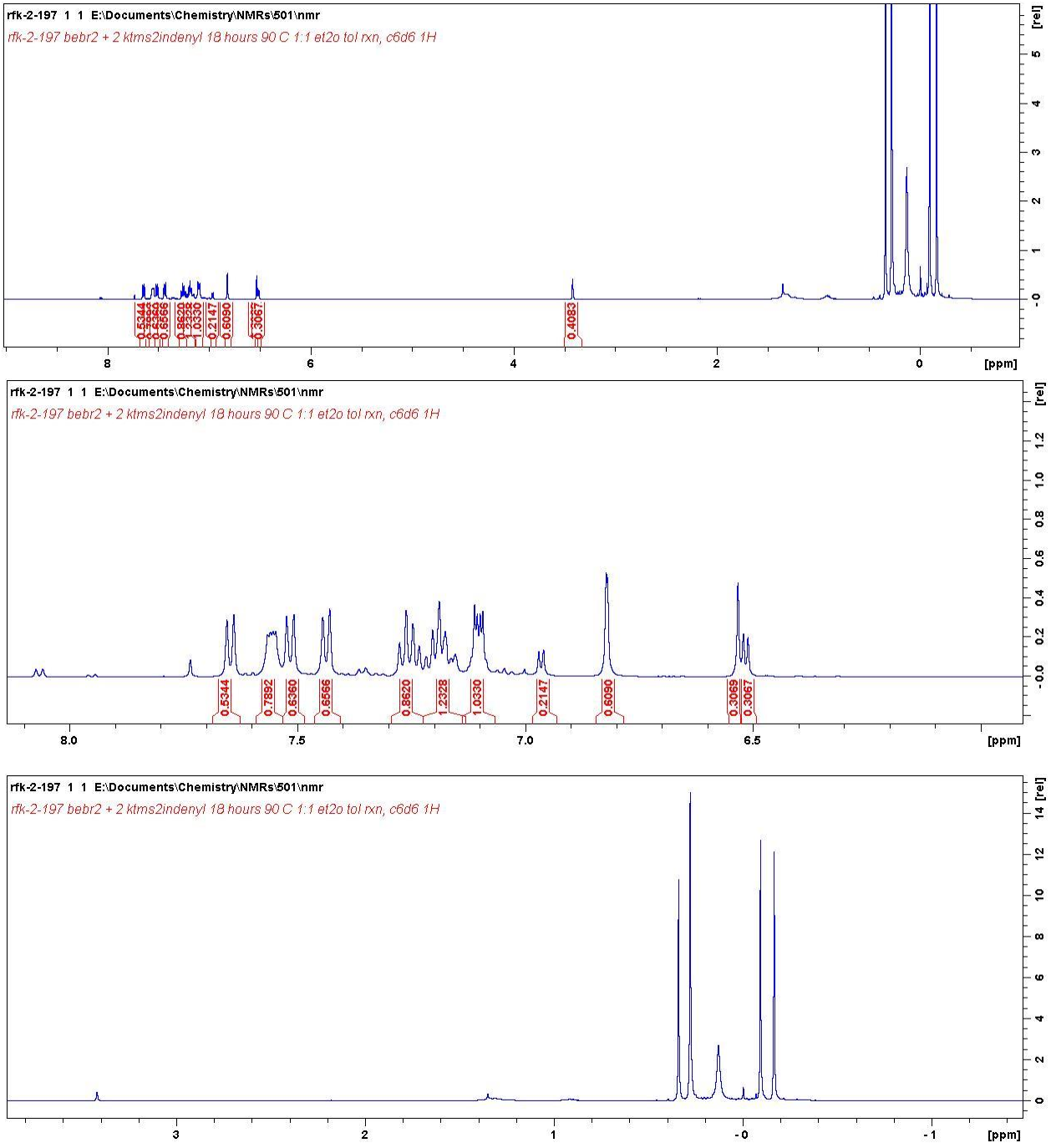

Figure 114. ^{9}Be NMR spectrum of high temperature reaction of 2 K[1,3-TMS_2Ind] + $BeBr_2$ for 18 hours

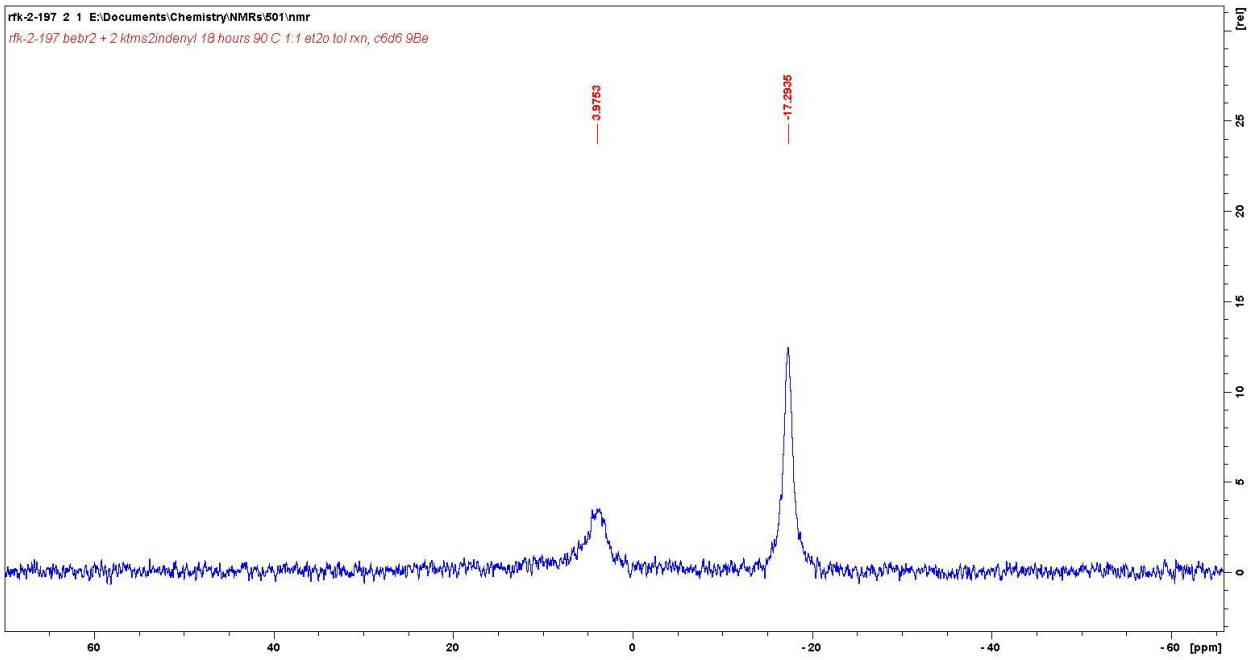

Solid-G Calculations

All coordinates used for Solid-G calculations came from optimized structures (B3PW91/def2TZVP) to normalize C-H distances (crystallographic X-H distances are often slightly short)

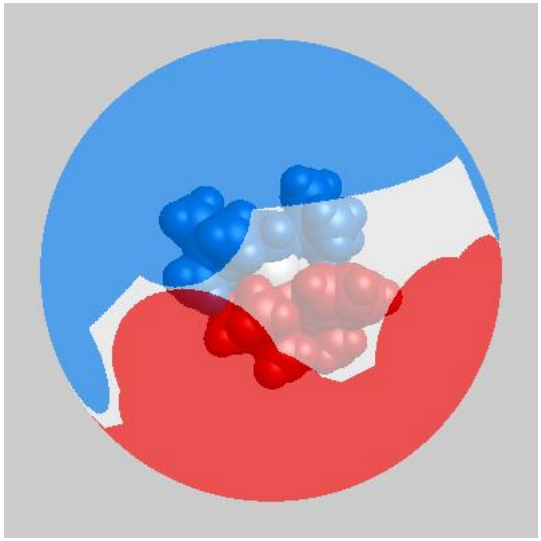

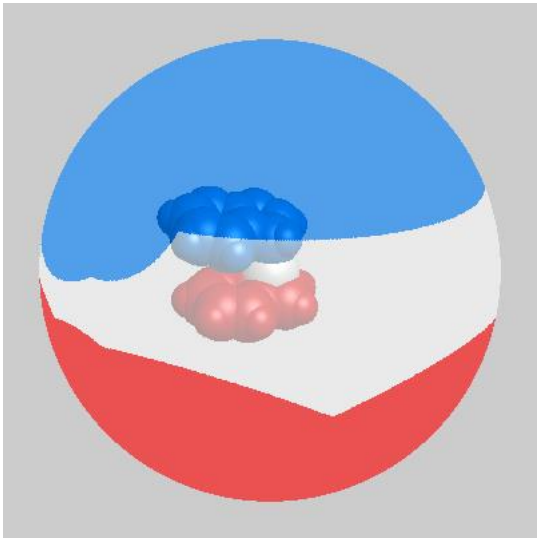

Figure 115. $[Be(1,3\text{-}TMS_2Ind)_2]$, $G_{complex}$ = 91.9% $Be[C_9H_7]_2$ $G_{complex}$ = 81.4%

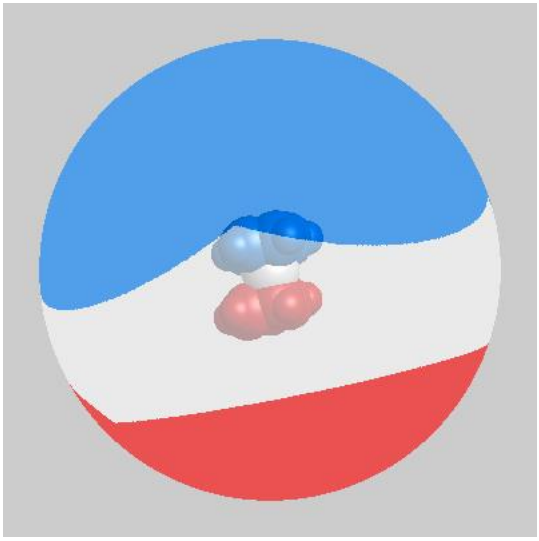

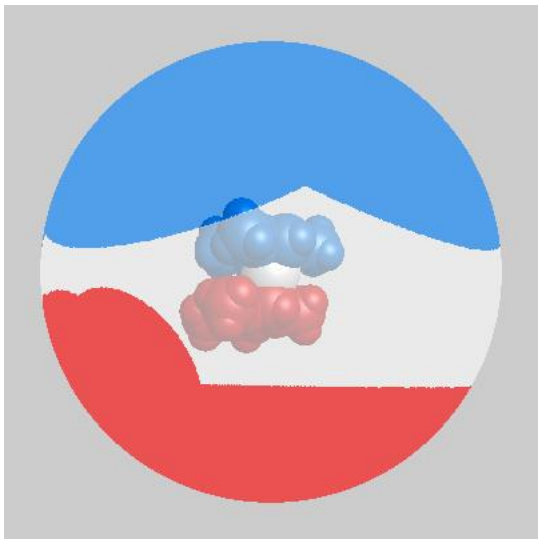

Figure 116. $[BeCp_2]$, $G_{complex}$ = 81.8% $[Be(^{Me4}Cp)_2]$, $G_{complex}$ = 84.7%

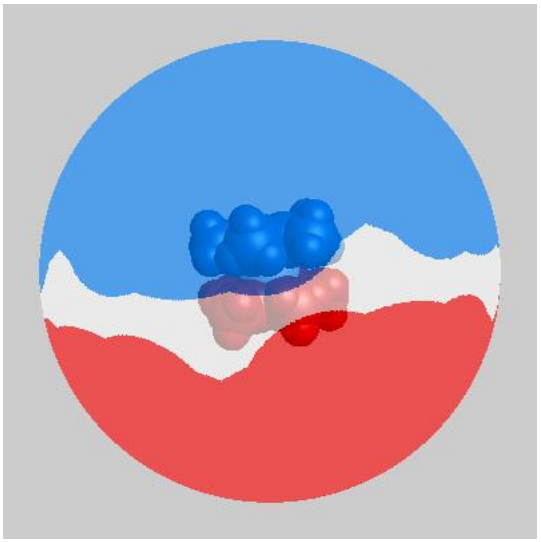

Figure 117. [$BeCp^*_2$], $G_{complex}$ = 90.6%

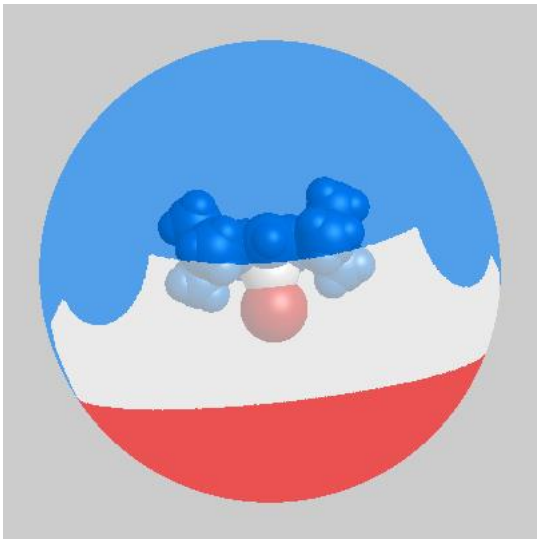

[Be(1,3-TMS_2Ind)Br] $G_{complex}$ = 86.2%

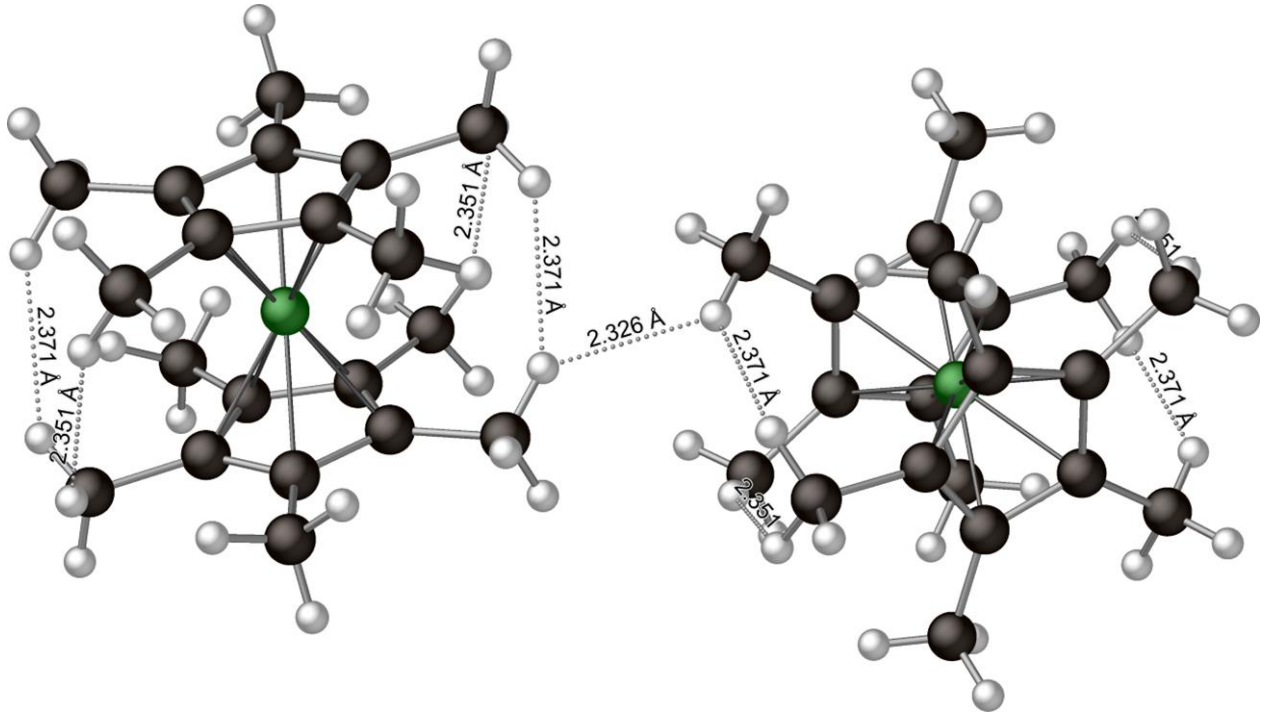

Figure 118. H···H contacts in [$BeCp^*_2$].

7.4 References

(1) Fischer, E. O.; Hofmann, H. P. Über Aromatenkomplexe von Metallen, XXV. Di-Cyclopentadienyl-Beryllium. *Chem. Ber.* **1959**, *92* (2), 482–486.

(2) Almenningen, A.; Bastiansen, O.; Haaland, A. Molecular Structure of Dicyclopentadienylberyllium $(C_5H_5)_2Be$. *J. Chem. Phys.* **1964**, *40* (11), 3434–3437.

(3) Almenningen, A.; Haaland, A.; Lusztyk, J. The Molecular Structure of Beryllocene, $(C_5H_5)_2Be$. A Reinvestigation by Gas Phase Electron Diffraction. *J. Organomet. Chem.* **1979**, *170* (3), 271–284.

(4) Lusztyk, J.; Starowieyski, K. B. The Raman Spectrum and Structure of Dicyclopentadienylberyllium. *J. Organomet. Chem.* **1979**, *170* (3), 293–297.

(5) Nugent, K. W.; Beattie, J. K.; Hambley, T. W.; Snow, M. R. A Precise Low-Temperature Crystal Structure of Bis(Cyclopentadienyl)Beryllium. *Aust. J. Chem.* **1984**, *37* (8), 1601–1606.

(6) Wong, C.-H.; Lee, T.-Y.; Chao, K.-J.; Lee, S. Crystal Structure of Bis(Cyclopentadienyl)Beryllium at -120 °C. *Acta Crystallogr. Sect. B* **1972**, *28* (6), 1662–1665.

(7) Wong, C.; Lee, T. Y.; Lee, T. J.; Chang, T. W.; Liu, C. S. Novel Structure of Beryllocene. *Inorg. Nucl. Chem. Lett.* **1973**, *9* (6), 667–673.

(8) Margl, P.; Schwarz, K.; Blöchl, P. E. Dynamics of Beryllocene. *J. Chem. Phys.* **1995**, *103* (2), 683–690.

(9) Margl, P.; Schwarz, K.; Bloechl, P. E. Fluxional Dynamics of Beryllocene. *J. Am. Chem. Soc.* **1994**, *116* (24), 11177–11178.

(10) Mire, L. W.; Wheeler, S. D.; Wagenseller, E.; Marynick, D. S. The Application of Density Functional Theory to Four Problems in Inorganic Chemistry: A Comparison to Traditional Ab Initio Methods. *Inorg. Chem.* **1998**, *37* (12), 3099–3106.

(11) Coates, G. E.; Glockling, F. Diisopropylberyllium and Some Beryllium Hydrides. *J. Chem. Soc.* **1954**, No. 0, 22–27.

(12) Coates, G. E.; Huck, N. D. 862. Dimethylberyllium. Part II. Co-Ordination Compounds. *J. Chem. Soc.* **1952**, No. 0, 4501–4511.

(13) Coates, G. E.; Smith, D. L.; Srivastava, R. C. T-Butylberyllium-Alkyls and -Aryls: Amine Complexes and Pyrolysis to Hydrides. *J. Chem. Soc. Dalt. Trans.* **1973**, No. 6, 618–622.

(14) Coates, G. E.; Wade, K.; Green, M. L. H. *Organometallic Compounds*; Metheun: London, 1967; Vol. 1.

(15) Buchner, M. R. Beryllium-Associated Diseases from a Chemist's Point of View. *Zeitschrift für Naturforsch. B* **2020**, *75* (5), 405–412.

(16) Buchner, M. R. Beryllium Coordination Chemistry and Its Implications on the Understanding of Metal Induced Immune Responses. *Chem. Commun.* **2020**, *56* (63), 8895–8907.

(17) Müller, M.; Buchner, M. R. Understanding the Localization of Berylliosis: Interaction of Be2+ with Carbohydrates and Related Biomimetic Ligands. *Chem. Eur. J.* **2019**, *25*, 16257.

(18) Fischer, E. O.; Seus, D. Notizen: Di-Indenyl-Eisen. *Z. Naturforsch. B* **1953**, *8* (11), 694.

(19) Beattie, J. K.; Nugent, K. W. Beryllocene and Related Slip-Sandwich Structures. *Inorg. Chim. Acta* **1992**, *198–200*, 309–318.

(20) Atwood, J. L.; Smith, K. D. Synthesis and Structure of Bis(Indenyl)Magnesium. *J. Am. Chem. Soc.* **1974**, *96* (4), 994–998.

(21) Overby, J. S.; Hanusa, T. P. Synthesis and Crystallographic Study of Indenyl and Isopropylated Indenyl Complexes of Calcium, Strontium, and Barium. *Organometallics* **1996**, *15* (9), 2205–2212.

(22) Neander, S.; Behrens, U.; Olbrich, F. Novel 18-Crown-6 Organometallic Rubidium and Cesium Complexes Containing Cyclopentadienyl, Indenyl, Pentamethylcyclopentadienyl, and Fluorenyl as Carbanions. *J. Organomet. Chem.* **2000**, *604* (1), 59–67.
(23) Buchanan, J. K.; Plieger, P. G. ^{9}Be Nuclear Magnetic Resonance Spectroscopy Trends in Discrete Complexes: An Update. *Z. Naturforsch. B* **2020**, *75* (5), 459–472.
(24) Burns, C. J.; Andersen, R. A. Organometallic Coordination Complexes of the Bis(Pentamethylcyclopentadienyl)-Alkaline Earth Compounds, $(Me_5C_5)_2ML_n$, Where M IS Mg, Ca, Sr, OR Ba and Me_5C_5BeCl. *J. Organomet. Chem.* **1987**, *325* (1), 31–37.
(25) del Mar Conejo, M.; Fernández, R.; del Río, D.; Carmona, E.; Monge, A.; Ruiz, C.; Márquez, A. M.; Fernández Sanz, J. Synthesis, Solid-State Structure, and Bonding Analysis of the Beryllocenes $[Be(C_5Me_4H)_2]$, $[Be(C_5Me_5)_2]$, and $[Be(C_5Me_5)(C_5Me_4H)]$. *Chem. Eur. J.* **2003**, *9* (18), 4452–4461.
(26) Gaines, D. F.; Coleson, K. M.; Hillenbrand, D. F. 9Be NMR of Beryllaboranes and Other Beryllium Compounds. *J. Magn. Reson.* **1981**, *44* (1), 84–88.
(27) Koby, R. F.; Doerr, A. M.; Rightmire, N. R.; Schley, N. D.; Long, B. K.; Hanusa, T. P. An η 3 - Bound Allyl Ligand on Magnesium in a Mechanochemically Generated Mg/K Allyl Complex. *Angew. Chemie Int. Ed.* **2020**, *132* (59), 9542–9549.
(28) Koby, R. F.; Hanusa, T. P.; Schley, N. D. Mechanochemically Driven Transformations in Organotin Chemistry: Stereochemical Rearrangement, Redox Behavior, and Dispersion-Stabilized Complexes. *J. Am. Chem. Soc.* **2018**, *140* (46), 15934–15942.
(29) Speight, I. R.; Chmely, S. C.; Hanusa, T. P.; Rheingold, A. L. Mechanochemically Directed Metathesis in Group 2 Chemistry: Calcium Amide Formation without Solvent. *Chem. Commun.* **2019**, *55*, 2202–2205.
(30) Speight, I. R.; Huskić, I.; Arhangelskis, M.; Titi, H. M.; Stein, R. S.; Hanusa, T. P.; Friščić, T. Disappearing Polymorphs in Metal–Organic Framework Chemistry: Unexpected Stabilization of a Layered Polymorph over an Interpenetrated Three-Dimensional Structure in Mercury Imidazolate. *Chem. Eur. J.* **2020**, *26* (8), 1811–1818.
(31) Koby, R. F.; Rightmire, N. R.; Schley, N. D.; Hanusa, T. P.; Brennessel, W. W. Halide Metathesis in Overdrive: Mechanochemical Synthesis of a Heterometallic Group 1 Allyl Complex. *Beilstein J. Org. Chem.* **2019**, *15*, 1856–1863.
(32) Koby, R. F.; Doerr, A. M.; Rightmire, N. R.; Schley, N. D.; Brennessel, W. W.; Long, B. K.; Hanusa, T. P. Mechanochemical Formation, Solution Rearrangements, and Catalytic Behavior of a Polymorphic Ca/K Allyl Complex. *Chem. Eur. J.* **2021**
(33) Rightmire, N. R.; Hanusa, T. P. Advances in Organometallic Synthesis with Mechanochemical Methods. *Dalton Trans.* **2016**, *45* (6), 2352–2362.
(34) Naglav, D.; Tobey, B.; Neumann, A.; Bläser, D.; Wölper, C.; Schulz, S. Synthesis, Solid-State Structures, and Computational Studies of Half-Sandwich Cp*BeX (X = Cl, Br, I) Compounds. *Organometallics* **2015**, *34* (12), 3072–3078.
(35) Guzei, I. A.; Wendt, M. An Improved Method for the Computation of Ligand Steric Effects Based on Solid Angles. *Dalton Trans.* **2006**, No. 33, 3991–3999.
(36) Bondi, A. Van Der Waals Volumes and Radii. *J. Phys. Chem.* **1964**, *68*, 441.
(37) Jaenschke, A.; Olbrich, F.; Behrens, U. Strukturen von Polaren Magnesiumorganylen: Synthese Und Struktur von Basen-Addukten Des Magnesiumindenids. *Z. Anorg. Allg. Chem.* **2009**, *635* (15), 2550–2557.
(38) Gritzo, H.; Schaper, F.; Brintzinger, H.-H. Bis(η^3-Indenyl)Bis(Tetrahydrofuran)Magnesium(II). *Acta Crystallogr. Sect. E* **2004**, *60* (8), m1108–

m1110.
(39) del Mar Conejo, M.; Fernández, R.; Gutiérrez-Puebla, E.; Monge, Á.; Ruiz, C.; Carmona, E. Synthesis and X-Ray Structures of [Be($C_5Me_4H)_2$] and [Be($C_5Me_5)_2$]. *Angew. Chem. Int. Ed.* **2000**, *39* (11), 1949–1951.
(40) Conejo, M. M.; Fernández, R.; del Río, D.; Carmona, E.; Monge, A.; Ruiz, C. Synthesis and Structural Characterization of Be(η^5-C_5Me_5)(η^1-C_5Me_4H). Evidence for Ring-Inversion Leading to Be(η^5-C_5Me_4H)(η^1-C_5Me_5). *Chem. Commun.* **2002**, No. 23, 2916–2917.
(41) Dewar, M. J. S.; Rzepa, H. S. Ground States of Molecules. 52. A MNDO SCF-MO Study of the Coordination of Beryllium-Indenyl and -Fluorenyl Complexes. *Inorg. Chem.* **1979**, *18* (3), 602–605.
(42) Kawakami, K.; Kuivila, H. G. Preparation and Spectral Characteristics of Some Allyltins. *J. Org. Chem.* **1969**, *34*, 1502.
(43) Weidner, U.; Schweig, A. Nature of the "Silicon β-Effect" in Allyltrimethylsilane. *Angew. Chem. Int. Ed. Engl.* **1972**, *11* (2), 146–147.
(44) Burshtein, K. Y.; Isaev, A. N.; Shorygin, P. P. σ-π Interaction in Some σ-Bonded Allyl Compounds. A MNDO Study. *J. Organomet. Chem.* **1989**, *361*, 21.
(45) Weiss, T.; Böhme, U.; Walfort, B.; Rheinwald, G.; Lang, H. Trimethylsilyl-Substituted Indenyl-$TiCl_3$ Half-Sandwich Complexes: Synthesis, Solid-State Structure, and Analysis of Substituent Effects. *Organometallics* **2005**, *24* (11), 2577–2581.
(46) O'Connor, J. M.; Casey, C. P. Ring-Slippage Chemistry of Transition Metal Cyclopentadienyl and Indenyl Complexes. *Chem. Rev.* **1987**, *87* (2), 307–318.
(47) Mrózek, O.; Vinklárek, J.; Růžičková, Z.; Honzíček, J. Indenyl Compounds with Constrained Hapticity: The Effect of Strong Intramolecular Coordination. *Eur. J. Inorg. Chem.* **2016**, *2016* (33), 5250–5264.
(48) Calhorda, M. J.; Romão, C. C.; Veiros, L. F. The Nature of the Indenyl Effect. *Chem. Eur. J.* **2002**, *8* (4), 868–875.
(49) Nguyen, K. T.; Lane, E. E.; McMillen, C. D.; Pienkos, J. A.; Wagenknecht, P. S. Is Indenyl a Stronger or Weaker Electron Donor Ligand than Cyclopentadienyl? Opposing Effects of Indenyl Electron Density and Ring Slipping on Electrochemical Potentials. *Organometallics* **2020**.
(50) Müller, M.; Pielnhofer, F.; Buchner, M. R. A Facile Synthesis for $BeCl_2$, $BeBr_2$ and BeI_2. *Dalton Trans.* **2018**, *47* (36), 12506–12510.
(51) Porskamp, P. A. T. W. Synthesis and Reactions of Functionalized Sulfines. [Sl: sn] 2007.
(52) Armarego, W. L. F.; Chai, C. L. L. Chapter 1 - Common Physical Techniques Used in Purification; Armarego, W. L. F., Chai, (Sixth Ed., Eds.; Butterworth-Heinemann: Oxford, 2009; pp 1–60.
(53) Dolomanov, O. V; Bourhis, L. J.; Gildea, R. J.; Howard, J. A. K.; Puschmann, H. OLEX2: A Complete Structure Solution, Refinement and Analysis Program. *J. Appl. Crystallogr.* **2009**, *42* (2), 339–341.
(54) Sheldrick, G. SHELXT - Integrated Space-Group and Crystal-Structure Determination. *Acta Crystallogr. Sect. A* **2015**, *71* (1), 3–8.
(55) Sheldrick, G. Crystal Structure Refinement with SHELXL. *Acta Crystallogr. Sect. C* **2015**, *71* (1), 3–8.
(56) M. J. Frisch, G. W. Trucks, H. B. Schlegel, G. E. Scuseria, M.; A. Robb, J. R. Cheeseman, G. Scalmani, V. Barone, B. Mennucci, G. A. Petersson, H.; Nakatsuji, M. Caricato, X. Li, H. P. Hratchian, A. F. Izmaylov, J. Bloino, G. Zheng, J. L.; Sonnenberg, M. Hada, M. Ehara, K. Toyota, R. Fukuda, J. Hasegawa, M. Ishida, T.; Nakajima, Y. Honda, O. Kitao, H. Nakai, T.

Vreven, J. A. Montgomery, Jr., J. E. Peralta, F.; Ogliaro, M. Bearpark, J. J. Heyd, E. Brothers, K. N. Kudin, V. N. Staroverov, R.; Kobayashi, J. Normand, K. Raghavachari, A. Rendell, J. C. Burant, S. S. Iyengar, J.; Tomasi, M. Cossi, N. Rega, J. M. Millam, M. Klene, J. E. Knox, J. B. Cross, V. Bakken, C.; Adamo, J. Jaramillo, R. Gomperts, R. E. Stratmann, O. Yazyev, A. J. Austin, R. Cammi, C.; Pomelli, J. W. Ochterski, R. L. Martin, K. Morokuma, V. G. Zakrzewski, G. A. Voth, P.; Salvador, J. J. Dannenberg, S. Dapprich, A. D. Daniels, Ö. Farkas, J. B. Foresman, J. V.; Ortiz, J. Cioslowski, and D. J. Fox, Gaussian, Inc., Wallingford CT, 2009. Gaussian16 Revision D.01. *http//www. gaussian. com/* **2009**.

(57) Perdew, J. P.; Wang, Y. Accurate and Simple Analytic Representation of the Electron-Gas Correlation Energy. *Phys. Rev. B* **1992**, *45* (23), 13244–13249.

(58) Grimme, S.; Antony, J.; Ehrlich, S.; Krieg, H. A Consistent and Accurate Ab Initio Parametrization of Density Functional Dispersion Correction (DFT-D) for the 94 Elements H-Pu. *J. Chem. Phys.* **2010**, *132* (15), 154104.

(59) Grimme, S.; Ehrlich, S.; Goerigk, L. Effect of the Damping Function in Dispersion Corrected Density Functional Theory. *J. Comput. Chem.* **2011**, *32* (7), 1456–1465.

(60) Rappoport, D.; Furche, F. Property-Optimized Gaussian Basis Sets for Molecular Response Calculations. *J. Chem. Phys.* **2010**, *133* (13), 134105.

(61) Lu, T.; Chen, F. Multiwfn: A Multifunctional Wavefunction Analyzer. *J. Comput. Chem.* **2012**, *33* (5), 580–592.

(62) Plieger, P. G.; John, K. D.; Keizer, T. S.; McCleskey, T. M.; Burrell, A. K.; Martin, R. L. Predicting 9Be Nuclear Magnetic Resonance Chemical Shielding Tensors Utilizing Density Functional Theory. *J. Am. Chem. Soc.* **2004**, *126* (44), 14651–14658.

(63) Iron, M. A. Evaluation of the Factors Impacting the Accuracy of 13C NMR Chemical Shift Predictions Using Density Functional Theory—The Advantage of Long-Range Corrected Functionals. *J. Chem. Theory Comput.* **2017**, *13* (11), 5798–5819.

(64) Frunzke, J.; Lein, M.; Frenking, G. Structures, Metal–Ligand Bond Strength, and Bonding Analysis of Ferrocene Derivatives with Group-15 Heteroligands $Fe(\eta^5\text{-}E_5)_2$ and $FeCp(\eta^5\text{-}E_5)$ (E = N, P, As, Sb). A Theoretical Study. *Organometallics* **2002**, *21* (16), 3351–3359.